AD-A995 336

DTIC ACCESSION NUMBER

Project 8.1a

LEVEL EFFECT OF THERMAL AND BLAST FORCES
FROM NUCLEAR DETONATORS ON BASIC
AIRCRAFT STRUCTURES AND
COMPONENTS

INVENTORY

DOCUMENT IDENTIFICATION

DISTRIBUTION STATEMENT

ACCESSION FOR		
NTIS	GRA&I	☒
DTIC	TAB	☐
UNANNOUNCED		☐
JUSTIFICATION		

BY
DISTRIBUTION /
AVAILABILITY CODES

DIST	AVAIL AND/OR SPECIAL
A-1	

QUALITY
INSPECTED
3

DISTRIBUTION STAMP

UNANNOUNCED

DTIC
S ELECTE D
DEC 17 1985
D

DATE ACCESSIONED

DATE RETURNED

85 12 16 012

DATE RECEIVED IN DTIC

REGISTERED OR CERTIFIED NO.

DTIC FORM 70A
DEC 83

DOCUMENT PROCESSING SHEET

PREVIOUS EDITION MAY BE USED UNTIL
STOCK IS EXHAUSTED.

TECHNICAL LIBRARY
of the
ARMED FORCES
SPECIAL WEAPONS PROJECT
SEP 16 1954

Operation

UPSHOT-KNOTHOLE

NEVADA PROVING GROUNDS

March - June 1953

Project 8.1a

Classification Changed to UNCLASSIFIED
By Authority of Jnt DoD/DOE Review
CN
By DNA Chf ISCM Date 23 Oct 1985
By DOE Lett to DNA Date 12 July 1985

EFFECTS OF THERMAL AND BLAST FORCES FROM
NUCLEAR DETONATIONS ON BASIC AIRCRAFT
STRUCTURES AND COMPONENTS

SECRET

Classification (Cancelled) (Changed to _____ 3/1/62
By Authority of AFSWC-3 Memo   9 Feb 62
By _____ Date 9 Feb 62

RESTRICTED DATA

This document contains restricted data as
defined in the Atomic Energy Act of 1946.
Its transmittal or the disclosure of its
contents in any manner to an unauthorized
person is prohibited.

Statement A
Approved for public release;
distribution unlimited

HEADQUARTERS FIELD COMMAND, ARMED FORCES SPECIAL WEAPONS PROJECT
SANDIA BASE, ALBUQUERQUE, NEW MEXICO

B 9985

UNCLASSIFIED

OPERATION UPSHOT-KNOTHOLE

Project 8.1a

EFFECTS OF THERMAL AND BLAST FORCES FROM NUCLEAR DETONATIONS ON BASIC AIRCRAFT STRUCTURES AND COMPONENTS

REPORT TO THE TEST DIRECTOR

by

E. J. Schlei and Staff
Division of Research
University of Dayton
and
G. T. James, Captain, USAF
and
L. J. Breidenbach
Wright Air Development Center

March 1954

Aircraft Laboratory
Wright Air Development Center
Dayton, Ohio

ABSTRACT

To augment the basic knowledge of the vulnerability and thermo-
elastic response of aircraft operating in the vicinity of a nuclear
detonation, various aircraft structural components were instrumented
for time-history temperature and strain response and exposed to the
thermal and/or blast inputs during Shots 9 and 10 of Operation
UPSHOT-KNOTHOLE. The specimens chosen for this investigation
were box beams, tension ties, stabilizer and elevator assemblies, and
structurally bonded metal hat, waffle, and honeycomb core type air-
craft panels. These stabilizers were preloaded to simulate an in-
flight condition and exposed in sets of three, such that one was shielded
from blast, one shielded from thermal radiation, and the other un-
shielded. In addition, structurally bonded metal aircraft panels were
instrumented for peak skin temperature determination with temp-tapes
and exposed to determine the threshold temperature for permanent
skin buckling and for bond release. A B-36 stabilizer and elevator
assembly and a B-36 wing outer panel were exposed and instrumented
with temp-tapes to investigate local panel damage. Samples of fabric
and foil control surface coverings were exposed in order to establish
a threshold of thermal damage for each type covering. Thermal and
blast inputs were measured at each of the four Project 8.1a instru-
mentation stations for both Shots 9 and 10. Test panel displays of air-
craft undercarriage components, comprising tire specimens, hydraulic
equipment, and related items, were exposed to relatively high thermal
inputs to establish a damage threshold for these components.

The data obtained during Shot 9 varied slightly from those antici-
pated because the inputs realized were lower than expected; however,
changes in the intended program for Shot 10, for the most part, offset
the effects of the Shot 9 inputs. Over 95 per cent of the instrumentation
channels on the box beams, tension ties, and stabilizer and elevator
assemblies produced usable response data. The data are consistent
and agree with those expected from general theoretical considerations.
Analysis of the above data should provide a better understanding of the
thermoelastic response of thick skinned specimens to unilateral heating

3

and an improved knowledge of the interaction of thermal and blast forces in causing aircraft damage. A wide range of damage, including bond release, was sustained by the bonded metal aircraft panels. For temperature rises up to about 350°F, waffle panels are less vulnerable to skin buckling than hat panels for the free edge condition. Of the panels tested, honeycomb core panels are the most vulnerable to bond release, with bond failure occurring at temperatures as low as 300°F. The overpressure required to produce panel buckling on the B-36 stabilizer and elevator assembly was found to be between 1.2 and 3.2 psi. Inputs of 23.1 cal/sq cm and 5.7 psi caused panel damage to the B-36 wing section ranging from moderate to complete destruction. Fabric and foil control surface coverings can be made to withstand satisfactorily thermal energies up to about 10 and 13 cal/sq cm, respectively.

FOREWORD

This report is one of the reports presenting the results of the 78 projects participating in the Military Effects Tests Program of Operation UPSHOT-KNOTHOLE, which included 11 test detonations. For readers interested in other pertinent test information, reference is made to WT-782, Summary Report of the Technical Director, Military Effects Program. This summary report includes the following information of possible general interest.

a. An over-all description of each detonation, including yield, height of burst, ground zero location, time of detonation, ambient atmospheric conditions at detonation, etc., for the 11 shots.

b. Compilation and correlation of all project results on the basic measurements of blast and shock, thermal radiation, and nuclear radiation.

c. Compilation and correlation of the various project results on weapons effects.

d. A summary of each project, including objectives and results.

e. A complete listing of all reports covering the Military Effects Tests Program.

PREFACE

This report is a presentation of the data obtained by Project 8.1a during Operation UPSHOT-KNOTHOLE. These data pertain primarily to individual structural components exposed under particular conditions; as a consequence, any extrapolation of these data should be made only with the particular specimens and the exposure conditions in mind. The discussion section, which is devoted primarily to the presentation of certain data phenomena as well as observations made during the field phase of the project, should be helpful to those who will utilize these data.

Naturally a project having the scope and magnitude of Project 8.1a can succeed only with the support and cooperation of many organizations and many individuals. The Aero-Elastic Laboratory of the Massachusetts Institute of Technology, the Allied Research Associates, Inc. of Boston, and the Department of Engineering of the University of California at Los Angeles were given the responsibility of recommending criteria to be investigated and specimens to be tested. The Director and Personnel of Program 9 supplied the technical motion picture photography during Shots 9 and 10. The Naval Radiological and Defense Laboratory supplied the calorimeters and the associated calibration data. The Personnel of the Signal Corps Electronics Laboratory, operating as Project 6.8, furnished the dosimeters employed at the instrumentation stations and reduced the resulting data. The Boeing Airplane Company furnished five honeycomb panels of the B-52 aircraft. The Consolidated Vultee Aircraft designed and fabricated the mounting jig for the B-36 elevator and stabilizer assembly. The Mechanical Branch and the Special Projects Branch of the Aircraft Laboratory of the Wright Air Development Center designed and fabricated the mounts and displayed the specimens sponsored by those Branches. Finally, special acknowledgment should be given for the support rendered by LCDR R.G. Preston, U.S.N., who was the Director of Program 8, and by all the other personnel of the Armed Forces Special Weapons Project whose coordinated efforts and spirit of cooperation made possible the successful recording of the required data. The authors of this report are grateful for this opportunity to acknowledge the support listed above.

CONTENTS

11

ILLUSTRATIONS

APPENDIX A   INSTRUMENTATION

APPENDIX B   THERMOELASTIC STUDY UTILIZING BOX BEAMS
AND TENSION TIES

15

16

17

18

19

20

23

24

APPENDIX D MISCELLANEOUS SPECIMENS

26

27

28

TABLES

31

32

CHAPTER 1

INTRODUCTION

1.1 BACKGROUND

The studies conducted by Project 8.1a in Operation UPSHOT-KNOTHOLE are a part of the Wright Air Development Center's (WADC) research and development program which is devoted to the study of the effects of nuclear weapons upon aircraft. Investigations consisting of physical experiments were initiated in 1946 and data were obtained during Operations CROSSROADS, GREENHOUSE, BUSTER-JANGLE, and TUMBLER-SNAPPER. Results of these operations and developments in the field of aircraft design, indicated the need for participation in UPSHOT-KNOTHOLE.

The program was planned by the Aircraft Laboratory of the WADC in consultation with the Aero-Elastic and Structures Research Laboratory of the Massachusetts Institute of Technology, Allied Research Associates, and the Division of Research of the University of Dayton. The University of Dayton was charged with the responsibility of the design, preparation, and instrumentation of test specimens; design and preparation of jigs and other test support equipment; the execution of the field operation, the reduction of data; and the preparation of the data report. The purpose of this report is to present the data obtained during UPSHOT-KNOTHOLE.

1.2 OBJECTIVE

1.2.1 Research and Development Program

The ultimate objective of the WADC research and development program is the development of critical operational criteria and the establishment of design criteria for aircraft of the future. A more immediate objective of the program is the determination of aircraft

vulnerability, with specific reference to the delivery of nuclear weapons.

1.2.2   Project 8.1a

The general objective of Project 8.1a was to obtain data on the response of aircraft components and selected test specimens to the thermal and/or blast phenomena produced by nuclear detonations.

The specific objectives were:

1. To determine the thermoelastic response of simple specimens representative of modern and future aircraft structural elements and components.

2. To determine the response of preloaded aircraft components (simulating flight conditions) to separate thermal and blast inputs and to coupled thermal and blast inputs.

3. To correlate buckling of aircraft structural panels with temperature rise using skin thickness, structural configuration, and edge restraint as parameters.

4. To perform an experimental check on theoretical predictions of overpressure damage to certain bonded metal structural configurations.

5. To test the effectiveness of modifications for fabric covered control surfaces designed to increase the thermal resistance of these components.

6. To determine the effects of thermal radiation on aircraft undercarriage components.

1.3   SCOPE OF PROGRAM

Major effort was directed toward displaying basic aircraft structures and components and obtaining the time-history temperature and strain responses of these specimens. A total of 220 channels of instrumentation were recorded by oscillographs at four stations; 105 channels during Shot 9 and 115 channels during Shot 10. Test specimens included 8 box beams, 8 tension ties, 13 horizontal stabilizer and elevator assemblies, and 6 aircraft panels. Exposures of each specimen were made at two or three different ranges.

Additional effort was expended in displaying other specimens including 31 aircraft panels, a B-36 stabilizer and elevator assembly, a B-36 wing section, 212 panels of protective control surface coverings and 99 aircraft undercarriage components. These specimens were instrumented for maximum temperature determination only. Response and damage to individual specimens were determined by visual inspection.

Thermal and blast inputs were measured at four ranges during Shots 9 and 10.

CHAPTER 2

PROCEDURE

2.1 BOX BEAMS AND TENSION TIES

The thermoelastic response of simple aircraft type structures was studied using specimens called box beams, which were long, slender structures consisting of two faces and two webs fastened together with screws and dowel pins, and tension ties, which were thin bars of rectangular cross-section stressed in tension. The specimens were made of aluminum and magnesium materials and each was mounted with its longitudinal axis in a vertical plane and with its front face normal to the intended burst point. The beams, rigidly clamped at one end, were exposed as cantilevers, as shown in Fig. 2.1; and the ties were loaded by leaf springs, such that the material stress at the peak of the thermal phase would be between yield and ultimate. A tension tie and its loading device are shown in Fig. 2.2.

Fig. 2.1 Box Beam and Mount
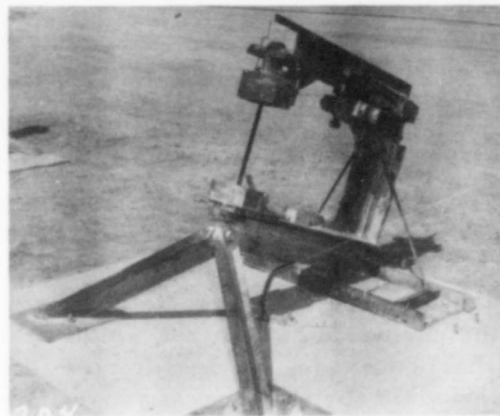
Fig. 2.2 Tension Tie and Loading Device

The absorptivity of the specimens was adjusted so as to achieve temperature rises up to a maximum of 400°F in the ties and in the front faces of the beams. At least one strain gage and one thermocouple were attached to each specimen to measure the time-history unit elongation and temperature of the metal.

Details of the thermoelastic study utilizing box beams and tension ties are given in Appendix B.

2.2   HORIZONTAL STABILIZER AND ELEVATOR ASSEMBLY (T-28)

The response of preloaded aircraft components to separate and coupled inputs was determined using horizontal stabilizer and elevator assemblies from T-28 aircraft. These specimens, representative of thin-skin, all-metal construction, were mounted vertically, with the chord oriented normal to blast incidence and with the control surface locked. A bending preload was applied to each stabilizer to simulate in-flight conditions. At each of three ranges, one assembly was exposed to thermal energy but shielded from blast, a second assembly was shielded from thermal but exposed to blast, and a third was exposed to both thermal and blast inputs, as shown in Fig. 2.3. Three
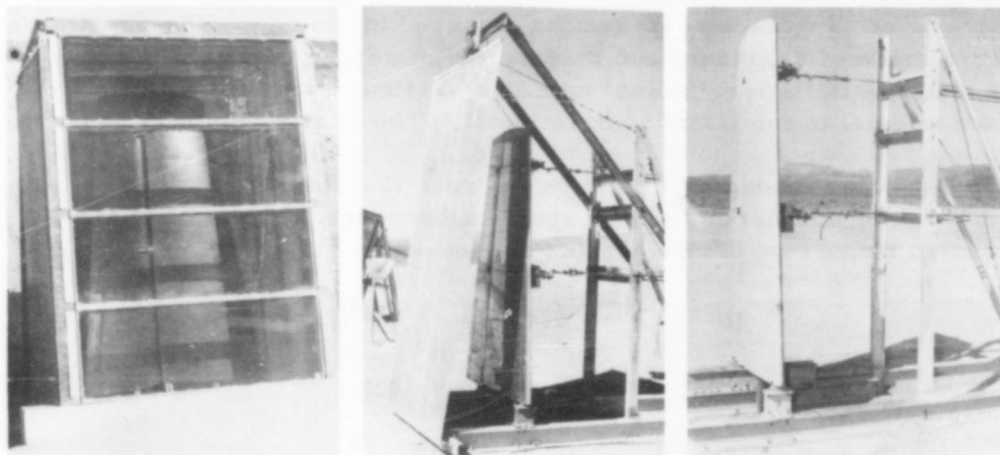
Fig. 2.3   One Set of T-28 Stabilizers.   Left to Right; Shielded from Blast, Shielded from Thermal, and Unshielded.

ranges were chosen such that the maximum stress in the rear spar of the unshielded stabilizer would be between yield and ultimate for the shortest range, at yield for the intermediate distance, and slightly below yield for the longest range. Instrumentation consisted of strain gages and thermocouples attached to the skin panels and spars of the specimens.

Details of the coupling study utilizing T-28 horizontal stabilizer

36

assemblies are given in Appendix C.

2.3 MISCELLANEOUS SPECIMENS

Miscellaneous specimens included bonded metal aircraft panels, B-36 components, control surface covering test panels, and aircraft undercarriage components.

2.3.1 Bonded Metal Aircraft Panels

The bonded metal aircraft panels used in the test were specimens representative of the "hat" stiffened sheet and "waffle" stiffened sheet constructions as used in the B-36 aircraft and of the "honeycomb core" sandwich type construction as used in the B-52 aircraft. A drawing of each type panel is shown in Fig. 2.4. The testing for

Hat Panel   Waffle Panel

Honeycomb Sandwich Panel
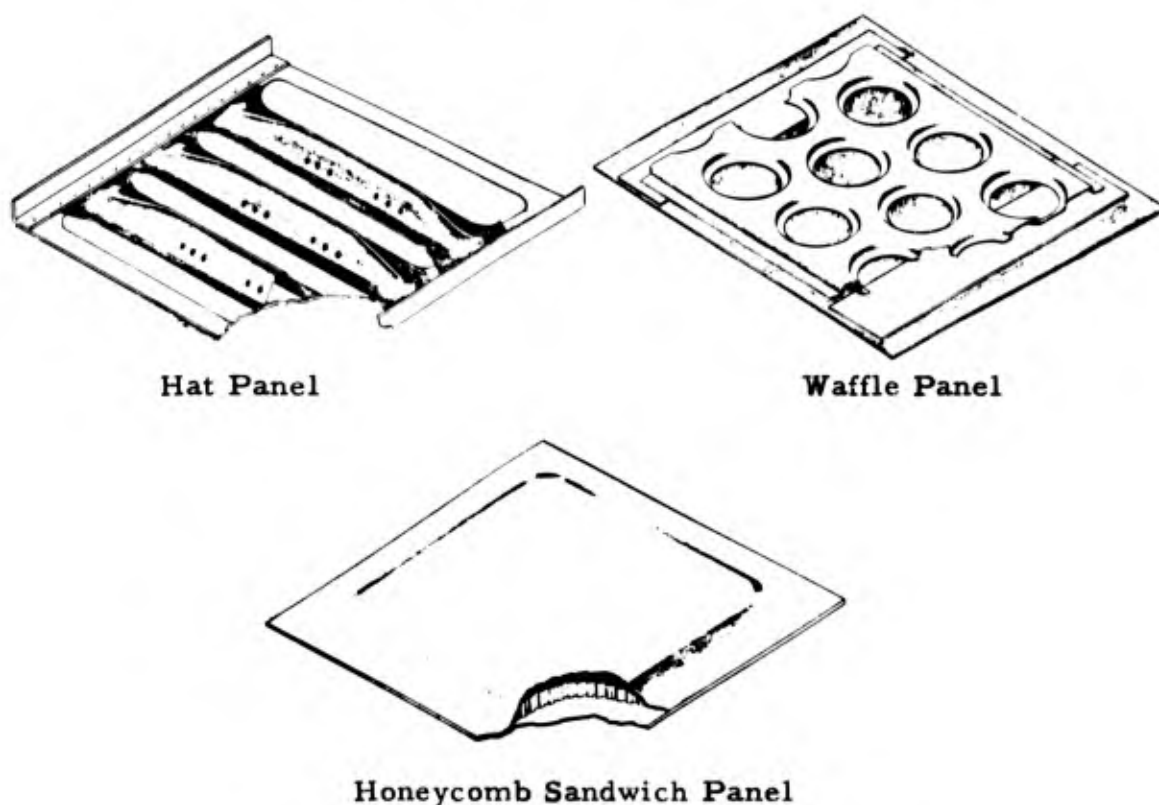
Fig. 2.4 Types of Bonded Metal Panels

thermoelastic buckling characteristics was accomplished by exposing the panels to the thermal energy while shielding them from the blast. Three bonded metal panels enclosed in blast shields are shown in Fig. 2.5. All panels were instrumented for peak skin temperature determination to facilitate correlation of buckling with skin temperature. In

37

Fig. 2.5 Typical Bonded Metal Panel Blast Shield Array

addition, six panels were instrumented for time-history measurements, three for strain and temperature data, and the remaining three for temperature information only.

2.3.2   B-36 Components

Theoretical predictions of local pressure damage were checked by exposing a left-hand horizontal stabilizer and elevator assembly of a B-36 aircraft. The effects of skin thickness, panel design, and temperature rise on overpressure and thermal damage were investigated using a 21 ft section of the left wing outer panel from the same type aircraft.

The horizontal stabilizer and elevator assembly was supported on a tubular steel framework, as shown in Fig. 2.6, in such a position

Fig. 2.6 The B-36 Stabilizer and Elevator Assembly
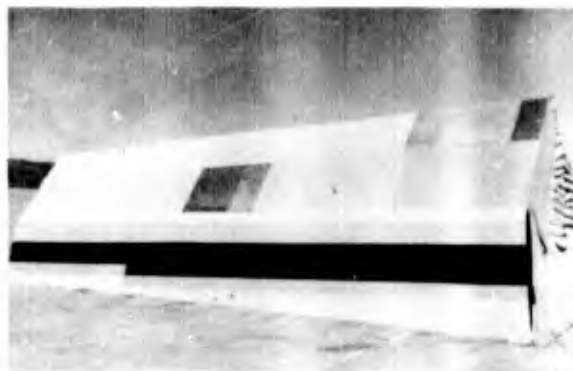
Fig. 2.7 The B-36 Wing Section
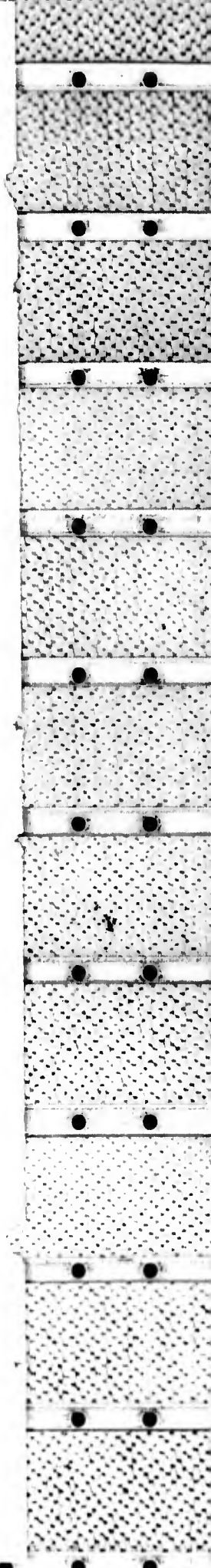
that the incidence of the blast wave would be similar to that of a bomb
delivery aircraft. Various panels on the stabilizer and elevator assem-
bly were instrumented for peak temperature determination using temp-
tapes.

The wing section, shown in Fig. 2.7, was placed with the front
spar touching the ground and the lower surface of the wing facing the
intended point of detonation. An earth embankment and steel cables
held the wing section in this inclined position. Skin panels on the wing
section were instrumented for peak skin temperature determination,
and an attempt was made to obtain different temperature rises for
similar panel thicknesses by varying the surface absorptivity.

2.3.3 Control Surface Covering Test Panels

Panels, consisting of a light metallic frame covered with fabric
or thin gage metal to represent aircraft control surfaces, were tested
to determine what protection against thermal radiation was afforded
these materials by dope, enamel, or a foil covering. The thin gage met-
al covering was bare magnesium alloy to test its effectiveness as a re-
placement for fabric. A variety of panels and exposure levels were
used to provide a large amount of visual inspection data. A set of panels,
displayed for exposure, is shown in Fig. 2.8.
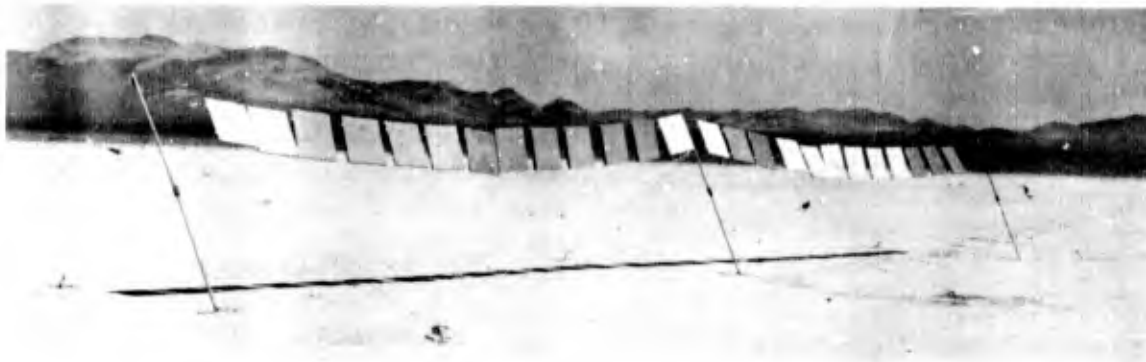
Fig. 2.8 Control Surface Covering Test Panels

2.3.4 Aircraft Undercarriage Components

Parts of aircraft undercarriages including tires, wheels, brakes,
and actuators were exposed at relatively high levels of thermal energy
to obtain visual damage data in an attempt to determine the esposure
limits of the metallic and rubber materials used in their construction.
The information could aid in the establishment of protective and main-
tenance measures for the prolongation of the service life of the com-
ponents. One set of equipment in exposure position is shown in Fig. 2.9.

39

Details of the miscellaneous specimens outlined above are given in Appendix D.

Fig. 2.9 Aircraft Undercarriage Components

2.4 INPUTS

Time-history measurements of total thermal energy and of over-pressure were made at each of the four stations fitted with oscillo-graphic instrumentation. Total gamma radiation was measured at the same four stations.

Total thermal energy meas-urements were obtained at each of the stations by means of calorim-eters furnished by the U.S. Naval Radiological Defense Laboratory. Energy incident at the location was measured by openly exposed calorimeters. In addition, calorimeters were mounted behind the glass panels of the stabilizer blast shields to measure the energy incident at the stabilizer and indirectly giving the thermal attenuation of the glass. Overpressure was measured by Statham and Consolidated gages with one of each type gage located at each station. Each gage was mounted in a hole at the center of a square plate which was oriented vertically in a plane passing through intended ground zero. Figure 2.10 shows a typical pressure gage, calorimeter, and mounting assembly.

Fig. 2.10 Pressure Gage, Calor-imeter and Mounting Assembly

Total gamma radiation was measured with film badges located along the lines of specimens and also inside the instrument shelters.

2.5 PROGRAM, SHOT 9

A schematic drawing of the arrangement of the specimens and instruments described above for Shot 9 is shown in Fig. 2.11. Fifteen different ranges are repre-sented, for purposes of clarity the four locations designed for oscillo-graphic instrumentation will be call-ed "Stations" and all other locations will be referred to as "Ranges." The numbers following the words Station and Range indicate the dis-tance in feet to intended ground zero.

40

Fig. 2.11 General Arrangement of Specimens and Instrument Shelters for Shot 9

2.5.1   Station 2300

Th. high temperature requirement of the beam and tie specimens indicated the need for Station 2300. The construction consisted of one large concrete base on which the specimens and instruments were mounted relatively close to each other. The instrument shelter was completely underground at the center of the base. The specimen display consisted of three box beams, three tension ties, and two sets of total thermal energy and overpressure measuring instruments, as shown in Fig. 2.12. All the beams and ties were made of 3/16 in.

Fig. 2.12 Test Array at Station 2300, Shot 9

thick material but differed in that:

1. One of each specimen was made of aluminum material and painted black.

2. A second pair was made of aluminum but painted gray, such that its temperature increase would be about one-half that of the black-painted items.

3. The third pair was made of magnesium material and colored a shade of gray, such that its temperature change would be the same as the change in temperature of the black aluminum specimens.

A total of 18 channels of oscillograph instrumentation were employed at Station 2300 during Shot 9 to record the desired information.

2.5.2   Station 6500

Station 6500 was the closest position to ground zero at which it was desirable to display a set of T-28 stabilizer assemblies. The construction consisted of a line of concrete bases which supported the specimens and their mounts or frames. The instrument shelter, of semi-buried, reinforced concrete design, was located at the center of, but behind the line of specimens with that portion above ground protected by earth fill. The detailed arrangement of the station, as shown in

42

Fig. 2.13, reading from left to right was:

Fig. 2.13 Display at Station 6500, Shot 9

1. A T-28 stabilizer, painted black and shielded from blast by a structural steel shelter but exposed to the thermal energy by means of the glass-paneled forward face of the enclosure. Also, inside the blast shield was a calorimeter.

2. A set of input instruments consisting of a Statham pressure gage and a calorimeter.

3. A box beam of magnesium material.

4. A tension tie of aluminum material.

5. A tension tie of magnesium material.

6. The second T-28 stabilizer, unshielded and painted gray.

7. A bonded metal waffle panel enclosed in its blast shield.

8. A camera tower to photograph item (6).

9. A box beam of aluminum material.

10. A second camera tower to photograph item (9).

11. The second set of input instruments consisting of a Consolidated pressure gage and a calorimeter.

12. A T-28 stabilizer, shielded from the thermal energy by a screen of aluminized asbestos cloth which was dropped and rolled up after the thermal phase was over but before the blast arrived.

13. A 5 ft camera tower designed to photograph, in motion, item (12).

The blast-shielded stabilizer was painted black to maximize the absorption of thermal energy which was attenuated about one-fourth by the glass panels. The unshielded stabilizer was painted a shade of gray, the reflection characteristics of which were such that the amount of thermal energy absorbed was approximately the same as that of the blast-shielded stabilizer.

Both beams and both ties were constructed of 1/8 in. thick material and were painted black in order that the temperature rise would be maximum.

43

Oscillograph instrumentation channels totaled 36 at Station 6500 during Shot 9.

2.5.3   Station 7200

Station 7200 consisted primarily of the second set of T-28 stabilizers. As at Station 6500, the construction consisted of a line of bases with the instrument shelter behind the center of the line. The design of the shelter at Station 7200, however, was different from that at Station 6500 in that it was completely above ground with a much larger earth embankment for protection.

Figure 2.14 shows the detailed arrangement; reading from

Fig. 2.14   Display at Station 7200, Shot 9

left to right there was:

1.   A T-28 stabilizer, unshielded.

2.   A set of input instruments.

3.   A bonded metal panel with free edges and inside a blast shield.

4.   A second T-28 stabilizer, inside a blast shield, which also contained a calorimeter.

5.   A bonded metal hat panel with fixed edges, enclosed in its blast shield.

6.   A set of input instruments.

7.   A T-28 stabilizer, shielded from thermal energy.

The total number of oscillograph channels used at Station 7200 during Shot 9 was 35.

2.5.4   Station 8800

The third set of T-28 stabilizers was located at Station 8800. With the exception that there were no bonded metal panels, the arrangement of the specimen and construction of Station 8800 were identical

44

to Station 7200.

Sixteen channels of data were recorded by an oscillograph at Station 8800 during Shot 9.

2.5.5 Other Shot 9 Displays

In addition to the stations where time-history data were recorded, several other locations were used to expose the remaining specimens. Bonded metal panels and their blast shields were located in groups of 2, 3, or 5 at ranges of 7400, 8400, 9400, 9700, and 10,800 ft. The B-36 wing section was positioned at the 4774 ft range; the B-36 stabilizer and elevator assembly at the 13,000 ft range. The Control Surface Covering Test Panels were situated at the 4000, 5500, 7000, and 10,000 ft ranges.

2.6 PROGRAM, SHOT 10

A schematic of the specimen and instrument arrangement for Shot 10 is shown in Fig. 2.15. Positioning was based on yield and burst height estimates of 14 KT and 500 ft above intended ground zero. Construction at the four oscillograph-instrumented stations was basically the same as for Shot 9, but many specimen mounts were reoriented in anticipation of the lowered height of burst. Some changes and additions to the original Shot 10 program were made after an evaluation of preliminary results of Shot 9.

2.6.1 Station 2300

The display at Station 2300 consisted of three box beams, three tension ties, and two sets of input instruments. The specimens can be described in pairs of one beam and one tie, because of their similar thickness, material, and absorptivity as listed below:

1. One pair was made of 3/16 in. thick aluminum material and painted black.

2. A second pair was made of 1/8 in. aluminum and painted black.

3. A third pair was made of 3/16 in. magnesium and painted gray, the same shade used for Shot 9.

The 3/16 in. thick aluminum beam was instrumented with six pairs of strain-gage thermocouple circuits. This was the main factor in the increase in number of oscillograph channels to a total of 36 for Station 2300 during Shot 10.

2.6.2 Range 3500 Feet

As a result of the lower-than-expected temperatures realized

45

Fig. 2.15 General Arrangement of Specimens and Instrument Shelters for Shot 10

46

during Shot 9, it was deemed advisable to expose an additional T-28 stabilizer to thermal energy only at a range where the desired temperatures would be attained. A range of 3500 ft was chosen, a stabilizer blast shield was moved from Station 8800 to that range, and the installation was made. To eliminate the need for an instrument shelter near the new location, a signal cable was laid between the 3500 ft range and Station 8800, and the oscillograph at that station was used to record the signals of two thermocouple circuits.

2.6.3 Station 6500

Three T-28 stabilizers, instrumented at three separate positions along the span, as opposed to the single position instrumentation of the Shot 9 stabilizers, were located at Station 6500 for Shot 10. Compared to the previous shot, mounting and shielding were similar but the preloads were almost doubled.

Input measurements were unchanged. On the base where a box beam had been mounted and photographed during Shot 9, a bonded metal hat panel with fixed edges was erected for purposes of a motion picture study of the reaction of the panel to the thermal energy. Fifty-four channels of oscillographic instrumentation were recorded during Shot 10 at Station 6500.

2.6.4 Station 7200

Three bonded metal panels, two of the "hat" type and one honeycomb core, and two sets of input instruments comprised the display at Station 7200 for Shot 10. The panels were instrumented with thermocouples which accounted for most of the 18 channels of data recorded at this station during Shot 10.

2.6.5 Station 8800

Two sets of input measurements were made at Station 8800. These, in addition to the two channels of data from the T-28 stabilizer at the 3500 ft range, made a total of six channels of instrumentation recorded at this station during Shot 10.

2.6.6 Other Shot 10 Displays

Bonded metal panels in their blast shields were located in groups of 2, 3, or 5, at ranges of 4000, 4250, 4400, 4800, and 5450 ft. The B-36 stabilizer and elevator assembly was placed at a range of 5300 ft. The Control Surface Covering Test Panels were positioned at ranges of 5500, 6000, 6500, and 7000 ft.

2.7 PROGRAM, SHOTS 3, 5, 6, AND 7

During Shot 5, three specimens of rubber tire material were exposed at ranges of 1180, 1650, and 2320 ft to aid in the determination of optimum exposure levels for the main body of components. During Shot 7, four pairs of panels on which the components were mounted were located at ranges of 1920, 2300, 3460, and 5000 ft.

During Shots 3, 5, and 6, various panels of glass and "Plexiglas" were exposed to obtain preliminary information on their thermal and blast resistance. The panels were mounted as the front surface of blast shields just as they would be used later with bonded metal panels and T-28 stabilizers. Also exposed at this time were several samples of the asbestos cloth used later as the stabilizer thermal shield.

CHAPTER 3

RESULTS

3.1 GENERAL

A summary of the results of the specimen response measurements obtained by Project 8.1a participation in six shots of the UPSHOT-KNOTHOLE series of nuclear explosions are presented in this chapter in the form of reduced oscillograph data, readings of peak temperature recording devices, photographs, and visual inspection data. Detailed results of the response measurements are included in Appendices B, C, D, and F; complete results of the input measurements made by Project 8.1a are presented in Appendix E. The general test conditions under which the data were obtained are given in Table 3.1.

The instrumentation equipment, including oscillographs, bridge balances, relay switching units, and blue boxes, operated satisfactorily. Of the total of 220 channels of oscillographic instrumentation during Shots 9 and 10, 212 channels produced usable data. The remaining 8 channels failed for various reasons, which included the breakage of thermocouple wire (2 channels), separation of the strain gage bond (2 channels), warping of pressure gage diaphragm (2 channels), breakage of strain gage lead wire (1 channel), and failure of one thermocouple channel for unknown reasons. In addition to the two strain gage bond failures mentioned above, the bond of one spare (unused) gage separated, making a total of 3 bond failures among the 161 strain gages installed on exposed specimens.

Of the 13 oscillograph rolls exposed, 11 produced excellent records. The two rolls at Station 2300 during Shot 10 were severely fogged by gamma radiation, but all channels were readable, using strong background lighting. The four instrument shelters used were very satisfactory and, because of their rugged, enclosed design, undoubtedly contributed largely to the success of the instrumentation effort. The effects of the electromagnetic interference that existed for

TABLE 3.1 - Test Conditions of Shots Participated in by Project 8.1

	Shot 3	Shot 5	Shot 6	Shot 7	Shot 9	Shot 10
Date	31 Mar	18 Apr	11 Apr	25 Apr	8 May	25 May
Time (GMT)	1259:59.995	1234:59.958	1244:59.781	1229:59.763	1529:55.362	1530:00.332
Location (Area)	T-7-5a	T-2	T-4a	T-1	FF	FF
Rad Chem Yield (KT)	0.20	23	0.22	43.4	26	14.9
Code Name	Ruth	Badger	Ray	Simon	Encore	Grable
Height of Burst (ft)	300 Tower	300 Tower	100 Tower	300 Tower	2423 Air	524 Air
Height of Burst (ft) (Scaled to 1 KT at Sea Level)	476	100	157	81	763	204
Ground Zero-Relative to Aiming Point (ft)					837 S 15 W	139 S 86 W
Atmospheric Pressure (mb)						
Ground Zero	873	862	869	870	900	901
Burst Height	863	852	866	860	825	884
Air Temperature (Degree F)						
Ground Zero	39.9	45.9	31.5	53.1	62.0	58.6
Burst Height	46.8	45.0	31.8	59.5	46.4	55.6
Relative Humidity (%)						
Ground Zero	48	40	43	26	19	32
Burst Height	32	39	40	26	23	23
Surface Wind - Direction and Velocity (knots)	360 04	360 09	045 05	340 05	190 05	360 04
Atmospheric Transmission (%/mi)	95.0	95.7	95.0	95.7	92.5	91.0

a few microseconds at the time of detonation were noticeable on the records made at Station 2300, and were violent on the channel recorded at Station 8800 with a signal cable extending to the range of 3600 ft during Shot 10, but caused no failure.

3.2 BOX BEAMS AND TENSION TIES

Eight box beams and eight tension ties were exposed during Shots 9 and 10. Three of the tension ties were stressed beyond the yield strength, as evidenced by permanent elongation, but none of the ties failed completely. There was no evidence of structural damage to the box beams, although the paint on some of the specimens were scorched.

Maximum temperatures of the tension ties and of the front faces of the box beams ranged from $173^{\circ}F$ to $404^{\circ}F$ during Shot 9 and from $323^{\circ}F$ to $591^{\circ}F$ during Shot 10, thus bracketing the desired $400^{\circ}F$ temperature rise.

Forty-two channels of strain gage and thermocouple instrumentation produced usable data. A typical pain of strain and temperature time-histories for box beams is shown in Fig. 3.1. A similar pair of measurements for tension ties is shown in Fig. 3.2. The complete set of data is presented in Appendix B.

3.3 HORIZONTAL STABILIZER ASSEMBLIES (T-28)

A total of thirteen T-28 horizontal stabilizer assemblies were exposed during Shots 9 and 10. Of this number, five were exposed to thermal but shielded from blast, four were exposed to blast but shielded from thermal, and the remaining four were exposed to both thermal and blast. All eight stabilizers of the last two groups, that is, all those exposed to blast were damaged beyond economical repair since permanent set occurred due to buckling of the rear spar web. For all practical purposes, the stabilizers exposed to thermal energy only were undamaged, with the one exception of the stabilizers at the range of 3500 ft during Shot 10. It was difficult to determine, by visual inspection, any appreciable difference in damage to two stabilizers, one of which was exposed to blast only and the other exposed to both thermal and blast. This was true at all three ranges. The heavy thermal damage inflicted on the stabilizer in the blast shield at the range of 3500 ft, where the inputs were 34.5 cal/sq cm and 5.8 psi, is shown in Fig. 3.3. Figure 3.4 shows the damage that was sustained by the three stabilizers located at Station 6500 during Shot 9 where the inputs were 14.8 cal/sq cm and 4.1 psi. A total of 83 channels of instrumentation produced usable time-history data on the stabilizers. Typical strain and temperature time-histories of a stabilizer rear spar are shown in Fig. 3.5, and similar measurements of an irradiated skin panel are shown in Fig. 3.6. The complete set of data for stabilizers is presented in Appendix C.

51
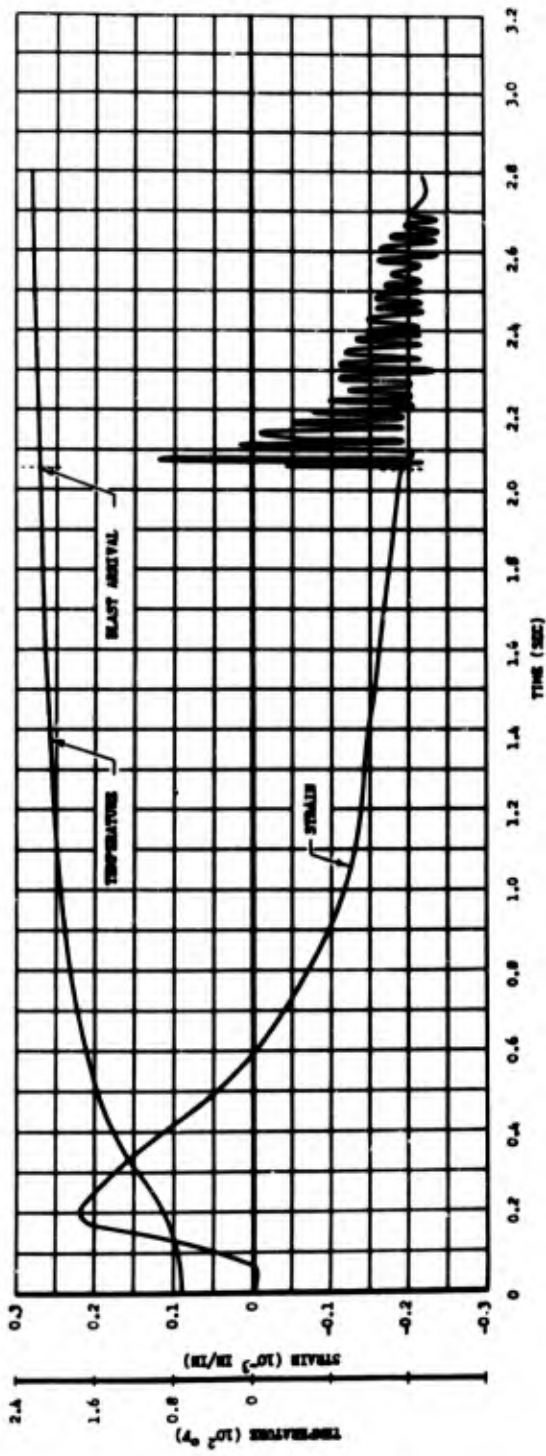
Fig. 3.1 Typical Box Beam Time-Histories of Strain and Temperature
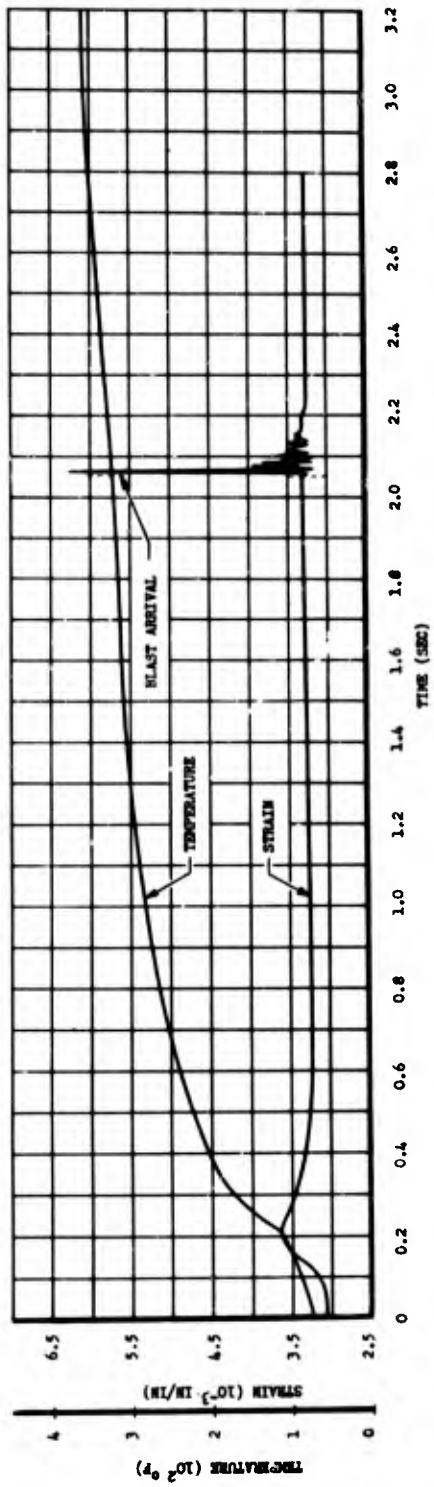
Fig. 3.2 Typical Tension Tie Time-Histories of Strain and Temperature

52

Fig. 3.3 Thermal Damage To
Stabilizer at Range
3500, Shot 10
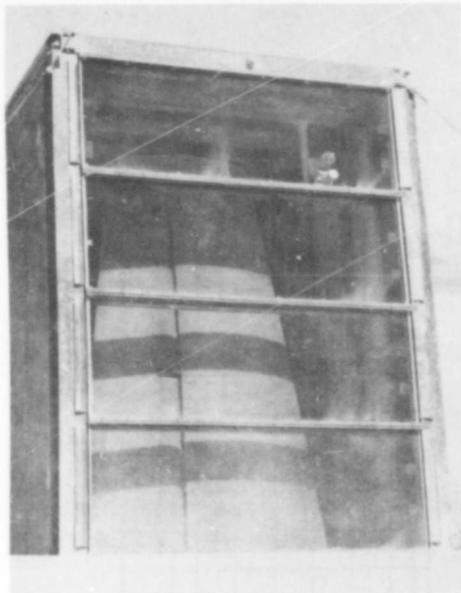
Fig. 3.4a Stabilizer Shield From
Blast Station 6500,
Shot 9

Fig. 3.4b Stabilizer Unshielded
Station 6500, Shot 9

Fig. 3.4c Stabilizer Shielded
From Thermal Station
6500, Shot 9

53
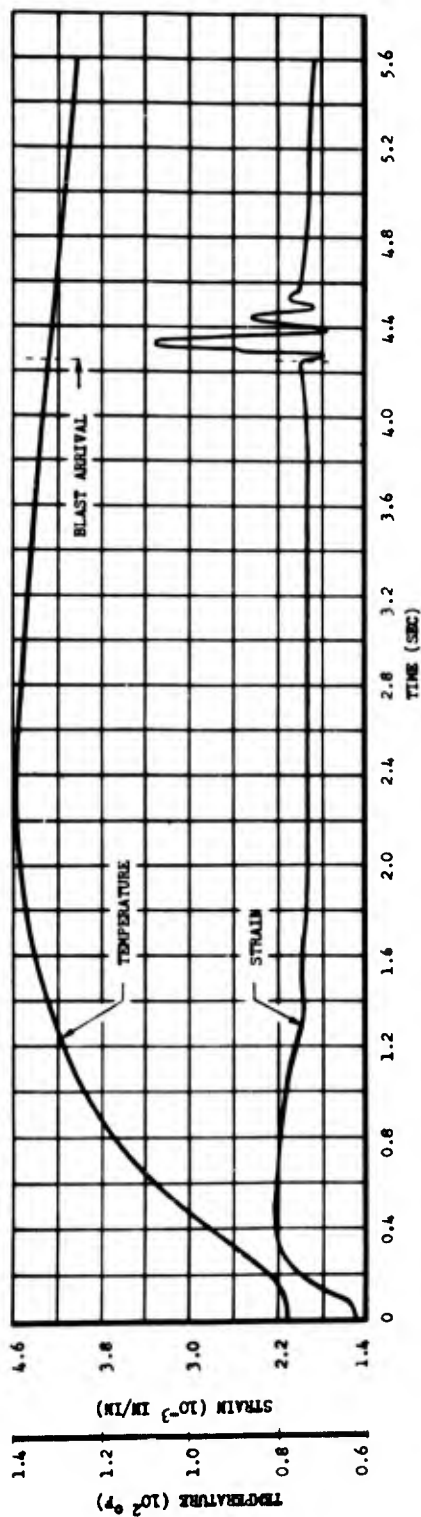
Fig. 3.5 Typical Stabilizer Rear Spar Time-Histories of Strain and Temperature
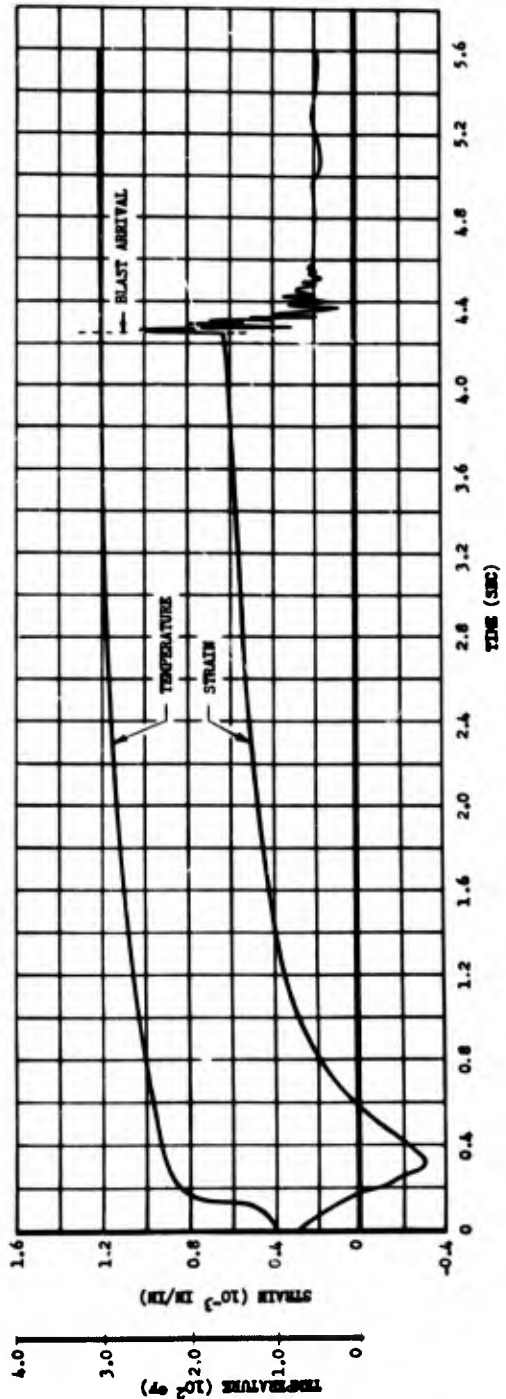
Fig. 3.6 Typical Stabilizer Skin Panel Time-Histories of Strain and Temperature

54

Good motion pictures showing the effects of the thermal and blast inputs on the stabilizers and the operation of the thermal shield were obtained. The operation of all blast and thermal shields and all mounting and loading frames was satisfactory.

3.4 MISCELLANEOUS SPECIMENS

A total of 36 bonded metal aircraft panels of three types, hat, waffle, and honeycomb core, were exposed during Shots 9 and 10. For each type of panel, a range of damage from negligible to severe was obtained. Bond release was apparent on at least one of each type panel.

Seven waffle panels were exposed. An example of damage to this type panel is shown in Fig. 3.7. Panel No. 5 sustained a maximum
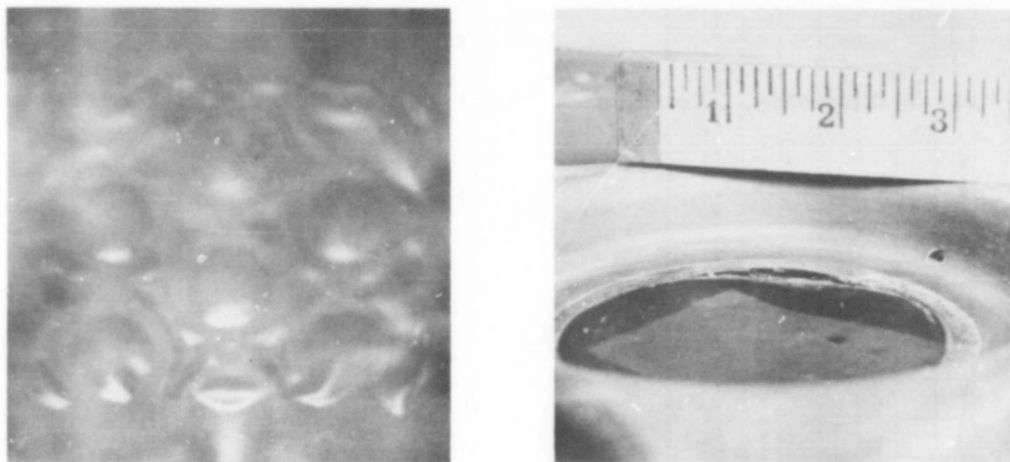
Fig. 3.7 Typical Damage to Waffle Panel

depth of buckle of 1/4 in. and a skin temperature rise of between 420°F and 514°F. Bond release occurred at four places, two on the doublers and two on the waffle stiffeners. Twelve time-histories of strain and temperature measurements of two waffle panels were obtained; these and all other data pertaining to bonded metal aircraft panels are presented in Appendix D.

Twenty-four hat panels were exposed. Figure 3.8 shows the damage inflicted on one of each of the four hat panel configurations tested. These four panels were located at Range 4800 during Shot 10. The two panels with 0.020 in. skin and free edges, the one completely and the other partially irradiated, were subjected to temperature rises between 430°F and 524°F, whereas the temperatures of the two panels with 0.025 in. skin, one with free edges and the other with fixed edges, were raised between 378°F and 404°F. On all four panels the maximum

55
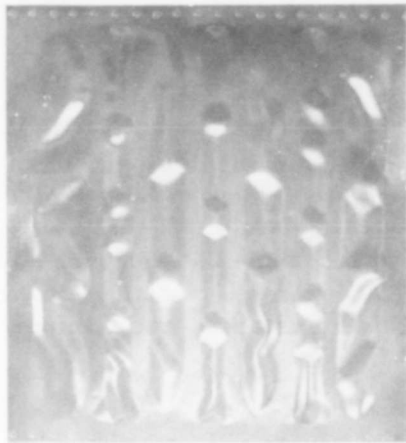
(a) 0.020" Skin, Free Edges
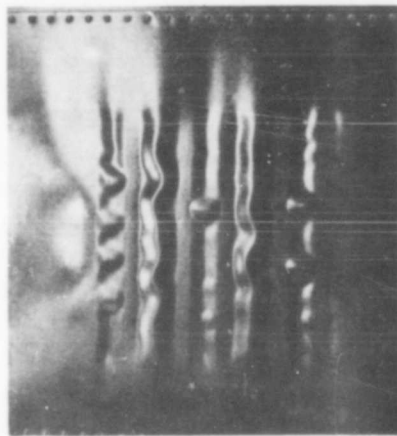
(b) 0.020" Skin, Partially Irradiated

(c) 0.025" Skin, Free Edges
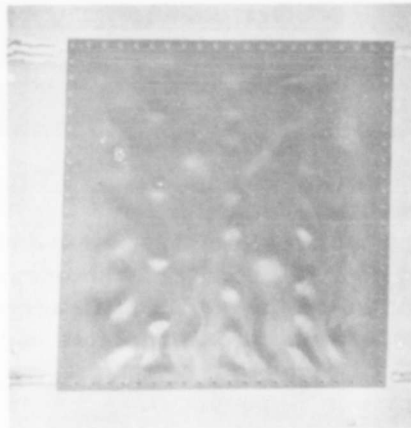
(d) 0.025" Skin Fixed Edges

Fig. 3.8 Damage of One Set of Hat Panels

depth of buckle was about 7/64 in.; however, no bond release was apparent on any of these four panels. At a higher thermal flux, two other hat panels with 0.025 in. skin experienced bond release when subjected to peak temperatures greater than 635°F. Fourteen channels of time-history strain and temperature data were obtained from three hat panels.

Five honeycomb core panels were exposed. The damage shown in Fig. 3.9 is representative of the reaction of honeycomb core panels
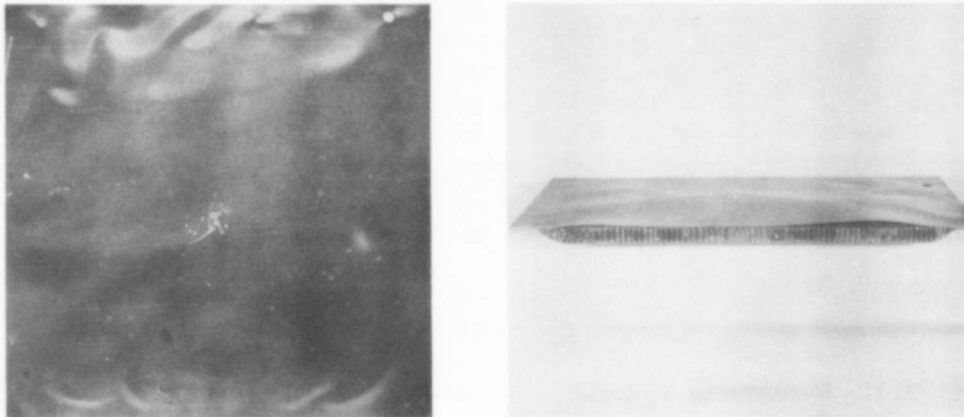
Fig. 3.9 Typical Damage to Honeycomb Core Panel

to the thermal input. The panel shown was No. 32 which was exposed during Shot 10 at a range of 4000 ft, where the total thermal energy incident normal to the panel was 18.5 cal/sq cm. For this type panel, bond release occurred at temperatures as low as 300°F. Two time-history temperature measurements were obtained from one panel.

The B-36 horizontal stabilizer and elevator assembly suffered very light damage during Shot 9 at a range of 13,585 ft, where the inputs were 3.3 cal/sq cm and 1.2 psi. During Shot 10 at a range of 5350 ft with inputs of 14.4 cal/sq cm and 3.2 psi, the assembly was damaged beyond economical repair. There was evidence of damage due to both thermal and blast inputs with the skin scorched and buckled, ribs and bulkheads crushed, and access doors opened and blown away.

The B-36 wing section, exposed during Shot 9 at input levels of 23 cal/sq cm and 5.7 psi, was very heavily damaged. Temp-tape data indicated that temperatures as high as 635°F were realized on skin panels. Thin aluminum and magnesium skins were scorched, and the adhesive bond between the hat stiffeners and the skin failed. Thicker skin was dished in between supporting stringers and ribs, bulkheads were crushed, and spar webs were buckled. In Appendix D of this

57

report are presented complete data, including photographs, of the two B-36 components.

A total of 213 test panels representing various control surface coverings were exposed during Shots 9 and 10 and were damaged within the range of negligible effect to complete destruction. Figure 3.10 shows the damage inflicted on a typical specimen. This panel of type "G" (see Table D.3a) was covered with cotton cloth treated with two brush coats of clear dope, four spray coats of aluminizing dope, and one coat of white enamel. It was exposed during Shot 10 at Range 7000 ft, where the thermal input level was 8.4 cal/sq cm. Details of the thermal damage sustained by each type of panel tested are given in Appendix D.

Fig. 3.10 Damage to Typical
Control Surface
Covering Panel

Three samples of rubber tire tread stock were exposed during Shot 5, and four pairs of panels displaying aircraft undercarriage components were exposed during Shot 7. An analysis of the results of the tread sample exposure was used to determine the position of the eight panels. For all types of components including tires, wheels, actuators, and related equipment, a range of damage from minor to severe was obtained. Detailed results of the exposure of the undercarriage components are given in Appendix D.

CHAPTER 4

DISCUSSION

4.1 GENERAL

The discussion material presented in this chapter is general in nature and is designed to acquaint the reader with significant aspects of the various data obtained. More detailed discussions appear in the sections which treat related specimens individually. The latter, more comprehensive discussions, are intended primarily to explain certain peculiarities of the data and the effect of employing special techniques and procedures and to present obvious data re-groupings that will facilitate evaluation and future analysis. In the application of the data it should be remembered that the results are specific in themselves, in that they were obtained from particular specimens exposed with definite orientations to certain inputs. Extrapolations, while entirely feasible, should not be undertaken until the conditions under which these data were obtained are thoroughly understood.

One unpredictable deviation from the program as planned for Shot 9 was the reduced input that resulted from the difference between intended and actual air zeros and from the lower-than-expected yield. Although the energy levels at the specimen locations were lower than planned, the data obtained should be useful in view of the compensating changes made in the Shot 10 program. These changes consisted of replacing one box beam and one tension tie by thinner specimens and of placing one additional blast-shielded T-28 stabilizer at a range of relatively high thermal energy.

The composite oscillographic instrumentation data are subject to different accuracy limitations dependent upon the particular type of measurement; hence, an unqualified statement as to over-all accuracy could be misleading. In the data obtained, for the least accurate measurement (strain measurements appreciably influenced by thermal effects), it was mathematically possible to realize errors up to 12.5

per cent; however, the majority of the data is believed to be accurate within 5 per cent. An estimation of errors involved in each type of measurement is presented in Appendix A of this report and are summarized in Table A.2. It is recommended that the values presented in the above table be employed to evaluate the accuracy of particular measurements. In general, input measurements and temperature data were more accurate than strain measurements.

The bakelite temperature-compensated strain gages used by Project 8.1a, although believed to be the best choice of available strain gages for the intended purpose, do not represent the ultimate in strain sensing devices where transient heating is a factor. In every respect the gages performed satisfactorily according to the manufacturers specifications, but the rapid temperature rises encountered by the test specimens produced large temperature gradients between the metal specimens and the strain sensing elements. The lag in response of the temperature-compensated strain gage was determined experimentally by a limited number of calibration plates exposed during Shots 9 and 10 and from additional data obtained in the laboratory.

4.2 BOX BEAMS AND TENSION TIES

Valid and meaningful thermoelastic response data were obtained from the exposure of the box beams and tension ties during the two shots on Frenchman Flat. Comparison of strain-temperature data from the two shots is complicated in that the thermal inputs were dissimilar because of the dust attenuation during the latter portion of the Shot 10 thermal phase. Higher peak temperatures, especially on the thicker aluminum tension ties, would have been desirable although temperatures sufficiently high to cause aluminum and magnesium ties to be stressed beyond the yield point were attained. Crossplots of the data, presented in Appendix B, show the data to be consistent and similar to that which would be expected from theoretical considerations. It is believed, therefore, that the thermoelastic data obtained are representative of the response of these specimens to unilateral heating of the type experienced in these tests.

Of particular interest was the strain developed in both the box beams and tension ties as a result of the temperature gradient that existed between the irradiated and nonirradiated surfaces during the early portion of the heating cycle. The magnitude of the temperature gradient is not known; however, thermocouples located on the nonirradiated side of a 3/16 in. thick face indicated a lag time of approximately 0.1 sec between time zero and initial thermal response. The temperature difference between the two faces at this time was undoubtedly considerable. As a result, the hotter side tended to expand, placing this portion in compression, which in turn caused a tensile stress to be developed on the cooler side where the strain gage was located. The net result

60

in both the box beam and tension tie strain measurements was for the strain gage to indicate a fictitious (i.e., not representative of the net effective) positive strain until the temperature gradient became negligible. This phenomenon is discussed in greater detail in Appendix B. Since blast response was not desired in tension tie strain data, blast effects were not reported. Certain of the box beam strain-time data include the blast response. The reaction of the box beam was such that the effect of blast can be readily eliminated by fairing the curve presented.

4.3 HORIZONTAL STABILIZER AND ELEVATOR ASSEMBLY (T-28)

The T-28 horizontal stabilizer elevator assemblies were exposed for the purpose of studying the interaction of the thermal and blast forcing functions both from the standpoint of physical damage production, as well as from the magnitude and nature of loads induced under the various exposure conditions. As mentioned in the results presentation, the actual inputs realized were such that the thermal coupling was too low to cause a marked difference in physical damage between irradiated and nonirradiated specimens. Nevertheless, the time-history strain and temperature data show the measured effects produced by the individual and combined thermal and blast inputs and, when thoroughly analyzed, should provide a better understanding of the phenomenon of thermal/blast coupling, as well as to provide accurate response data for the condition of isolated thermal and blast inputs.

The effect of exposing a stressed structure to reasonably high thermal inputs alone was demonstrated in Shot 10, wherein thermal weakening was sufficient to allow the preload to cause permanent deformation of the structure. If inputs had been as high as anticipated, a greater spread of coupling data would have been obtained. Certain of the strain gages responded to the thermal input in a manner analogous to that described for the box beams and tension ties above. A peculiarity common to all rear spar strain measurements (Station 24.75) made on stabilizers exposed to blast was the occurrence of a momentary decrease in strain at shock arrival followed by a large increase in strain. This phenomenon is probably caused by the influence of the higher modes of vibration prevalent at blast arrival. The above phenomena plus other pertinent characteristics of the data are discussed in detail in Appendix C.

4.4 MISCELLANEOUS SPECIMENS

From the visual inpection and peak temperature data of the bonded metal aircraft panels, the following observations were made. Two different types of buckles, differing in size and in initiating temperature, occurred to both hat and waffle panels. With an ambient

61

temperature of about 100°F, temperature rises at the start of permanent buckling were lowest (50°F) for fixed edge hat panels, higher (100°F) for free edge hat and honeycomb core panels, and highest (200°F) for waffle panels. However, at skin temperature rises of 450°F for all types of panels, the depth of buckle was greatest for waffle panels, less for hat panels, and least for honeycomb core panels. The ratios of panel weights were:

Type	Relative Weight
Waffle	1.00
Hat, 0.020	1.40
Hat, 0.025	1.53
Honeycomb	1.59

The change in the skin thickness of hat panels from 0.020 in. to 0.025 in. had little effect on the depth of buckle. Fixed edges and partial irradiation of hat panels caused appreciable increases in the depth of buckle. The attachment of large area bonds was affected at lower temperatures than that of small area bonds. Bond release initiation temperatures were highest for hat panels, lower for waffle panels, and lowest for honeycomb core panels. Detailed discussion of the above statements and a presentation and discussion of normalized temperature distribution curves are presented in Appendix D.

The B-36 stabilizer assembly was essentially undamaged by 1.2 psi overpressure under the conditions tested, whereas an overpressure of 3.2 psi caused damage beyond economical repair. Therefore, the threshold of critical damage of the test configuration was between 1.2 and 3.2 psi overpressure; however, in applying this result to a complete B-36, the effects of the different mounting of the assembly (the jig-type full span support used by Project 8.1a compared to the cantilever attachment to a fuselage of some flexibility) should be considered. A similar observation can be made concerning the mounting of the B-36 wing section, which besides obtaining thermal and local overpressure damage data, provided an excellent example of the varying degrees of damage of the light construction aft of the rear spar compared to the heavier construction of the wing box.

The results of the tests of control surface covering panels indicated that fabric-covered panels, although their resistance to the thermal input was increased by white enamel, were without exception more vulnerable than metal foil-covered panels. Curves of damage as a function of thermal inputs for various panels are presented in Appendix D.

For the aircraft undercarriage components a satisfactory range of thermal damage was obtained. The correlation of this damage with

62

thermal energy incident to the specimens was subject to possible large inaccuracies due to the large amount of dust and smoke surrounding the panels and to the lack of time-history instrumentation. This problem is disucssed in Appendix D.

4.5   INPUTS

The time-histories of total thermal energy and overpressure inputs for both Shots 9 and 10 were measured at the four primary locations of Project 8.1a. Usable data were obtained from 19 thermal energy channels and from 14 overpressure channels; curves drawn through the plotted points agree relatively well with blast line data. The thermal energies measured along the 8.1 line at a height of about 5 ft above the ground between limits of 5 and 55 cal/sq cm were consistently lower than blast line data, the difference increasing with the higher values of thermal energy. The thermal energies measured along the Project 8.1a line ranged from 5 to 55 cal/sq cm and agreed very well with the finalized NRDL data. The thermal energies measured inside the blast shields indicated, for a given range, an incident energy level of about three-fourths the value outside the shield.

The overpressure measurements made along the 8.1 line during Shot 9 between limits of 2 and 12 psi, bracketed the blast line data, whereas the readings for Shot 10, between 1 and 10 psi, were slightly higher than the blast line measurements. Diaphragm type pressure gages used at Station 2300, although shielded from direct thermal radiation, were seriously affected during the thermal phase, probably by heated air. The effect was detectable but negligible at Station 6500. Orifice type pressure gages at the same locations were apparently unaffected. The responses of the two types of gages to the blast phase were very similar.

Gamma radiation measurements, made with "cigarette case" dosimeters, indicated, in general, very good attenuation of the radiation by the instrument shelters. The incident radiation level during Shot 10 at Station 2300 was greater than anticipated by a factor of more than two and resulted in very dark but readable oscillograph records.

4.6   SPECIAL EQUIPMENT AND TECHNIQUES

Panels of glass exposed during Shots 3, 5, and 6 on a trail basis and used as the front faces of blast shields during Shots 9 and 10 had the strength required to withstand the blast phase and sufficiently good transmission characteristics to make practical their use in exposing a specimen to thermal radiation while shielding it from blast. Time-history instrumentation established the thermal transmission of 3/4 in. thick glass as about 75 per cent. No breakage occurred as a result of the blast input, but two panels were broken by debris missiles.

63

The use of a special, silicone-base paint for absorptivity control was, in general, satisfactory but several disadvantages were experienced. The solubility of the paint in acetone and other common cleaning solutions made difficult the cleaning of a painted surface, which, at the same time, was highly vulnerable to scratches.

Discoloration, scorching, and blistering of the paint occurred on some of the specimens. These effects appeared to be a function, not only of the peak temperature attained by the specimen, but also of the energy level of the incident thermal radiation. In some instances gray paint turned dark during irradiation, thus changing the absorptivity. These points are discussed in greater detail in Appendix F.

CHAPTER 5

CONCLUSIONS AND RECOMMENDATIONS

5.1 CONCLUSIONS

It is concluded that:

1. Sufficient data were obtained to afford a reasonably complete analysis of the "Coupling Study Utilizing T-28 Stabilizer and Elevator Assemblies" and of the "Thermoelastic Studies Utilizing Box Beams and Tension Ties."

2. The thermal energies at the T-28 stabilizer exposure sites were, in general, too low to cause a significant difference in damage between irradiated and nonirradiated stabilizers.

3. Bonded metal waffle panels are less vulnerable to permanent skin buckling than bonded metal hat panels for temperature rises less than $350^\circ F$.

4. The threshold of permanent skin buckling for bonded metal fixed edge hat panels is as little as about $50^\circ F$ temperature rise.

5. Failure of the adhesive bond of bonded metal honeycomb core panels occurs at temperatures as low as $300^\circ F$ ($\triangle t = 188^\circ F$).

6. The threshold of critical overpressure damage for the B-36 stabilizer and elevator assembly lies between 1.2 and 3.2 psi.

7. Serious thermal damage of the B-36 wing section results from exposure to 23.1 cal/sq cm.

8. Fabric covered control surfaces can be processed to withstand thermal energies up to 10 cal/sq cm without apparent damage, whereas foil covered surfaces, although only slightly more thermal resistant at the low damage level, appear to be capable of withstanding thermal inputs up to twice that of the fabric coverings before critical damage is encountered.

9. Glass panels are suitable material for the blast shielding of test specimens at input levels of 6.6 psi and 54 cal/sq cm, and 6.2 psi and 29.6 cal/sq cm, respectively, for 3/8 in. x 20 in. x 20 in. and

65

7/8 in. x 24 in. x 66 in. panels.

10. The buried and semi-buried instrumentation shelters are satisfactory.

5.2 RECOMMENDATIONS

It is recommended that:

1. The data presented in this report be further processed for application to current vulnerability problems and for the establishment or modification of design criteria.

2. Buried or semi-buried instrumentation shelters be used in future test programs.

3. Efforts be continued to develop a high-temperature strain gage and adhesive.

4. The use of glass panels to isolate thermal inputs from blast inputs be studied further.

5. Control of absorptivity be studied further.

APPENDIX A

INSTRUMENTATION

A.1 GENERAL

Instrumentation of Project 8.1a test specimens consisted of three types: time-history, peak temperature, and photographic. The time-history instrumentation employed sensing elements to convert physical phenomena into electrical signals and oscillographs to make a permanent record of the variations of the phenomena with time. The quantities measured were the unit elongation and temperature of metal specimens and overpressure and total thermal energy inputs. Peak temperature instrumentation made use of temp-tapes attached to metal specimens to indicate the maximum temperature to which the metal was raised. Photographic instrumentation consisted of motion picture cameras trained on certain specimens to record their response to the thermal and blast phases.

A.2 TIME-HISTORY RECORDING EQUIPMENT

The basic recording instrument used was the Consolidated Engineering's 18-channel recording oscillograph, type 5-114 P-3, of which six were used during Shot 9 and seven during Shot 10.

The following is a brief summary of the more important features of the type 5-114 P-3 oscillograph:

Active data channels . . . . . . 18, plus 1 dynamic reference
Power . . . . 26 volts d.c.
Paper width . . . . 7 in.
Paper length used . . . . . . 125 ft
Record speed used . . . . . . 28.8 in./sec
Approximate maximum
   recording time . . . . 45 sec
Time base indication . . . . . lines every 0.01 sec

Each oscillograph generates its own time base which is recorded on the photo-sensitive paper every 0.01 of a second; however, if the time-history data from two or more oscillographs are to be compared and analyzed in conjunction with each other, it is necessary that a time base calibration be established for each instrument. The calibrations were obtained by recording a 60 cycle power line frequency simultaneously in each of the seven oscillographs for a period of slightly over 10 sec. The exact frequency at the time of recording was obtained from the power company, and thus by counting cycles, a true 10 sec time interval was established. The time base lines generated during this true 10 sec interval were counted and correction factors were determined for each oscillograph. All time-history data presented in this report have been corrected with their respective time correction factors.

A. 2. 1   Auxiliary Equipment

Strain and overpressure quantities were measured with variable resistance type sensing elements requiring a bridge balance unit which supplied the excitation voltage, provided a means of balancing the bridge circuit, and incorporated a method of adjusting the output resistance of the circuit to a value which would provide critical damping of the galvanometer in the oscillograph.

The measurements of temperature and total thermal energy were made with thermocouple sensing elements which required only attenuating and damping resistors as auxiliary equipment. The purpose of these resistors was to attenuate the thermocouple output and to provide critical damping of the galvanometer in the oscillograph.

Since the oscillographs were required to operate remotely during the test, a relay switching unit was designed to incorporate the following features:

1. Accept the timing signals from the Test Control Point and convert them into the closing of relays to warm up the equipment, start the oscillographs just before detonation, and keep them running until after their paper supply was exhausted.

2. Provide interlocking circuits so that instantaneous opening of any relay by the blast or ground shock would not inadvertently stop the operation of the equipment.

Six 24-volt aircraft batteries supplied the power for each station during the tests. These batteries were continously augmented with a selenium rectifier during preshot checks and calibrations. The rectifier was automatically disconnected by the -5 sec timing signal. The batteries were kept in a charged condition by conventional tungar bulb battery chargers. Two 12 volt batteries in parallel supplied the

68

bridge voltage for all strain gage channels and pressure transducers at each station, completely independent of all other circuits.

To facilitate the plotting of time-history data as a function of time after detonation, the exact instant of detonation was recorded on the dynamic reference trace on each oscillograph record. This was accomplished by a photocell-triggered circuit (E. G. & G. Blue Box, MK III), sensitive to a high rate of change of light intensity, which produced an electrical impulse at time zero. In order to minimize blast damage, the blue box proper was installed inside the instrument shelter and the phototube was removed and mounted in a conduit box outside the shelter. A typical installation of the conduit box with phototube inside is shown in Fig. A.1.

Fig. A.1 Typical Phototube Installation for Blue Box

A.2.2   Sensing Elements

The sensing elements used included strain gages, thermocouples, pressure transducers, and calorimeters.

A.2.2.1   Strain Gages

Where time-history deformations of certain specimens were required, resistance-type strain gages were employed to measure time-history unit elongations at various locations on the specimens. Baldwin temperature-compensated strain gages, type EBDF-13D, EBDF-7D, and EBDFR-13D, were used for this purpose and were bonded to the specimen by use of a suitable adhesive. These gages have a compensating characteristic which corrects for the strain caused by gradual temperature rises but not entirely for rapid temperature rises. The correction for strain produced by rapid temperature rises is discussed in para. A.2.3.1. Although this type of gage has certain limitations, including its response to transients, it was selected for use at all strain installations as the best available for the intended purpose. This gage was selected also because of its negligible transverse sensitivity, i.e., the gage indicates strain parallel to the major axis of the gage only. In several cases, where biaxial strains were of interest, equiangular rosette type gages were installed. All strain gages installed were capable of responding to true strain to within plus or minus 1 per cent.

All gages were of the bakelite type in order to resist

substantially the peak temperatures which would be encountered. For installations which would experience peak temperatures greater than 250°F, the gages were bonded to the test specimen with a phenolic resin adhesive ("Bakelite Cement", Bakelite Corporation of America). At some locations, where the peak temperatures would not exceed 250°F, an epon resin adhesive (Type A-2, Armstrong Products Co.) was used as the bonding agent. Both types of adhesive proved to be entirely satisfactory.

In general, a strain gage indicates all elongations of the specimen on which it is mounted, including expansion due to temperature rise which must be compensated for in order to obtain strain measurements which are proportional to the actual stress in the material. The usual method of compensation for strain caused by thermal expansion consists of a duplicate strain gage installation on similar material free to expand, coupled electrically with the strain gage on the specimen to give a true strain measurement; however, this method could not be employed during these tests because of difficulty in obtaining comparable temperature-time responses at both strain gage installations.

A. 2. 2. 2   Thermocouples

All time-history temperature measurements were made using copper-constantan thermocouples as the sensing elements. Wires of 0.005 in. diameter were used in order to prevent excessive heat conduction away from thin specimens and to minimize the thermal lag between the specimen and thermocouple junction. Laboratory tests, conducted prior to thermocouple installation, revealed that the thermal lag of the junction was negligible during rapid temperature rises such as would be encountered by the specimens when exposed to thermal radiation from a nuclear explosion.

The thermocouple wires were attached to the specimen separately, about 1/8 in. apart, by a special capacitance discharge welding technique which is described in detail in Capacitance Welding Technique for the Installation of Thermocouples, WADCTR 53-289.

A. 2. 2. 3   Pressure Transducers

The pressure transducers selected for the measurement of overpressure at each of the stations were the Statham Scientific Instruments Model P6, orifice type, and the CEC's (Consolidated Engineering Corporation's) Model 4-310, diaphragm type, which employed temperature-compensated, four active arm and two active arms strain gages, respectively, for their sensing elements. Selection of these transducers was based on their signal output, which required no

amplification, and on their availability. Because of the different type transducers (orifice and diaphragm type), one of each type was placed at each station in order to draw comparison between them, as well as to measure the blast overpressure. Both types of transducers were available in various pressure ranges. A list of the pressure ranges and natural frequencies of the transducers used is given in Table A.1, appearing at the end of this appendix. The frequency response of a complete pressure gage circuit was limited by the galvanometer used which was specified to have a flat ($\pm 5\%$) amplitude response in the range of from 0 to 90 cycles/sec.

The Statham P6 transducer was a differential pressure gage which had an orifice approximately 1/4 in. in diameter. The reference pressure nipple in the rear was removed and the hole was plugged with a screw which permitted sufficient leakage to allow for the gradual variations of atmospheric pressure.

The CEC 4-310 pressure transducer was a differential pressure instrument which had a diaphragm approximately 1/2 in. in diameter and was adaptable to flush-mounting. This transducer had been on the market only a short time when the decision was made to use it on UPSHOT-KNOTHOLE; however, the value of a comparison between orifice and diaphragm type transducers was considered to outweigh the fact that it was a new instrument.

A.2.2.4   Calorimeters

The calorimeters used for total thermal energy measurements were obtained from the Naval Radiological Defense Laboratory (NRDL), by whom the calorimeters were designed and manufactured. This particular type of calorimeter was chosen because it had been proven reliable on other operations of this nature, because it consists of a simple thermocouple circuit which required no auxiliary equipment, and also because it is easy to install, maintain, and operate.

The calorimeter sensing element is a black circular disc of known emissivity, conductivity, and heat capacity with a thermocouple fastened to the rear surface. At the rear of the calorimeter are two large solid copper blocks which form the cold-junctions of the thermocouple. The disc, thermocouple, and cold-junction blocks are encased in a cadmium plated steel cylinder and wired as shown schematically in Fig. A.2. The front of the calorimeter is a quartz window, having a thermal transmissibility of 92 per cent. The aperture of the case was designed to afford the instrument a 90° field of view. The calorimeters were mounted on welded, steel pipe supports approximately 5 ft above the ground, as displayed in Fig. A.2, and were positioned such that the disc was normal to the line from the instrument to the intended burst point.

71
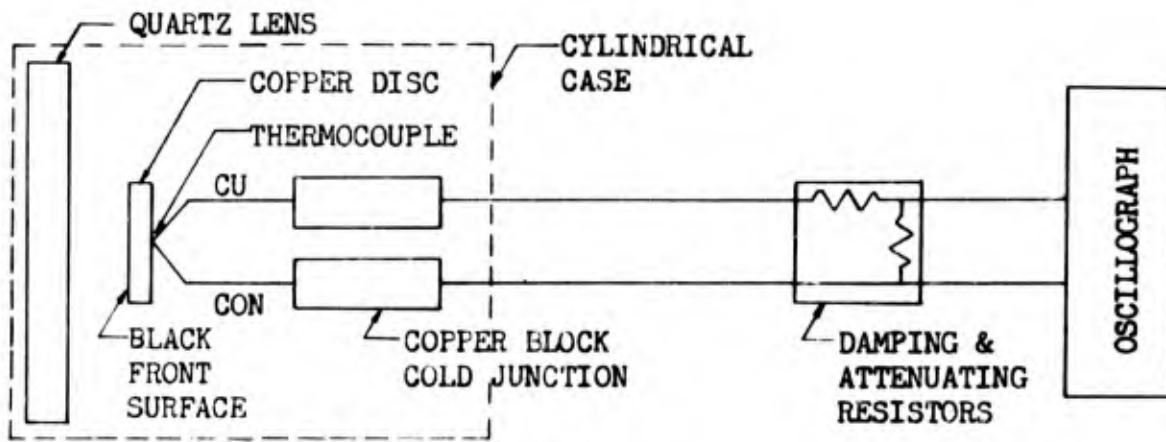
SCHEMATIC OF
CALORIMETER CIRCUIT
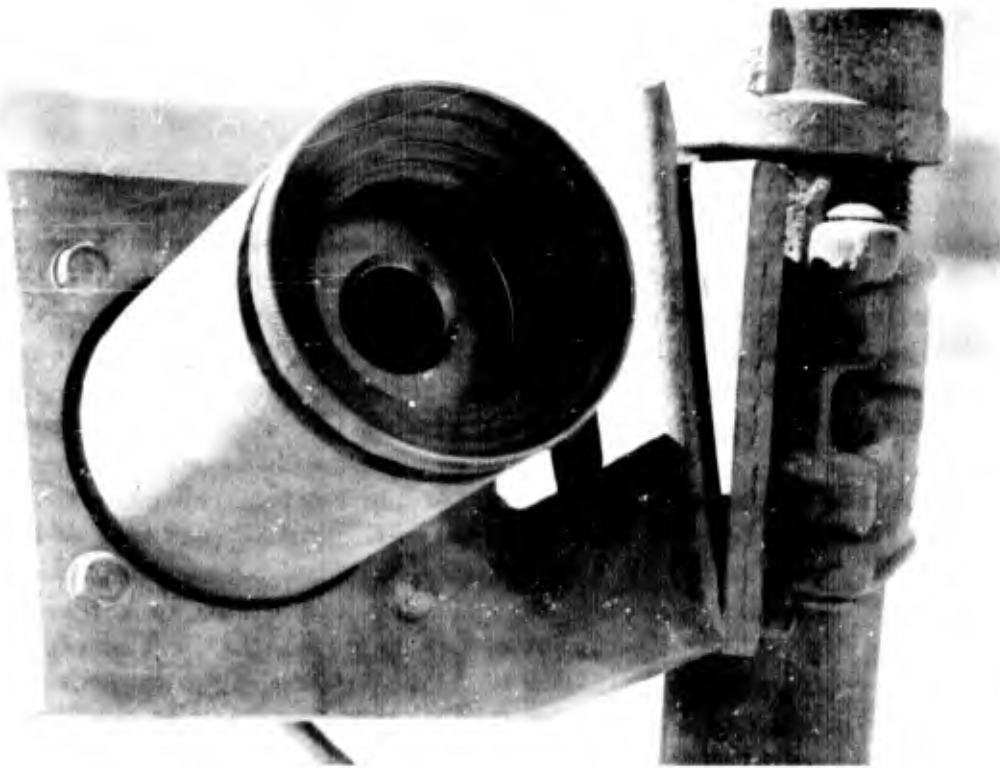
Fig. A.2 Schematic Wiring Diagram of Calorimeter Circuit and a
Typical Calorimeter Installation

A.2.3   Calibration

Both the experimental and the arithmetic methods were used for the calibration of the various sensing elements. An experimental calibration was obtained by recording the respective instrument responses to a series of known "loads" applied to the sensing elements. From the "load" and response data, calibration curves were drawn. In some instances when it was impractical to obtain an accurate measurement of the calibrating input to a sensing element, use was made of an arithmetic calibration obtained by computing the relationship between a given input and the corresponding response of the sensing element.

Because of the extreme sensitivity of the equipment and transducers used, it was necessary to employ a calibration procedure which would nullify the effects on the initial calibration to the changes in galvanometer, transducer, and over-all circuit sensitivity which can occur as a result of shipping the equipment to the test site, changing the galvanometer, or changing the bridge voltage. The system used to compensate for the sensitivity changes in circuits calibrated by the experimental method is known as the "Calibration Normalizing Procedure" and is described below in four phases.

Phase I   Calibration Record

Step A - Record the zero (no input applied to the transducer) galvanometer position on the oscillogram presented in Fig. A.3a. Note: The lengths a, b, c, d, and e on Fig. A.3a represent galvanometer trace readings and are obtained by measuring in inches the distance between the reference trace and the active galvanometer trace. The deflection due to an applied input to the transducer is the difference between the corresponding active trace reading and the zero reading; a positive deflection is obtained if, due to an applied load a trace reading is greater than its zero reading.

Step B - The cal-plus and cal-minus signals, shown in Fig. A.3a, are obtained by shunting the resistance R_p alternately across each of two adjacent arms of the bridge. Cal-plus is defined as the positive deflection whereas cal-minus is the negative deflection resulting from unbalancing the bridge with R_p. Both "cal" signals are recorded on the oscillogram.

Step C - Known increments of the input to be measured are applied to the transducer and are recorded; the resulting readings are represented by d and e in Fig. A.3a.

Phase II   Reduction of Calibration Record

Step A - Obtain the active trace readings which

73

72

include the zero, cal-plus, cal-minus, and calibrating increments shown in Fig. A. 3a.

Step B - Obtain the deflections in inches by subtraction and convert the deflections into per cent of cal-plus or cal-minus when the sign of the deflection is plus or minus, respectively. Sample calculations are present in Fig. A. 3a.

Step C - Plot a calibration curve in terms of per cent "cal" and applied input as shown in Fig. A. 3c.

Phase III   Preshot "Cal" Signals

Step A - Obtain "cal" deflections by following the same procedure stated in A and B of Phase I, using the same values of R_p. Note: Because the deflections due to the "cal" resistor, R_p, might be slightly different for the test system than for the laboratory system, "cal" signals are recorded on the day prior to a test. By using the calibrate ("cal") deflections obtained on the day prior to the shot to convert the test deflections to per cent of cal-plus or cal-minus, any changes of circuit sensitivity are compensated, making possible the use of the original calibration curve described in Phase II, Step C.

Phase IV   Reduction of Test Record

Step A - After test has been run, obtain readings of the active trace.

Step B - Obtain the deflections in inches by subtraction and convert the deflections into per cent of calibrate as shown in Fig. A. 3d using the deflections of cal-plus and cal-minus obtained from the preshot record.

Step C - Convert the test deflections, which are in terms of per cent of calibrate, into equivalent values of the measured input by use of the original calibration curve.

A. 2. 3. 1   Strain Gage

For load-response calibration of the strain gage sensing elements, an arithmetic procedure was used for all specimens except tension ties. The experimental calibration of tension ties is discussed in Appendix B. Formula A. 1 gives the strain-response ratio or cal-factor (ϵ /d) derived from the analysis of a Wheatstone bridge circuit in which the strain gage is used as a variable resistance.

$$\epsilon / d = \frac{R}{(R + Rc) \, d_1 \, n \, Kg} \qquad \text{A. 1}$$

where:
  ϵ is unit strain (in. /in.)
  d   is the galvanometer deflection due to ϵ (in.)

74

CALIBRATION RECORD

(a) = Zero reading of the active trace in inches
(b)-(a) = 100 per cent of cal-plus deflection in inches (Positive deflection)
(c)-(a) = 100 per cent of cal-minus deflection in inches (Negative deflection)
(d)-(a) = Deflection in inches due to a known applied input (Example 1)
(e)-(a) = Deflection in inches due to a known applied input (Example 2)

$$\frac{(d)-(a)}{(b)-(a)} \times 100 = \text{Deflection of trace in per cent cal-plus}$$

$$\frac{(e)-(a)}{(c)-(a)} \times 100 = \text{Deflection of trace in per cent cal-minus}$$

(a)

Wheatstone-bridge
Known Resistors = R and Rp
Variable Resistor = Rsg

(b)
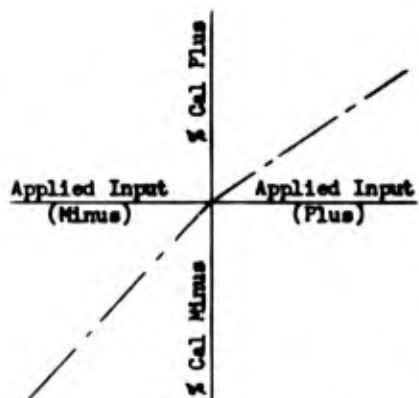
CALIBRATION CURVE

(c)
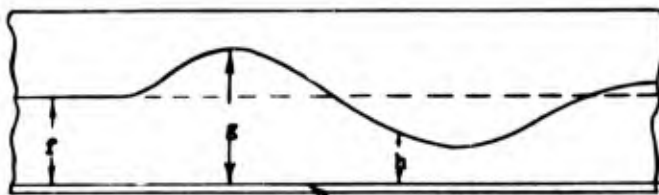
TEST RECORD

Let
(N) = 100 per cent cal-plus on preshot record
(O) = 100 per cent cal-minus on preshot record
(f) = Zero position of trace

Then
(g)-(f) = Deflection in inches due to applied input by test (Example 3)
(h)-(f) = Deflection in inches due to applied input by test (Example 4)

$$\frac{(g)-(f)}{(n)} \times 100 = \text{Test deflection of trace in per cent cal-plus}$$

$$\frac{(h)-(f)}{(o)} \times 100 = \text{Test deflection of trace in per cent cal-minus}$$

(d)

Fig. A.3 Method for Expression Galvanometer Deflections According
to Calibration Normalizing Procedure

75

R is the strain gage resistance (ohms)

Rc is a known calibrating resistance connected in parallel
with one arm of the bridge (ohms)

d_1 is the galvanometer deflection due to Rc (in.)

n is the number of strain gages in the bridge

Kg is the gage factor, the ratio of the unit change of
electrical resistance to the unit strain of the gage
wires; this figure is supplied by the gage manufacturer

The value of the galvanometer deflection, d_1, caused by the unbalanc-
ing resistor, Rc, was determined by a laboratory test and then em-
ployed in the calculation of the strain-response ratio.

Although "temperature-compensated" strain gages were
used, corrections for rapid changes of specimen temperature were
required because the full benefit of the inherent compensation character-
istic of the strain·gage was not realized unless the wires of the gage
were, at all times, at the same temperature as the specimen. This
condition was met only for relatively slow changes in temperature pri-
marily because of the poor heat transfer qualities of the adhesive and
of the bakelite body of the strain gage. Also, temperature compensated
gages were not available for magnesium and consequently a temperature
correction was required when these gages were applied to the magnes-
ium specimens. Correction data were obtained from laboratory tests
and from exposures of special calibration specimens during Shots 9
and 10. Examinations of the data revealed the need for individual cor-
rection of each strain measurement on each specimen that experienced
either a rate of temperature rise greater than $80^{\circ}F/sec$ or a total
temperature rise greater than $150^{\circ}F$. Correction curves, similar to
the one shown in Fig. A.4, were drawn as required. It should be noted
that the strain corrections are largest at about the midpoint of the
change of temperature when the rate of temperature rise of the speci-
men material is high and are less at higher temperatures. As a result,
inaccuracies on the correction curve could permit a considerable per-
centage error in the strain curve during the initial part of the thermal
phase where the actual strain is small and the correction is large;
however, this error, if present, should be much less as the tempera-
ture and resulting actual strain increase.

A.2.3.2   Thermocouple

The voltage output of a copper-constantan thermocouple,
made from the same reels of wire used in instrumenting the specimens,
was measured in a laboratory test and found to agree closely with the
standard Leeds and Northrup conversion table (38 calibration).

The "calibration" or sensitivity check of each thermocouple
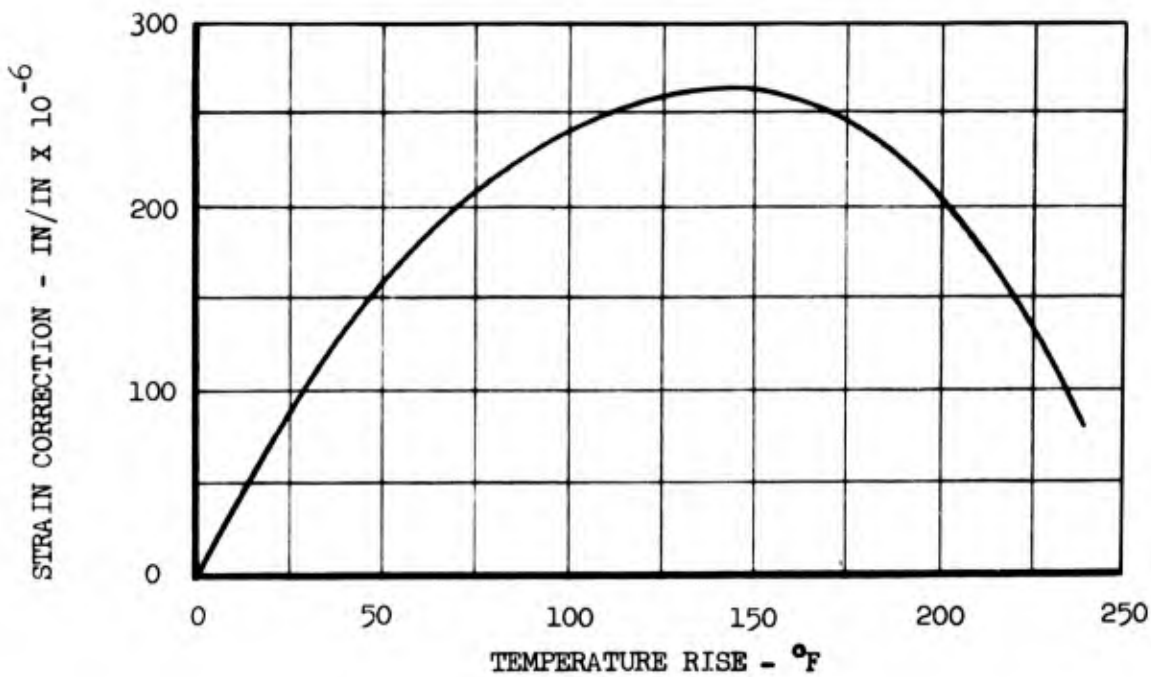
Fig. A.4 Typical Strain Gage Correction Curve

circuit was accomplished by inserting an accurately-measured voltage into the complete circuit including the thermocouple, attenuating and damping resistors, lead wires, and oscillograph galvanometer. The resulting deflection of the galvanometer was recorded; measured, and converted into a "cal-factor" in terms of millivolts per inch. Thereafter, by means of the cal-factor and the conversion table, readings of the thermocouple circuit were reduced to temperature data.

A.2.3.3   Pressure Gage

A static calibration of each pressure transducer was made in the laboratory and checked in the field by application of pressure and vacuum measured by a mercury manometer. No attempt was made to calibrate the gages under dynamic pressure conditions; however, the frequency responses of the galvanometers used in the gage circuits were checked in the laboratory.

A.2.3.4   Calorimeter

Instrument calibration factors in terms of calories/sq cm/ millivolt were supplied by NRDL. The calorimeter circuit sensitivities were checked and recorded by the same method used for thermocouple

77

circuits. Thus, by means of the circuit cal-factor (millivolt per inch) and the instrument factor, readings of the calorimeter circuit were reduced to total thermal energy.

A.2.4 Estimation of Errors

This estimation of errors was made in terms of the probable maximum error, i.e., the error obtained by adding the usual inaccuracies of the instrumentation and data reduction with no allowance for possible error compensation. In all instances when an error was estimated, the largest probable error was chosen so that over-all conservatism would be attained. The errors for each type of measurement are summarized in tabular form at the end of this section. A block diagram in the form of a flow sheet is presented in Fig. A.5 for the purpose of outlining the various steps where error can be introduced.

A.2.4.1 Errors Common to All Types of Measurements

Errors in recording the electrical outputs from the sensing elements occurred in both the experimental calibration and in the obtaining of the test data. According to the manufacturer of the oscillograph, the recording error is negligible for galvanometer deflections which are less than one inch. For larger deflections, however, the system becomes slightly non-linear. The degree of non-linearity for deflections of the magnitude encountered in calibration and testing have been determined by laboratory tests to be approximately 1 per cent. Accordingly, a 1 per cent error was assigned to the various recording operations in the preparation and execution phases.

One per cent errors as a result of human error in reading the oscillograms were introduced in both the preparation and the resolution phases. Where galvanometer deflections were above 1 in. the reading error was actually less than 1 per cent. Errors are also introduced when the data obtained by measuring the oscillograph trace deflections are plotted as curves. Experience has shown that errors of this type are relatively small; thus, an assigned error of 1 per cent is believed adequate to account for inaccuracies introduced by plotting and reproduction.

A.2.4.2 Errors Which Vary With Type of Measurement

Whereas most of the steps involved in obtaining an experimental calibration are the same for all types of measurements utilizing this type of calibration, the step involving the application of calibrating inputs introduces different errors for different types of measurements. For thermal energy and temperature channels, an error of 1/2 per cent was assumed for the determining of the electrical inputs utilized

78

PREPARATION   EXECUTION   RESOLUTION

SENSING ELEMENT
Pressure Gage Only
1%

ANALYTICAL
CALIBRATION

GAGE FACTOR
1%

DERIVATION
OF FORMULA
1/2%

EXPERIMENTAL
CALIBRATION

CALIBRATING
INPUTS

Thermal Energy . . . 1/2%
Temperature 1/2%
Overpressure 1%
Strain (Tension
  Ties Only) . . . 1%

RECORDING OF
CALIBRATION DATA
1%

REDUCTION OF
CALIBRATION DATA
1%

RECORDING OF
TEST DATA
1%

REDUCTION
OF TEST DATA

Preshot Electrical
Calibration Records . . . 1%
Test Records 1%

MISCELLANEOUS

(1) Strain Temp. Compensation
    Box Beams 6%
    Tension Tie 3%
    Stab. Skin 5%
    Stab. Spar 1%
(2) Thermal Energy Heat
    Loss Correction . . . 1/2%

PLOTTING AND
REPRODUCTION OF
DATA CURVES
1%

79

Fig A.5 Procedure for Obtaining Estimated Errors

to evaluate individual circuit sensitivities. The inherent accuracy of the pressure sensing elements was 1 per cent. In applying inputs to the pressure gages during their calibration, a maximum probable error of 1 per cent occurred as a result of reading the graduations of the mercury manometer. The tension tie calibration involved human error in reading the loads applied by a testing machine; an estimate of 1 per cent for the error in this procedure was made.

The errors involved in an analytical calibration were estimated to be 1 1/2 per cent. Of this error, 1 per cent was allowed for strain gage calibration factor error in accordance with manufacturer specifications; the remaining 1/2 per cent error was introduced in the derivation of the analytical formula. In order to substantiate the analytical calibrations, comparisons between analytical calibration factors and experimental calibration factors were made. Tension tie specimens were used because the simplicity of the specimens made possible the computation of accurate stress-strain relationships. As a result of the comparisons of the strain gage circuit sensitivities obtained by both of these methods, it was determined that the average deviation between two comparable sensitivities was 0.7 per cent. The maximum and minimum deviations were +3 per cent and -1.5 per cent, respectively, and were, from a consideration of relative accuracies of the two methods, primarily a result of inaccuracies in the experimental calibration.

For those strain gage channels requiring a temperature compensation calibration (all channels exposed to thermal energy except for T-28 stabilizer spars) an average error of 5 per cent was estimated for the thermal phase of the measurement. For the blast phase, however, the temperature compensation error for the box beam and stabilizer strain measurements was negligible because the magnitude of the blast-induced strains was very high with respect to the temperature strain correction. The 5 per cent error for the tension tie specimens prevailed during the blast phase because there was no appreciable change in strain evident in the tension tie time-history measurements as a result of blast impingement.

In general, the error due to temperature compensation of strain gages is not known definitely, but it is evident that the error is dependent on the peak strain and the peak temperature to which a given specimen is subjected. The box beam, stabilizer skin, and tension tie strains were relatively small; the first two were lower than the tension tie strains, with the box beam strains the lowest. The above specimens attained rather high temperatures which made large strain corrections necessary, and therefore, could introduce significant error in the final data. The average strain correction for the box beams, for instance, was about 56 per cent of the peak box beam strain measured. Considering the ratios of corrected strain to peak strain, errors of 6 per cent, 5 per cent, and 3 per cent were assumed for the box beams,

stabilizer skins, and tension ties, respectively. Since the T-28 stabilizer spar temperature rise was small no temperature compensation was used; however, a 1 per cent error was assumed for these measurements as a result of neglecting the temperature effects. The temperature compensation errors appear in the miscellaneous correction step of the resolution phase, Fig. A. 5.

Other miscellaneous corrections were applied to the total thermal energy data when correcting the recorded trace for the heat losses of the sensing element. The 1/2 per cent error assigned to this operation was a result of the correction approximations which were used.

A. 2. 4. 3   Summary of Errors

A summary of the errors which have been described is presented in Table A. 2, appearing at the rear of this appendix. In this table the errors in the preparation, execution, and the resolution phases have been compiled and totaled for each specimen type, the sum of the errors being the maximum error. The maximum error, listed in the last column of Table A. 2, represents the accuracy limitations within which 67 per cent of the data will be. These limits were determined by statistical methods using the maximum errors involved in each step of a particular measurement.

A. 3   PEAK TEMPERATURE INSTRUMENTATION

The peak temperature instrumentation was accomplished by means of temp-tapes, a device consisting of 24 sensing elements each of which melts at a particular given temperature in the range from 123 to 635°F. The temp-tapes used by Project 8. 1a are described in detail in _Measurement of Peak Temperatures with Thermal Sensitive Indicators,_ WADC Technical Report 53-471. The temp-tapes were used to obtain peak temperatures to supplement the time-history data and to obtain peak temperature data on specimens which were not oscillographically instrumented.

Two different designs for temp-tapes, as shown in Fig. A. 6, were used depending upon the space available for installation: type A temp-tape, four columns and six rows, 2 in. by 3 1/2 in. ; type D temp-tapes two columns and 12 rows, 5/8 in. by 5 in. All temp-tapes were installed on the unexposed surface of the skin to be instrumented. Before affixing the temp-tape to the surface, the metal was thoroughly cleansed with acetone and/or steelwool.

The temp-tapes were calibrated at the Naval Material Laboratory Brooklyn, N. Y., using a high intensity heat source with an exposure time of from 2 to 3 sec so as to simulate temperature rises caused by thermal energy from a nuclear explosion. The results of the calibration,

81
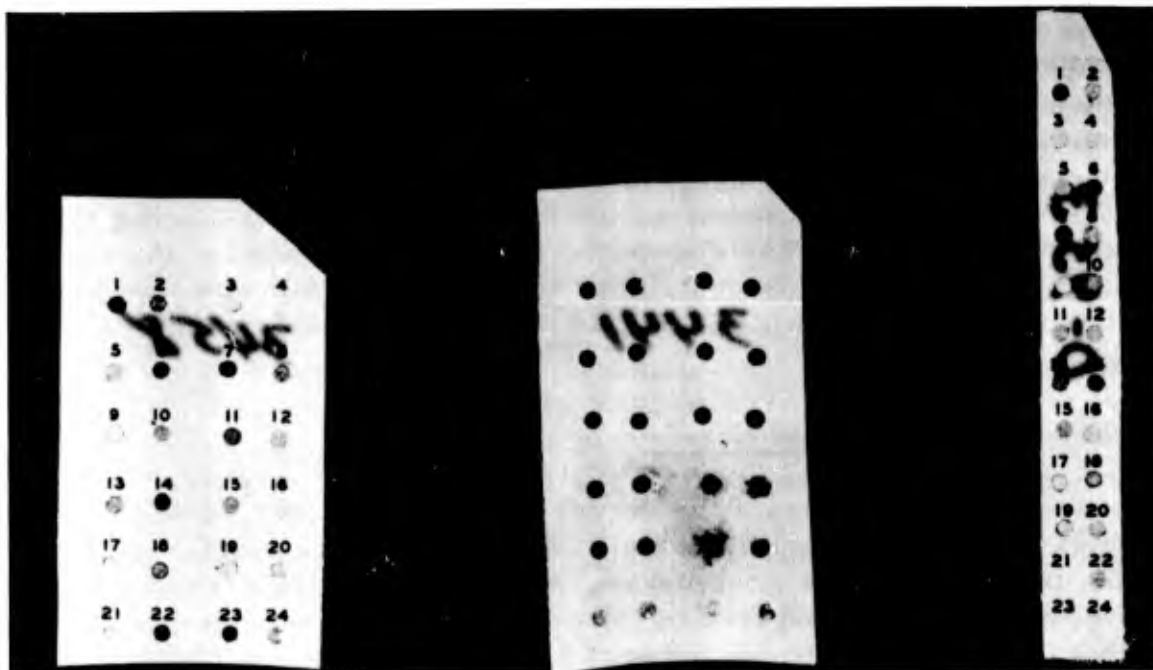
Type A
Not Melted

Type A
Melted

Type D
Not Melted

Fig. A.6 Type A and D Temp-tapes, Including a Temp-tape with all
Elements Melted (Numbers Indicate Element Number)

including a list of the sensing elements, are given in Table A.3, appearing at the end of this appendix. With exclusion of the last four elements which were eutectic alloys, all sensing elements were pigment coated papers. Upon melting, the pigment papers turn a black color and the eutectic alloys become sporatic and disfigured as shown in Fig. A.6. The estimated reliability of the calibration is plus or minus 5 per cent; however, because of possible variance in the degree of contact of the sensing elements with the specimen, the over-all estimated reliability of temp-tape data is ±10 per cent. A field check of the temp-tape calibration was performed by installing temp-tapes near each accessible thermocouple installation on all specimens. Table A.4, appearing at the end of this appendix, gives a summary of the data obtained from this check. The results of this field check were, in general, favorable in that the calibration appears to be valid for temp-tapes mounted on 0.025 in. skin; however, the calibrated temperatures are possibly low for temp-tapes mounted on thicker skins. There are insufficient data to change with any degree of certitude the calibrated temperature of any of the elements. Calibrations are being repeated using various skin thicknesses and exposure times, but the results are not available at this writing.

Temp-tapes were also placed by thermocouple installations on the tension ties and on the spar cap of the T-28 stabilizers; however, because of the thermal radiation received by the temp-tapes, there was very poor agreement with the thermocouple data. In general, the data from these temp-tapes were much higher than the thermocouple data.

Not infrequently, one or more of the temp-tapes at an installation would indicate a peak temperature lower than the other temp-tapes, indicating the need for having at least three and preferably more temp-tapes at each installation. Because one or more of the temp-tapes at an installation may indicate a peak temperature lower than that actually attained, the temperature range presented in this report for a particular installation is the maximum temperature range indicated by any of one or more of the temp-tapes at this installation.

Difficulty was encountered in reading the temp-tapes because elements No. 1, 6, 7, and 10 had turned a darker color, prior to the time of installation, and it was difficult to determine whether or not they had melted. The elements were analyzed very carefully; however, there still remains some doubt about peak temperatures indicated by these elements. The over-all estimated reliability of the peak temperature data indicated by temp-tapes may be taken as plus or minus 10°F.

A.4 PHOTOGRAPHY

Motion picture coverage of the response of the test specimens to thermal and blast inputs was accomplished by means of one each GSAP (Gun Sight Aiming Point) camera and High-speed Eastman Camera trained on each item to be photographed. The GSAP camera was used to record the response of the specimen during the thermal phase and the High-speed Eastman for specimen response during the blast phase. The cameras were mounted about 5 1/2 ft above the ground on pedestals as can be seen in Fig. 2.13.

Table A.5, appearing at the end of this appendix, lists the test specimens which were photographed including the information pertaining to each film which was exposed.

TABLE A.1 - Pressure Transducers

Installation No.		Ground Range (ft)	Shot	Transducer Range (psi)	Natural Frequency (cps)
Statham Model P-6	163	2300	9	±15	1100
	165	6500	9	± 7.5	900
	167	7200	9	± 5	900
	169	8800	9	± 4	750
	171	2300	10	±10	950
	173	6500	10	± 2	600
	175	7200	10	± 2	600
	176	8800	10	± 2	600
	177	8800	10	± 4	750
Consolidated Type 4-310	162	2300	9	-5 to +10	2000
	164	6500	9	-5 to +10	2000
	166	7200	9	-1 to + 4	2000
	168	8800	9	-1 to + 4	2000
	170	2300	10	-5 to +10	2000
	172	6500	10	-1 to + 4	2000
	174	7200	10	-1 to + 4	2000

TABLE A.2 - Estimated Errors in Various Types of Measurements

Measurements	Preparation (%)	Execution (%)	Resolution (%)	Probable Maximum Error (%)	Maximum Error in 67% of Data (%)
Box Beam Strain	2 1/2	1	9	12 1/2	3
Tension Tie Strain	3	1	6	10	3
Stabilizer Skin Strain	2 1/2	1	8	11 1/2	3
Stabilizer Spar Strain	2 1/2	1	4	7 1/2	2
Temperature	2 1/2	1	3	6 1/2	2
Pressure	4	1	3	8	2
Thermal Energy	2 1/2	1	3 1/2	7	2

84

TABLE A.3 - Temp-tape Sensing Elements and Calibration

Element Number	Name	Calibrated Melting Temperature ($^\circ$F)
1	Triphenyl phosphate	123
2	5-di-n-butyl thiourea	144
3	Tri-p-cresyl phosphate	178
4	Sucrose ecta-acetate	171
5	Sorbitol hexa-acetate	195
6	Thiazolidine thione	232
7	Acetanilide	225
8	Hydroquinone dibenzyl ether	253
9	Benzoin	265
10	Adipic acid	142
11	Cholesterol	288
12	Benzanilide	309
13	p-chloroacetanilide	331
14	Succinic acid	364
15	N-phenylsulfanilimide	377
16	m-dinitro benzoic acid	368
17	Anthracene	424
18	Hexachlorobenzene	442
19	Phthalimide	465
20	Phenolphthalein	488
21	Alloy 0000-10 (82.6% Cd-17.4% Zn)	515
22	Bismuth (100%)	517
23	Alloy 0000-11 (92.5% Cd-7.5% Sb)	540
24	Cadmium	635

TABLE A.4 - Summary of Peak Temperature Data For Field Check of Temp-tape Calibration

Peak Temperature (°F)		Frequency of Temp-tape Reading	Skin Thickness (in.)	Thermocouple Inst. No.	Name of Specimen
Thermo-couple	Temp-tape				
639	635	3	0.025	86	T-28 Stab.
	540-634	1			
414	377-423	4	0.025	55	T-28 Stab.
401	377-423	4	0.025	144	Hat Panel
395	377-423	4	0.025	146	Hat Panel
376	377-423	4	0.025	66	T-28 Stab.
364	377-423	4	0.025	51	T-28 Stab.
330	331-363	2	0.025	72	T-28 Stab.
	309-330	2			
312	288-308	4	0.025	106	T-28 Stab.
303	309-330	2	0.025	102	T-28 Stab.
	288-308	2			
302	288-308	3	0.025	123	T-28 Stab.
	265-287	1			
300	288-308	1	0.025	161	Hat Panel
	265-287	1			
	253-264	2			
298	288-308	4	0.025	121	T-28 Stab.
293	288-308	3	0.025	119	T-28 Stab.
	265-287	1			
202	288-308	2	0.025	79	T-28 Stab.
	265-287	1			
	253-264	1			
254	253-264	3	0.025	83	T-28 Stab.
	225-231	1			
124	123	4	0.025	91	T-28 Stab.
99	123	4	0.025	61	T-28 Stab.
87	123	4	0.025	48	T-28 Stab.
87	123	4	0.025	76	T-28 Stab.
568	517-539	4	1/8	14	Box Beam
210	195-224	4	1/8	10	Box Beam
197	178-194	4	1/8	8	Box Beam
412	424-441	1	3/16	12	Box Beam
	377-423	3			
362	377-423	4	3/16	2	Box Beam
325	288-308	4	3/16	16	Box Beam
311	288-308	4	3/16	6	Box Beam
236	253-263	1	3/16	4	Box Beam
	232-252	2			
	178-194	1			
235	232-252	1	*	148	Hat Panel
220	195-225	1	*	159	Hat Panel
	171-177	1			
183	178-194	1	*	18	Box Beam
	144-170	1			
162	144-170	1	*	22	Box Beam
	123	1			
160	144-170	3	*	150	Honeycomb Panel
140	144-170	4	*	26	Box Beam

* Substructure

TABLE A.5 - Motion Picture Information for Project 8. la Specimens

Shot No.	Location	Subject	Camera Type	Film Speed (Frames/sec)	Film[a] Type and No.
9	Station 6500	T-28 Stabilizer with Thermal Shield	EHS GSAP	606[b] 64	BX, 16651 KC. 16652
		Box Beam	EHS GSAP	531[b] 63	BX, 16653 KC. 16654
		T-28 Stabilizer, Unshielded	EHS GSAP	563[b] 62	BX, 16655 KC, 16656
10	Station 6500	T-28 Stabilizer with Thermal Shield	EHS GSAP	519 62	BX, 16769 KC, 16770
		Bonded Metal Panel (No. 13)	EHS GSAP	602 63	BX, 16771 KC, 16772
		T-28 Stabilizer, Unshielded	EHS GSAP	595 61	BX, 16773 KC, 16774
	5300 ft Range	B-36 Stabilizer and Elevator Assembly	EHS GSAP	519 61	BX, 16768 KC, 16767

a   KC-Kodachrome, BX-Background X

b   At time of shock arrival

APPENDIX B

THERMOELASTIC STUDY UTILIZING BOX BEAMS AND TENSION TIES

B.1 GENERAL

The thermoelastic study consisted of exposure of simple box beam structures and preloaded bars of rectangular cross-section, typical of simple aircraft structures and structural elements, which shall be referred to as "Box Beams" and "Tension Ties", respectively. Time-history thermal and mechanical responses of these specimens were of primary interest during the thermal phase.

B.2 PROCEDURE

The basic materials from which the box beams and tension ties were fabricated consisted of 3/16 and 1/8 in. thick 75S-T6 aluminum and FS1h magnesium alloys. Because neither of the materials could be procured from any one manufacturer, the tensile properties of three specimens of the material from each manufacturer were determined experimentally and are compiled in Table B.1. All material used was cut from rolled plate stock such that the longitudinal axis of the specimen was in the direction of the rolling. Care was exercised in avoiding temperatures which might alter the physical properties of the materials, and in inspecting for surface scratches and other deformities. Typical stress-strain curves for the aluminum and magnesium alloys are presented in Figs. B.1 and B.2.

B.2.1 Box Beam

The box beams utilized during these tests consisted of simple aircraft box beam type structures having two faces with two webs between them, to which the faces were attached by screws and dowels. The general box beam specifications are indicated in Fig. B.3. A

88

TABLE B.1 - Tensile Properties of Materials for Box Beams and Tension Ties
(Tested at 75°F)

SPECIMEN COMPONENT	MATERIAL	SIZE OF TEST SAMPLE (IN.)	ULTIMATE TENSILE STRENGTH PSI	YIELD STRENGTH PSI	MODULUS OF ELASTICITY 10^6 PSI	ELONGATION IN./IN.	SOURCE
1/8" AL BOX BEAM FACES AND 1/8" AL TENSION TIES	75S-T6 AL (ROLLED PLATE)	1/8 x 3/4 x 12	83,100	78,000	10.35	13.7%	REYNOLDS
3/16" AL BOX BEAM FACES AND 3/16" AL TENSION TIES	75S-T6 AL (ROLLED PLATE)	3/16 x 3/4 x 12	80,500	75,250	10.06	12.0%	KAISER
1/4" AL BOX BEAM WEBS	75S-T6 AL (EXTRUDED BAR)	1/4 x 1 1/2 x 12	85,000	80,000	10.07	16.3%	ALCOA
1/8" MG BOX BEAM FACES AND 1/8" MG TENSION TIES	FS1H MG (ROLLED PLATE)	1/8 x 3/4 x 12	41,000	33,200	5.97	4.3%	ALCOA
3/16" MG BOX BEAM FACES AND 3/16 MG TENSION TIES	FS1H MG (ROLLED PLATE)	3/16 x 3/4 x 12	42,300	33,000	6.45	10.0%	DOW
1/4" MG BOX BEAM WEBS	FS1H MG (ROLLED PLATE)	1/4 x 1 1/2 x 12	40,000	31,000	6.66	17.0%	DOW
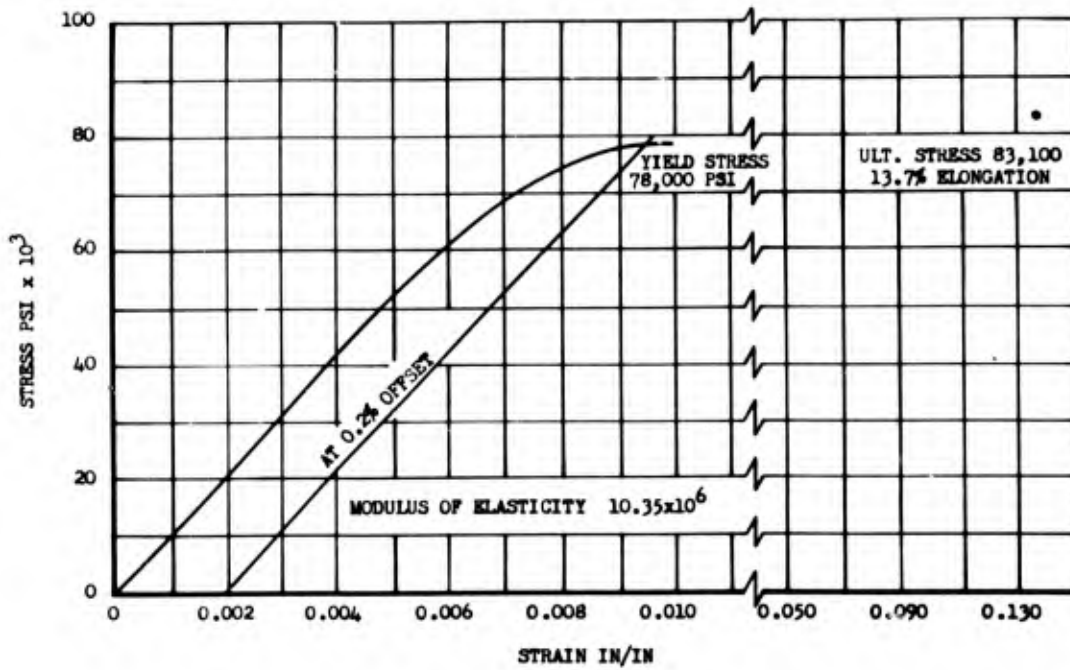
Fig. B.1 Typical Stress-strain Curve for 75S-T6 Aluminum
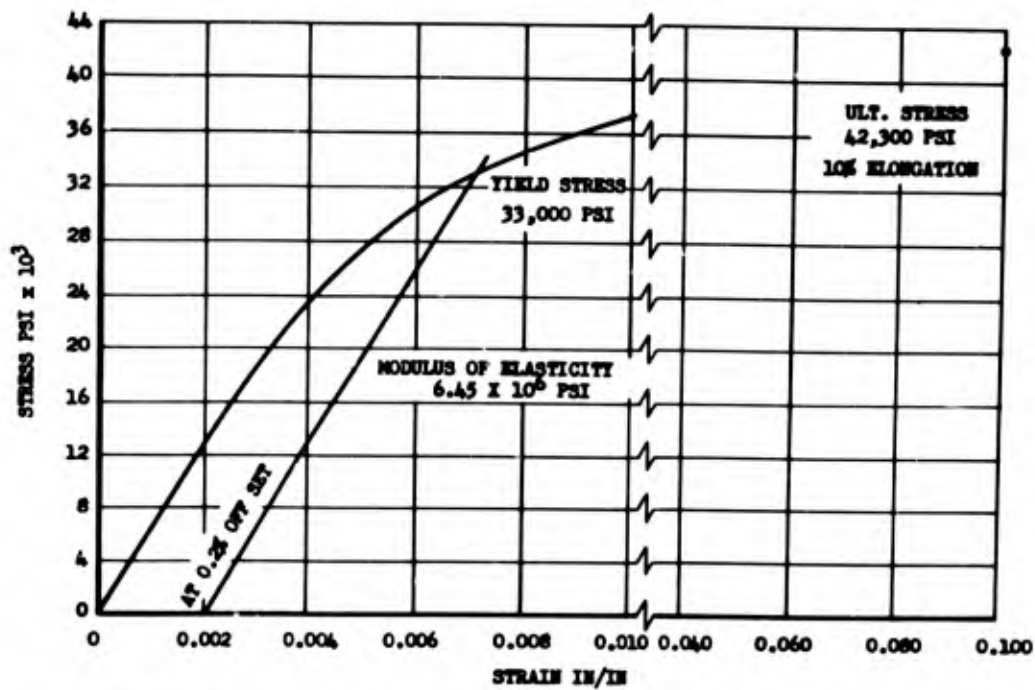
Fig. B.2 Typical Stress-strain Curve for FS1h Magnesium

90

Fig. B.3 Details of Box Beam Construction

NOTE: EDGES TO BE BOLTED
MACHINED SQUARE (WEB ONLY)

CHART

PLATE	A	B
$T_t = 3/16"$	1/8"	

2 TO EACH ASSEMBLY

SCREW LENGTHS

PLATE TYPE	LENGTHS ⑤ & ⑥
A	9/16"
B	1/2"

HOLES:

DOWEL ④ REAM PLATE③
7/16" DEEP FOR ALL PLATE TYPES

SCREWS ⑤ & ⑥ TAP PLATE③
7/16" DEEP WITH 8-32 BOTTOM TAP

⑥ 90,000 PSI ULT. SHEARING
STRESS. REAR SIDE ONLY. NO
DOWEL PINS USED.

④ PRESS FIT 1" ON
CENTERS. 90,000 PSI
ULT. SHEARING STRESS

⑤ 90,000 PSI ULT.
SHEARING STRESS.
FRONT SIDE ONLY
1" ON CENTERS

PC. NO.	NAME	MATERIAL	QUAN.
-6	8-32 HEX SOCKET TYPE CAP SCREWS	STEEL (SEE NOTE)	152
-5	8-32 FLATHEAD MACHINE SCREWS	STEEL (SEE NOTE)	76
-4	11/64" DOWEL PINS, 1/2" LONG	STEEL (SEE NOTE)	76
-3	1/4" X 1 1/2" X 48" WEB	STEEL	2
-2	T_t" X 6" X 48" BACK PLATE (SEE CHART)		1
-1	T_t" X 6" X 48" FRONT PLATE		1

91

Fig. B.4 Universal Mounting Fixture with Box Beam Installed

block of metal was bolted to both faces and both webs at the free end of the box beam to prevent possible failure of the end fasteners. The beams were mounted rigidly in cantilever fashion, 2 ft above the ground, in mounts as shown in Fig. B.4, such that 3 ft of the box beam extended above the mount, and the front face was normal to the intended line of direct radiation at burst time. Nine aluminum box beams were fabricated of which 6 had 3/16 in. faces and 3 had 1/8 in. faces, and 7 magnesium box beams were made of which 4 had 3/16 in. faces and 3 1/8 in. faces.

Time-history instrumentation on the box beams consisted of two strain gages and one thermocouple on the inside of the front surface, 1 ft above the attachment fitting. In addition, one box beam had similar installations at three locations on one web and at two locations on the rear surface, as shown in Fig. B.5. The two strain gages at each

          ⊗ Location common to all box beams

          x Additional locations, one box beam only
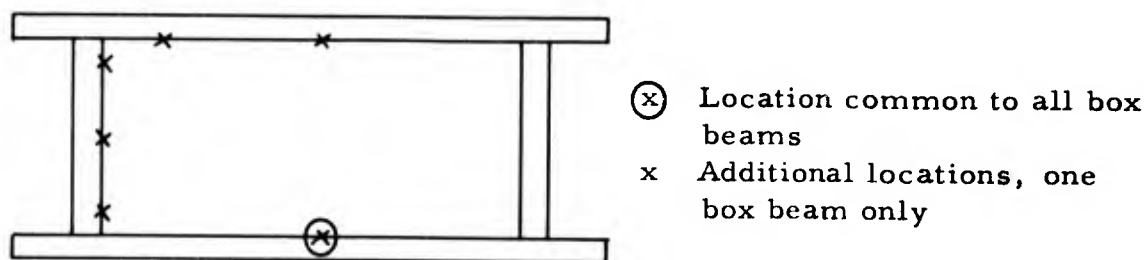
Fig. B.5 Instrumentation Locations on Cross Section of Box Beam

installation were connected as opposite arms of the strain bridge so as to provide a sufficiently large gage output. The gages were mounted so as to be sensitive to strain in the direction of the longitudinal axis only. A pictoral representation of the instrumentation locations is given in Fig. B.6 for the 2-channel box beams and in Fig. B.7 for the 12-channel box beam. In addition to the oscillographic instrumentation, peak temperature indicating devices (temp-tapes) were installed at various locations on each box beam, as shown in Fig. B.8. Calibration of the time-history instrumentation is discussed in Appendix A.

B.2.2   Tension Ties

The tension tie specimens were rectangular cross-sectional bars, 3/4 in. wide and 18 in. long, stressed in tension. They were mounted with the 3/4 in. face normal to the intended burst point, in a "C" frame type mount as shown in Fig. B.9, where the leaf springs were used to apply (and hold constant during the thermal phase) the specified preloads. Only the center 12 in. of the total length of the tension ties were exposed. The preloads applied to the tension ties

93

ERDF-13D
STRAIN GAGE

• COPPER - CONSTANTAN
THERMOCOUPLE JUNCTION
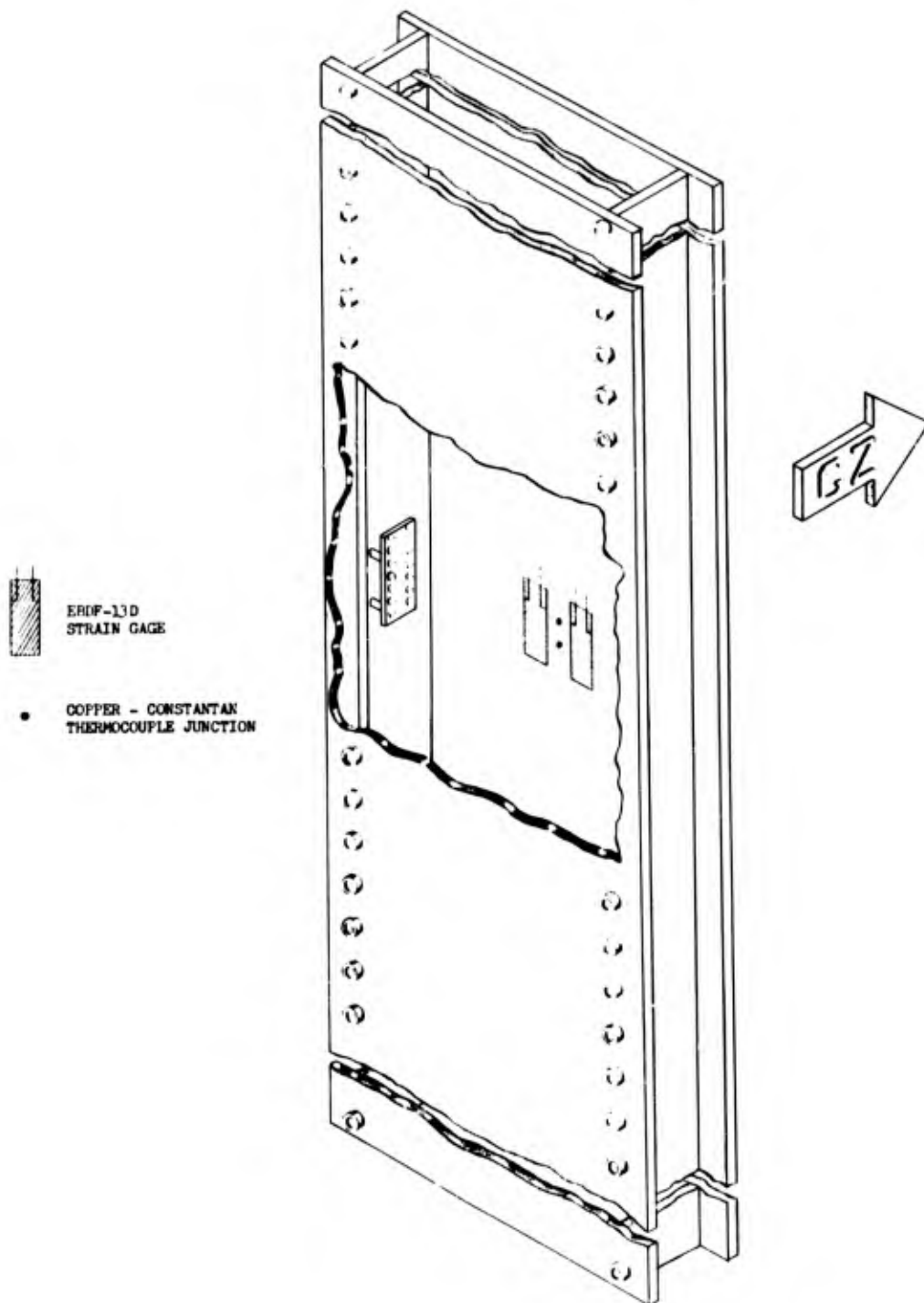
Fig. B.6 Instrumentation of Box Beams for Shots 9 and 10. Center
Line of Instrumentation was Located 12 in. Above Clamping
Device. Refer to Installation Nos. 1 to 14 Inclusive for
Graphs Pertaining to this Structure.

94
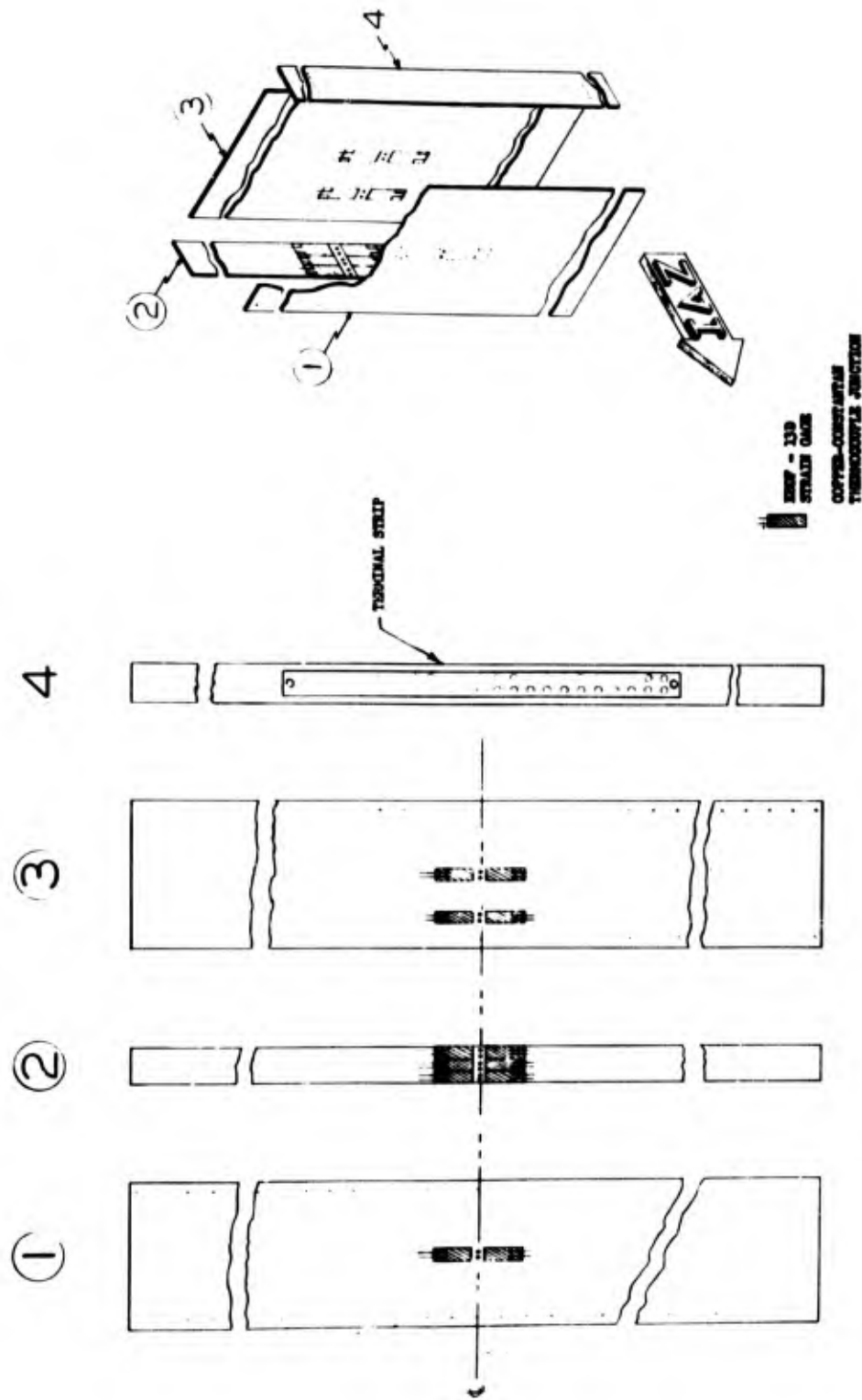
Fig. B.7 Instrumentation of 12-channel Box Beam for Shot 10. Center Line of Instrumentation was Located 12 in. Above Clamping Fixture. Refer to Installation Nos. 15 to 26 Inclusive for Graphs Pertaining to this Structure.

95
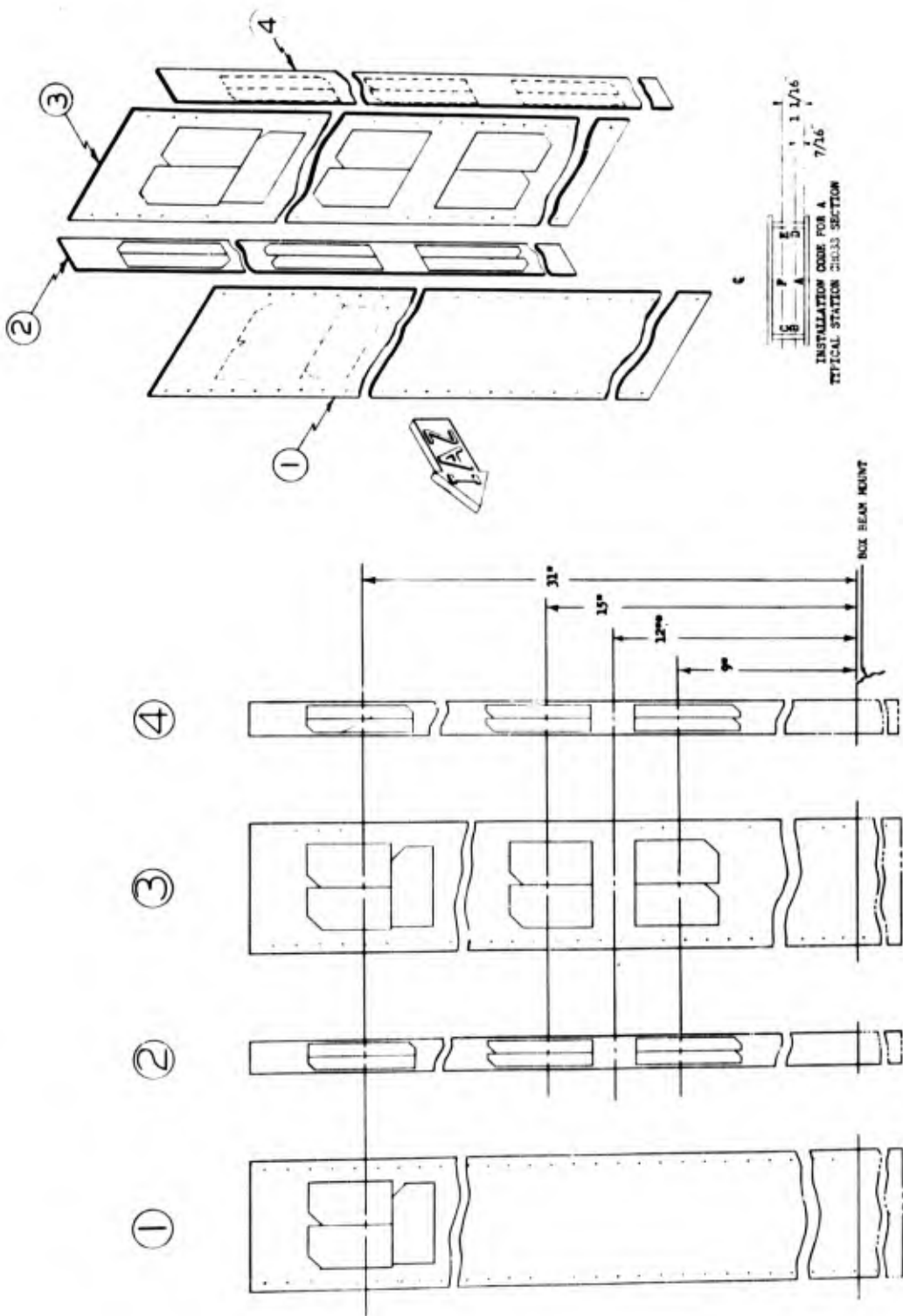
Fig. B.8 Location of Temp-tape Instrumentation on Box Beams

ALIGNMENT
INDICATOR

LEAF SPRINGS

UPPER GRIPPING BLOCK

TENSION TIE SPECIMEN

LOWER GRIPPING BLOCK

WEDGE TYPE
SPECIMEN GRIPS

B.P.

LOAD MONITOR
STRAIN GAGE

LOADING SCREW

THERMOCOUPLE
COLD JUNCTION
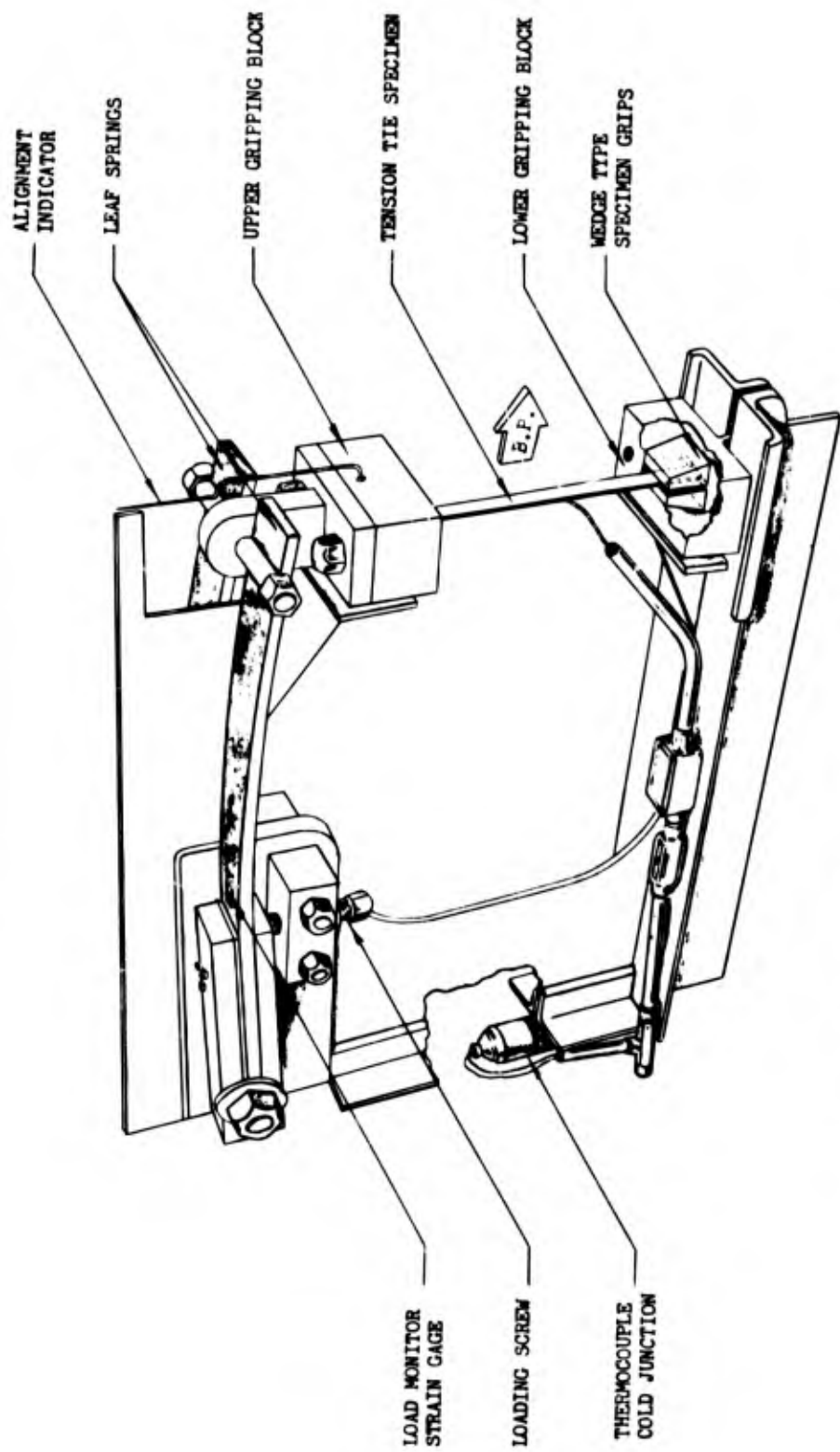
Fig. B.9 "C" Frame Mount for Tension Ties

were measured by strain gages on the springs. All forces, exclusive of the pure tensile load, were minimized by means of special adjustments on the mount. Light metal shields were placed over the leaf springs in order to minimize the change in tensile load due to thermal response of the springs.

Instrumentation on the tension ties consisted of one strain gage and one thermocouple installed on the center of the rear face, as shown in Fig. B.10. The strain gages were mounted so as to measure the strain parallel to the longitudinal axis only.

The calibration of the tension ties was determined experimentally by applying known tensile stresses to the ties, calculating the strain and recording the gage output. From these data, calibration curves were drawn. Calibration of the thermocouple is discussed in Appendix A.

B.2.3   Exposure Program

During Shots 9 and 10, eight box beams and eight tension ties were exposed as shown in Figs. B.11 and B.12. It was originally planned that all specimens at Station 2300 would be 3/16 in. thick; however, after analysis of the Shot 9 data it was deemed advisable to attain a higher temperature on two specimens, and thus one each 1/8 in. aluminum tension tie and box beam were exposed during Shot 10, instead of the proposed 3/16 in. tension tie and box beam. The temperature rise of the specimens was controlled by painting them to regulate the thermal energy absorption.

B.3   RESULTS

A total of 46 channels of information were recorded, of which 42 channels yielded usable data and one channel yielded data during the thermal phase only. Table B.2 lists the oscillographic installation numbers for the box beams and tension ties, including the quantity measured and figure references.

No visible damage was sustained by any of the specimens other than some paint scorching, except during Shot 10, when there was evidence of minor pitting probably caused by small stones or sand blasting.

B.3.1   Box Beams

A summary of the peak temperature and strain data obtained on each box beam specimen is given in Table B.3. A comparison of the time-history temperature and strain data during the thermal phase for the front face of each box beam is shown in Figs. B.13 through B.20. Time-history strain data during the thermal phase of each

THERMOCOUPLE

STRAIN GAGE

$\frac{3}{4}$"

A

A

18"

EXPOSED LENGTH
12"

6"

IAZ

METAL WIRE
SHIELD

HEAT RESISTANT TAPE

BAKELITE CEMENT

STRAIN GAGE

PAINTED FACE

SECTION A-A

CAPACITANCE WELDED
THERMOCOUPLE
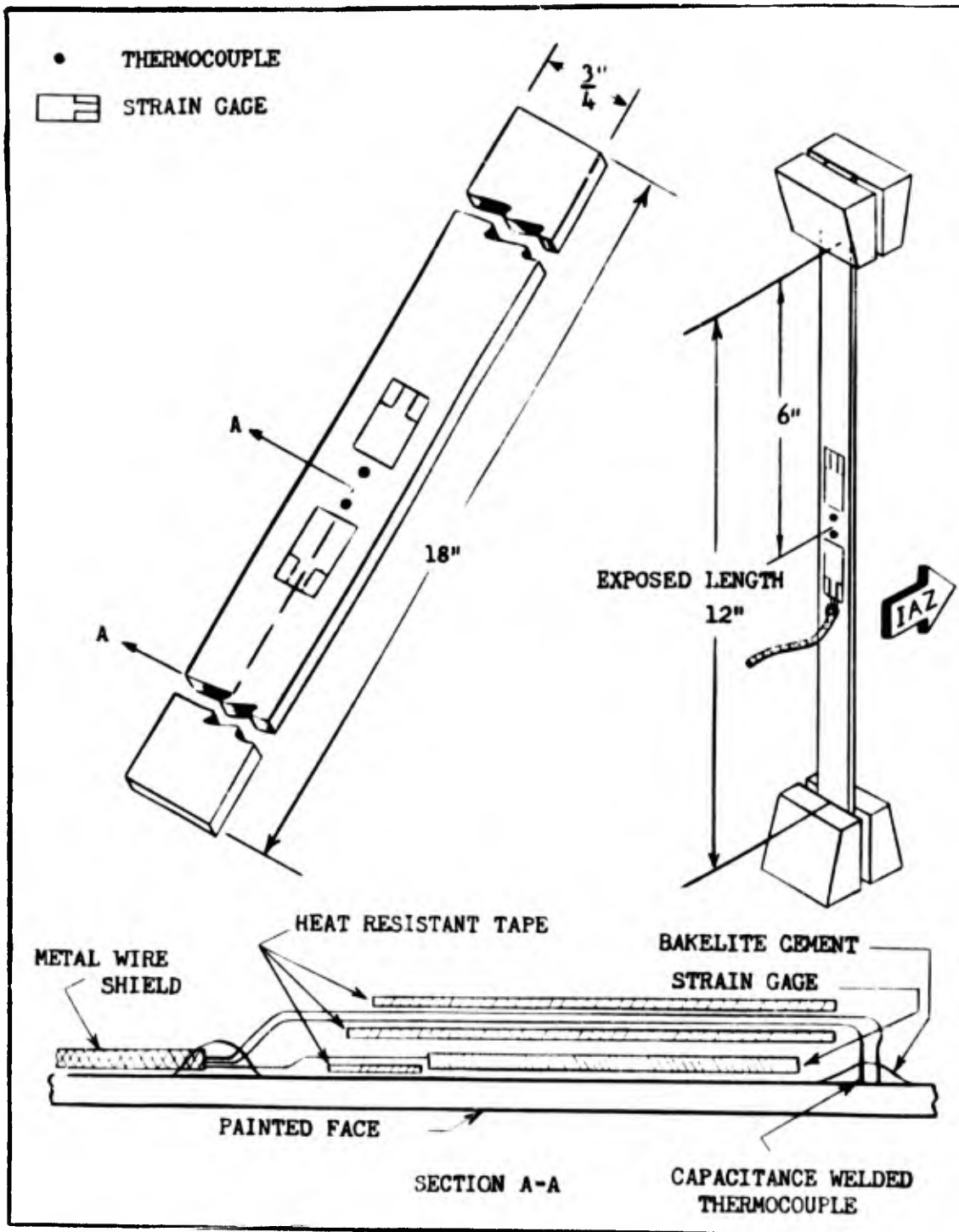
Fig. B.10 Location of Tension Tie Instrumentation

99

Fig. B.11 Schematic of Box Beam and Tension Tie Program, Shot 9
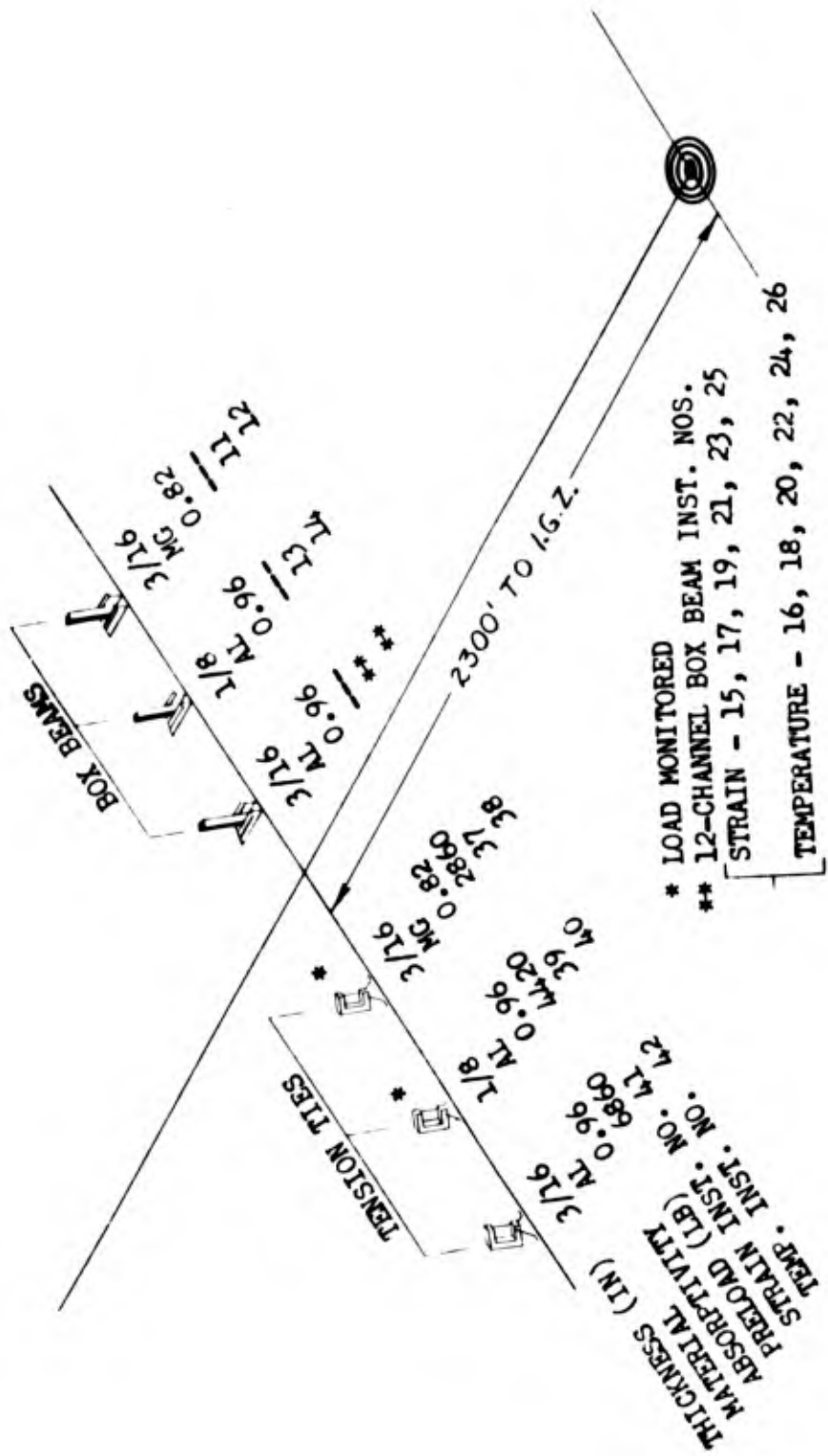
Fig. B.12 Schematic of Box Beam and Tension Tie Program, Shot 10

TABLE B.2 - Index to Oscillographic Instrumentation (Box Beam and Tension Tie Specimens) Box Beams

INST. NO.	QUANTITY MEASURED	FIGURE REFERENCE	MATERIAL	THICKNESS (IN.)	ABSORP-TIVITY	STATION
SHOT 9						
1	STRAIN	B.13, B.26, B.50	MAGNESIUM	3/16	0.82	2300
2	TEMPERATURE	B.13, B.22, B.50				
3	STRAIN	B.14, B.27, B.49	ALUMINUM	3/16	0.48	2300
4	TEMPERATURE	B.14, B.22, B.49				
5	STRAIN	B.15, B.28, B.49	ALUMINUM	3/16	0.96	2300
6	TEMPERATURE	B.15, B.22, B.49				
7	STRAIN	B.16, B.29, B.52	ALUMINUM	1/8	0.96	6500
8	TEMPERATURE	B.16, B.23, B.52				
9	STRAIN	B.17, B.30, B.52	MAGNESIUM	1/8	0.96	6500
10	TEMPERATURE	B.17, B.23, B.52				
SHOT 10						
11	STRAIN	B.18, B.31, B.50	MAGNESIUM	3/16	0.82	2300
12	TEMPERATURE	B.18, B.24, B.50				
13	STRAIN	B.19, B.32, B.51	ALUMINUM	1/8	0.96	2300
14	TEMPERATURE	B.19, B.24, B.51				
15	STRAIN	B.20, B.21, B.48, B.49		3/16	0.96	
16	TEMPERATURE	B.20, B.24, B.25, B.48, B.49				
17	STRAIN	B.21, B.33, B.48		1/4	-	
18	TEMPERATURE	B.25				
19	STRAIN	B.21, B.34, B.48		1/4	-	
20	TEMPERATURE	B.25	ALUMINUM			2300
21	STRAIN	B.21, B.35, B.48		1/4	-	
22	TEMPERATURE	B.25				
23	STRAIN	B.21, B.36, B.48		3/16	-	
24	TEMPERATURE	B.25				
25	STRAIN	B.21, B.37, B.48		3/16	-	
26	TEMPERATURE	B.25				

TENSION TIES

INST. NO.	QUANTITY MEASURED	FIGURE REFERENCE	MATERIAL	THICKNESS (IN.)	ABSORP-TIVITY	STATION
SHOT 9						
27	STRAIN	B.38, B.54	MAGNESIUM	3/16	0.82	2300
28	TEMPERATURE	B.38, B.45				
29	STRAIN	B.39, B.52	ALUMINUM	3/16	0.48	2300
30	TEMPERATURE	B.39, B.45				
31	STRAIN	B.40, B.53	ALUMINUM	3/16	0.96	2300
32	TEMPERATURE	B.40, B.45				
33	STRAIN		MAGNESIUM	1/8	0.96	6500
34	TEMPERATURE					
35	STRAIN	B.41, B.53	ALUMINUM	1/8	0.96	6500
36	TEMPERATURE	B.41, B.46				
SHOT 10						
37	STRAIN	B.42, B.54	MAGNESIUM	3/16	0.82	2300
38	TEMPERATURE	B.42, B.49				
39	STRAIN	B.45, B.53	ALUMINUM	1/8	0.96	2300
40	TEMPERATURE	B.43, B.47				
41	STRAIN	B.44, B.53	ALUMINUM	3/16	0.96	2300
42	TEMPERATURE	B.44, B.47				

TENSION TIES LEAF SPRING

INST. NO.	QUANTITY MEASURED	FIGURE REFERENCE				STATION
SHOT 9						
43	LOAD MONITOR	B.38				2300
44	LOAD MONITOR	B.41				6500
SHOT 10						
45	LOAD MONITOR	B.43				2300
46	LOAD MONITOR	B.42				2300

TABLE B.3 – Summary of Box Beam Data

MATERIAL	MG	AL	AL	MG	AL	MG	AL	AL	AL	AL	AL	AL	AL
THICKNESS (IN.)	3/16	3/16	3/16	1/8	1/8	3/16	1/8	3/16	1/4	1/4	1/4	3/16	3/16
ABSORPTIVITY	0.82	0.48	0.96	0.96	0.96	0.82	0.96	0.96					
STATION	2300	2300	2300	6500	6500	2300	2300	2300	2300	2300	2300	2300	2300
SHOT NO.	9	9	9	9	9	10	9	10	10	10	10	10	10
TEMPERATURE INST. NO.	2	4	6	10	8	12	14	16	18	20	22	24	26
STRAIN INST. NO.	1	3	5	9	7	11	13	15	17	19	21	23	25
INST. LOCATION	A	A	A	A	A	A	A	A	B	C	D	E	P
AMBIENT TEMPERATURE (°F)	83	71	84	73	83	79	75	89	83	76	81	86	87
TEMPERATURE OF EXPOSED FACE AT BLAST ARRIVAL (°F)	348	216	295	206	194	388	552	318	98	86	89	98	101
PEAK TEMPERATURE (°F)	362	236	312	210	197	412	568	323	183	172	162	150	140
TIME TO REACH PEAK TEMPERATURE (SEC)	4.0	6.5	4.5	7.0	6.75	3.0	1.4	1.04	7.5	18	42	44	44
STRAIN OF EXPOSED FACE AT BLAST ARRIVAL (10^{-3} IN./IN.)	-0.865	-0.890	-0.440	-0.565		-0.510	-1.060			1.250	0.475	0.078	0.020
PEAK STRAIN (10^{-3} IN./IN.)	-0.930	-0.224	-0.537	-0.565	-0.565	-1.080	-1.440	-0.258	1.310	1.310	0.500	0.078	0.043
TIME TO REACH PEAK STRAIN (SEC)	3.1	3.0	6.0	5.2	5.2	2.8	1.98	0.88	1.2	1.7	0.93		2.3

D E
C
B
P
A
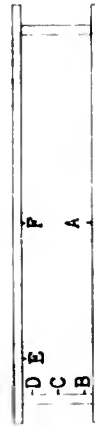
INSTALLATION LOCATIONS
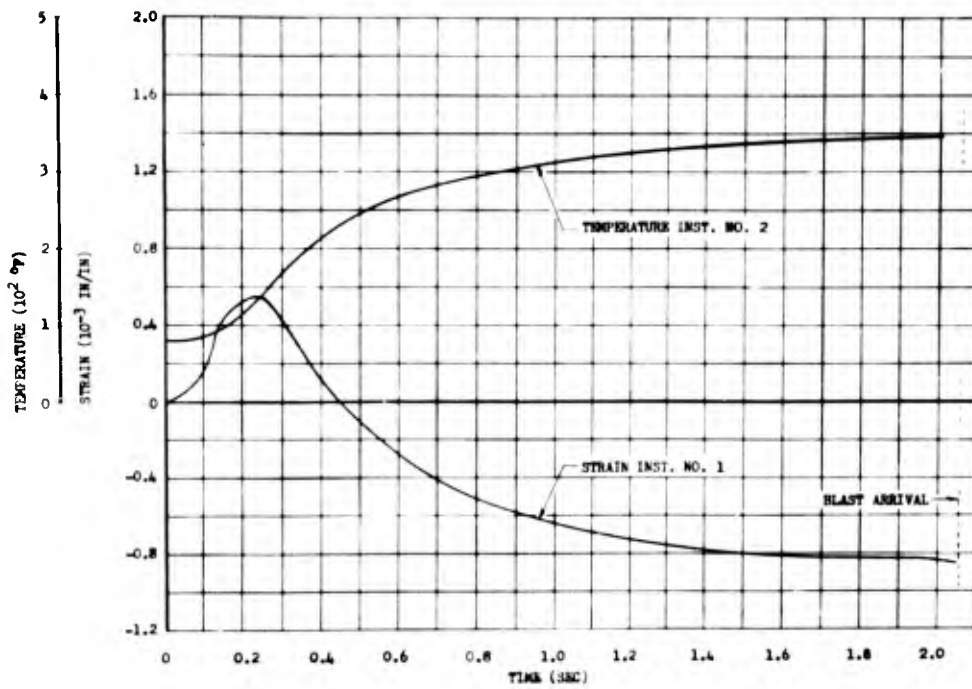
Fig. B.13 Exposed Face Strain and Temperature Rise as a Function of
Time of 3/16 in. Mg Box Beam (Absorptivity 0.82), Before
Blast Arrival, for Station 2300, Shot 9
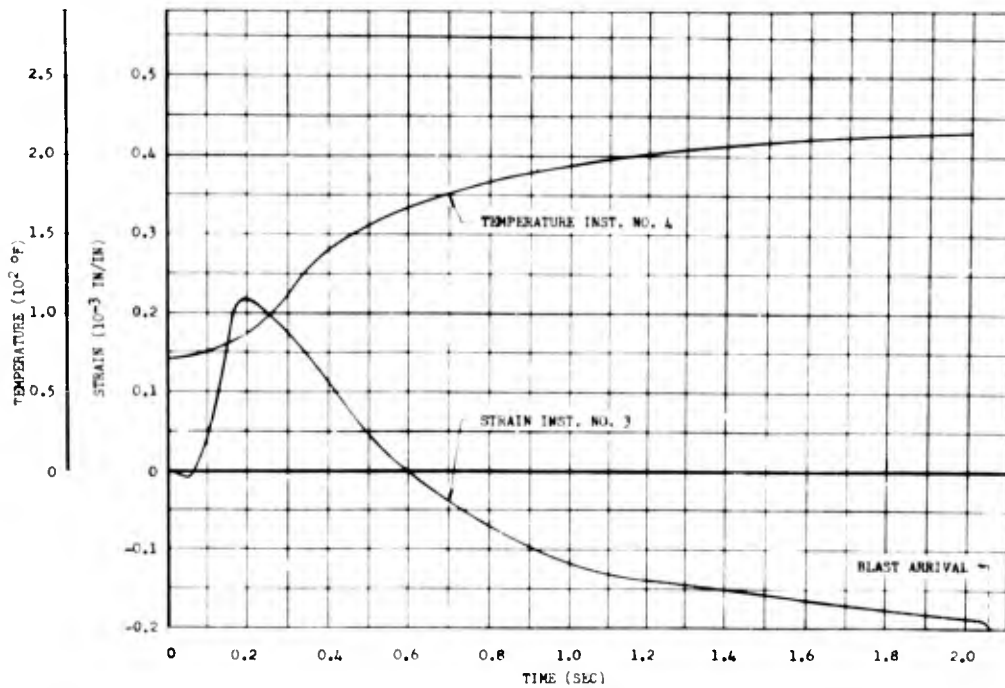
Fig. B.14 Exposed Face Strain and Temperature Rise as a Function of
Time of 3/16 in. of Al Box Beam (Absorptivity 0.48), Before
Blast Arrival, for Station 2300, Shot 9

104
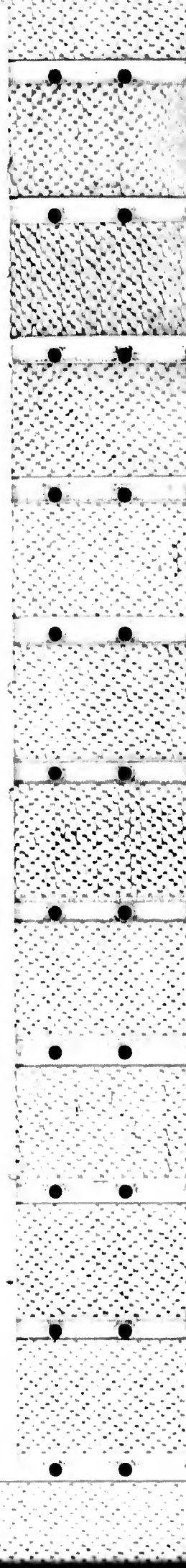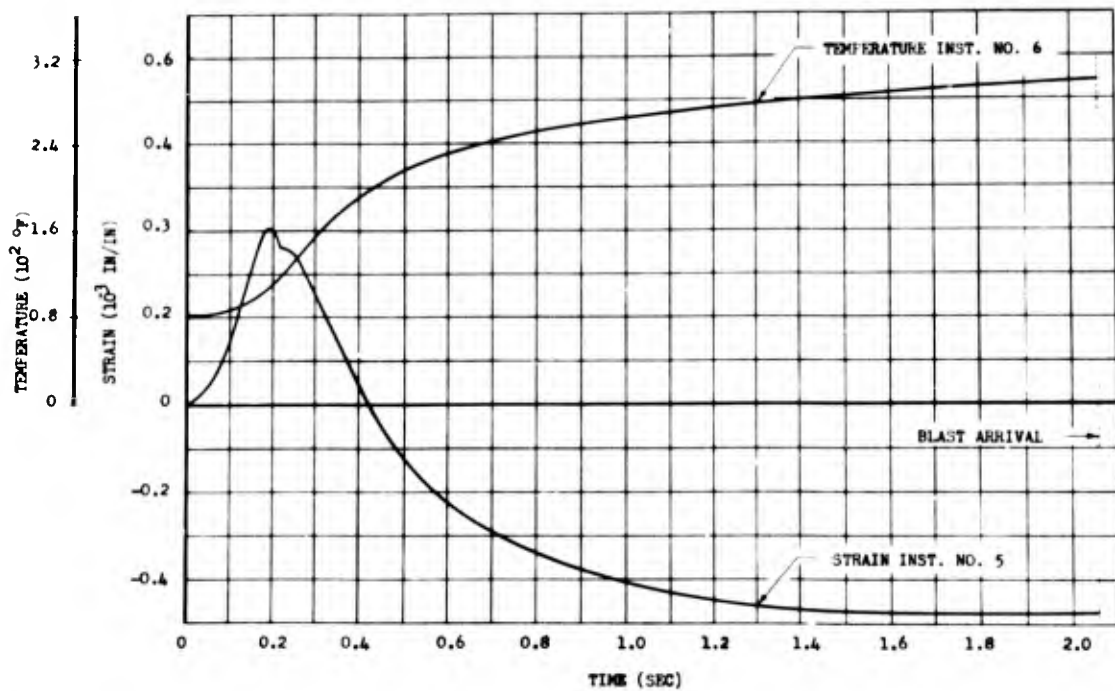
Fig. B. 15 Exposed Face Strain and Temperature Rise as a Function of Time of 3/16 in. Al Box Beam (Absorptivity 0.96), Before Blast Arrival, for Station 2300, Shot 9
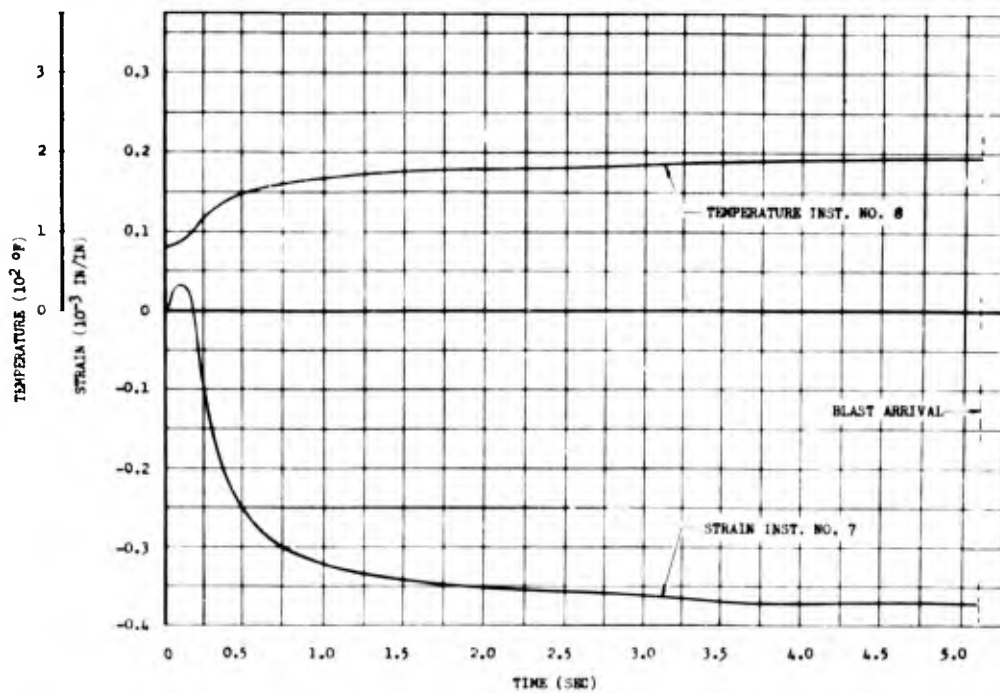
Fig. B. 16 Exposed Face Strain and Temperature Rise as a Function of Time of 1/8 in. Al Box Beam (Absorptivity 0.96), Before Blast Arrival, for Station 6500, Shot 9

105
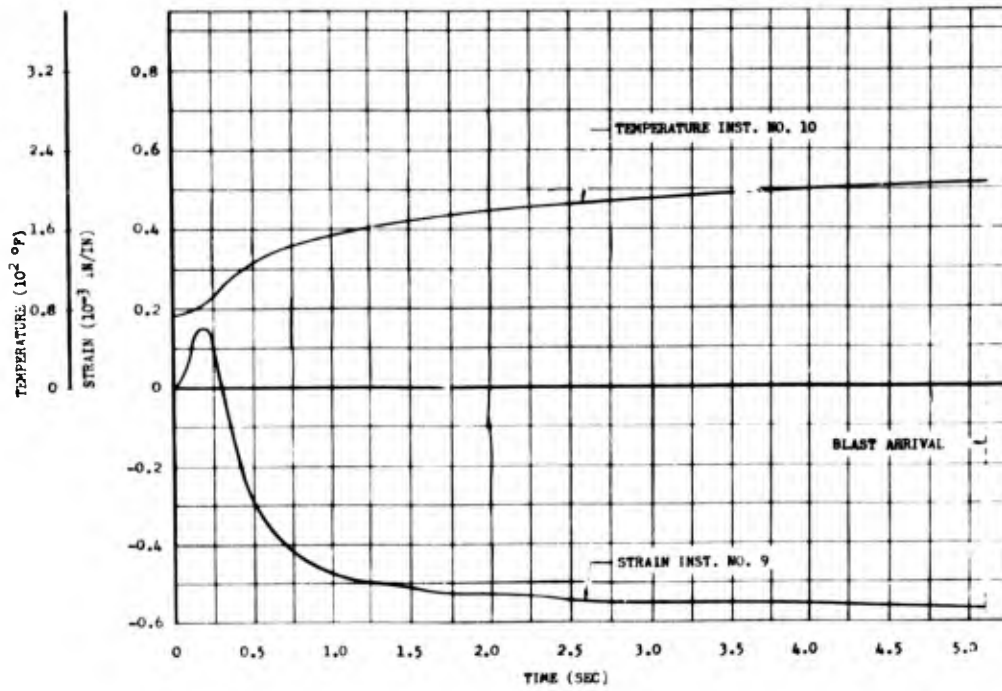
Fig. B.17 Exposed Face Strain and Temperature Rise as a Function of
Time of 1/8 in. Mg Box Beam (Absorptivity 0.96), Before
Blast Arrival, for Station 6500, Shot 9
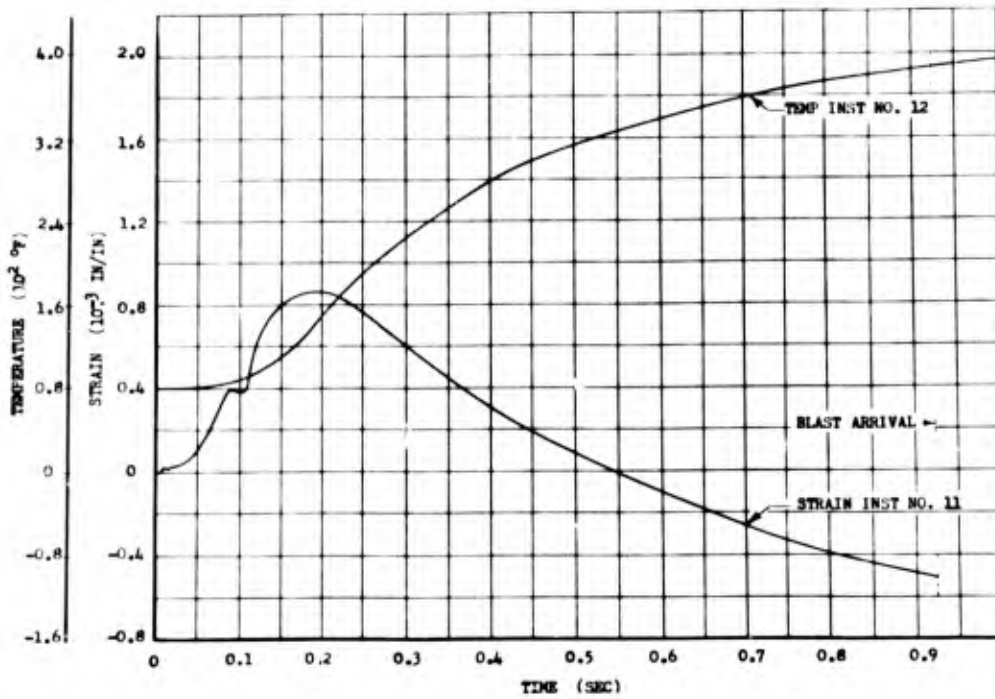
Fig. B.18 Exposed Face Strain and Temperature Rise as a Function of
Time of 3/16 in. Mg Box Beam (Absorptivity 0.82), Before
Blast Arrival, for Station 2300, Shot 10

106
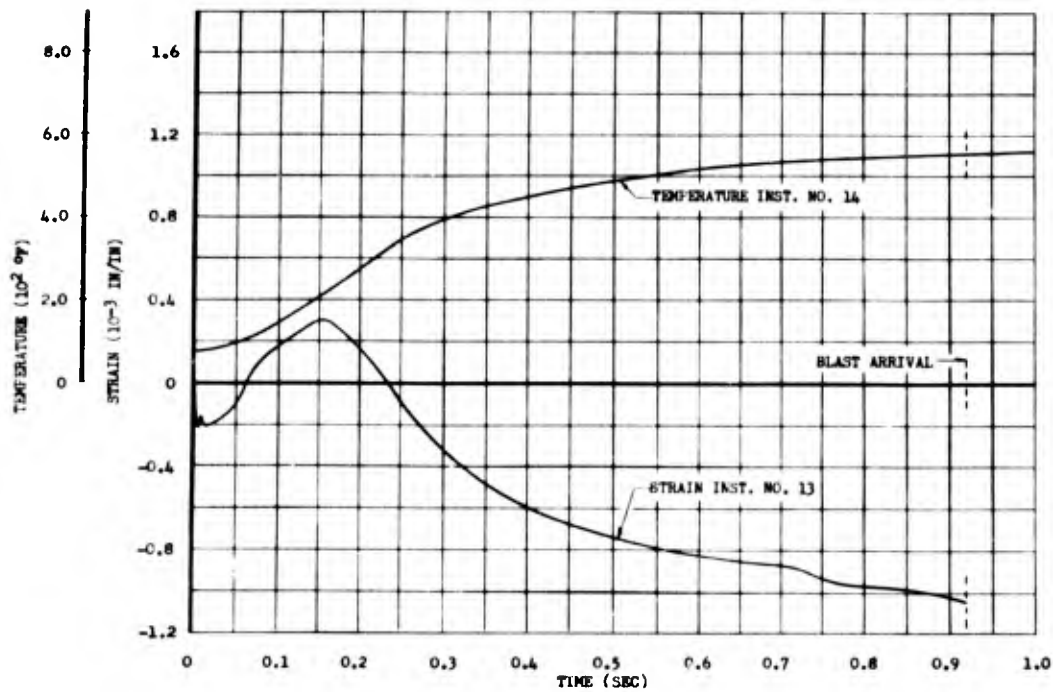
Fig. B.19 Exposed Face Strain and Temperature Rise as a Function of Time of 1/8 in. Al Box Beam (Absorptivity 0.96), Before Blast Arrival, for Station 2300, Shot 10
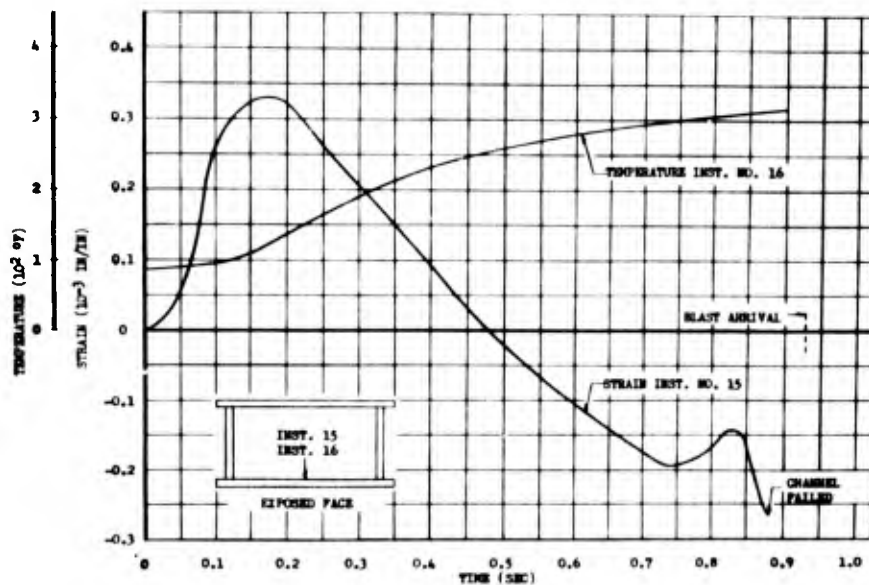
Fig. B.20 Exposed Face Strain and Temperature Rise as a Function of Time of 3/16 in. Al Box Beam (Absorptivity 0.96), Before Blast Arrival, for Station 2300, Shot 10

107

installation on the 12-channel box beam are shown in Fig. B.21. The complete time-history temperature data for the front face of each box beam at Station 2300, Shot 9, are given in Fig. B.22, at Station 6500, Shot 9, in Fig. B.23, and at Station 2300, Shot 10, in Fig. B.24. In addition, all the time-history temperature data for the 12-channel box beam are shown in Fig. B.25. The time-history strain response curves during the blast phase for each box beam are shown in Figs. B.26 through B.37. The peak temperature data obtained from the temp-tape installation are summarized in Table B.4.

B.3.2   Tension Ties

A summary of the peak temperature and strain data obtained on each tension tie specimen is given in Table B.5. Included in this table is the measured elongation over a 10 in. interval and a summary of the cross-sectional areas for every inch, 5 in. above and 5 in. below the strain gage. Because of the change in cross-sectional area, all load data are presented as total load rather than unit load.

A comparison of the time-history temperature, strain, and load data for each tension tie is shown in Figs. B.38 through B.44. The complete time-history temperature data are shown for each tension tie at Station 2300, Shot 9, in Fig. B.45, at Station 6500, Shot 9, in Fig. B.46 and at Station 2300, Shot 10, in Fig. B.47. No time-history data were available for the 1/8 in. magnesium (abs. 0.96) tie at Station 6500, Shot 9. The temperature-time curve for Inst. No. 28 (indicated as a broken line in Figs. B.38 and B.45) was extrapolated parallel to comparable measured time-history data and is believed to be within ±10 per cent. The tensile load vs time data, indicated by broken line curves in Fig. B.39 through B.44, were calculated from the time-history temperature and strain data for the particular tension tie and also from analysis of measured load-time data from other tension ties and are believed to be within ±5 per cent.

B.4   DISCUSSION

The thermal and blast inputs realized during Shot 9 were somewhat lower than expected because of a lower than predicted yield which, coupled with the bombing error, substantially reduced the energy levels at the test stations. The time-history temperature curves obtained at Station 2300 during Shot 10 rose more rapidly and peaked much sooner than comparable temperature data obtained during Shot 9 because the dust raised by the shock front during Shot 10 highly attenuated the radiant energy reaching this exposure station.

An unexpected phenomenon common to all the box beam and tension tie strain data is the appearance of a large positive strain pulse beginning at time zero. In all probability this is caused by a temperature

gradient through the instrumented skin of the specimens. Since the exposed face was restrained from buckling, the initial temperature distribution produced tensile strain in the rear fiber where the strain gage was mounted. However, in the case of the box beams, the net effective reaction of the exposed face expansion upon the webs and rear face was still tensile strain, as seen from Figs. B.21 and B.48 for the 12-channel box beam. It would appear, therefore, that during the initial heating of the specimen, the strain of the exposed face is not representative of the effect of this face upon the restraining members of the box beam.

B.4.1   Box Beams

To aid in the analysis of the box beam data, curves of strain vs temperature rise are present in Figs. B.48 through B.52. In general, these curves are extended to the peak temperature attained by the particular specimen, unless this is prohibited by the failure of both the strain and temperature channel. The oscillations caused by the blast wave were omitted so as to present the response of the specimen to the thermal energy only.

B.4.2   Tension Ties

Stress-strain curves for the tension ties are shown in Fig. B.53 and B.54 for aluminum and magnesium specimens, respectively. The values of stress used in preparation of these curves were computed from the preshot cross-sectional areas and load curve presented in para. B.3.2 for each tension tie. The values of strain were taken from the strain-time curves presented in para. B.3.2 for each specimen; however, an interpolation of the first portion of the curve was made to eliminate the initial positive strain caused by the temperature gradient.

As is indicated in Fig. B.53, the only aluminum tension tie to yield during either shot was the 1/8 in. thick specimen at Station 2300 during Shot 10. It attained a temperature of 580°F and a 0.2 per cent elongation at the strain gage after 1.005 sec exposure. Two magnesium tension ties exceeded the yield point. The first was the 1/8 in. thick specimen at Station 6500 during Shot 9, and the second was the 3/16 in. thick specimen at Station 2300 during Shot 10. No time-history data were available from the 1/8 in. thick specimen; however, it elongated 7/32 in. over a 10 in. length for an average elongation of 2.2 per cent. The second magnesium specimen attained a temperature of 273°F and elongated 0.2 per cent at the strain gage after 0.38 sec exposure time.

109
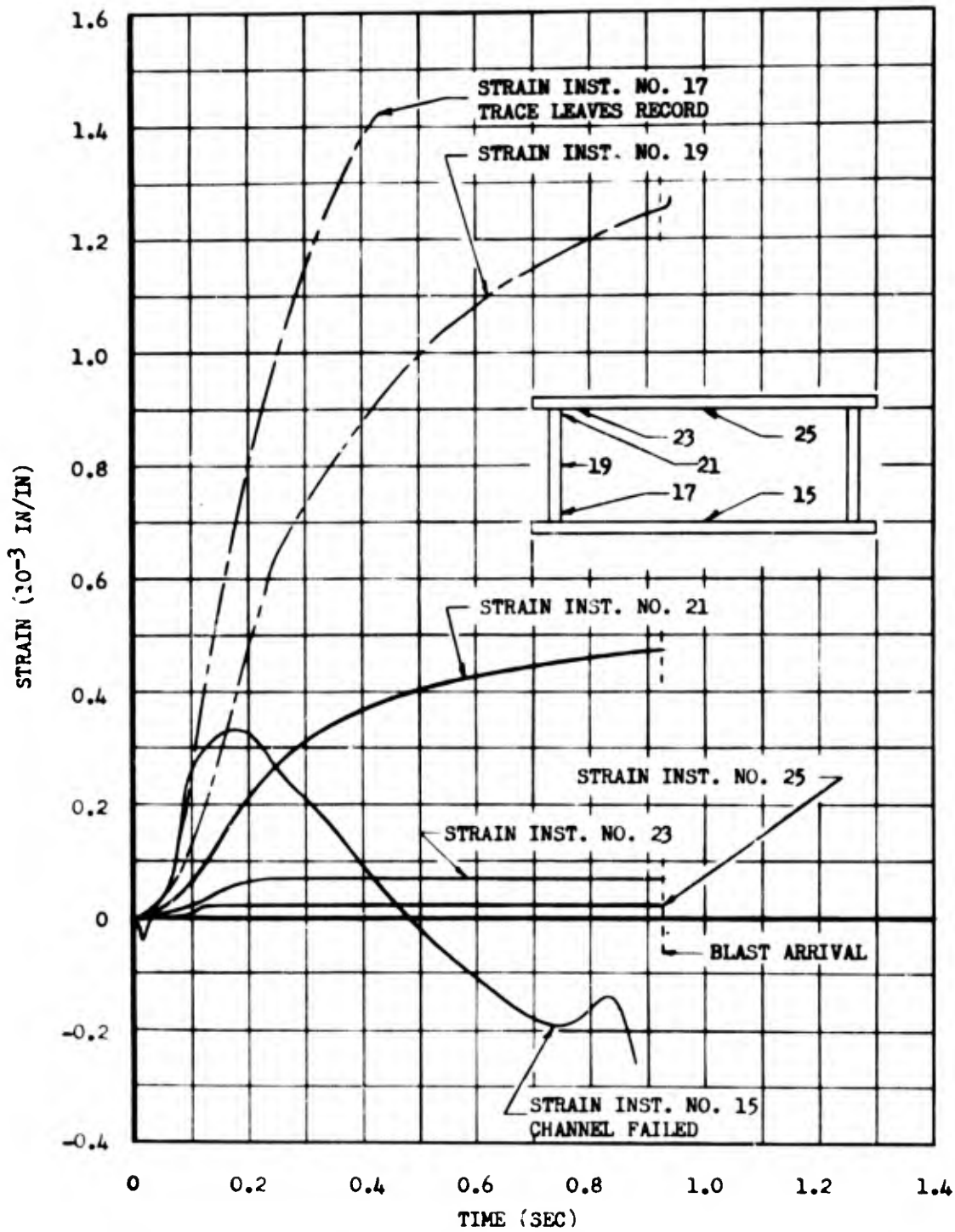
Fig. B.21 Strains as a Function of Time of 3/16 in. Al Box Beam, (Absorptivity 0.96), Before Blast Arrival, Station 2300, Shot 10

110
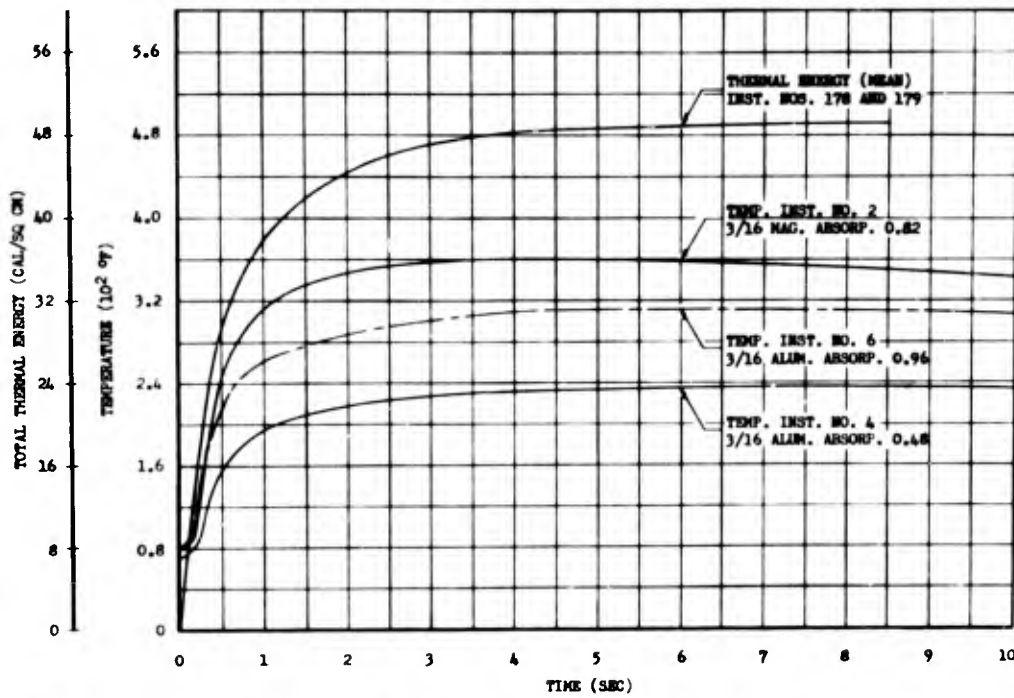
Fig. B.22 Comparison of Box Beam Temperatures and Thermal Energy
as a Function of Time for Station 2300, Shot 9
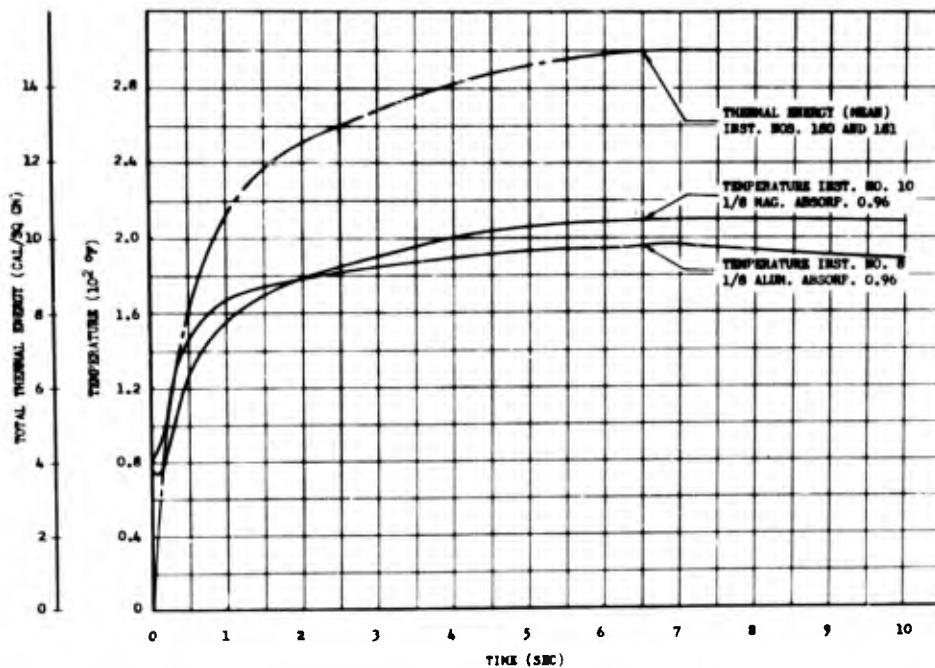
Fig. B.23 Comparison of Box Beam Temperatures and Thermal Energy
as a Function of Time for Station 6500, Shot 9

111
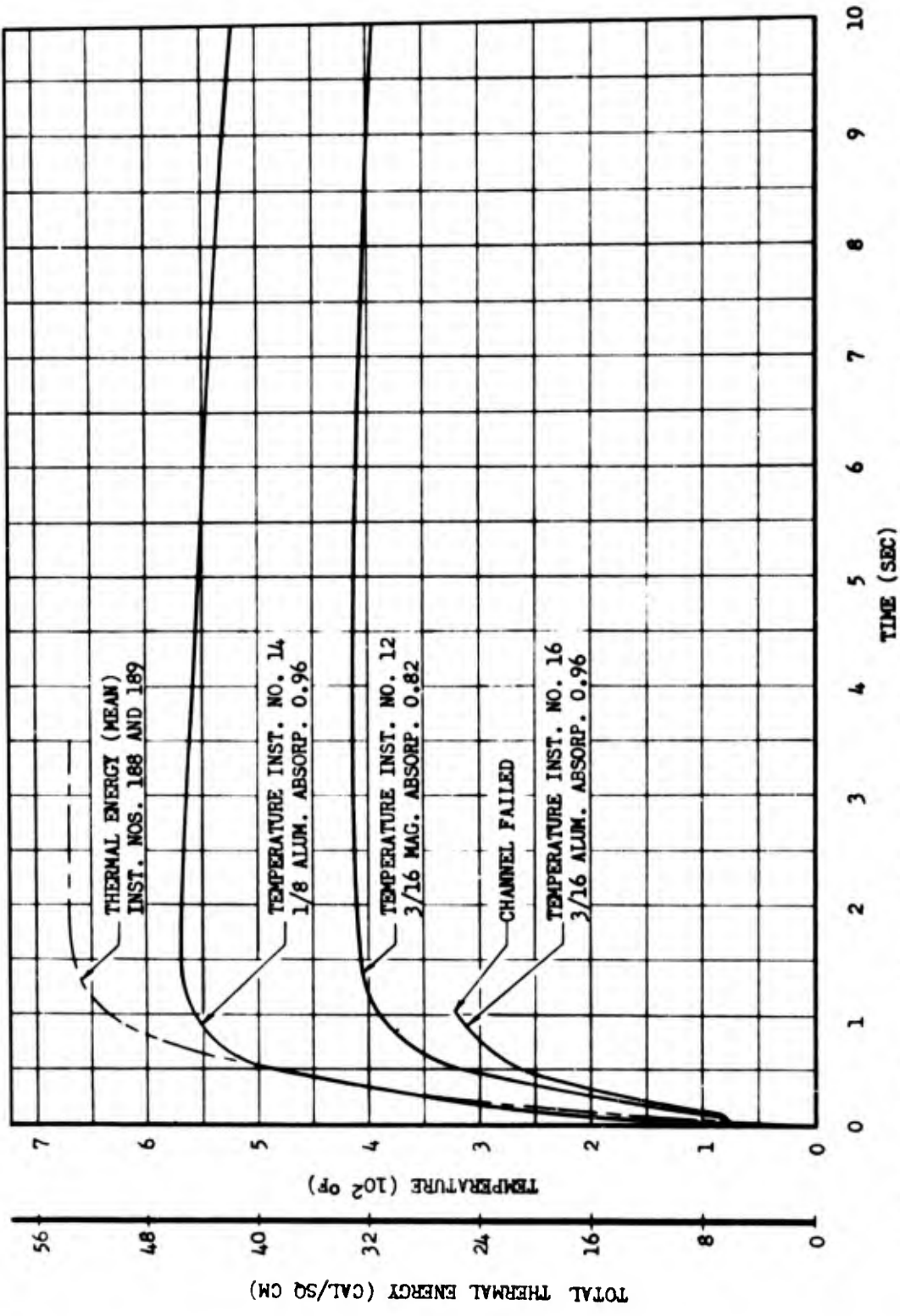
Fig. B.24 Comparison of Box Beam Temperatures and Thermal Energy as a Function of Time for Station 2300, Shot 10

112
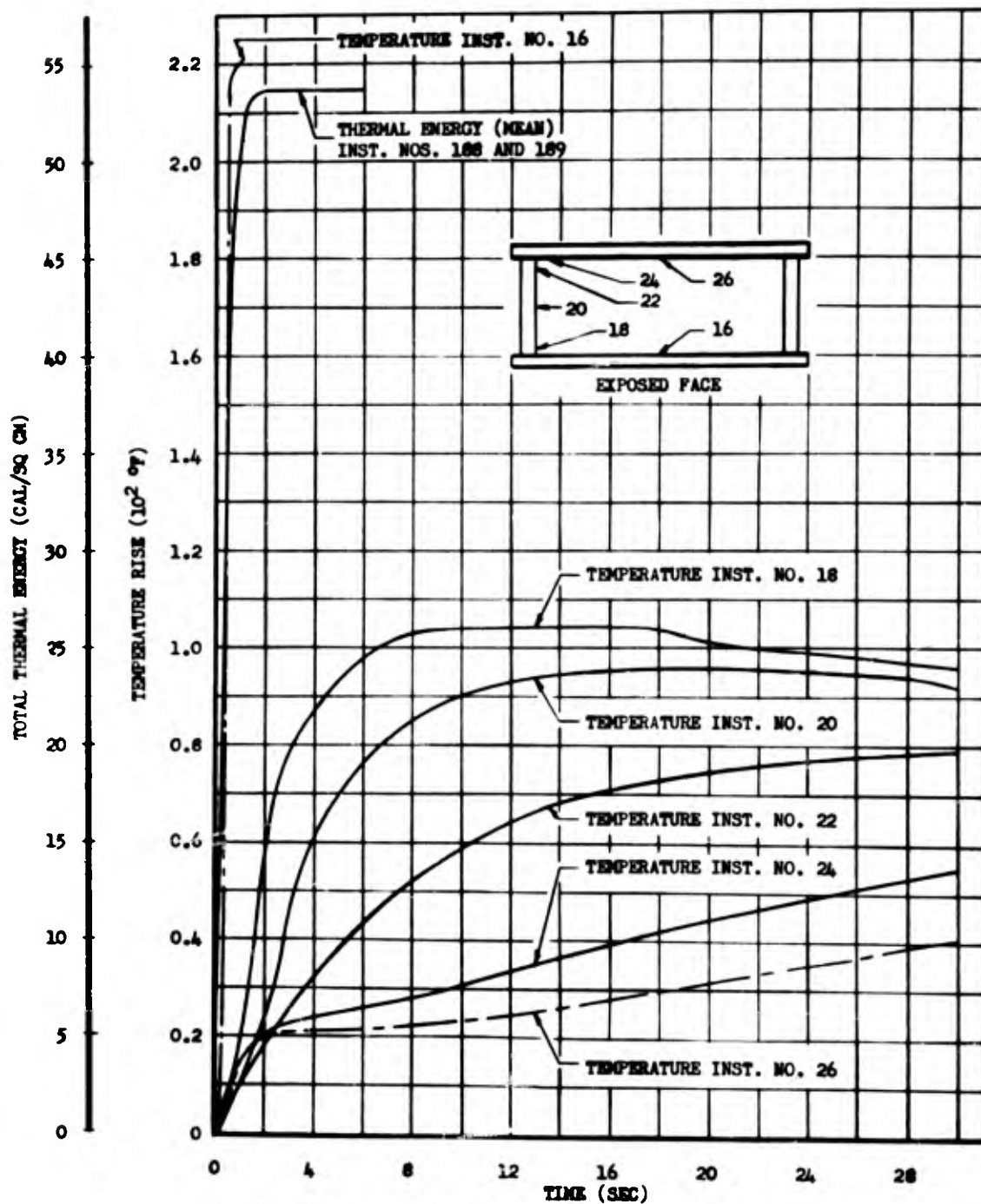
Fig. B.25 Comparison of Time-Temperature Data of 3/16 in. Al Box
Beams (Absorptivity 0.96), and Thermal Energy as a
Function of Time for Station 2300, Shot 10

113

TABLE B.4 - Peak Temperature Attained on Box Beams (Temp-Tape Data)

	SHOT 9					SHOT 10		
	STATION 2300			STATION 6500		STATION 2300		
THICKNESS* (IN.)	3/16 MAG	3/16 AL	3/16 AL	1/8 AL	1/8 MAG	3/16 MAG	1/8 AL	3/16 AL
MATERIAL ABSORPTIVITY	0.82	0.48	0.96	0.96	0.96	0.82	0.96	0.96
LOCATION CODE**			PEAK TEMPERATURE (°F)					
9" STATION								
a	360***	236***	311***	196***	209***	412***	573***	>322***
b	178-195	144-170	171-177	<123	<123	195-224	178-194	184***
c	144-170	123	144-170	<123	<123	178-194	178-194	>162***
d	195-224	144-170	171-177	<123	<123	178-194	195-224	144-170
e	144-170	<123	144-170	<123	<123	171-177	178-194	<123
f	144-170	<123	144-170	<123	<123	144-170	144-170	>139***
15" STATION								
a	360***	236***	311***	196***	209***	412***	573***	>322***
b	232-252	171-177	232-252	<123	<123	232-252	225-231	178-194
c	178-194	144-170	171-177	<123	<123	178-194	178-194	144-160
d	195-224	144-170	195-224	<123	<123	232-252	232-252	178-194
e	178-194	144-170	144-170	<123	<123	178-194	178-194	144-160
f	144-170	<123	144-170	<123	<123	144-170	178-194	>139***
31" STATION								
a	377-423	232-252	309-330	195-224		377-423	517-539	288-308
b	178-194	144-170	171-178	<123		195-224	225-231	178-194
c	178-194	<123	171-178	<123		178-194	144-170	144-160
d	178-194	144-170	171-178	<123		195-224	178-194	171-178
e	178-194	<123	171-178	<123		178-194	144-170	171-178
f	144-170	<123	<122	<123		144-170	144-170	<123

* THIS APPLIES TO LOCATIONS a AND f. OTHER LOCATIONS ARE 1/4" THICK.

** FOR LOCATION ON BOX BEAM SEE FIG. B.9.

*** THERMOCOUPLE VALUE.

114

TABLE B.5 - Summary of Tension Tie Data

MATERIAL	MG	AL	AL	MG	AL	MG	AL	AL
THICKNESS (IN.)	3/16	3/16	3/16	1/8	1/8	3/16	1/8	3/16
ABSORPTIVITY	0.82	0.48	0.96	0.96	0.96	0.82	0.96	0.96
STATION	2300	2300	2300	6500	6500	2300	2300	2300
SHOT NUMBER	9	9	9	9	9	10	10	10
PRELOAD (LB)	1560	4810	4810	2960	6520	2860	4420	6860
TEMPERATURE INST. NO.	28	30	32	34	36	38	40	42
STRAIN INST. NO.	27	29	31	33	35	37	39	41
AMBIENT TEMPERATURE (°F)	63	62	77		69	69	70	68
PEAK TEMPERATURE (°F)	404	261.5	365		173	421	591	334
TIME TO REACH PEAK TEMPERATURE (SEC)	4.50	8.05	6.60		6.25	2.50	1.50	1.42
PEAK STRAIN* (10^{-3} IN./IN.)	2.60	4.40	3.65		7.546	1.79	9.79	5.466
TIME TO REACH PEAK STRAIN (SEC)	0.285	0.285	0.203		0.250	9.85	1.66	0.242
ELONGATION OVER 10 IN. LENGTH (IN.)	0	0	0	7/32	0	7/16	1/4	1/32
ACTUAL PRESHOT THICKNESS OF TIE (IN.)	0.195	0.190	0.190	0.124	0.125	0.192	0.125	0.194
PRESHOT CROSS-SECTIONAL AREA AT STRAIN GAGE (SQ IN.)	0.146	0.143	0.142	0.093	0.094	0.143	0.094	0.146

POSTSHOT CROSS-SECTIONAL AREA AS INDICATED (SQ IN.)
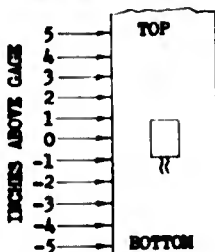
INCHES ABOVE GAGE	TOP / BOTTOM	MG	AL	AL	MG	AL	MG	AL	AL
5	5	0.150	0.142	0.142	0.092	0.094	0.142	0.094	0.145
4	4	0.148	0.142	0.142	0.092	0.094	0.139	0.094	0.144
3	3	0.148	0.142	0.142	0.091	0.094	0.138	0.092	0.144
2	2	0.147	0.142	0.141	0.089	0.093	0.137	0.093	0.144
1	1	0.146	0.143	0.141	0.087	0.093	0.136	0.090	0.144
0	0	0.146	0.142	0.140	0.087	0.093	0.136	0.092	0.144
-1	-1	0.146	0.142	0.140	0.087	0.093	0.137	0.092	0.144
-2	-2	0.147	0.142	0.140	0.090	0.094	0.138	0.092	0.144
-3	-3	0.147	0.143	0.141	0.091	0.093	0.138	0.093	0.144
-4	-4	0.147	0.142	0.142	0.091	0.094	0.139	0.092	0.144
-5	-5	0.148	0.142	0.141	0.091	0.094	0.139	0.092	0.144

* DUE TO THERMAL ONLY

115
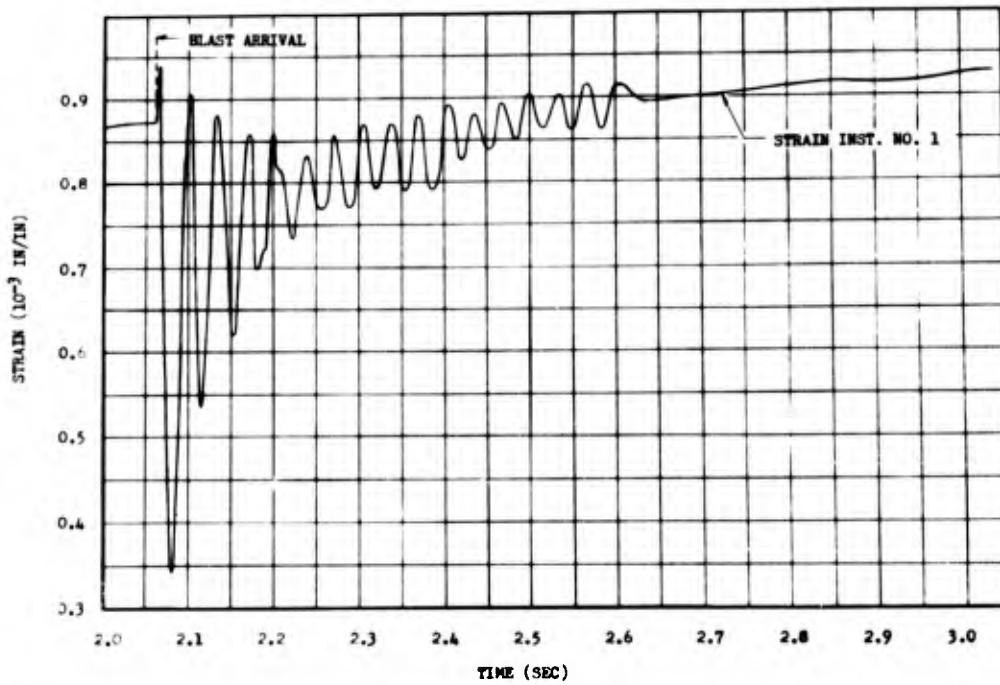
Fig. B.26 Exposed Face Strain as a Function of Time of 3/16 in. Mg
Box Beam (Absorptivity 0.82), for Station 2300, Shot 9
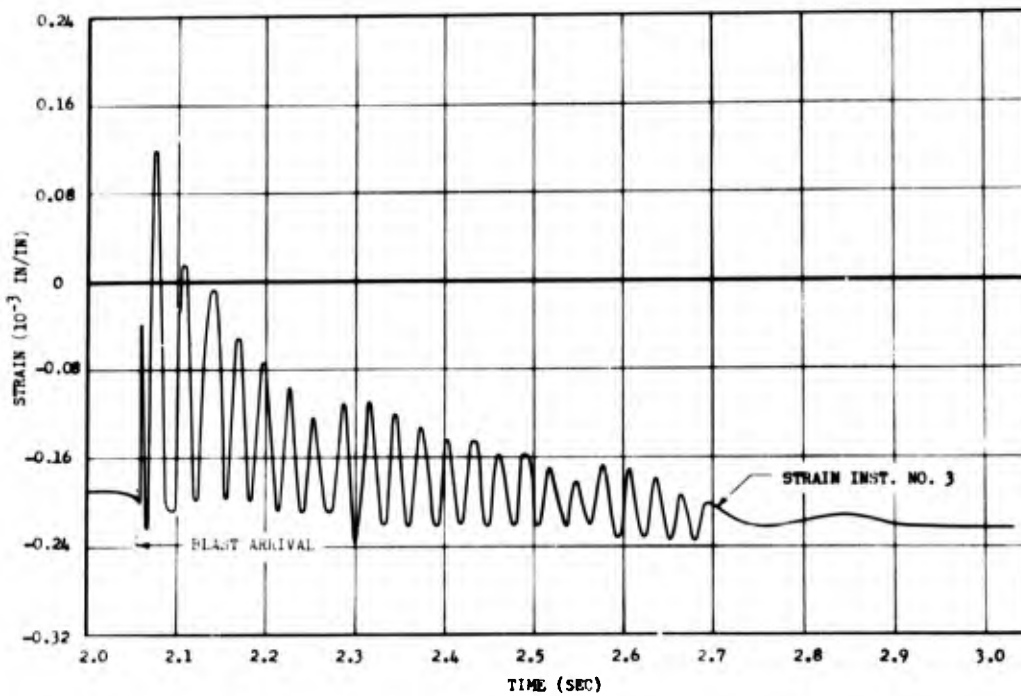
Fig. B.27 Exposed Face Strain as a Function of Time of 3/16 in. Al
Box Beam, (Absorptivity 0.48), for Station 2300, Shot 9

116
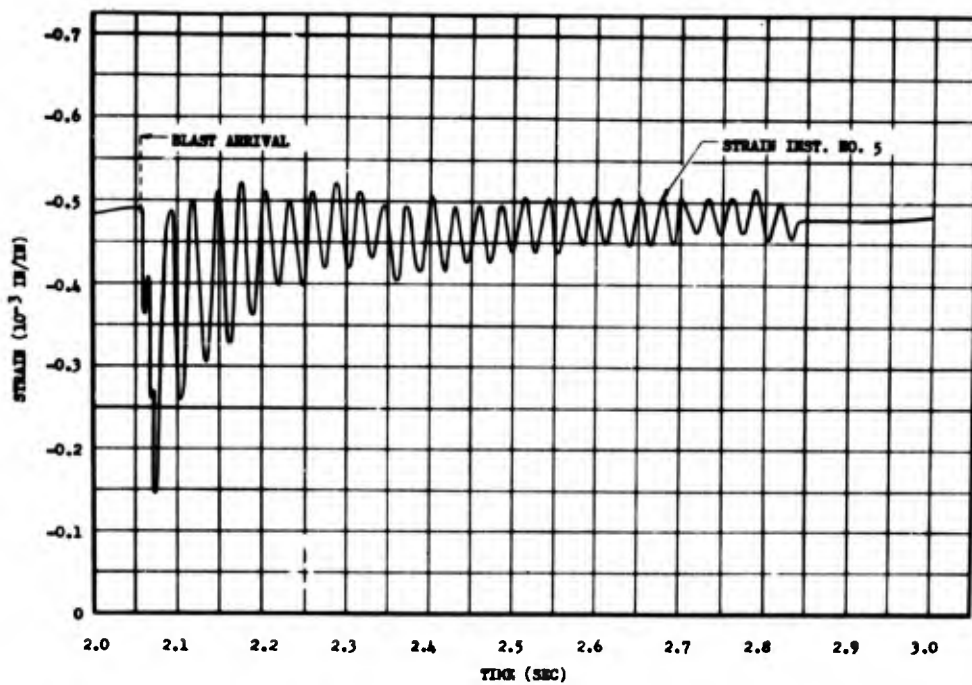
Fig. B.28 Exposed Face Strain as a Function of Time of 3/16 in. Al
Box Beam (Absorptivity 0.96), After Blast Arrival, for
Station 2300, Shot 9
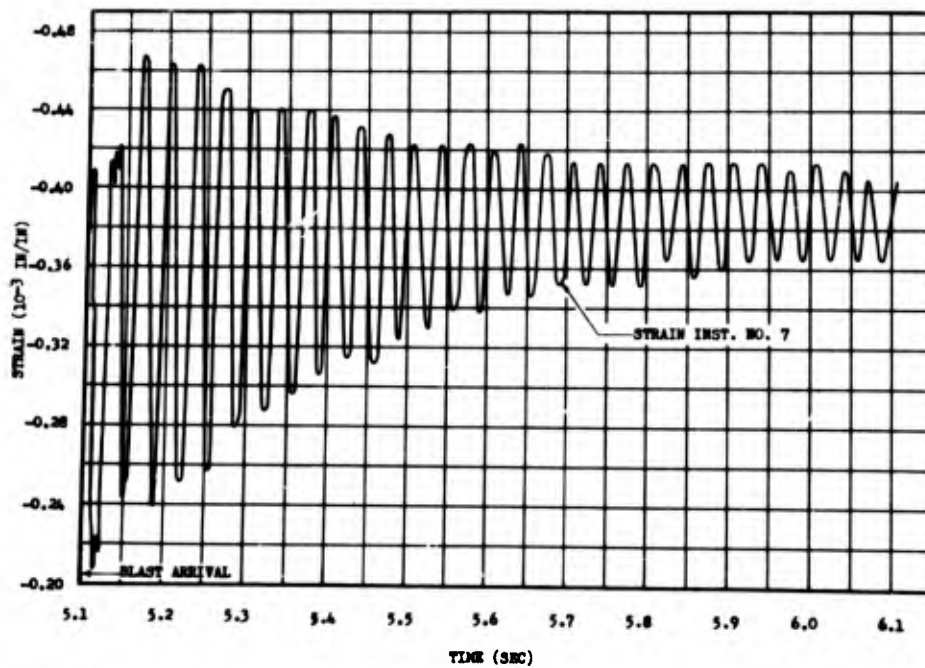
Fig. B.29 Exposed Face Strain as a Function of Time of 1/8 in. Al
Box Beam (Absorptivity 0.96), After Blast Arrival, for
Station 6500, Shot 9

117
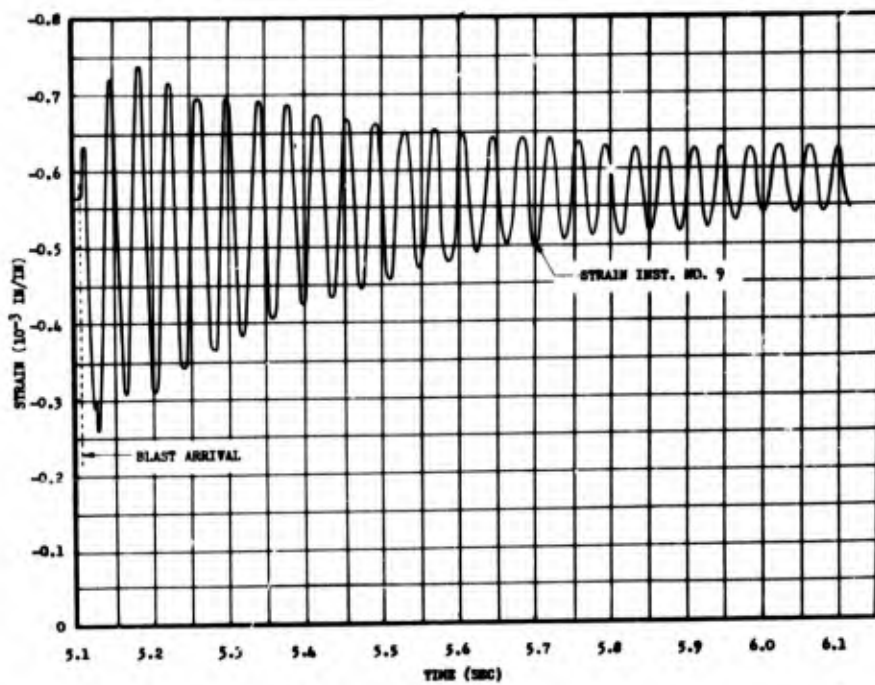
Fig. B.30 Exposed Face Strain as a Function of Time of 1/8 in. Mg
Box Beam (Absorptivity 0.96), After Blast Arrival, for
Station 6500, Shot 9
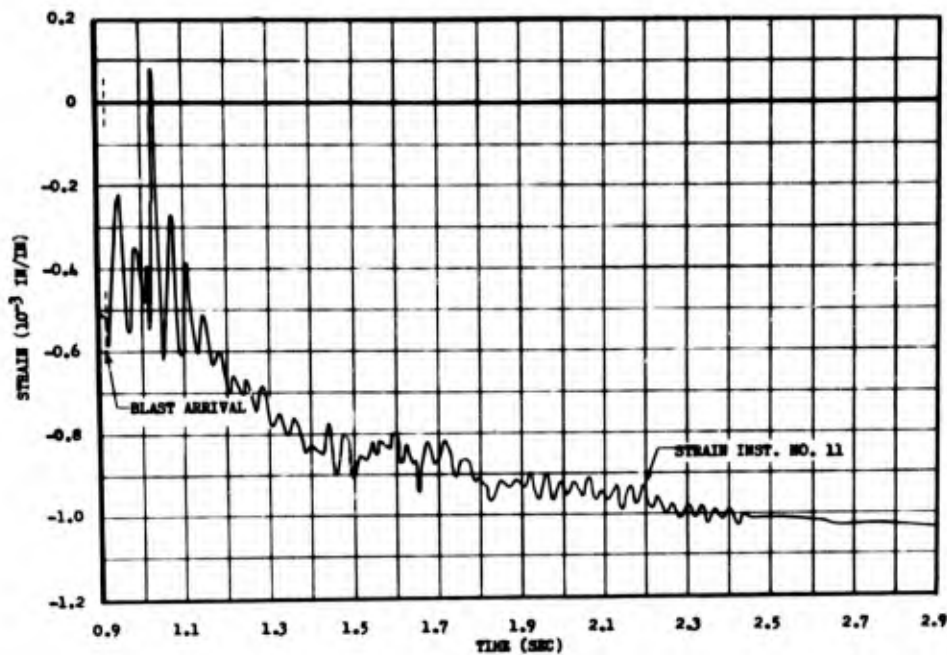
Fig. B.31 Exposed Face Strain as a Function of Time of 3/16 in. Mg
Box Beam (Absorptivity 0.82), After Blast Arrival for
Station 2300, Shot 10

118
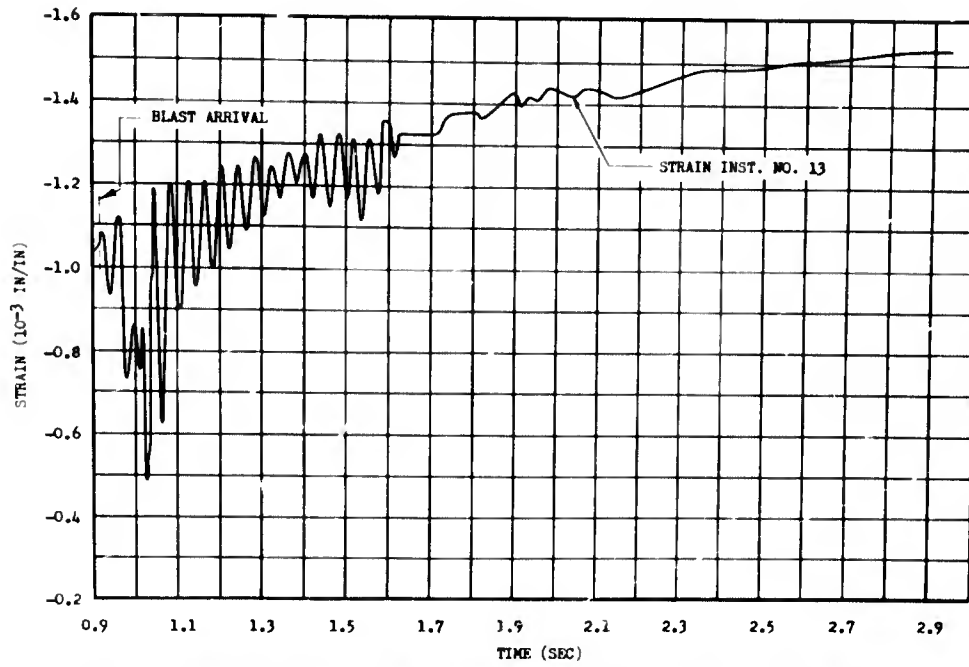
Fig. B.32 Exposed Face Strain as a Function of Time of 1/8 in. Al Box Beam (Absorptivity 0.96), After Blast Arrival, for Station 2300, Shot 10
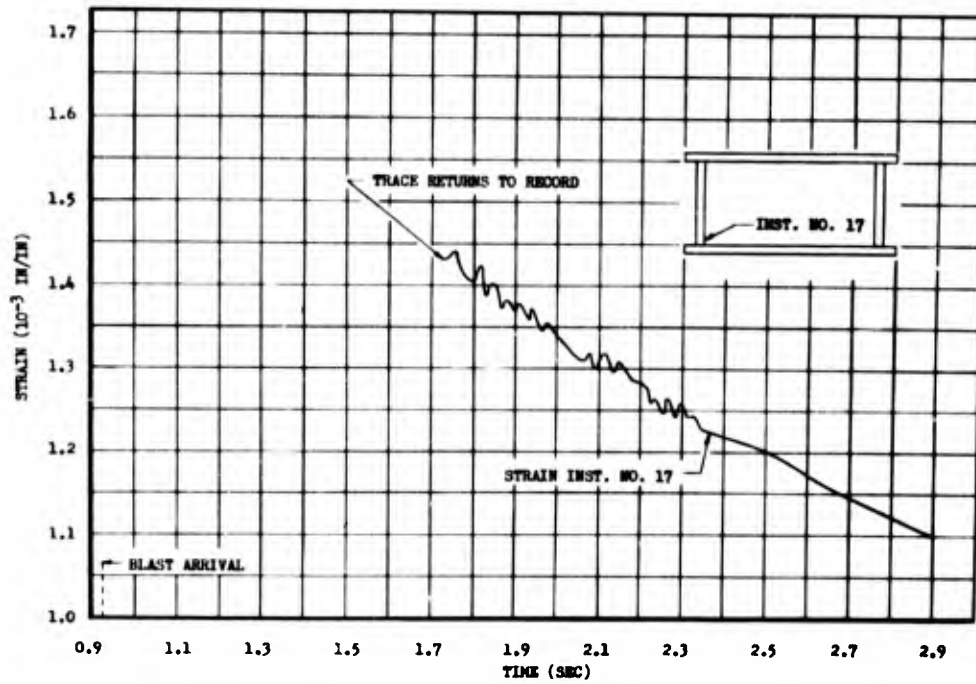
Fig. B.33 Web Strain as a Function of Time of 3/16 in. Al Box Beam (Absorptivity 0.96), After Blast Arrival, for Station 2300, Shot 10

119
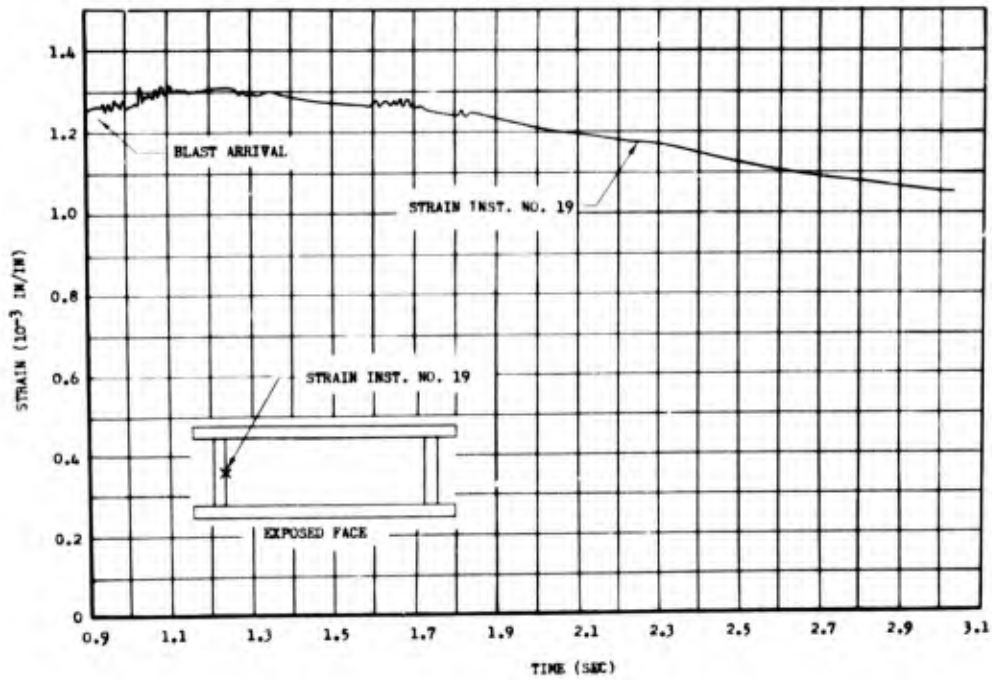
Fig. B.34 Web Strain as a Function of Time of 3/16 in. Al Box Beam
(Absorptivity 0.96), After Blast Arrival, for Station 2300,
Shot 10
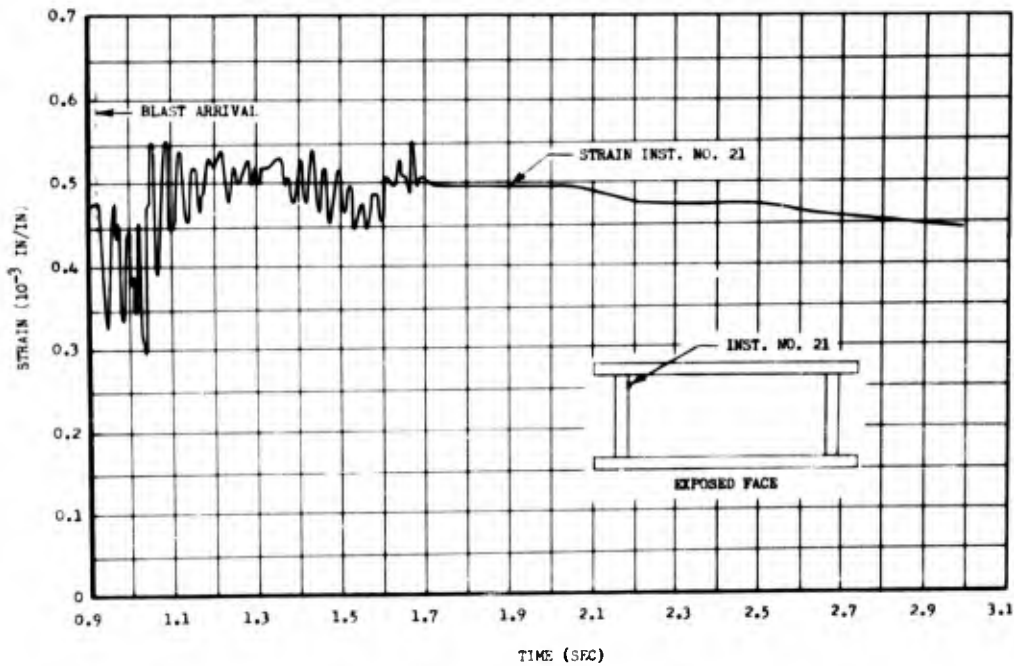
Fig. B.35 Web Strain as a Function of Time of 3/16 in. Al Box Beam
(Absorptivity 0.96), After Blast Arrival, for Station 2300,
Shot 10

120
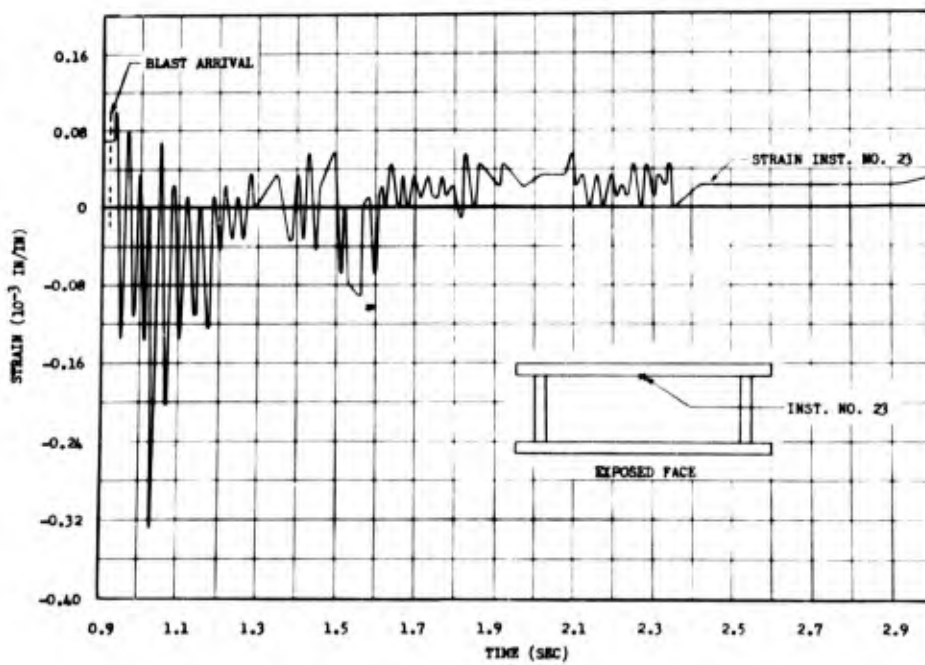
Fig. B.36 Rear Face Strain as a Function of Time of 3/16 in. Al Box Beam (Absorptivity 0.96), After Blast Arrival, for Station 2300, Shot 10
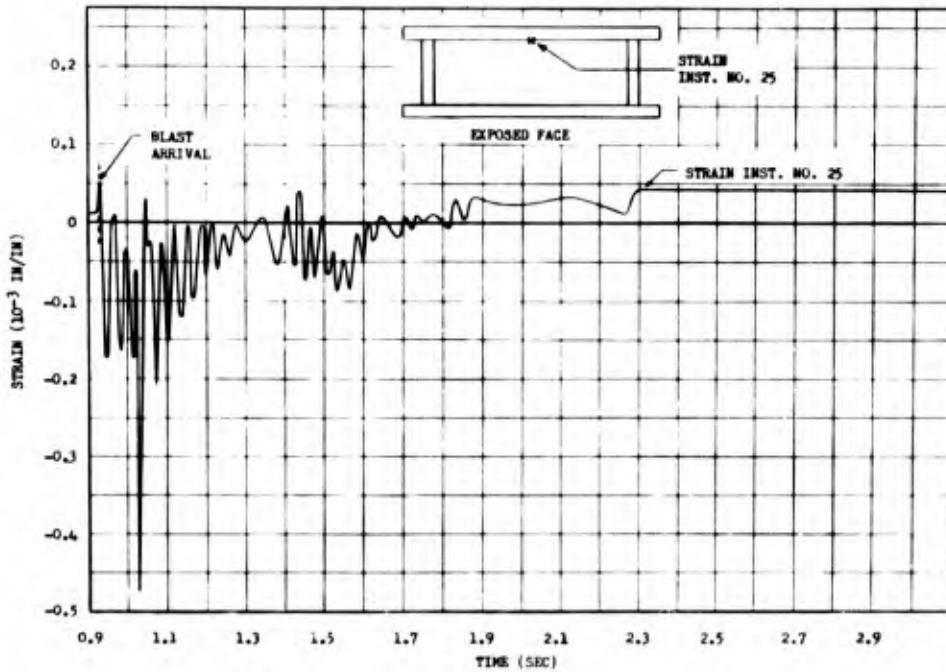
Fig. B.37 Rear Face Strain as a Function of Time of 3/16 in. Al Box Beam (Absorptivity 0.96), After Blast Arrival, for Station 2300, Shot 10

121
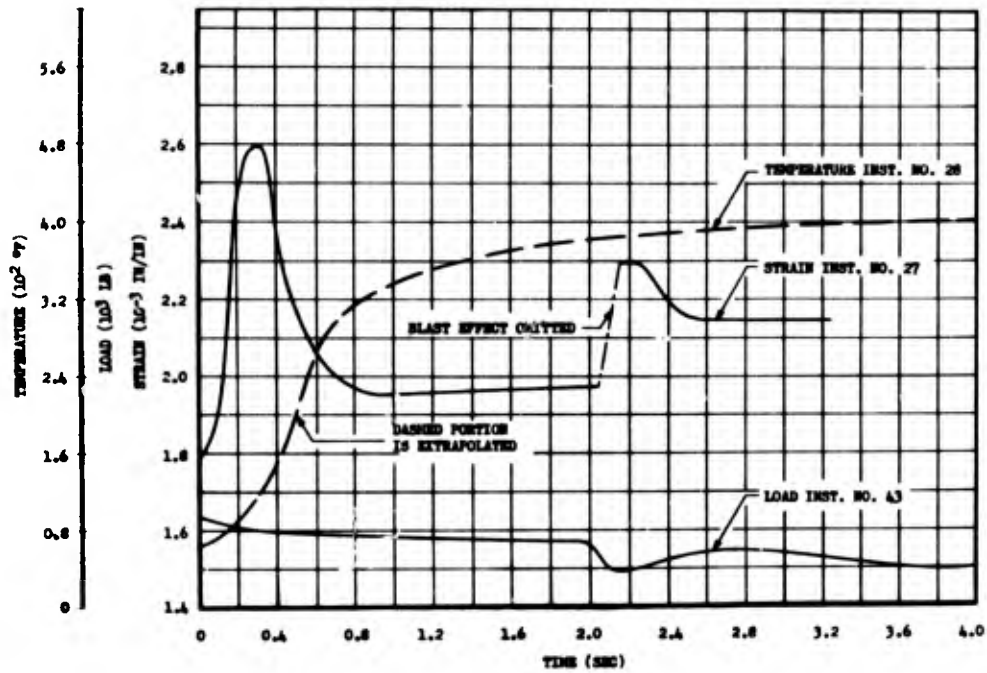
Fig. B.38 Strain, Temperature Rise, and Load as a Function of Time of 3/16 in. Mg Tension Tie (Absorptivity 0.82), for Station 2300, Shot 9. Cross-sectional area was 0.146 sq in.
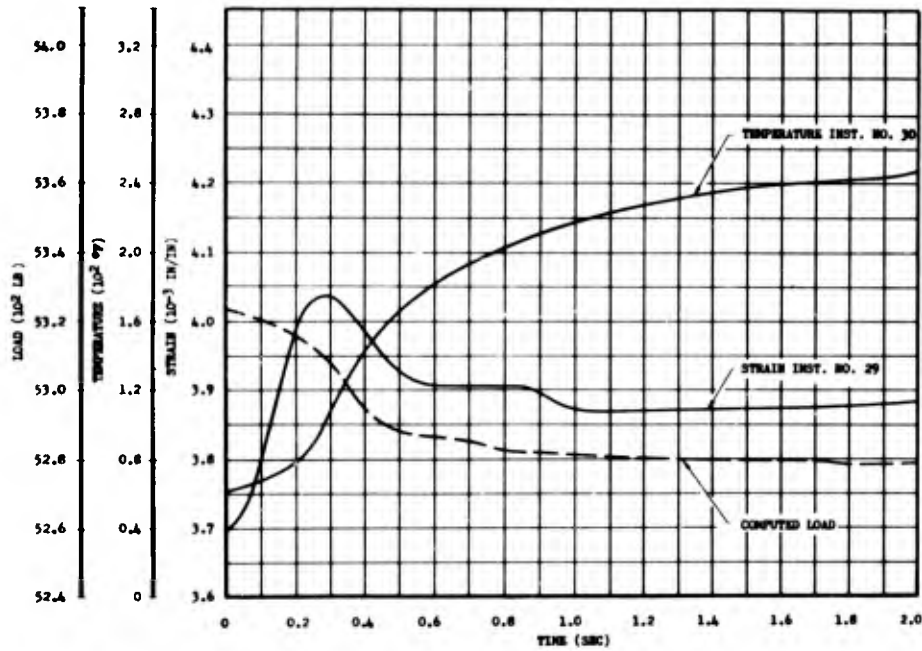
Fig. B.39 Strain, Temperature Rise, and Load as a Function of Time of 3/16 in. Al Tension Tie (Absorptivity 0.48), for Station 2300, Shot 9. Cross-sectional area was 0.143 sq in.
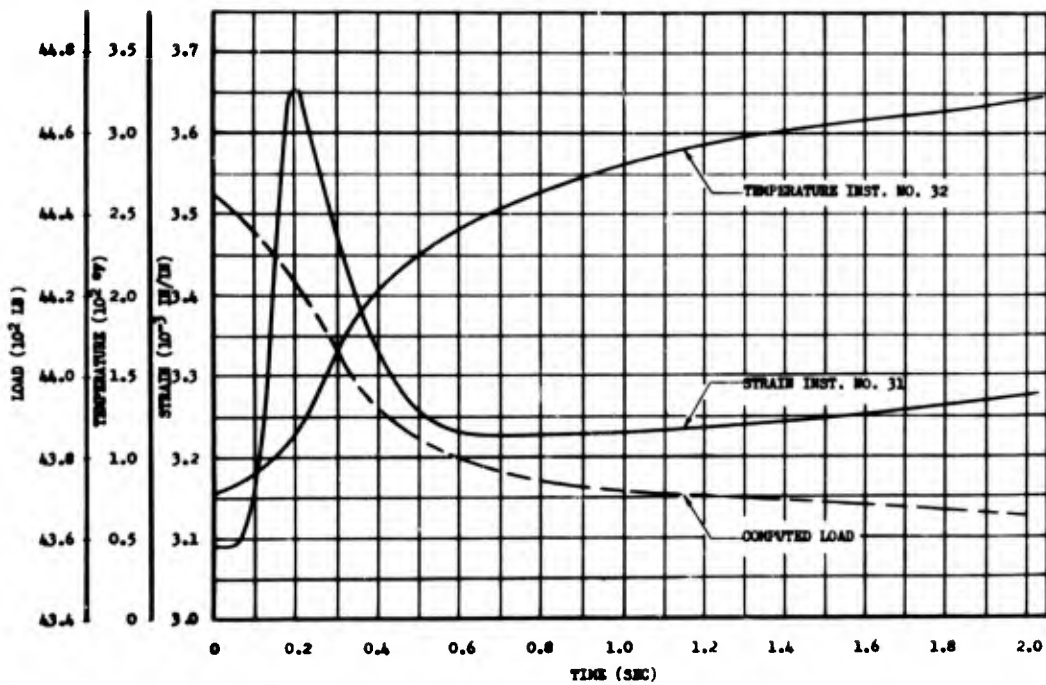
Fig. B.40 Strain, Temperature Rise, and Load as a Function of Time
of 3/16 in. Al Tension Tie (Absorptivity 0.96), for Station
2300, Shot 9. Cross-sectional area was 0.142 sq in.
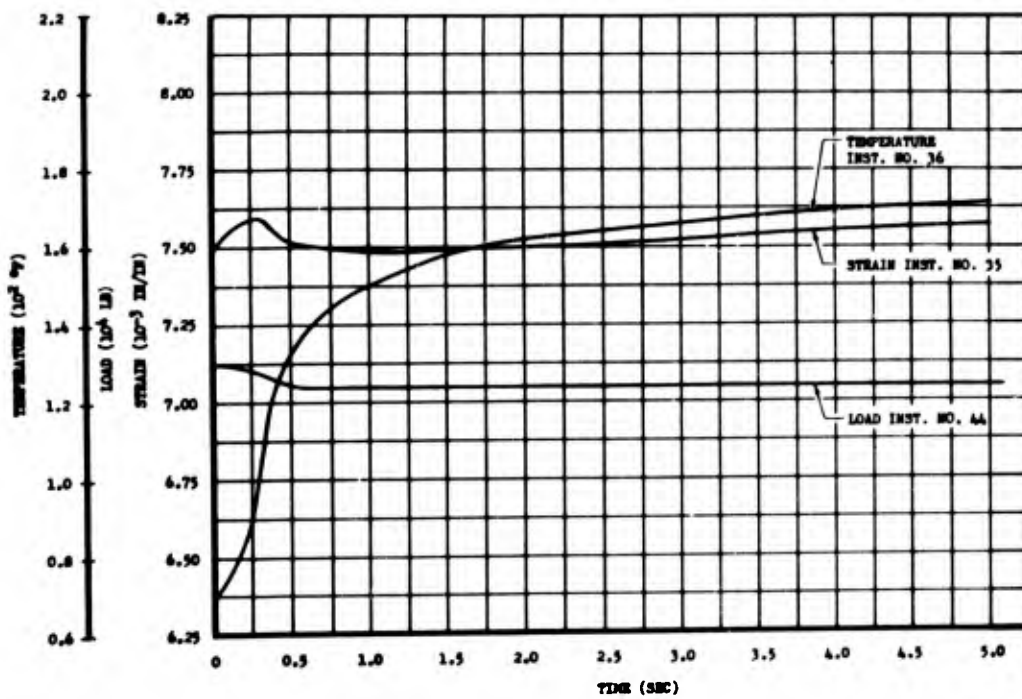
Fig. B.41 Strain, Temperature Rise, and Load as a Function of Time
of 1/8 in. Al Tension Tie (Absorptivity 0.96), for Station
6500, Shot 9. Cross-sectional area was 0.094 sq in.

123
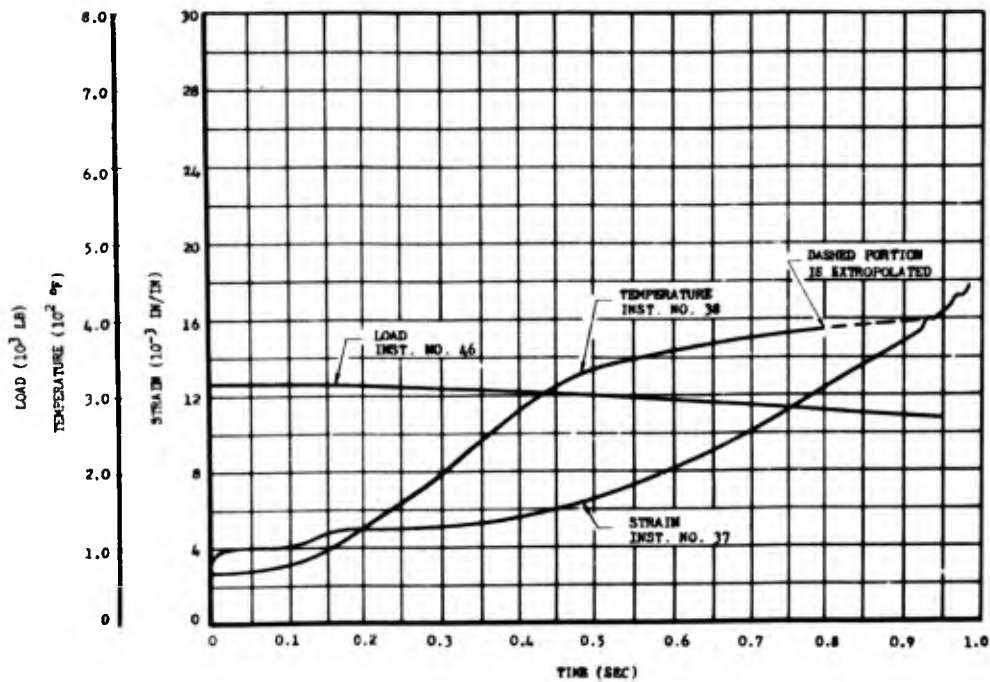
Fig. B.42 Strain, Temperature Rise, and Load as a Function of Time of 3/16 in. Mg Tension Tie (Absorptivity 0.82), for Station 2300, Shot 10. Cross-sectional area was 0.143 sq in.
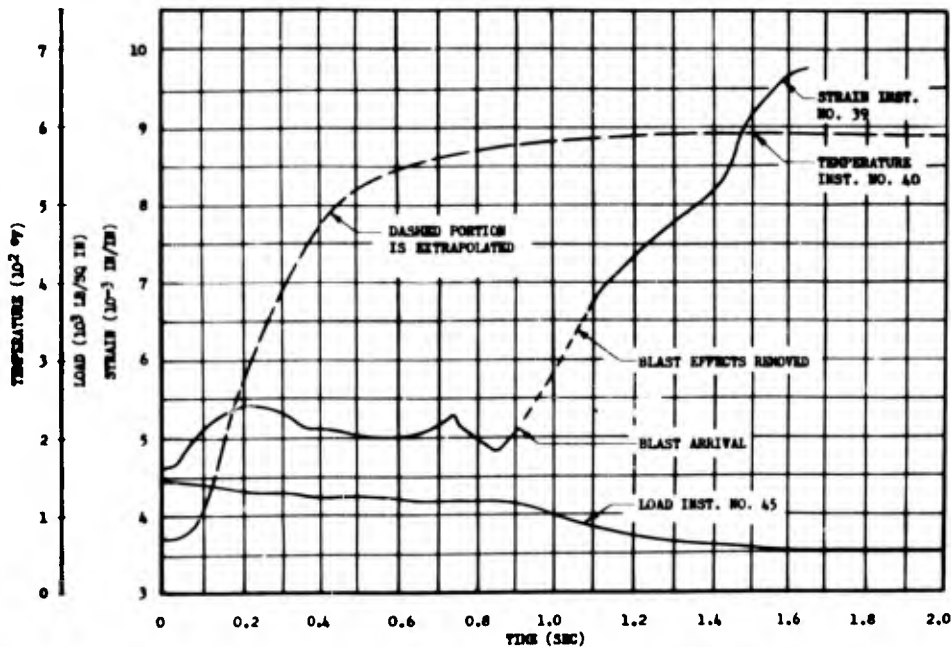
Fig. B.43 Strain, Temperature Rise, and Load as a Function of Time of 1/8 in. Al Tension Tie (Absorptivity 0.96), for Station 2300, Shot 10. Cross-sectional area was 0.094 sq in.

124
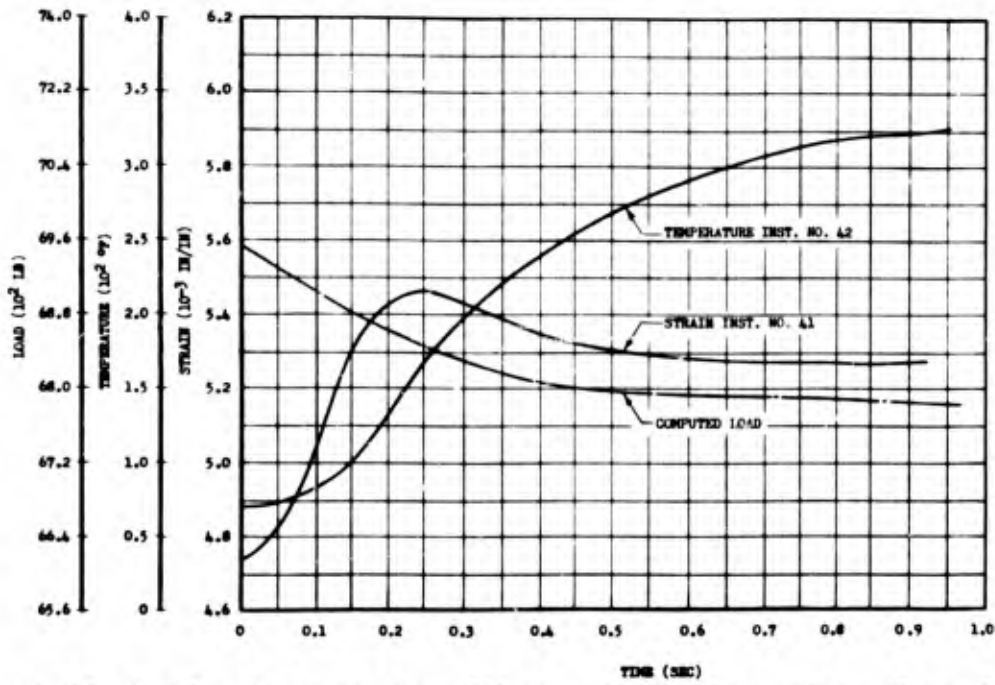
Fig. B. 44 Strain, Temperature Rise, and Load as a Function of Time of 3/16 in. Al Tension Tie (Absorptivity 0. 96), for Station 2300, Shot 10. Cross-sectional area was 0. 146 sq in.
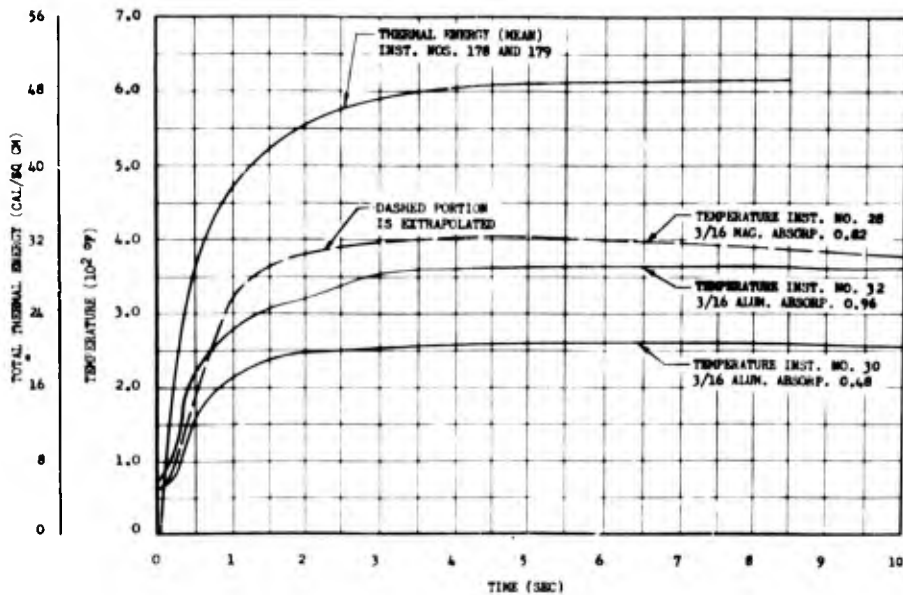
Fig. B. 45 Comparison of Temperature Rise and Thermal Energy as a Function of Time for Tension Ties at Station 2300, Shot 9

125
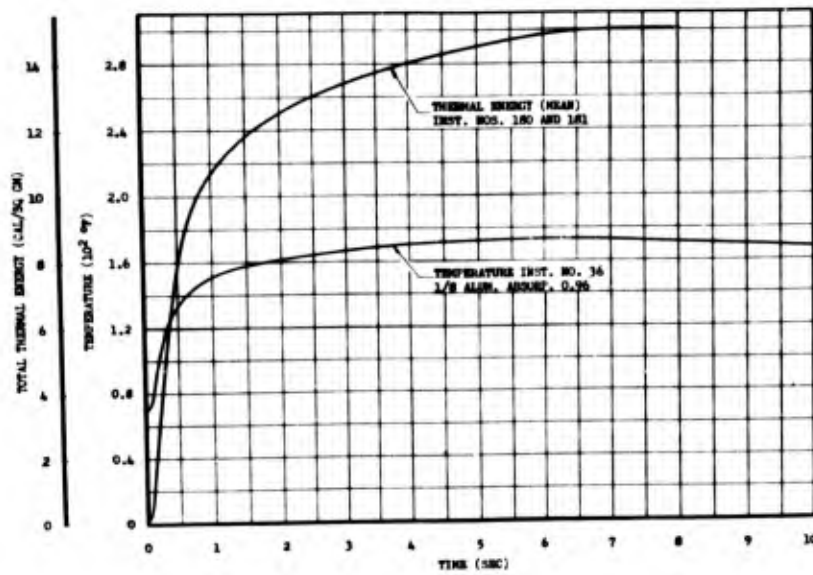
Fig. B. 46 Comparison of Temperature Rise and Thermal Energy as a
Function of Time for Tension Ties at Station 6500, Shot 9
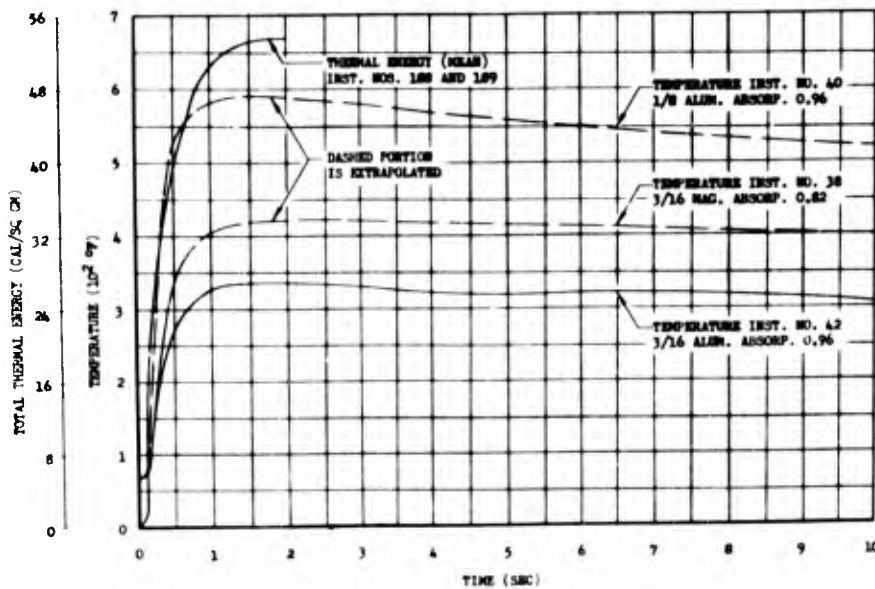
Fig. B. 47 Comparison of Temperature Rise and Thermal Energy as a
Function of Time for Tension Ties at Station 2300, Shot 10

126
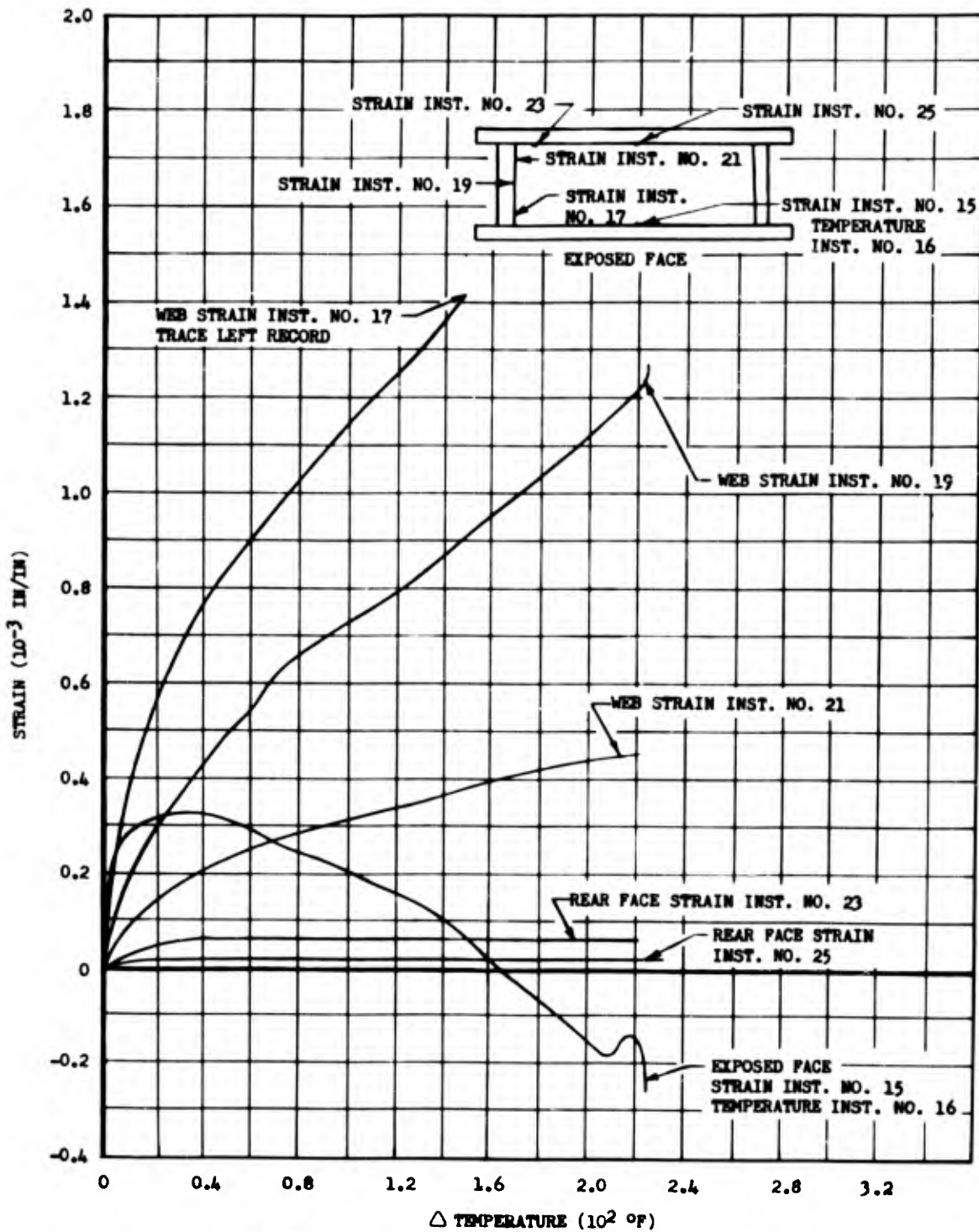
Fig. B.48 Comparison of Exposed Face, Web, and Rear Face Strains
as a Function of Exposed Face Temperature Rise of 3/16 in.
Al Box Beam (Absorptivity 0.96), Station 2300, Shot 10

127
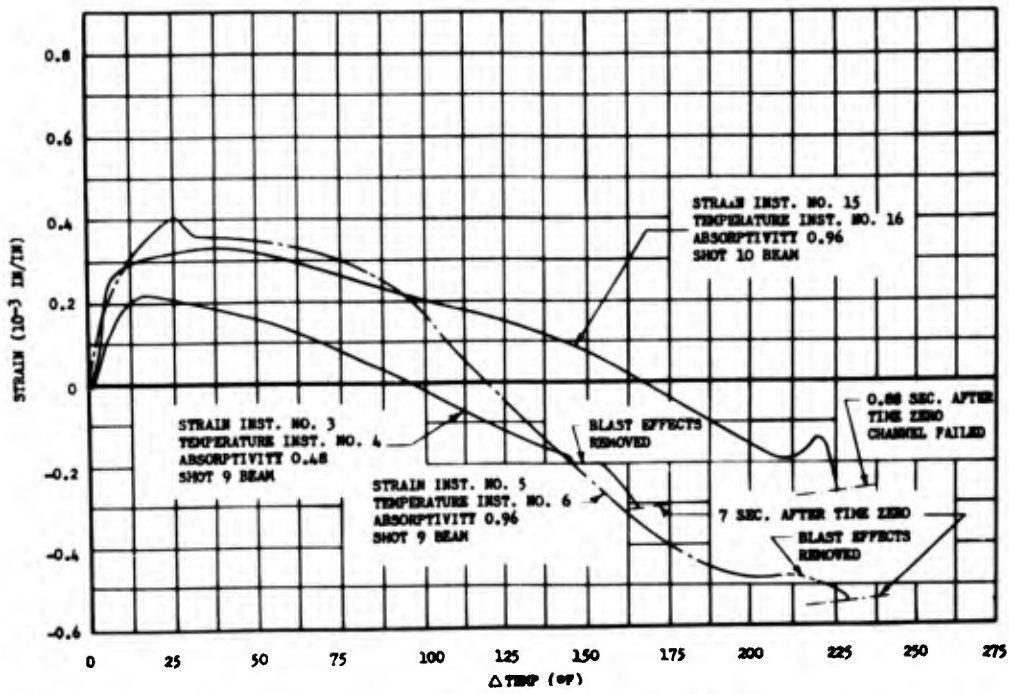
Fig. B.49 Comparison of Exposed Face Strain as a Function of Temperature Rise of 3/16 in. Al Box Beams, at Station 2300
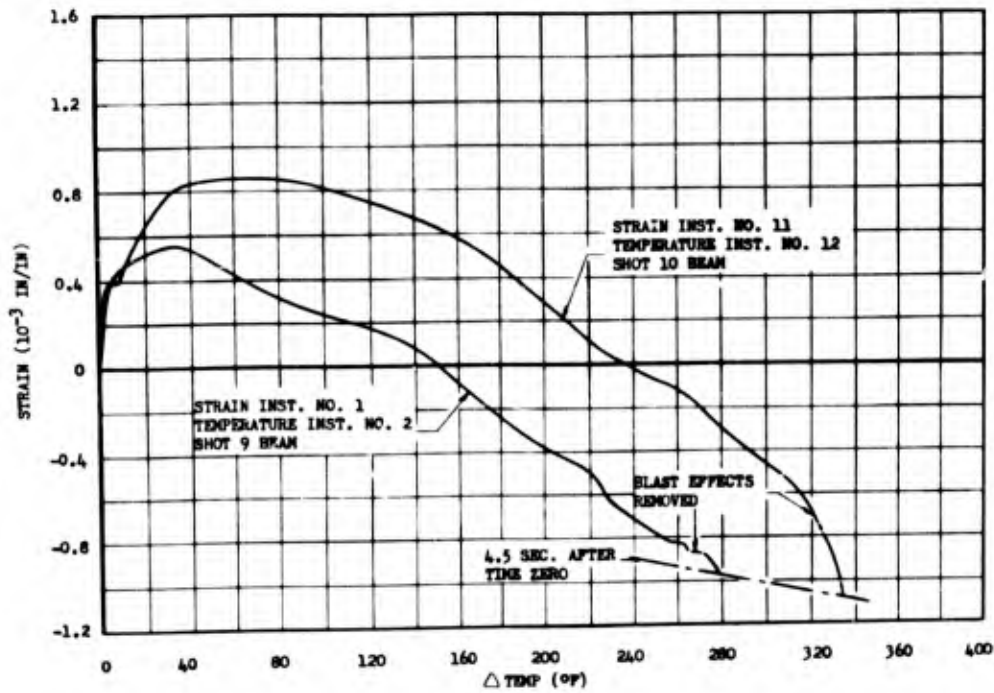
Fig. B.50 Comparison of Exposed Face Strains as a Function of Temperature Rise of 3/16 in. Mg Box Beams (Absorptivity 0.82) at Station 2300

128
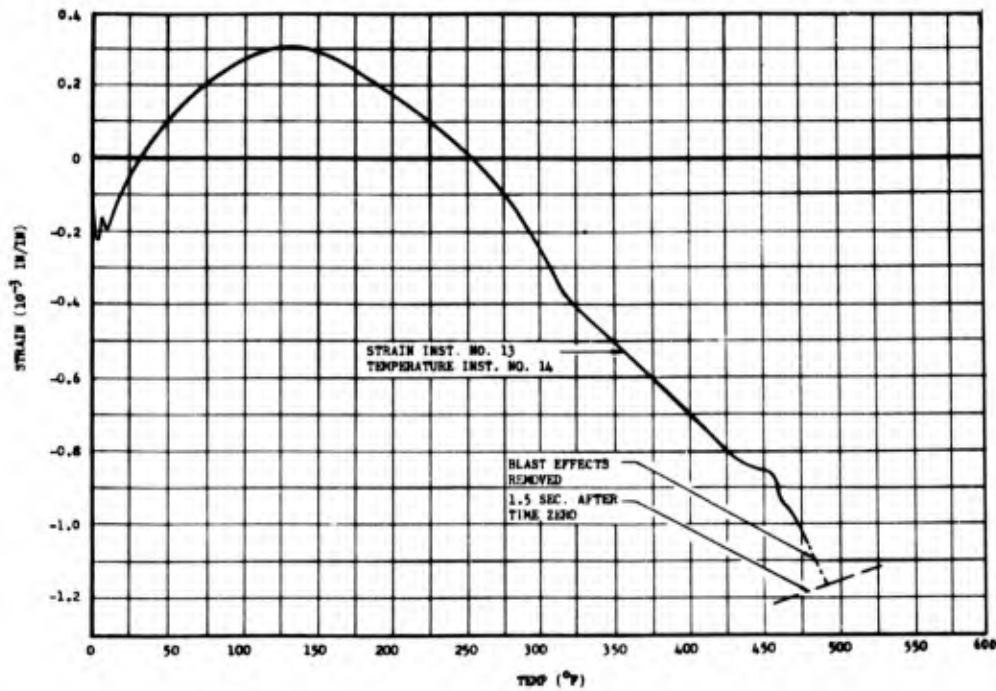
Fig. B.51 Exposed Face Strain as a Function of Temperature Rise of
1/8 in. Al Box Beam (Absorptivity 0.96), at Station 2300,
Shot 10
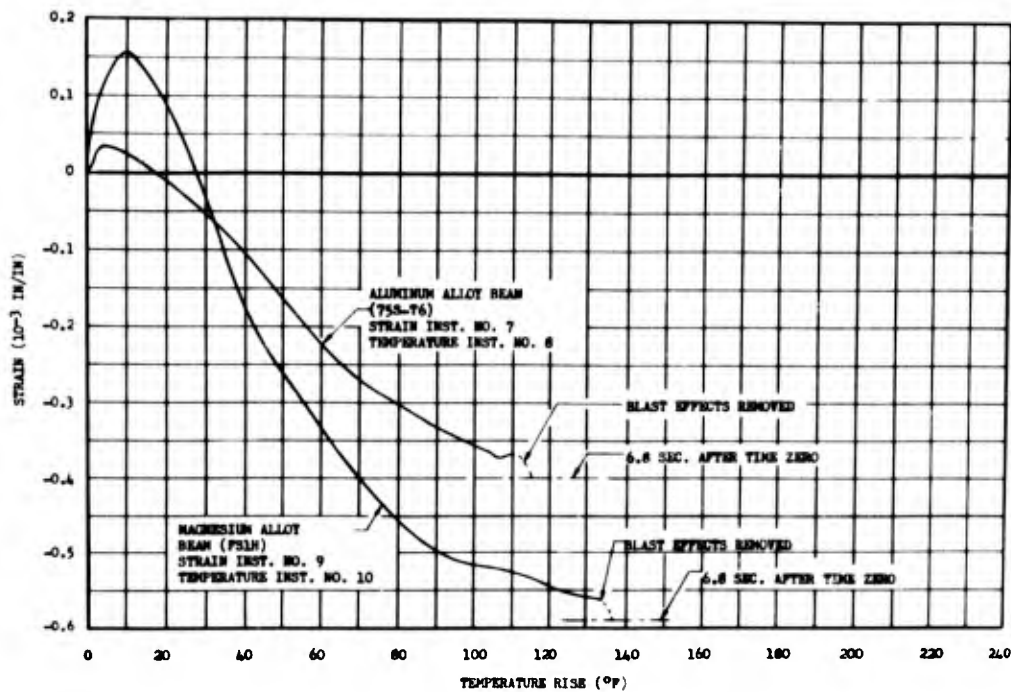
Fig. B.52 Comparison of Exposed Face Strains as a Function of
Temperature Rise of 1/8 in. Box Beam Specimens (Absorp-
tivity 0.96), at Station 6500, Shot 9

129
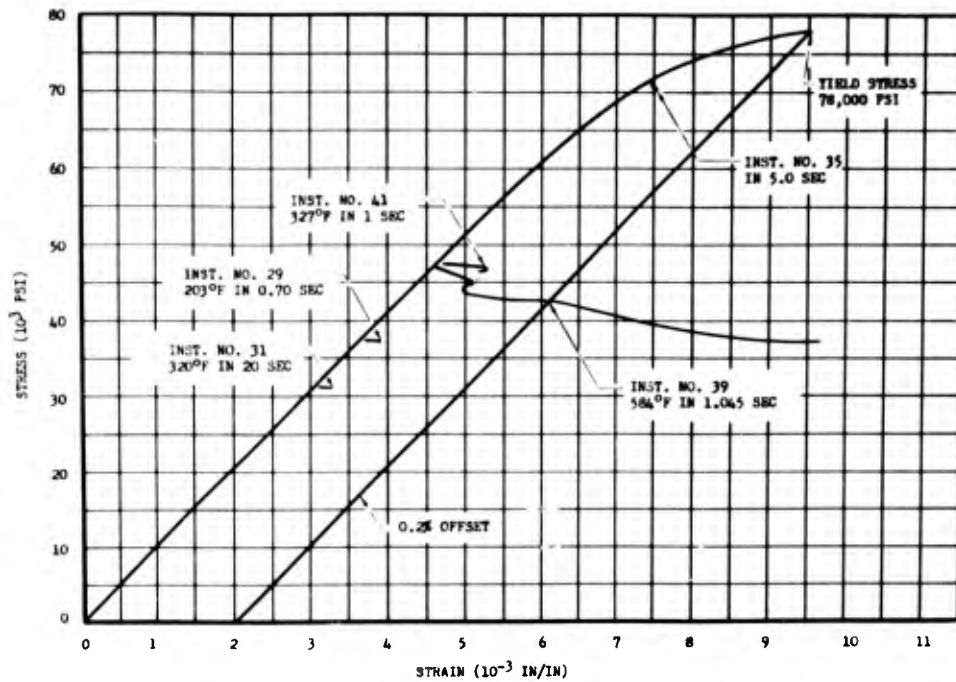
Fig. B.53 Stress-strain Diagram of the 75S-T6 Aluminum Alloy
Tension Tie
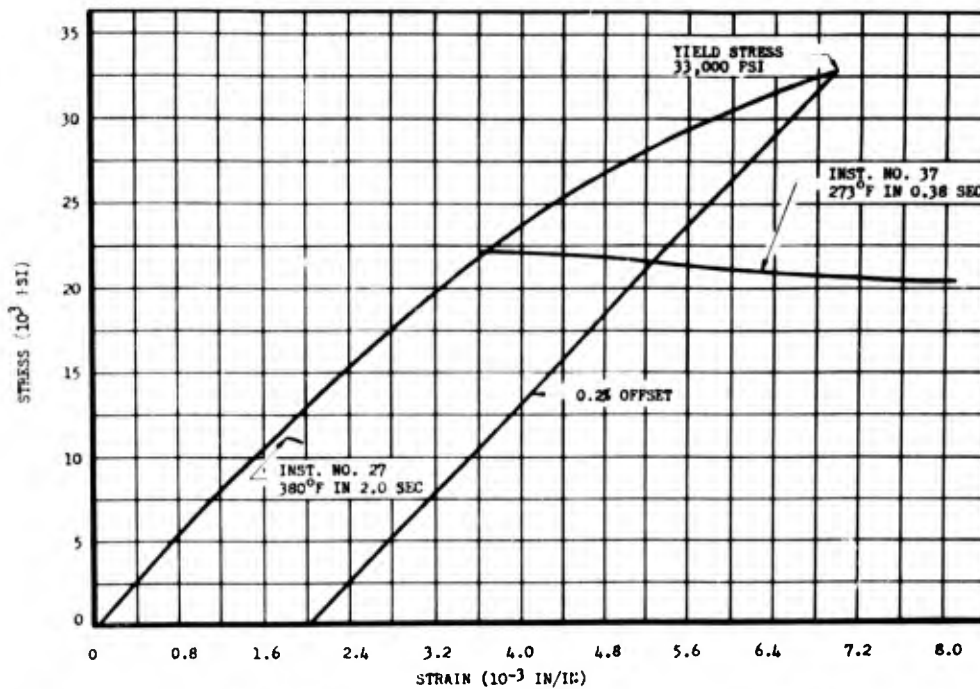
Fig. B.54 Stress-strain Diagram of the FS1h Magnesium Alloy
Tension Ties

130

APPENDIX C

COUPLING STUDY UTILIZING
T-28 HORIZONTAL STABILIZER ASSEMBLIES

C.1 GENERAL

The horizontal stabilizer and elevator assembly (T-28) was used in the coupling study as a typical aircraft structure; factors such as availability, ease in mounting and preloading, and size influenced the choice of the T-28 assembly.

The T-28 horizontal tail assembly has a slightly tapered platform as shown in Fig. C.1 and Fig. C.2. The internal structure consists of two spars and closely-spaced ribs (no stringers). The assembly employs a symmetrical airfoil and design so that the left-hand and right-hand components are interchangeable. The rear spar carried all of the bending loads, whereas the shear loads are transferred to the fuselage by both spars and the elevator fuselage attachment.
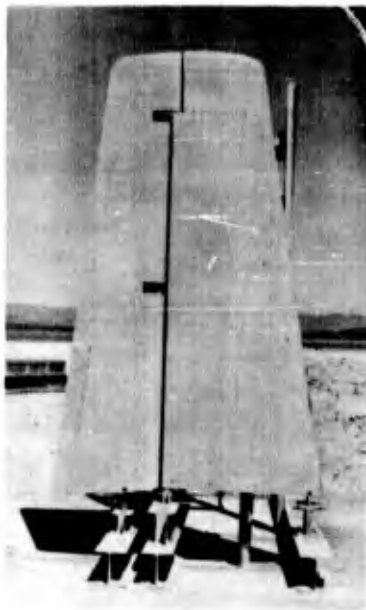
Fig. C.1 T-28 Horizontal
Stabilizer
Assembly

C.2 PROCEDURE

The two modifications made to the stabilizers may be seen in Fig. C.3. The first modification, which was required at all instrumented stations, consisted of removable access panels constructed on the nonirradiated side of each stabilizer. The opening and the patch were fabricated in accordance with Air Force specifications so that the basic structural integrity was maintained. The second modification, also on

131

Fig. C.2 Planform View of T-28 Horizontal Stabilizer Assembly
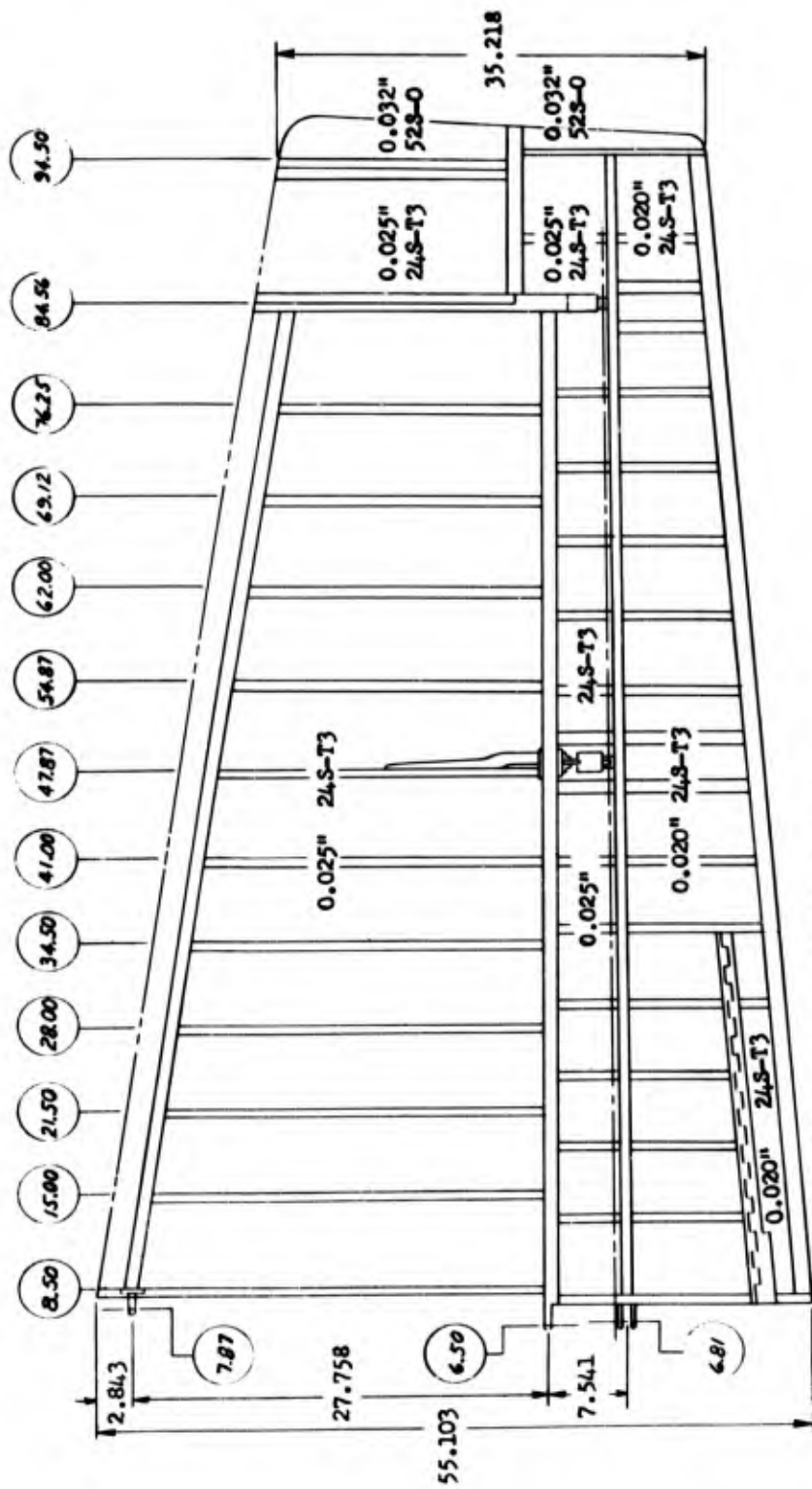
FRONT SPAR - 0.032" 24S-T3 CHANNEL L
REAR SPAR - 0.040" 24S-T3 WEB, 75S-T6 SPAR CAP IC
RIBS - 0.016" AND 0.051" 24S-T3

132

Fig. C.3 Stabilizer Loading Attachments and Access Panel

133

the unexposed side, consisted of mounting steel clips on the front and rear spars at stabilizer Stations 47.75 and 83.5 so that preloads could be applied. The addition of an access panel in the skin next to the inboard front spar load attachment was required for access to fastenings which secured the load attachment fitting. All other clips were riveted to the structure. Existing holes were used for all bolts and rivets.

Six of the nine stabilizers exposed during Shot 9 were instrumented with strain gage and thermocouple installations on the skin and the rear spar cap at Station 24.75 as shown in Fig. C.4. The spar cap thermocouple was eliminated on the three remaining stabilizers exposed only to blast inputs because the predicted temperature rise was relatively low. Duplicate strain gage and thermocouple installations were made at all instrumented positions as spares in the event of sensing element failure prior to the test. Strain gage rosettes were used in place of the single element gages for the skin panel strain measurements on the three stabilizers located at the 7200 ft station. All single element gages were oriented with the gage axes parallel to the rear spar; the rosette was mounted with one element parallel to the rear spar. The skin gages and rosettes were placed in the center of the stabilizer skin panel at Station 24.75.

To obtain further information on temperature distribution, temp-tapes (Section A. 3) were placed at various locations on the inside of the exposed stabilizer surface, as shown in Fig. C.5.

Three of the four stabilizers exposed during Shot 10 were instrumented as close as possible to Stations 24.75, 44.25, and 65.88, as shown in Fig. C.6; the fourth stabilizer had been previously exposed during Shot 9, and consequently was instrumented as shown in Fig. C.4. On the two stabilizers exposed to thermal inputs main and spare strain gage thermocouple installations were mounted on the inside surface of the rear spar-cap flange adjacent to the exposed side and in the center of the skin panels at the three spanwise stations. In addition, at Station 24.75, two strain gages and two thermocouples were applied to the inside of the front spar flange adjacent to the exposed surface, and two strain gages were applied to the rear spar-cap flange on the nonirradiated side. All skin and rear spar strain gages were oriented exactly as those used during Shot 9; front spar gages were mounted with the gage axes parallel to the front spar. Only one thermocouple, placed next to the strain rosette at Station 24.75, was applied to the stabilizer exposed to blast input only during Shot 10. Again, temp-tapes were used during Shot 10 to determine peak skin and flange temperatures at the various positions shown in Fig. C.7.

Each stabilizer exposed to blast during both shots was oriented such that the rear spar and the chord line were normal to the shock wave propagation. The stabilizers exposed to thermal radiation were at an angle of 16° with the horizontal at Stations 6500, 7200, and 8800. At this angle, the plane of the stabilizers was approximately normal to

134
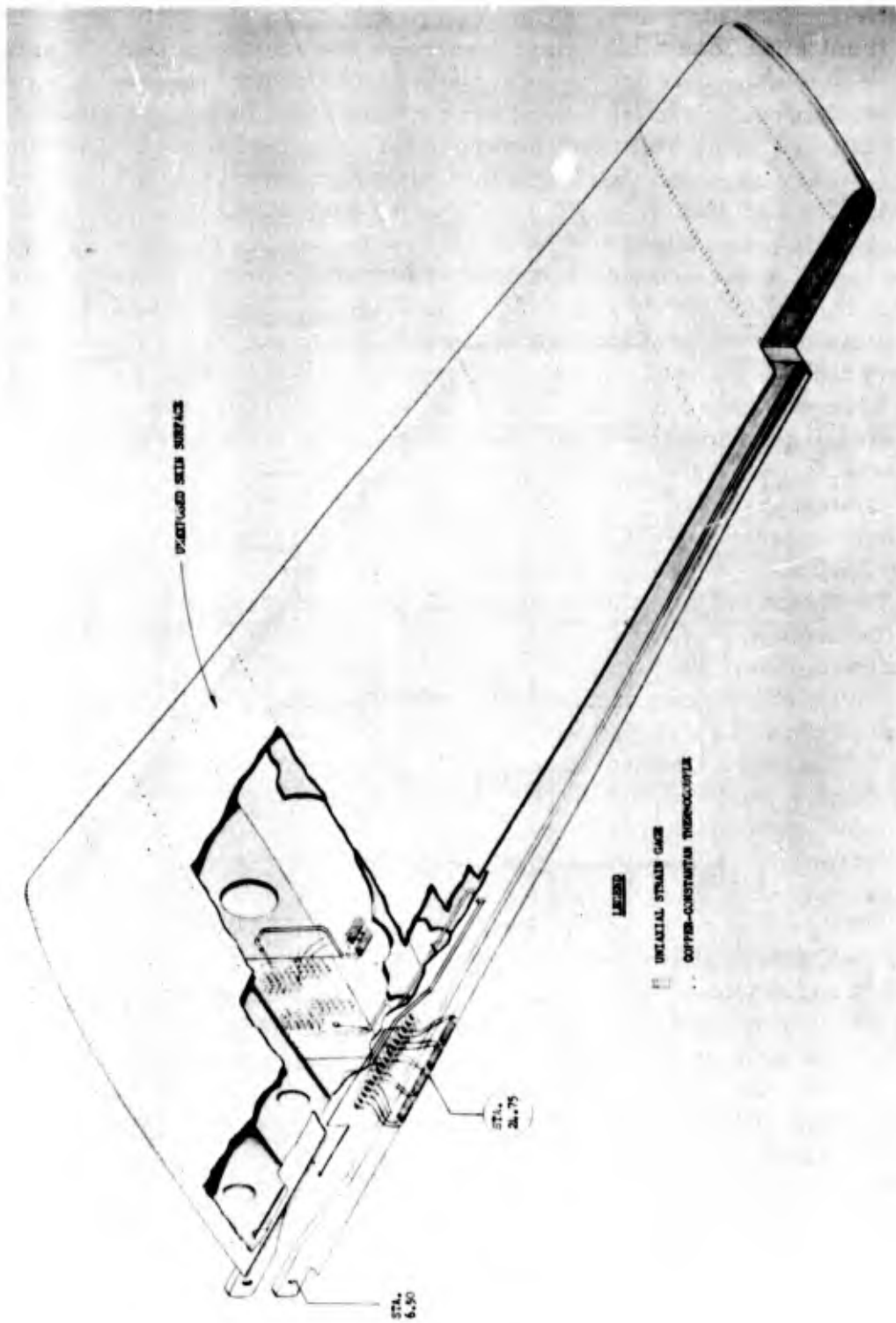
Fig. C.4 Location of T-28 Stabilizer Instrumentation for Shot 9

NOTE: ALL DIMENSIONS AND STATIONS EXPRESSED IN INCHES
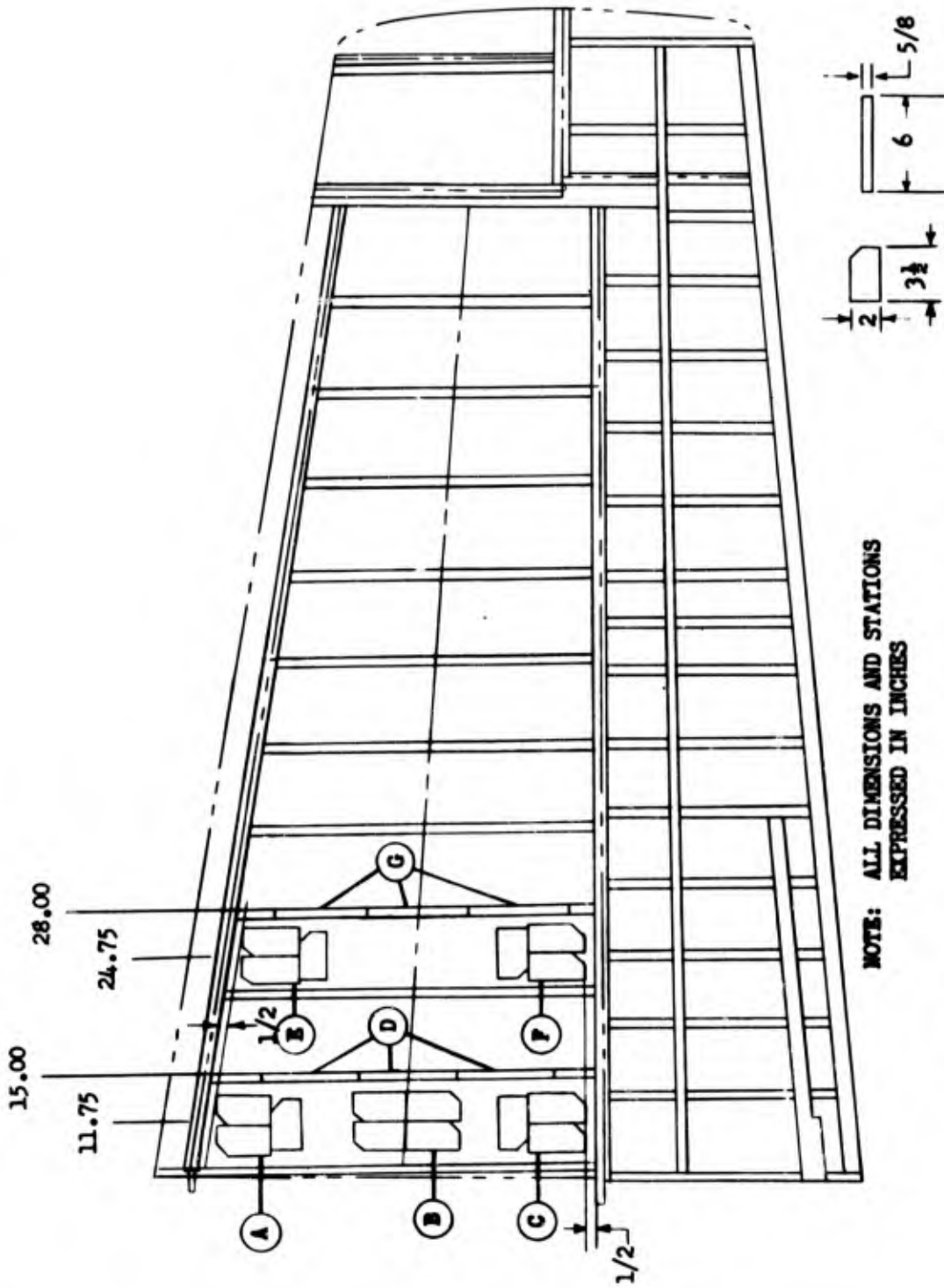
Fig. C.5 Location of Temp-tapes on T-28 Stabilizer for Shot 9

136
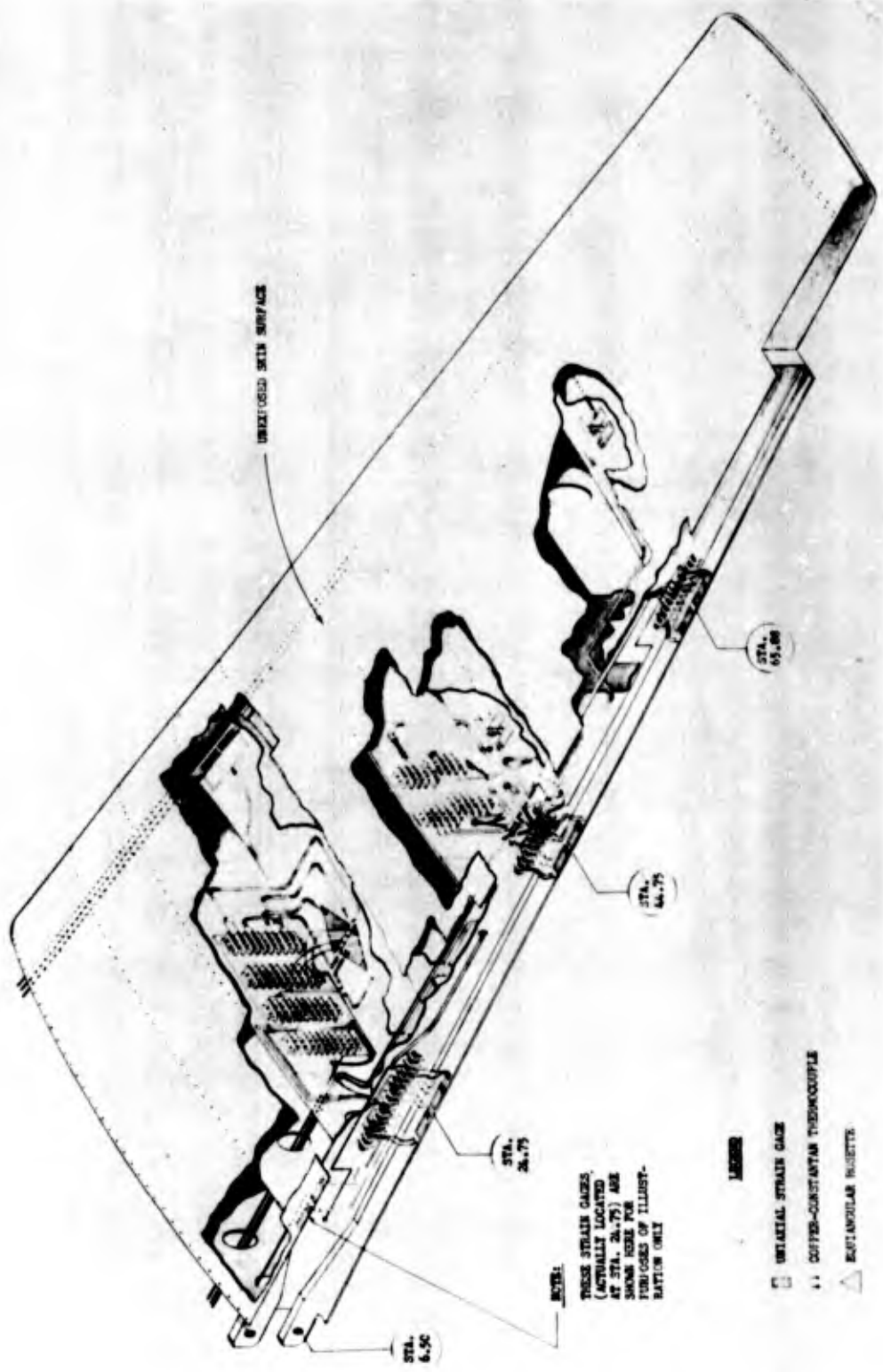
Fig. C.6 Location of T-28 Stabilizer Instrumentation for Shot 10

137
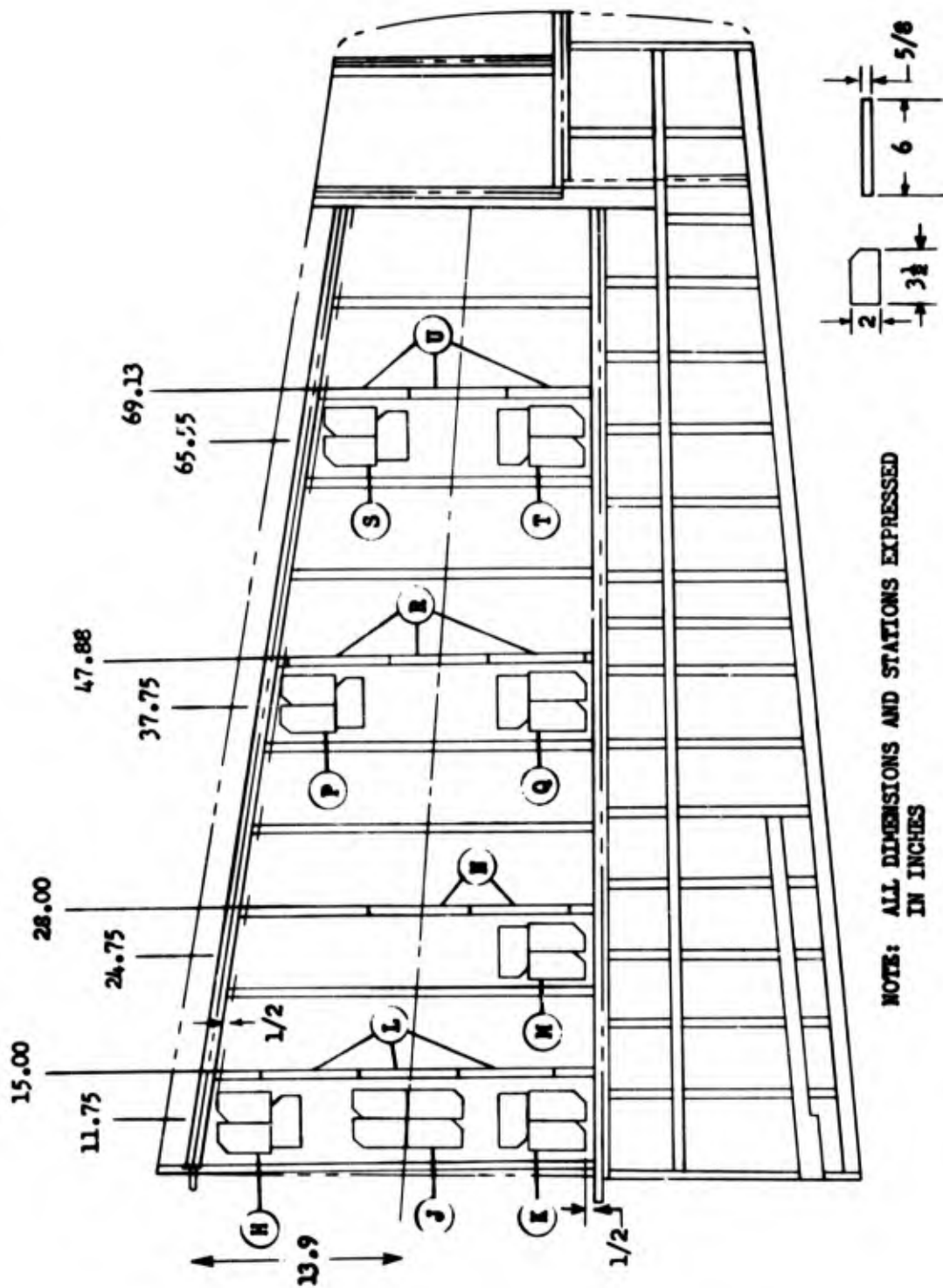
Fig. C.7 Location of Temp-tapes on T-28 Stabilizer for Shot 10

NOTE: ALL DIMENSIONS AND STATIONS EXPRESSED IN INCHES

138
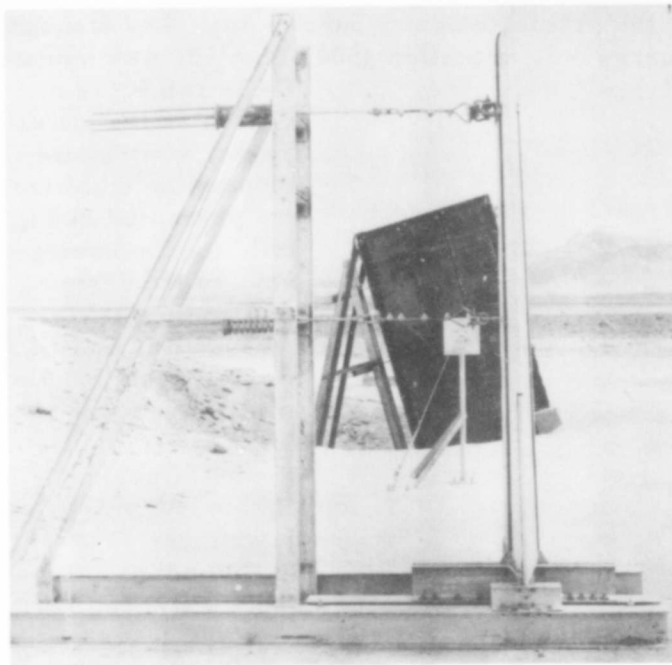
Fig. C.8 Installations on Level and Slanted Concrete Bases
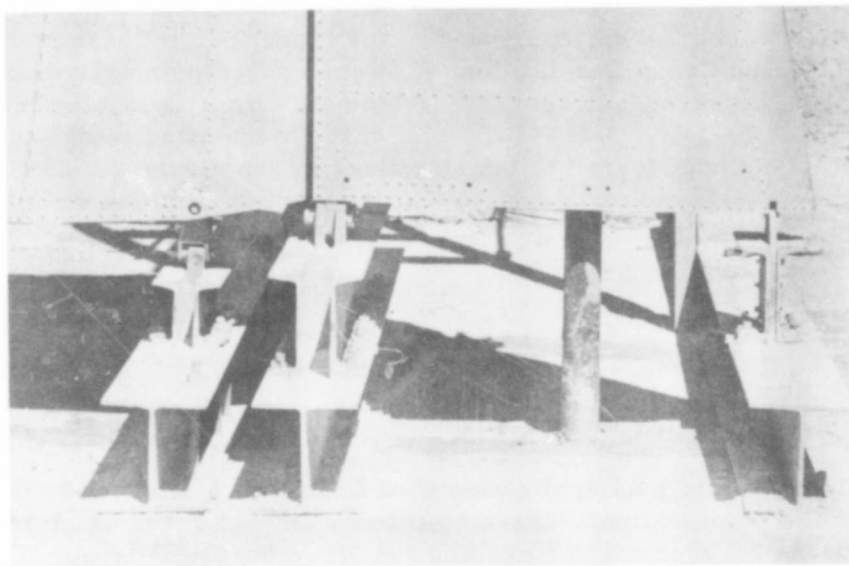
Fig. C.9 Stabilizer Mounting Fixtures

139

the line from the predicted Shot 9 burst point. The stabilizer exposed to thermal energy only at Station 3500, Shot 10, was mounted vertically. These two types of installations as well as the stabilizer loading frame, a structure designed to support the stabilizer preloads, are presented in Fig. C.8. The stabilizer mounting fixtures which were designed to accommodate the stabilizer fittings are presented in Fig. C.9.

The quantity of preload necessary to produce the desired spar stress due to the combined effects of preload, thermal radiation and overpressure was determined to be 11,800 psi and 20,700 psi at Station 24.75 for Shots 9 and 10, respectively. Identical loads were applied to all stabilizers exposed during a given shot.

The preload was applied at the two outboard elevator hinge attachments on the rear spar and at equivalent chord stations on the front spar. These points were chosen primarily because the stabilizer is locally reinforced at the hinge attachments to withstand the load transferred to the stabilizer by the elevator. The following forces were applied as effective at the neutral axis (38.5 per cent chord):

Fig. C.10 Flexible Connection Between the Springs and the Cross Bar Loading Linkage

Shot 9	Outboard	190 lb
	Inboard	1000 lb
Shot 10	Outboard	340 lb
	Inboard	1700 lb

To facilitate load application cross bars were attached to the clips at the front and rear spars by flexible linkages (Fig. C.10). The connections between the springs and the cross bars were made flexible so that side oscillations would not be restricted. A picture of the lower springs and the spring holding mechanism is presented in Fig. C.11.
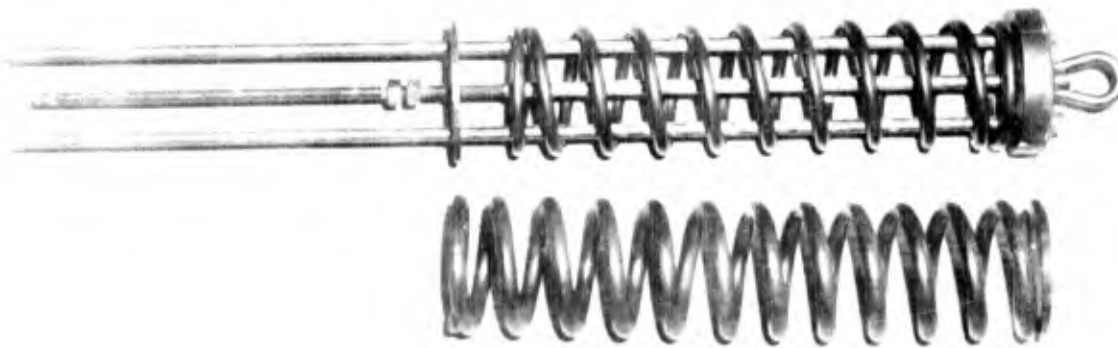
Fig. C.11 Stabilizer Loading Springs Used With Lower Loading Attach-
ment in Shot 9 and Shot 10. The Smaller Spring, Shown
With the Holder, Was Used During Shot 9.

Calibration curves were obtained by the arithmetical calibration
procedure which is described in Appendix A. Each stabilizer was
mounted and loaded as shown in Fig. C.12. The applied preloads were
greater than those expected to be used during the test, thus providing
an adequate check of the load attachments and the mounting fixtures.
By recording all of the strain gage outputs for each incremental load,
the quality of the strain gage installations was also checked.

The thermal shielding for the tests was obtained by placing a 5 ft
by 9 ft reflective, fireproof, curtain in front of the stabilizer. The
curtain was dropped 3 1/2 sec after time zero by a time-delay release
mechanism activated by the light from the bomb burst. The shield
operation may be seen in Fig. C.13.

The blast shield was a 9 1/2 ft high, 6 1/2 ft wide, and 5 1/2 ft
deep steel enclosure with a glass window in the side facing ground zero,
as shown in Fig. C.14. Additional details concerning the strength and
transmission of the glass may be found in Appendix F.

The exposure conditions and deployment of the stabilizers for
Shots 9 and 10 are presented in Fig. C.15 and Fig. C.16, respectively.
Also shown on these diagrams are the absorptivity, type of measure-
ments, and the installation numbers for each stabilizer.

C.3 RESULTS

During Shots 9 and 10, 83 of the 86 channels recording affects on
stabilizers yielded usable data. The three failures occurred as a

141
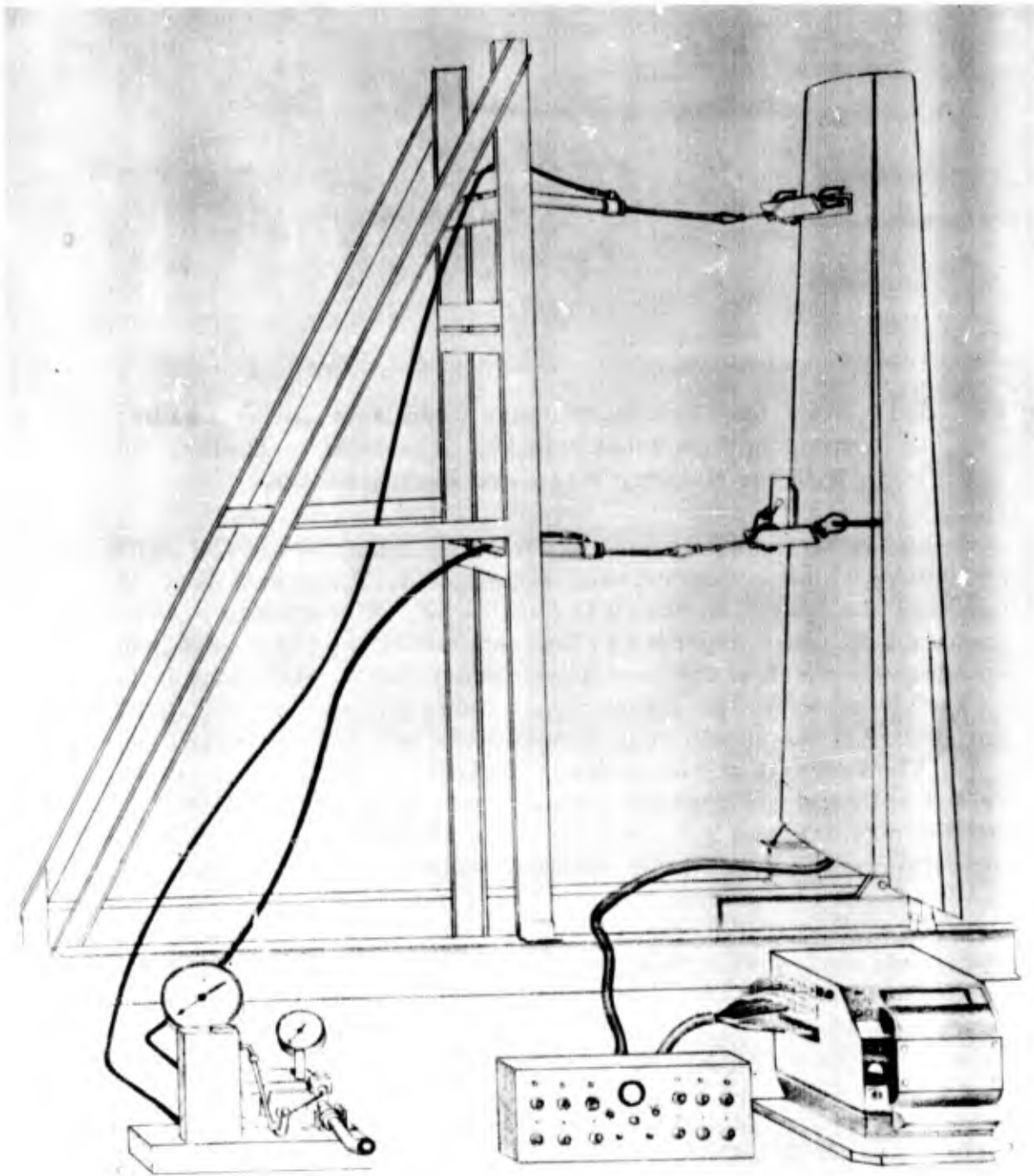
Fig. C.12 Calibration Apparatus for T-28 Stabilizer Calibration

142
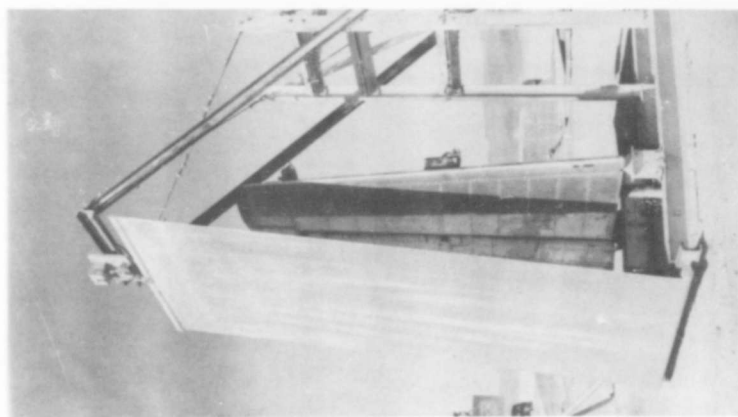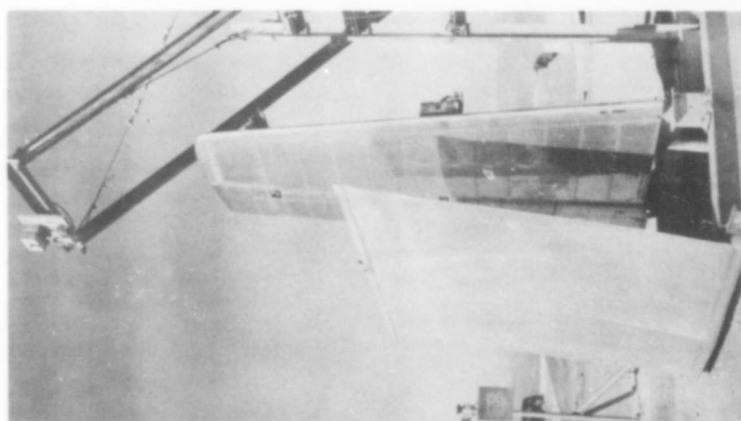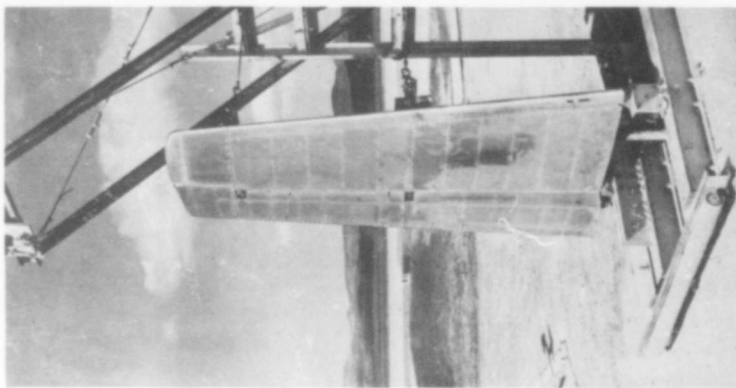
Fig. C.13 Thermal Shield Operation Sequence

143
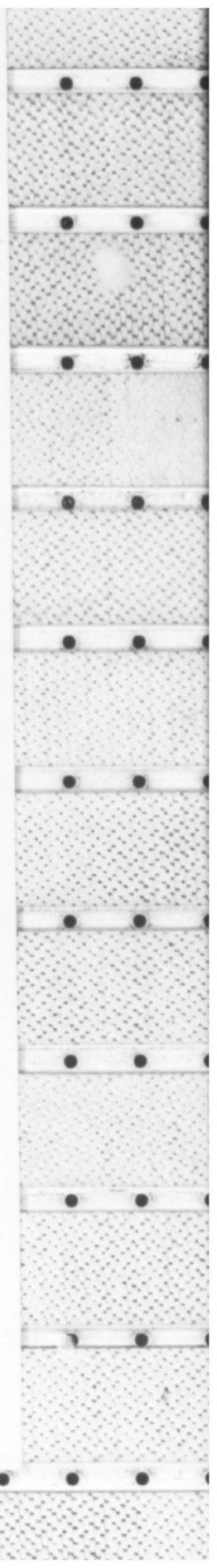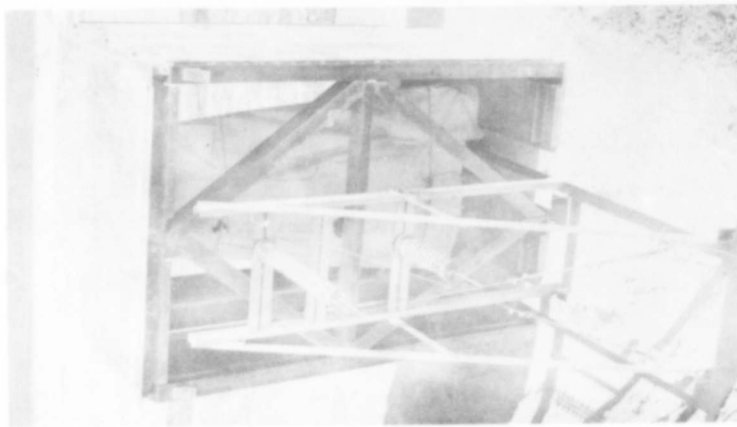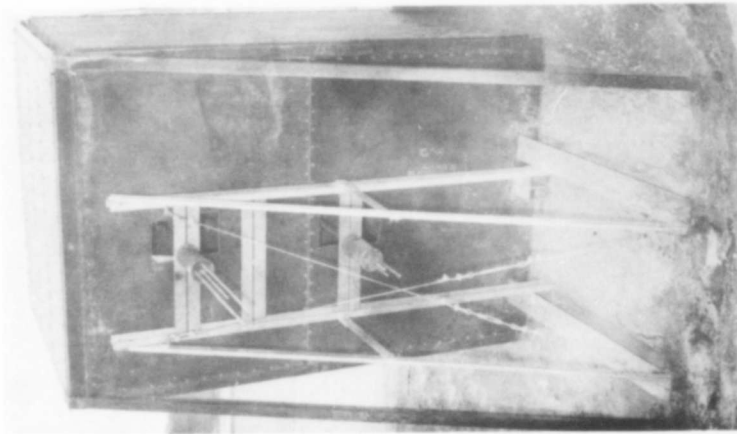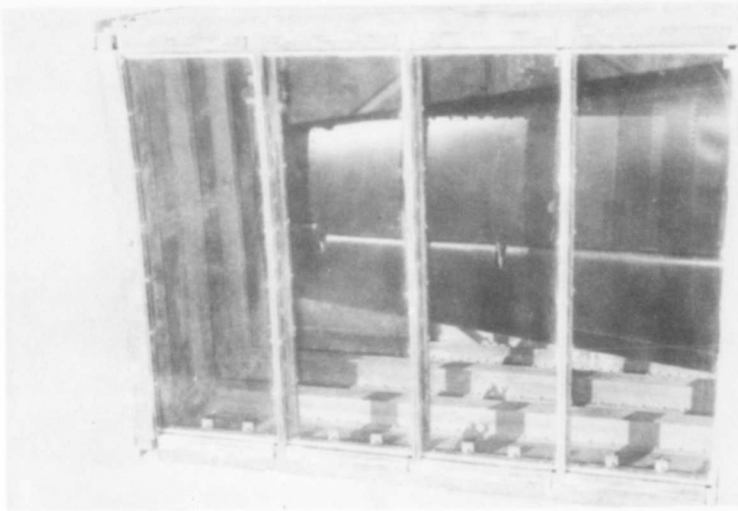
Fig. C.14 Blast Shield with Test Stabilizer in Place

144
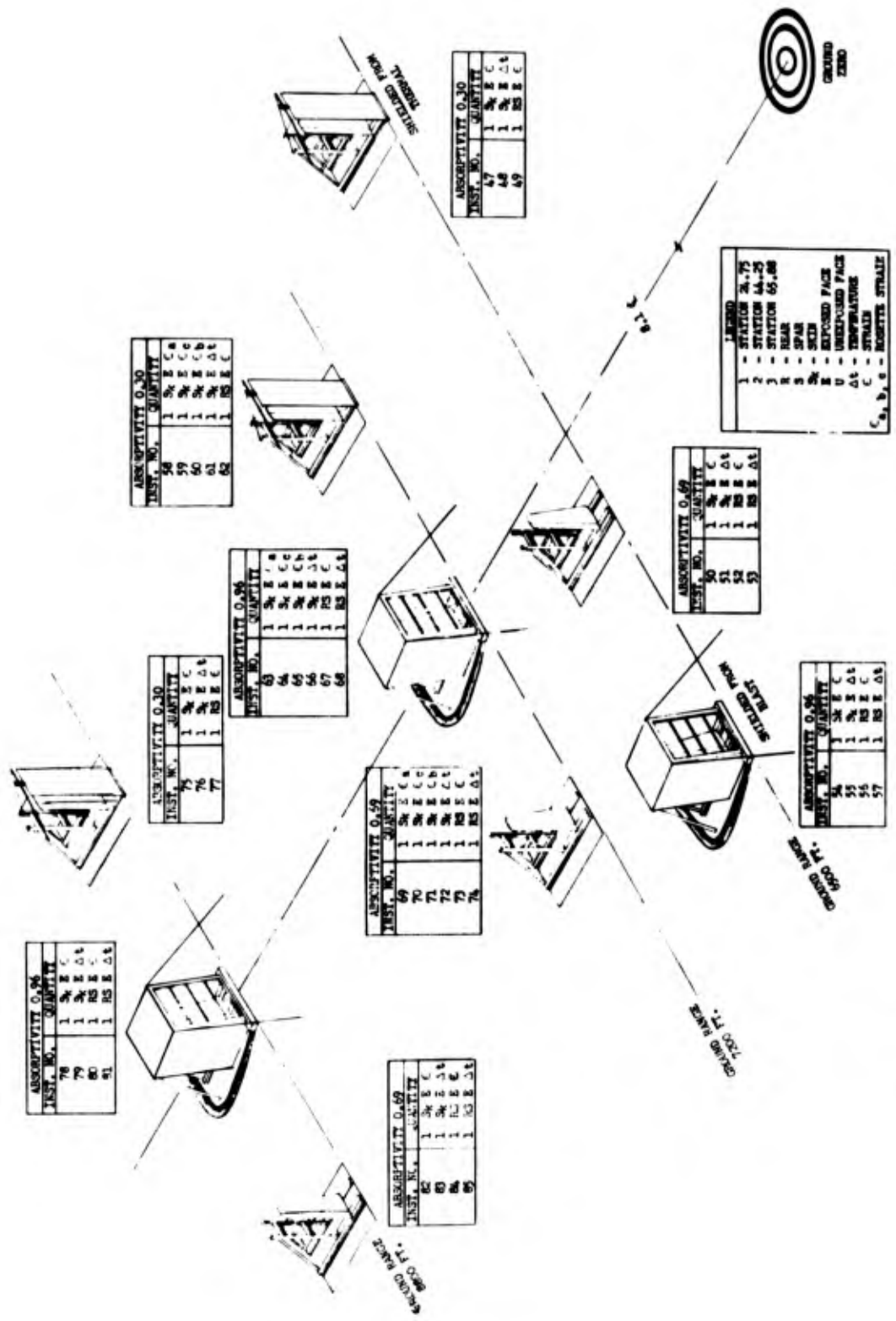
Fig. C.15 Schematic of T-28 Stabilizer Program for Shot 9

Fig. C.16 Schematic of T-28 Stabilizer Program for Shot 10

146

result of (1) a broken strain gage lead, (2) a thermocouple high resistance connection, and (3) the failure of one strain gage bond. In addition, four thermocouple circuits were broken as a result of the blast impingement on the skin surfaces; these data are reported as usable information because a major part of each measurement was recorded prior to the failure.

Every channel of usable data is represented in the graphical presentation of this section; the curves are grouped in such a way that comparisons can readily be made. An installation number (Inst No.) was assigned to each measurement to facilitate cross reference.

In addition to time-history instrumentation, stabilizer data were obtained from still and motion picture photography, by visual specimen examination and damage repair estimates, and by peak temperature (temp-tape) measurements.

A comparison of predicted and actual inputs and ranges is presented in Table C.1.

TABLE C.1 - Comparison of Predicted and Actual Inputs Received

	Ground Range (ft)		Slant Range (ft)		Thermal Energy (cal/sq cm)		Peak Overpressure (psi)		Δt on Gray 0.025 Skin (°F)		Incident Angle to Vertical Specimen
	Predicted	Actual	Predicted	Actual	Predicted	Actual	Predicted	Actual	Predicted	Actual	
Shot 9	6500	7098	6945	7500	16.9	14.9	5.2	4.1	528	300	19.5°
	7200	7796	7610	8163	13.8	12.0	4.4	3.5	432	240	17.8°
	8800	9391	9140	9699	9.4	8.3	3.2	2.5	294	168	14.9°
Shot 10	3500	3552	3550	3591	32.5	*34.5	5.3	*5.8	**500	540	0
	6500	6537	6519	6558	8.5	9.3	2.2	2.2	266	200	4.8°

* Obtained from Preliminary Blast Line Data
** Black 0.025 Skin Results Listed Here, and Prediction is Based on 72% of Thermal Energy Received at Station Due to Glass Attenuation

C.3.1   Spar Data

Maximum strains and temperatures obtained from time-history instrumentation and other pertinent information for all stabilizer spar measurements obtained during Shots 9 and 10 are presented in Table C.2. The graphs of spar strain as a function of time for all valid measurements are presented in Fig. C.27 to C.42, inclusive; the graph figure number for a particular measurement is listed in col (7) of Table C.2.

C.3.2   Skin Data

All of the pertinent oscillographic strain and temperature data

147

TABLE C.2 - Results Obtained From T-28 Stabilizer Spar Measurements, Shots 9 and 10

(1) SHOT NO.	(2) EXPOSURE	(3) ABSORB.	(4) QUANTITY MEASURED	(5) STABILIZER STATION (INCHES)	(6) INSTALLATION NUMBER	(7) GRAPH FIGURE NUMBER	(8) ACTUAL GROUND RANGE (FEET)	(9) PRELOAD STRAIN	(10) MAXIMUM THERMAL STRAIN 10⁻⁶ IN./IN.	(11) MAXIMUM BLAST STRAIN	(12) MAXIMUM STRAIN	(13) AMBIENT TEMP	(14) PEAK TEMP (°F)	(15) ΔT MAXIMUM	(16) TIME TO REACH ΔT MAXIMUM (SECONDS)
SHOT 9	THERMAL ONLY	0.96	STRAIN	24.75	56	C.27	7098	1120	1960	1460	790				
			TEMP	24.25	57	C.28	7098					99	179	80	2.85
			STRAIN	24.75	67	C.27	7725	1160	1080	1625	700	102	166	64	3.00
			TEMP	24.75	68	C.28	7725								
			STRAIN	24.75	80	C.27	9191	1075	1625	1576	550	102	146	44	2.90
			TEMP	24.75	81	C.28	9191					82	264	182	2.55
SHOT 10	THERMAL ONLY	0.96	TEMP	24.75	87	C.30	5552		1235		1146				
			**TEMP	24.75	124	C.31;C.32	6537	85		1057		74	149	75	11.70
			**TEMP	24.75	125	C.31	6537								
			STRAIN	24.75	126	C.27;C.29	6537	1620	2675	2410	655	88	150	62	2.75
			TEMP	24.75	127	C.30	6537								
			***STRAIN	24.75	128	C.42	6537	-2565	-2950	-3130	-565				
			TEMP	44.25	129	C.30	6537	240	1080	1080	840				
			STRAIN	65.88	130	C.29	6537	150	665	510	515	66	146	60	2.60
			TEMP	65.88	131	C.28	6537					87	140	53	1.50
SHOT 9	BLAST ONLY	0.30	STRAIN	24.75	49	C.34	7098	800	800	4270	3470				
			**STRAIN	24.75	62		7725	920	995	3190	3470				
			STRAIN	24.75	77	C.34	9191	900	920	2960	2060				
SHOT 10	BLAST ONLY	0.30	***STRAIN	24.75	94	C.33;C.32	6537	170	211	-95	-265				
			STRAIN	24.75	95	C.33;C.35	6537	1600	1830	3540	1740				
			***STRAIN	24.75	96	C.42	6537	-2600	-2800	-5480	-3020				
			STRAIN	44.25	97	C.35	6537	450	467	1365	915				
			STRAIN	65.88	98	C.35	6537	240	290	1425	1165				
SHOT 9	THERMAL & BLAST	0.69	STRAIN	24.75	52	C.36;C.37	7098	950	1480	5000	4050				
			TEMP	24.75	53	C.38	7098					68	145	77	2.95
			STRAIN	24.75	72	C.36;C.37	7725	1100	1750	5000	3900				
			TEMP	24.75	74	C.38	7725					65	119	54	1.00
			STRAIN	24.75	84	C.36;C.37	9191	1100	1550	3675	2575				
			TEMP	24.75	85	C.38	9191					71	116	45	2.21
SHOT 10	THERMAL & BLAST	0.69	***STRAIN	24.75	107	C.31;C.32	6537	20	980	1170	1020				
			**TEMP	24.75	108	C.39;C.40	6537					96	176	80	11.00
			STRAIN	24.75	109	C.39;C.40	6537	1530	2200	3390	1760	78	119	61	2.40
			TEMP	24.75	110	C.38	6537								
			***STRAIN	44.25	111	C.42	6537	-2115	-2070	-3900	-1785				
			STRAIN	44.25	112	C.39;C.40	6537	170	840	2140	1970	80	145	65	2.65
			TEMP	65.88	113	C.40	6537								
			STRAIN	65.88	114	C.39;C.40	6537	75	550	1199	1315	67	150	61	1.25
			TEMP	65.88	115	C.41	6537								

* NO VALID MEASUREMENT OBTAINED
** FRONT SPAR MEASUREMENT - ALL OTHERS REAR SPAR
*** UNEXPOSED SIDE OF STABILIZER - ALL OTHERS ON EXPOSED SIDE

148

TABLE C.3 - Results Obtained From T-28 Stabilizer Skin Data, Shots 9 and 10

SHOT NO.	EXPOSURE	ABSORP.	QUANTITY MEASURED	STABILIZER STATION (INCHES)	INSTALLATION NUMBER	GRAPH FIGURE NUMBER	ACTUAL GROUND RANGE FEET	PRELOAD STRAIN	MAXIMUM THERMAL STRAIN	MAXIMUM BLAST STRAIN 10⁻⁶ IN/IN	MAXIMUM STRAIN	AMBIENT TEMP	PEAK TEMP °F	Δt MAXIMUM	TIME TO REACH MAXIMUM SECOND
SHOT 9	THERMAL	0.96	STRAIN	24.75	54	C.43	7098	430	1090	1185	755				
			TEMP	24.75	55	C.43	7098					96	414	318	5.15
			STRAIN A	24.75	63	C.43; C.44	7796	270	-85	-280	-950				
			STRAIN C	24.75	64	C.44	7796	320	40	3	317				
			STRAIN B	24.75	65	C.44	7796	50	-1220	-760	-1280				
			TEMP	44.25	66	C.43	7296					108	376	288	5.25
			STRAIN	44.25	78	C.43	9191	270	-15	550	-285				
			TEMP	24.75	79	C.43	9191					91	202	111	4.30
SHOT 10	THERMAL	0.96	TEMP	24.75	86	C.49; C.55	1552					100	639	539	3.15
			STRAIN C	24.75	116	C.47; C.48	6537	390	-160	-55	-550				
			STRAIN B	24.75	117	C.46; C.47; C.48	6537	1070	-880	-1200	-2270				
			TEMP	24.75	118	C.47; C.48	6537	-30	-288	171	-268				
			STRAIN	44.25	119	C.49; C.55	6537	655	55	280	500	81	293	212	3.90
			TEMP	44.25	120	C.46	6537					86	298	212	4.80
			STRAIN	65.88	121	C.49	9191	200	-850	-688	-1050				
			TEMP	65.88	122	C.49	6537					92	301	211	4.60
SHOT 9	BLAST	0.30	STRAIN B	24.75	47	C.50	7098	280	280	1165	242				
			TEMP	24.75	48	C.52	7098					68	87	19	6.55
			STRAIN A	24.75	58	C.50; C.51	7796	215	215	925	365				
			STRAIN C	24.75	59	C.51	7796	215	215	440	238				
			STRAIN B	24.75	60	C.52	7296	0	0	-675	-675				
			TEMP	44.25	61	C.49	7296					68	99	31	2.10
			STRAIN	44.25	72	C.50	9191	285	285	920	635				
			TEMP	24.75	76	C.52	9191					63	87	24	2.10
SHOT 10	BLAST	0.30	STRAIN B	24.75	88	C.54	6537	51	98	335	242				
			STRAIN A	24.75	89	C.53; C.54	6537	440	410	775	365				
			STRAIN C	24.75	90	C.54	6537	32	32	86	238				
			**TEMP	44.25	91	C.55	6537		720	1430	750	52	123	71	4.25
			STRAIN	65.88	93	C.53	6537	190	155	720	570				
SHOT 9	THERMAL & BLAST	0.69	STRAIN	24.75	50	C.55; C.56	7098	400	-960	2400	1900	89	316	275	5.1
			**TEMP	24.75	51	C.55; C.56; C.57; C.58	7098								
			STRAIN A	24.75	69	C.57; C.58	7296	200	-1120	-280	-1520				
			STRAIN C	24.75	70	C.57; C.58	7296	180	-260	-1175	-1335				
			STRAIN B	24.75	71	C.58	7296	50	-790	-1790	-1800				
			TEMP	44.25	72	C.59	7796					91	330	239	5.70
			**STRAIN	24.75	82		9191								
			**TEMP	24.75	83	C.59	9191					86	254	168	3.70
SHOT 10	THERMAL & BLAST	0.69	STRAIN A	24.75	99	C.60; C.61; C.62; C.63	6537	310	-350	1020	710				
			STRAIN B	24.75	100	C.60; C.62; C.63	6537	190	-1320	-1050	-1510				
			STRAIN C	24.75	101	C.61; C.62; C.63	6537	260	-20	690	430				
			TEMP	24.75	102	C.64; C.65	6537					100	303.5	202.5	4.90
			STRAIN	44.25	103	C.61	6537	530	690	1085	495				
			**TEMP	44.25	104	C.60; C.61	6537								
			STRAIN	65.88	105	C.60; C.64	6537	100	1280	1520	1420				
			TEMP	65.88	106	C.64	6537					104	312.5	204.5	4.80

* NO VALID DATA OBTAINED
** THERMOCOUPLE BROKE AT BLAST ARRIVAL

149

for all stabilizer skin measurements obtained during Shots 9 and 10 are presented in Table C.3. The time-histories of all skin temperatures and uniaxial strains are included in Figs. C.43 to C.65, as listed in col (7) of Table C.3. The results of the biaxial strain computations (obtained from the rosette strain measurements) are listed in Table C.4; time-history graphs of maximum, minimum, and shear strain and the angle of the maximum strain axis are presented in

TABLE C.4 - Stabilizer Skin Rosette Data

Shot No.	Input to Which Exposed	Actual Ground Range (ft)	Figure Reference	Installation Numbers	Maximum Preload Strain	Largest Principle Strain (10^{-6} in./in.)	Maximum Shear Strain
9	Blast	7796	C.70; C.71	58, 59, 60	370	990	780
9	Thermal	7796	C.66; C.67	63, 64, 65	410	890	850
9	Thermal & Blast	7796	C.74; C.75	69, 70, 71	230	1440	1500
10	Blast	6537	C.72; C.73	88, 89, 90	450	820	480
10	Thermal	6537	C.68; C.69	116, 117, 118	1100	170	900
10	Thermal & Blast	6537	C.76; C.77	99, 100, 101	310	1300	1220

Note: All Rosettes Located at Stabilizer Station 24.75

Figs. C.66 to C.77, inclusive.

The rosette computations were made by means of the nomograph[1] presented in Fig. C.17. The sample computation worked out to explain the use of the nomograph may be followed in the order of the numbered, dashed lines. In addition to the information explaining the use of Fig. C.17, the following information is needed to complete the computations.

1. Construct angle ON'N = 30°
2. Layout OR = MN. OR is always positive

---

[1] Hewson, T. A., "A Nomograph Solution to the Strain Rosette Equations", Experimental Stress Analysis, V4, n1, Addison-Wesley Press, Cambridge, 1946, p 26.

150

Fig. C.17 Nomograph for Equiangular Rosette Computations by T.A. Hewson (Referenced in Text)

3. The rosette was oriented on the stabilizer as shown in Fig. C.18

To compute the angle of the principal strain use the following convention.

Let γ = the angle measured (positive in the counter-clockwise direction) from the OA axis of the strain rosette to the axis of the maximum strain, ϵ_1 or ϵ_{MAX}. "O" is the vertex of the angle γ.

The angle γ may be computed from formula:

$$\tan 2\gamma = \frac{3(\epsilon_C - \epsilon_B)}{2\epsilon_A - \epsilon_B - \epsilon_C}$$

To obtain the proper orientation of angle γ, as shown in the rosette drawing in Fig. C.18, use the following convention

Fig. C.18 Strain Rosette Orientation

Case I	$\epsilon_C > \epsilon_B$	$0 < \gamma < 90°$
Case II	$\epsilon_B > \epsilon_C$	$0 > \gamma > -90°$
Case III	$\epsilon_B = \epsilon_C$	

(a)	$\epsilon_A > \epsilon_B$	$\gamma = 0$ and $\epsilon_A = \epsilon_1$ or ϵ_{MAX}
(b)	$\epsilon_A < \epsilon_B$	$\gamma = 90°$ and $\epsilon_A = \epsilon_2$ or ϵ_{MIN}

C.3.3 Peak Temperature Data

Peak temperature data obtained from temp-tapes located on various stabilizers are presented in Tables C.5 and C.6 for Shots 9 and 10, respectively. Representative skin temperature data obtained by thermocouple and temp-tape measurement are presented in Fig. C.19 and Fig. C.20 as an aid in temperature distribution studies.

C.3.4 Visual Damage Survey

All stabilizers exposed during Shots 9 and 10 were individually

TABLE C.5 - Peak Temperatures Attained on T-28 Stabilizers; Shot 9 (Temp-tape Data)

Station (ft)	6500		7200		8800	
Exposed to	Thermal	Thermal & Blast	Thermal	Thermal & Blast	Thermal	Thermal & Blast
Absorptivity	0.96	0.69	0.96	0.69	0.96	0.69
Location Code*	Peak Temperature Range (°F)					
a	377-423	377-423	288-308	309-330	232-252	225-231
b	377-423	377-423	331-363	309-330	265-287	225-231
c	377-423	377-423	364-368	288-308	265-287	225-231
d	232-252	232-252	232-252	178-194	171-177	144-160
e	377-423	377-423	331-363	288-308	265-287	253-264
f	377-423	377-423	377-423	288-308	288-308	225-231
g	232-252	232-252	232-252	195-224	195-224	171-178

Note: Locations d and g are double thickness (0.025" skin plus 0.032" rib flange). All other locations are on 0.025" aluminum skin.
* For location on stabilizers see Fig. C.5

TABLE C.6 - Peak Temperatures Attained on T-28 Stabilizers; Shot 10 (Temp-tape Data)

Station (ft)	6500		3500
Exposed To	Thermal	Thermal & Blast	Thermal
Absorptivity	0.96	0.69	0.96
Location Code*	Peak Temperature Range (°F)		
h	144-170	288-308	635
j	178-194	288-308	635
k	178-194	288-308	635
l	144-170	178-194	
m	288-308	288-308	635
n	195-224	195-224	
p	288-308	288-308	
q	309-330	288-308	
r	195-224	195-224	
s	265-287	288-308	
t	309-330	288-308	
u	195-224	195-224	

Note: Locations l, n, r, and u are double thickness (0.025" skin plus 0.032" rib flange). All other locations are on 0.025" aluminum skin.
* For location on stabilizers see Fig. C.7

153
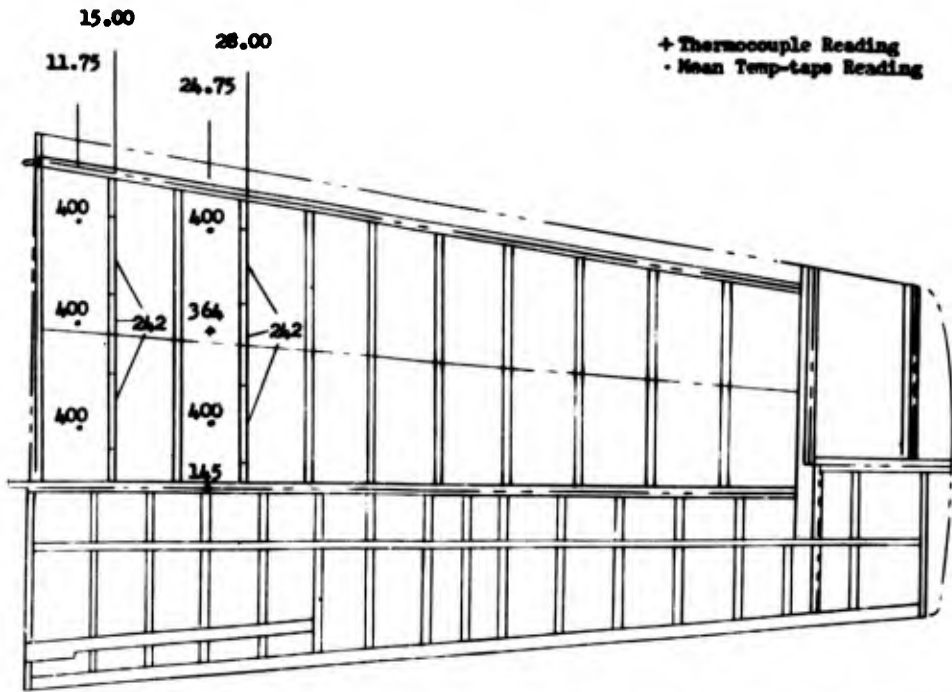
Fig. C.19 Peak Temperature Distribution for the Stabilizer Exposed to Both Thermal and Blast Inputs at Station 6500, Shot 9
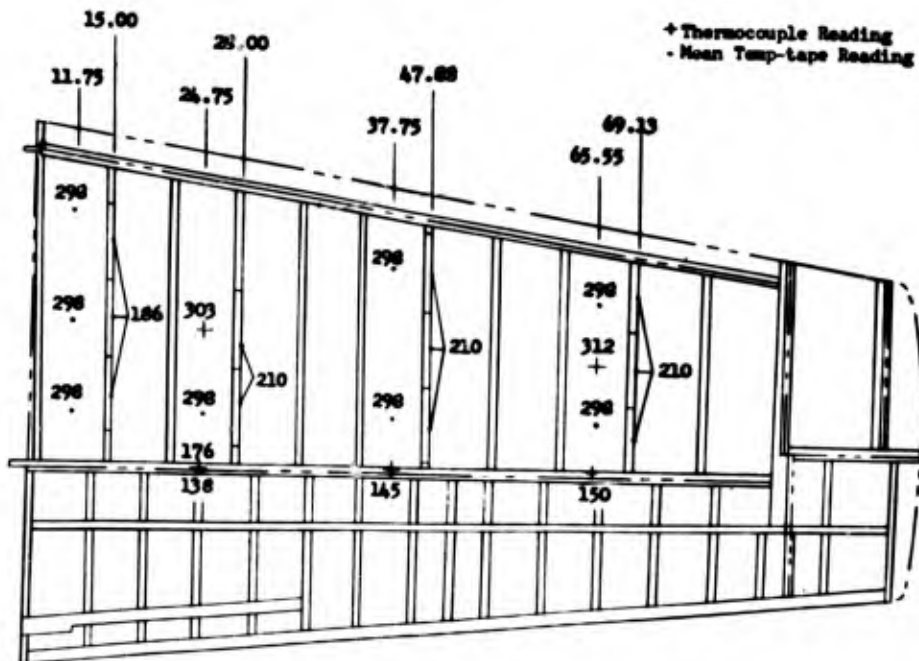
Fig. C.20 Peak Temperature Distribution for the Stabilizer Exposed to Thermal and Blast Inputs at Station 6500, Shot 10

154

inspected for damage. Damage in the form of spar buckling and skin wrinkling was predominant. A diagonal wrinkle, shown in Fig. C.21, starting at the intersection of the rear spar and the station 7.5 rib (exposed side) was detected on nearly all installations exposed to blast. The structure was reinforced by a doubler at this point. Another typical failure, shown in Fig. C.22, consisted of a skin buckle on the
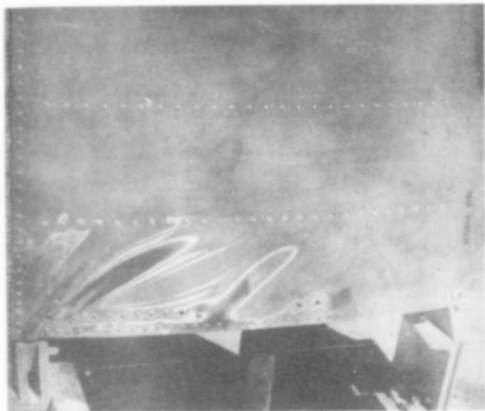
Fig. C.21 Typical Skin Buckle on Irradiated Surface at Intersection of Rear Spar and Root Rib
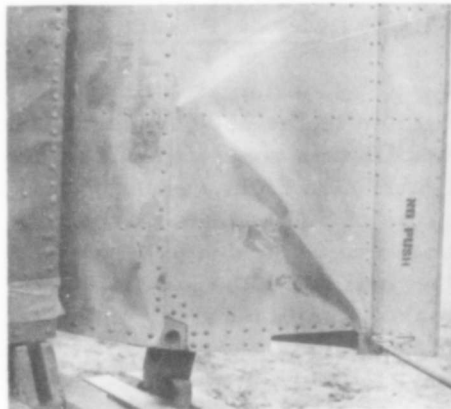
Fig. C.22 Typical Root Buckle on Unexposed Side of Elevator

unexposed side of the elevator at the intersection of the root elevator rib and the elevator trim tab. A failure evident on all stabilizers exposed to blast was a series of parallel, diagonal buckles in the rear spar web beginning at the reinforced root web section and extending outboard to station 40. No similar effects on the rear spar web of stabilizers exposed only to thermal energy were discovered. As a result of the spar web buckles, permanent set in the affected stabilizers was observed both from the postshot inspection and from the difference in the preload strains measured before and after the shot. A typical web buckle is presented in Fig. C.23.
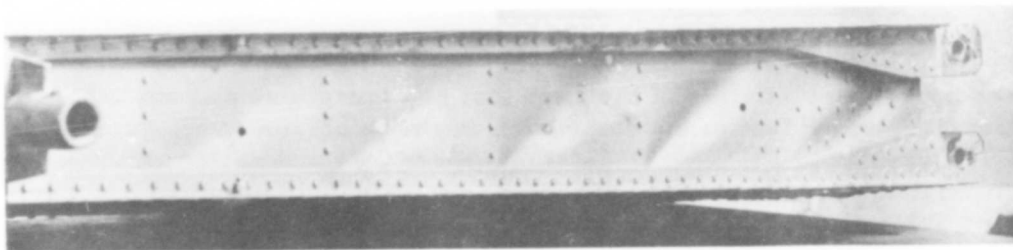
Fig. C.23 Typical Rear Spar Web Buckles

Over-all views of typically damaged stabilizers exposed only to blast, and exposed to both thermal and blast inputs, are presented in Fig. C.24 and Fig. C.25, respectively. The stabilizer exposed to thermal energy only, Station 3500, Shot 10, was damaged beyond economical repair, and a picture of its damage may be seen in Fig. C.26; no visual damage was observed on the other stabilizers exposed to thermal energy only because of the lower inputs.

C.3.5 Motion Picture Data

Motion picture coverage of the T-28 stabilizer program was limited to the 6500 ft station during Shots 9 and 10. A typical camera installation consisted of two cameras, an Eastman High-speed and a GSAP (Gun Sight Aiming Point) set to expose film at the approximate rates of 550 and 64 frames per second, respectively. The slower speed camera was used to photograph the stabilizer response to both thermal and blast inputs, whereas the high-speed camera was used to make possible a study of the stabilizer blast response. During each of the two shots, the two stabilizers exposed to blast inputs at Station 6500 were photographed. More details concerning the cameras, film, and film speed which were used may be found in Appendix A.

At Station 6500 where overpressure was 3.9 psi and 2.2 psi for Shots 9 and 10, stabilizer tip deflections of 8 and 3 in., respectively, were observed. No difference in the response of either of the two stabilizers photographed during a given shot was detected. As a result of the large deflections and rapid oscillation of the tips of the stabilizers during Shot 9, a considerable amount of slack was observed in the linkage of the outboard loading device. Because of the slack, the entire upper loading linkage "flapped" for a very short time until the upper loading spring elongated. This phenomenon was not observed during Shot 10.

No other new data were obtained from the motion pictures. However, they substantiated the stabilizer frequency of oscillation, torsional action on the structure, and the elevator oscillation, indicated by other data.

C.4 DISCUSSION

The purpose of this discussion is to point out phenomena caused by known peculiarities of the field test configurations and any other factors not evident in the data which might be helpful in future analyses. Notes pertaining to instrumentation procedures and performance have been made for the purpose of aiding in the planning of future programs.

Most of the strain and temperature curves which were presented in Section C.3 have been re-plotted in normalized form; i.e., in terms

Fig. C.25 Over-all Damage Sustained by Stabilizer Exposed to Both Thermal and Blast Inputs, Station 6500, Shot 9

Fig. C.24 Over-all Damage Sustained by Stabilizer Exposed to Blast Only, Station 6500, Shot 9

Fig. C.26 Over-all Damage Sustained by Stabilizer Exposed to Thermal
Radiation Only, Station 3500, Shot 10

158

of per cent of peak strain or temperature, to facilitate comparison. By plotting on the same graph all of the normalized temperature and strain vs time curves obtained from similar instrumentation installations, it was possible to obtain one average or typical curve which represents all of the temperature measurements and one typical curve representing all of the strain curves on the composite graph. These normalized curves are presented as composite plots of corresponding temperature and strain measurements in Figs. C.78 to C.82, inclusive.

From the normalized composite plots described above, crossplots of per cent peak strain as a function of per cent peak temperature were plotted for every strain-temperature pair. The crossplots are presented in Figs. C.83 and C.84. It should be kept in mind that these crossplots represent only typical or average results and are presented not as specific data but merely as material for generalized discussion.

C.4.1 Pertinent Characteristics of Curves

Whereas most of the graphs of strain and temperature measurements present no problem in understanding their various peaks and curve forms, in some instances unexpected variations occur which may not be so readily understandable. The response to thermal radiation of the T-28 stabilizer rear spar-cap strain gages (irradiated side) was very similar to the response of comparable gages on the box beam and tension tie specimens (Appendix B). As shown in the normalized average curve, Fig. C.78, as well as in Figs. C.27 and C.29, the spar-cap strain increases to a peak at about 0.4 sec, decreases a considerable amount, and then increases until the blast wave arrives. If the stabilizer is shielded from blast, the strain continues to rise. The "hump" in the curve, described above, is probably caused by local strains which result from non-uniform heating of the stabilizer skin and spar-cap. As the hot, expanding skin which was attached to the spar-cap exerted local tension on the cooler, relatively non-expanding spar-cap, a local spar-cap strain could have been produced. As the heat transferred to the spar-cap, the strain decreased as the skin and spar tended toward thermal equilibrium. Finally, as the stabilizer spar became heated and the skin on the irradiated side, because of expansion, had decreased its resistance to bending, the stabilizer deflected slightly, causing a strain increase in the spar-caps. The foregoing hypothesis is substantiated by the absence of the "hump" in the rear spar-cap strain measurement on the unexposed side. (See Fig. C.85).

Another result subject to question is the unequal magnitude of the preload strains obtained from the spar-caps on opposite sides of the spar. Inasmuch as the spar and the airfoil were symmetrical, it

159

would seem logical that strain gages placed equal distances on either side of the spar web center line would record bending strains of equal magnitude. As shown in Fig. C.85, there is a considerable discrepancy in the strains recorded at the two locations. In the preloaded position, however, there was a considerable amount of buckling on the compression side (unexposed side), and consequently very little of the skin was capable of resisting bending. Under these conditions, the structure was no longer symmetrical because all of the skin on the tension side was resisting bending, thereby causing a shift of the neutral axis toward the tension side, resulting in greater bending strains in the spar-cap under compression.

The blast phase of stabilizer rear spar-cap measurements as a function of time is presented in Fig. C.34 and Fig. C.37. At the time of blast arrival (the beginning time on the graphs) there is a deflection in the direction opposite to that of the primary bending moment. This deflection is a very rapid one which has a frequency much higher than either the first or second mode vibration, and the amplitude of the deflection is relatively small. Mathematical analyses of similar structures indicate that third mode vibrations may exist, causing initial root deflections toward the blast. Superposition of the first cycle of the third bending mode upon the first mode deflections, which are comparatively small initially, indicates the initial root bending would be in the direction opposite to the disturbing force. The presence of this higher mode is indicated by the variations from a true sine wave of the first two cycles; the higher mode damps out rapidly, and thereafter a pure sinusoidal vibration occurs.

In analyzing the skin strain data, care should be taken not to use those portions of the time-history curve where buckling took place. In most of these measurements the buckling occurred as a result of the shock impingement; however, some thermal buckling was observed. Although the skin strain vs time curves indicate the strain sensed by the strain gages at various time intervals, it must not be assumed that all of these strains are proportional to stress and, consequently, applicable for obtaining stress at a given time. For the most part, the strains can be used to compute stress; however, when the skin buckles, or "oilcans," strain is increasing without a proportionate increase in stress. Typical examples of buckling caused by blast impingement and by thermal radiation are presented in Figs. C.56 and C.60, respectively.

C.4.2   Thermoelastic Data

A complete presentation of thermoelastic data is beyond the scope of this report. Only examples of the thermal-strain response will be presented. Rear spar and skin strain-temperature curves are presented in Figs. C.83 and C.84, respectively, and represent all of the stabilizers exposed during Shot 9. Other strain-temperature curves are presented in Figs. C.86 and C.87. The hook at the end of the spar-

cap strain-temperature curve, Fig. C.83, occurred as a result of increased bending strain after the peak temperature was attained. It appears that a higher strain level was maintained longer for the stabilizer exposed to both inputs, Fig. C.83, but that a higher peak strain was finally attained by the stabilizer exposed to thermal radiation only. The hooks at the end of the skin strain-temperature curves, Fig. C.84, were not as prominent as those for the spar crossplots of these parameters because the skin strain was only slightly affected by the small changes in preload, whereas it was appreciably affected by temperature changes. As the temperature reached its peak, the skin strain was not changing rapidly, therefore, minimizing the hook in the curve for the skin strain-temperature relationship.

A plot of the normalized front spar strain vs temperature rise is presented in Fig. C.87 for the stabilizers exposed to thermal inputs during Shot 10. Inasmuch as the front spar flange had two layers of skin over it, and consequently did not change in temperature rapidly, the strain due to thermal radiation did not decrease appreciably after the peak strain was attained.

C.4.3   Coupling

The effects of the coupling of the thermal and blast inputs on the stabilizers were not conclusive, although the peak rear spar-cap strains were from 15 per cent to 20 per cent higher on the stabilizers exposed to both inputs than on the stabilizers exposed to blast only during Shot 9. During Shot 10, however, the stabilizer exposed to blast only was subjected to rear spar-cap strains which were actually 32 per cent higher than the same measurement on the stabilizer exposed to both inputs.

A comparison of damage sustained by the various stabilizers also indicates that there was very little difference between the two stabilizers exposed to blast inputs at each station. Thermal damage was nearly nonexistent; the blast input was almost entirely responsible for the damage incurred. A comparison of Figs. C.24 and C.25, which show the damage sustained by stabilizers at Station 6500, Shot 9, exposed to blast only and to both inputs, respectively, seems to indicate that the damage sustained by both of the stabilizers was not radically different. Closer examination of the stabilizers, however, shows that the stabilizer exposed to both inputs sustained slightly greater damage; the elevator control horn attaching bolt sheared, enabling the elevator to deflect considerably. At stations located farther than 6500 ft from intended ground zero, the difference in damage between the two stabilizers exposed to blast at a given station was even less noticeable.

More pronounced coupling effects would have been observed had Shot 9 inputs been as high as planned; skin temperatures of 650°F were predicted for the stabilizer exposed to thermal energy only at

161

Station 6500. As an indication of the thermal damage which should have been sustained at Station 6500, Shot 9, refer to Fig. C.26, the stabilizer exposed to thermal energy only at Station 3500, Shot 10. This stabilizer was subjected to a skin temperature of 640°F, and consequently, the skin was very severely buckled on the irradiated side. In fact, the structure was sufficiently weakened to permit the preloading spring to bend the stabilizer and thereby buckle the skin at the intersection of the root rib and rear spar; this type of buckle is shown in Fig. C.21.

C.4.4   Operation of Mounting and Loading Devices

The mounting and loading frames were satisfactory in that no structural failure occurred and no difficulty was experienced in using them. Equally satisfactory were the load attachments, which were fastened to the stabilizer and the linkages and connections which were parts of the loading mechanism. Less inertia and friction of the springs and holders would have eliminated the "flapping" of the upper linkage during Shot 9, as was observed from motion picture data.

Upon reviewing the data from Shots 9 and 10, it appeared that preloads were not applied uniformly to all stabilizers on a given shot; the spring preloads were adjusted by carefully measuring the spring length specified by the individual spring calibration curves. After the test series when the springs were recalibrated, it was discovered that the lower springs' calibrations were very similar to the preshot values, whereas a wide variation was obtained between the two calibrations of the upper springs. The variation was probably caused by non-uniform friction in the spring guides which occurred as the spring was compressed.

C.4.5   Operation of Shields

Thermal shielding was very satisfactory during Shot 9 in that very low skin temperature rises were measured on all three installations. As can be observed from the crossplot of these three temperature-time curves, Fig. C.52, the maximum temperature rise was 31°F, whereas the average temperature rise of all installations was 25°F. The marked change in slope of the curve at 3.5 sec, 1.75 sec, and 3 sec on the curves of installations numbered 48, 61, and 76, respectively, indicate the time when the thermal shield was released. The higher temperature rise of installation 61, located at a horizontal range of 7796 ft, was probably the result of an early release of the shield at that station; the early release made it possible for this stabilizer to absorb more thermal energy.

The shielding effect of the one thermal shield used during Shot 10 was not very apparent from the shape of the skin temperature-

162

time curve of the thermally shielded stabilizer; however, a definite decrease in the maximum temperature rise was apparent. As seen in Fig. C.65, the stabilizer skin shielded from thermal energy (exposed to blast only) was subjected to a temperature rise of $70^{\circ}F$, whereas the other stabilizers located at the same station underwent temperature changes in excess of $200^{\circ}F$. This shield was badly charred as a result of the thermal input (the same shield had been used previously during Shot 9), a factor which might have caused less thermal shielding than expected. Documentary motion pictures substantiated the fact that the shield at Station 6500, Shot 10, dropped about 3 sec after time zero, as planned. After each shot, some charring was discovered on all shields, but it was mostly near the top of the shield and was generally insignificant except for the charring which occurred during Shot 10. No difficulty was encountered in the release and rolling mechanisms, and interference of the shield with the stabilizer did not occur.

Excellent shielding from blast was obtained on both Shots 9 and 10, although some leakage through openings in the structure occurred. The amount of strain in the spar due to blast at Station 24.75 for the different stabilizers shielded from blast is presented in Fig. C.27. The strain amplitude, due to blast, varies from 60×10^{-6} in./in. to 170×10^{-6} in./in. depending on the range and shot. By comparison, as shown in Fig. C.34 which presents the spar strain at Station 24.75 of all stabilizers exposed to blast only, the strain amplitude of the stabilizers exposed only to blast varied from 930×10^{-6} in./in. to 1950 $\times 10^{-6}$ in./in., which indicated that the shield attenuated the blast effects by approximately 92 per cent.

No structural failures of the blast shield occurred, and no fractures, cracks, or discolorations of the glass window were discovered in any of the blast shields exposed during Shots 9 and 10, even though the glass was subjected to overpressure and thermal energy levels as high as 6.2 psi and 29.6 cal/sq cm, respectively. From the thermal measurements made both inside and outside the blast shield, it was estimated that the glass transmitted about 75 per cent of the incident thermal energy.

C.4.6 Instrumentation

During the preparation stages of this test, the problem of obtaining strain measurements on skin which is subject to buckling was considered. It was known that the effects of buckling on a strain reading can be compensated by applying strain gages on both surfaces of the skin such that the strain gages were directly opposite each other, and by incorporating the two gages in opposite arms of a Wheatstone-bridge circuit the increased strain due to buckling is essentially canceled out. Prior to the test, however, it was decided that a strain gage mounted on the irradiated surface would be influenced too much by the

163

radiant energy to yield reliable data. Therefore, a compromise instrumentation plan utilizing only one strain gage mounted on the inside surface of the irradiated skin was decided upon.

During Shot 10, one strain gage was mounted on a 0.025 in. thick plate and exposed directly to thermal radiation but not to blast; the strain gage was protected from direct thermal radiation by a layer of aluminum foil. As a result of the test, no adverse effects on the gage, its bond, its wiring, or its response to strain inputs were observed. It is believed that strain gages (bakelite type) protected by aluminum foil can be bonded on surfaces receiving 10 cal/sq cm thermal energy, and possibly more, without ill effects.
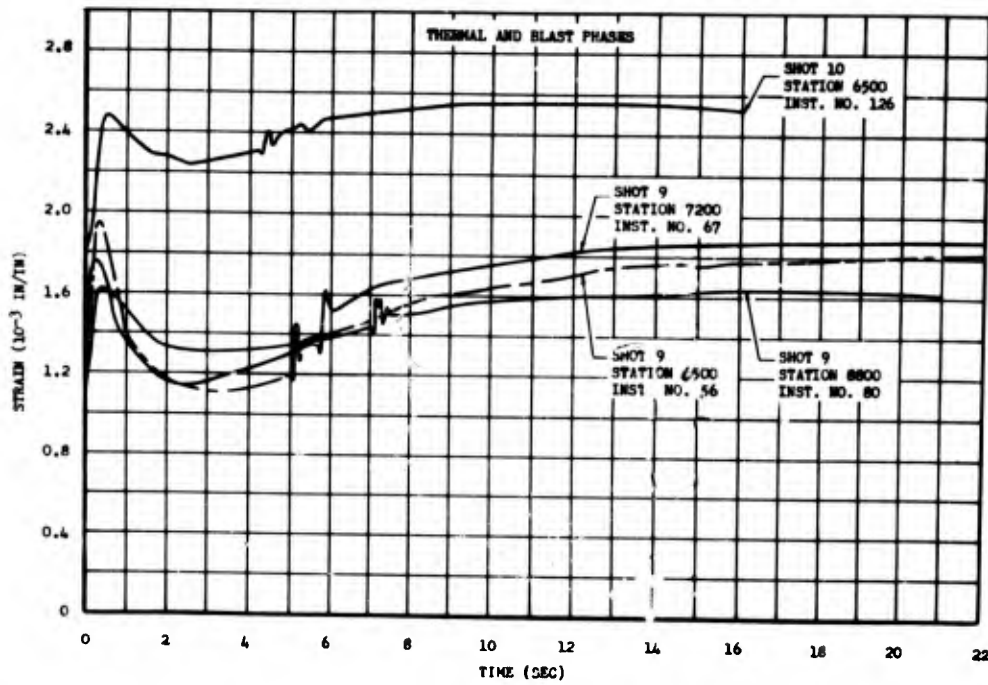
Fig. C.27 Comparison of Rear Spar-cap Strain (Exposed Side) vs Time From Stabilizers Exposed to Thermal Energy Only, Stabilizer Station 24.75
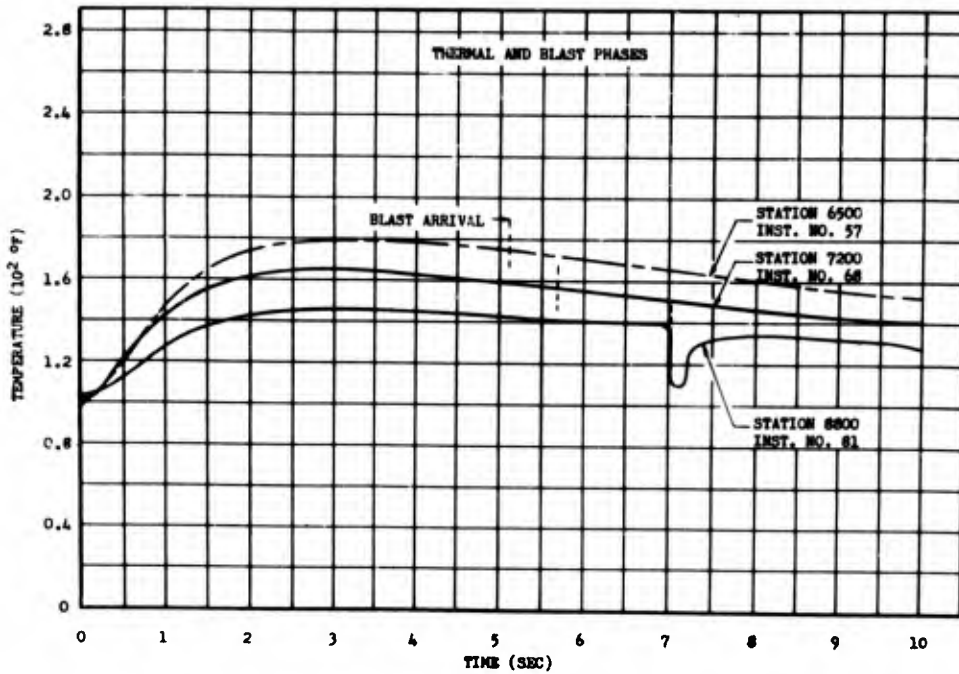
Fig. C.28 Comparison of Rear Spar-cap Temperature (Exposed Side) vs Time from Stabilizers Exposed to Thermal Energy Only, Stabilizer Station 24.75

165
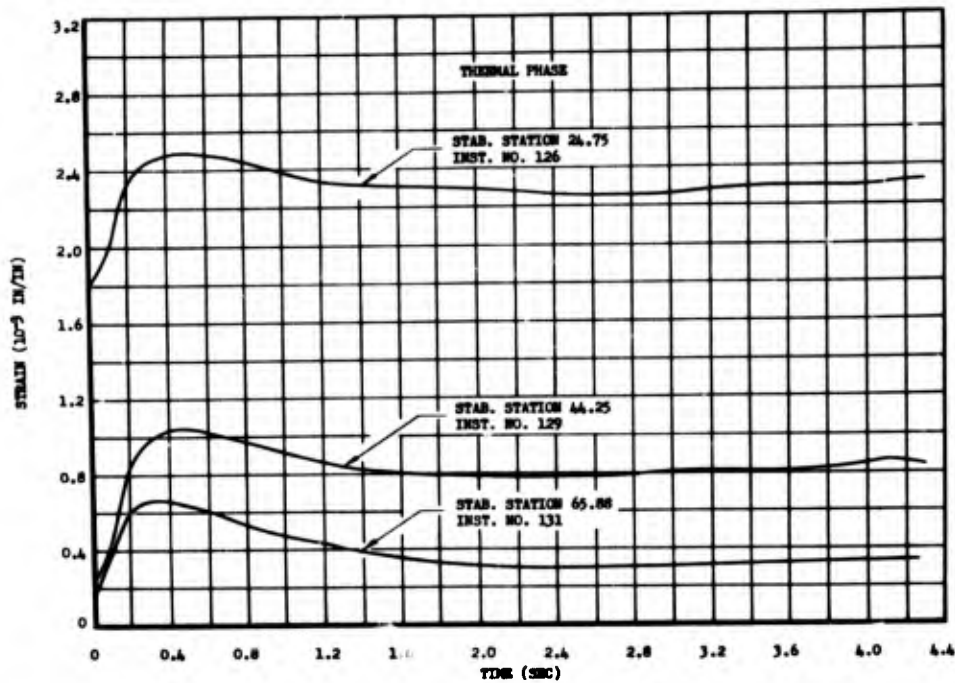
Fig. C.29 Comparison of the Rear Spar-cap Strain (Exposed Side) vs
Time Measurements at Various Stabilizer Stations, From
the Stabilizer Exposed to Thermal Energy Only, Station 6500,
Shot 10
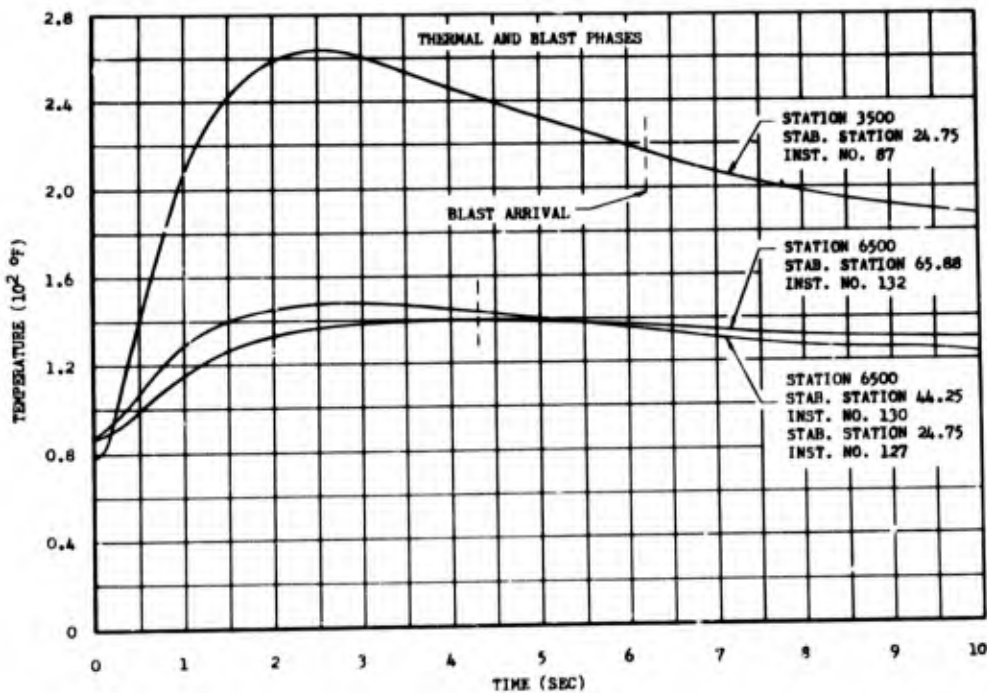
Fig. C.30 Comparison of the Rear Spar-cap Temperature (Exposed
Side) vs Time Measurements From All Stabilizers Exposed
to Thermal Energy Only, Shot 10

166
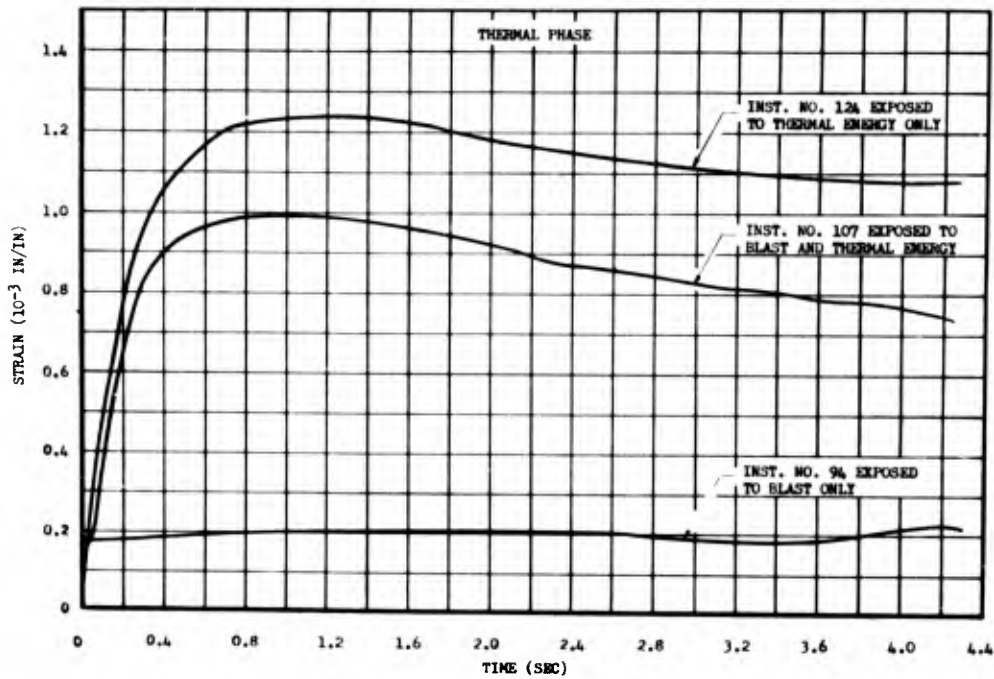
Fig. C.31 Comparison of Front Spar Flange Strain vs Time Measurements From All Stabilizers Exposed at Station 6500, Shot 10, Stabilizer Station 24.75
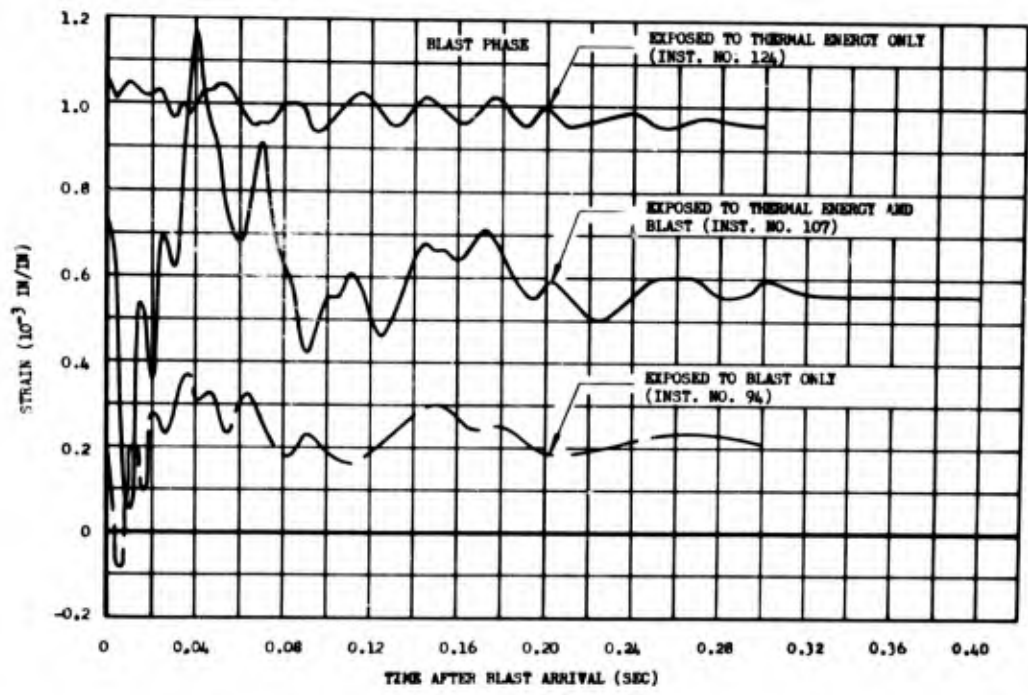
Fig. C.32 Comparison of Front Spar Flange Strain vs Time Measurements From All Stabilizers Exposed at Station 6500, Shot 10, Stabilizer Station 24.75

167
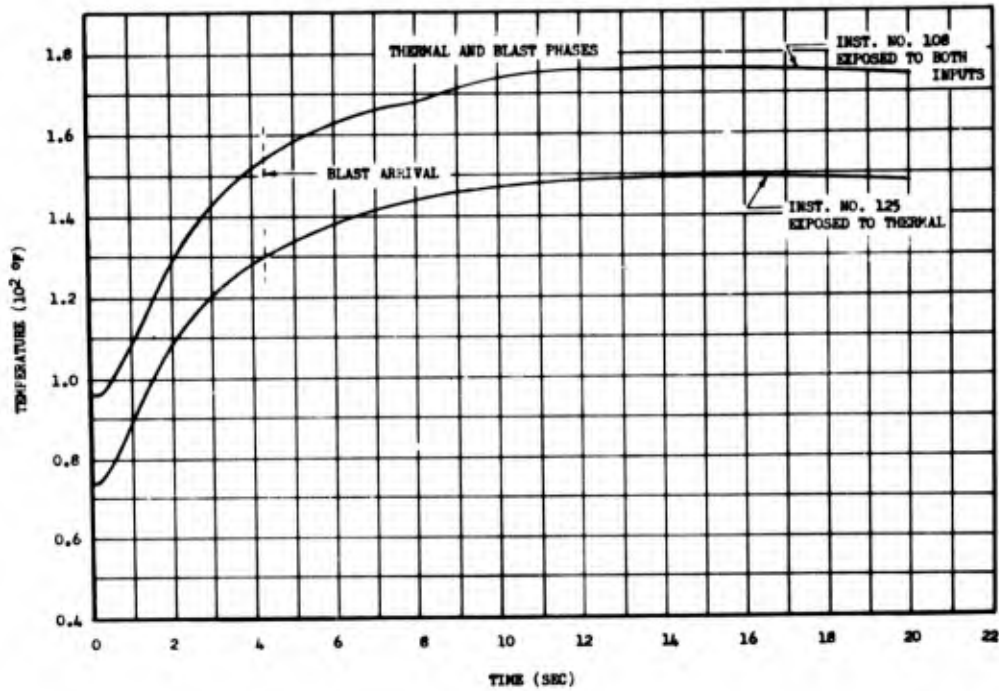
Fig. C. 33 Comparison of the Front Spar Temperature vs Time From
All Stabilizers Exposed to Thermal Energy, Station 6500,
Shot 10
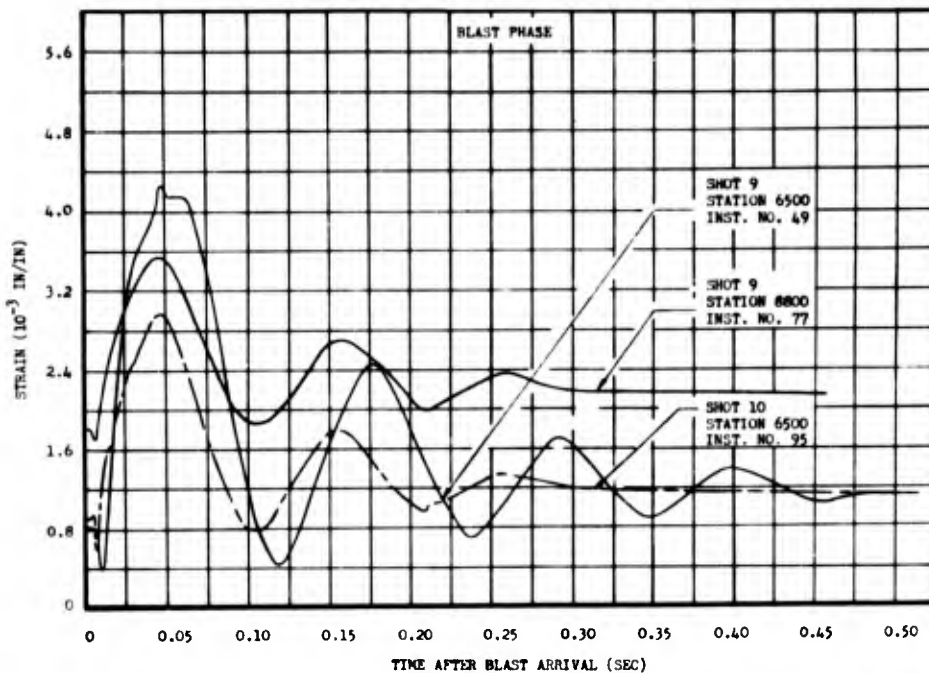
Fig. C. 34 Comparison of the Rear Spar-cap Strain (Exposed Side) vs
Time From Stabilizers Exposed to Blast Only, Stabilizer
Station 24. 75

168
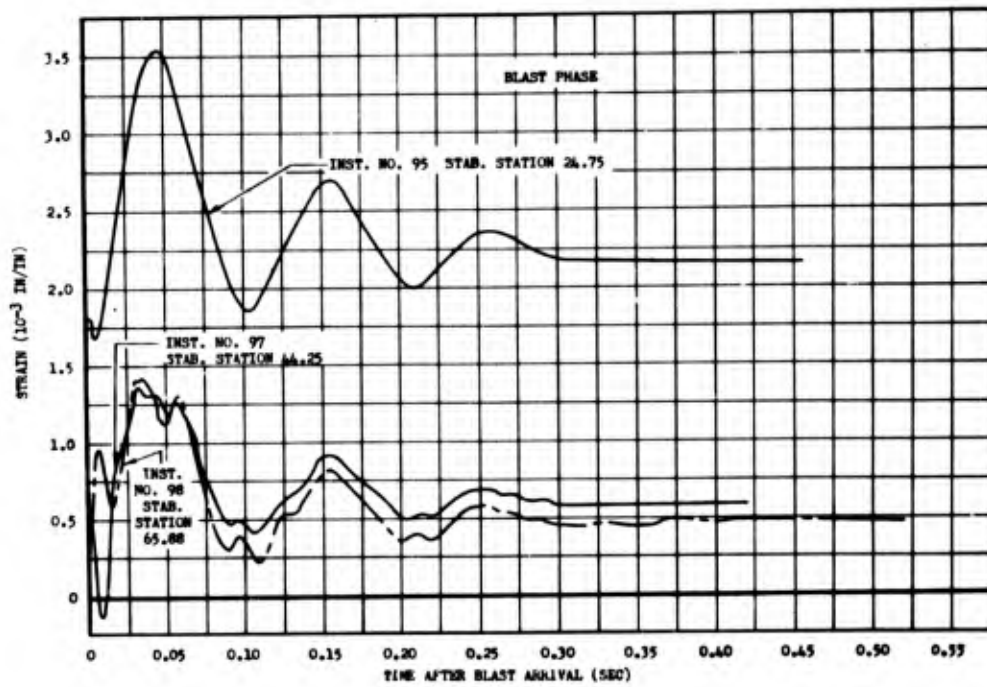
Fig. C.35 Comparison of the Rear Spar-cap Strain (Exposed Side) vs Time Stabilizer Exposed to Blast Only, Station 6500, Shot 10
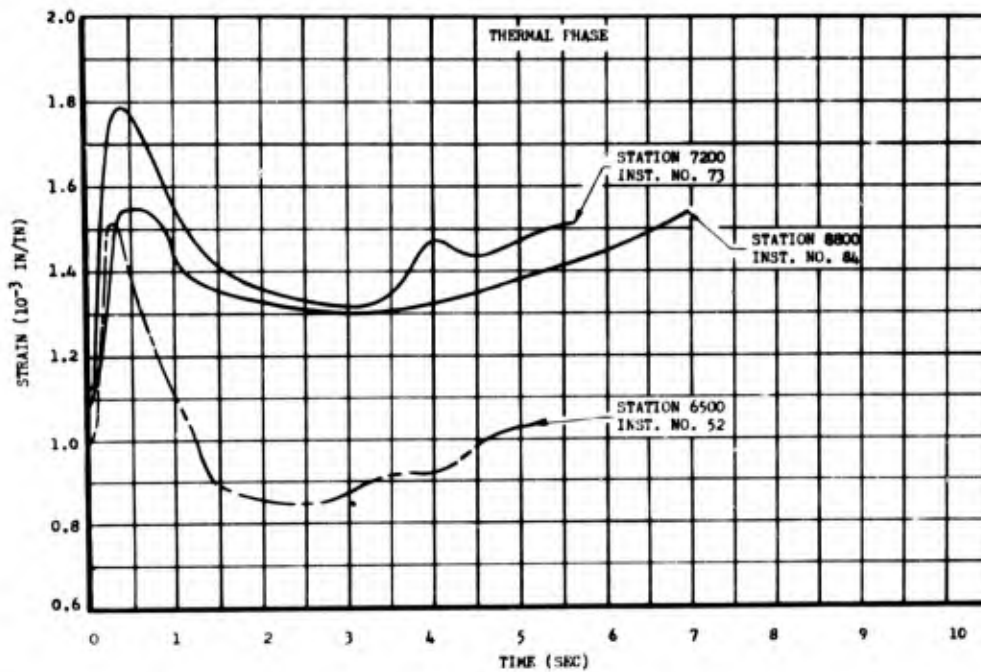
Fig. C.36 Comparison of the Rear Spar-cap Strain vs Time of All Stabilizers Exposed to Both Blast and Thermal Inputs, Shot 9, Stabilizer Station 24.75, Exposed Side

169
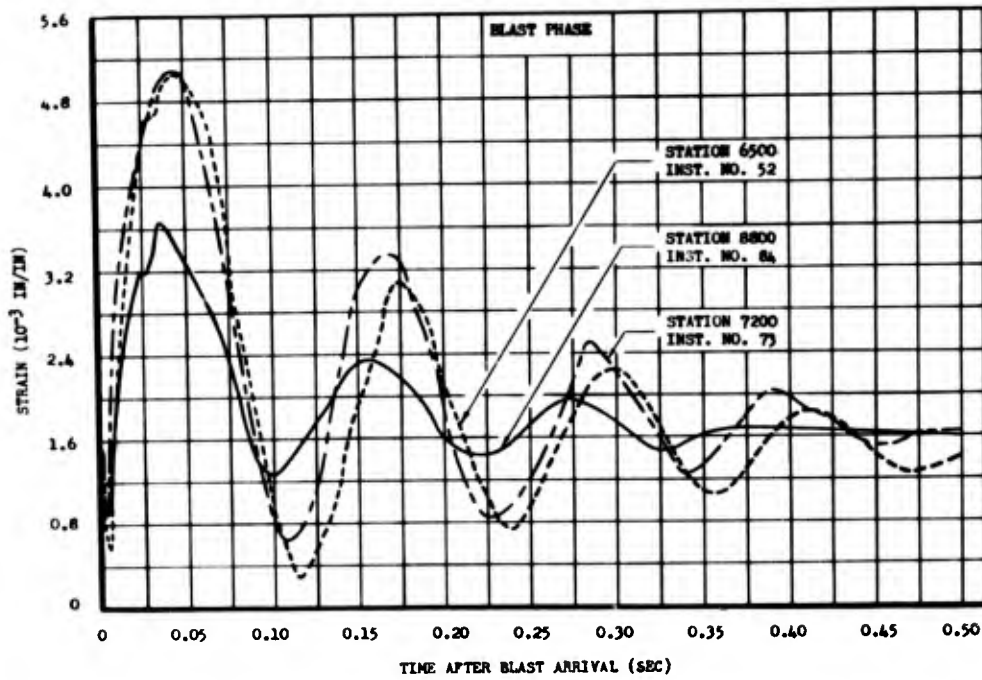
Fig. C.37 Comparison of the Rear Spar-cap Strain (Exposed Side) vs
Time for All Stabilizers Exposed to Both Thermal and Blast
Inputs, Shot 9, Stabilizer Station 24.75
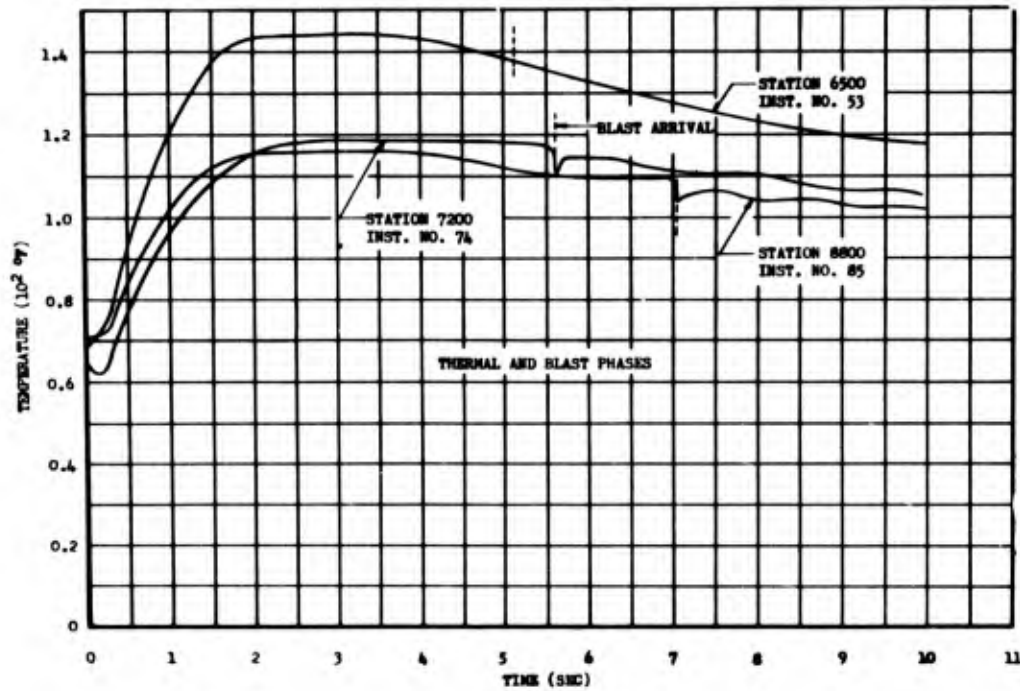
Fig. C.38 Comparison of the Rear Spar-cap Temperature (Exposed
Side) vs Time at Stabilizer Station 24.75 for All Stabilizers
Exposed to Both Thermal and Blast Inputs, Shot 9

170
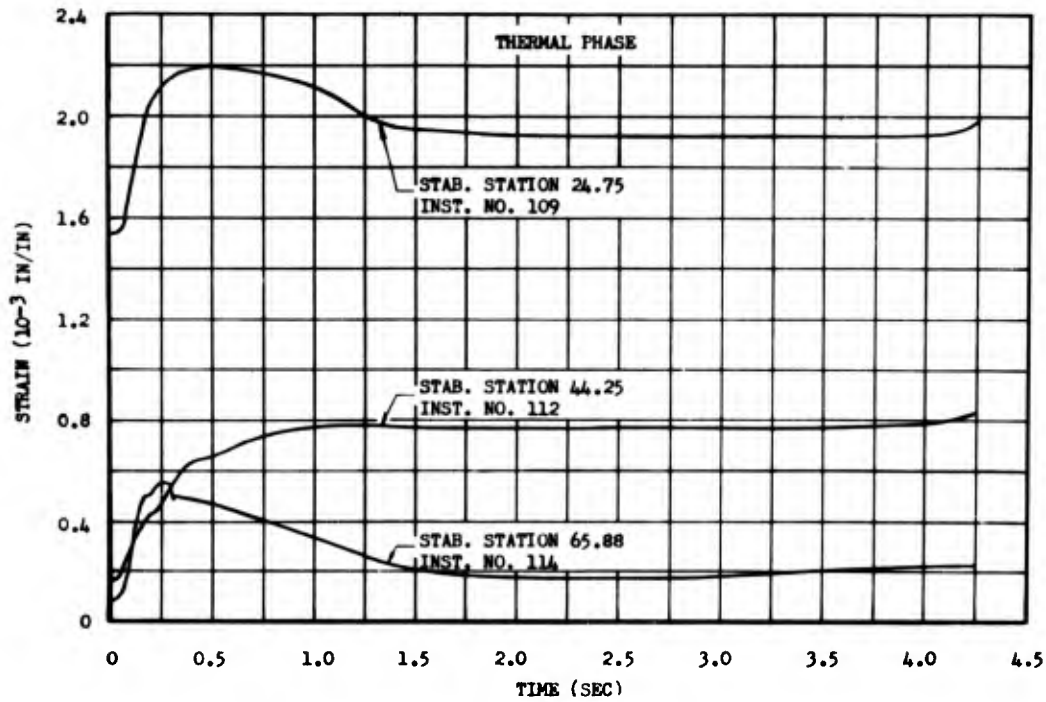
Fig. C.39 Comparison of the Rear Spar-cap Strain (Exposed Side) vs Time for Stabilizer Exposed to Both Thermal and Blast Inputs, Station 6500, Shot 10
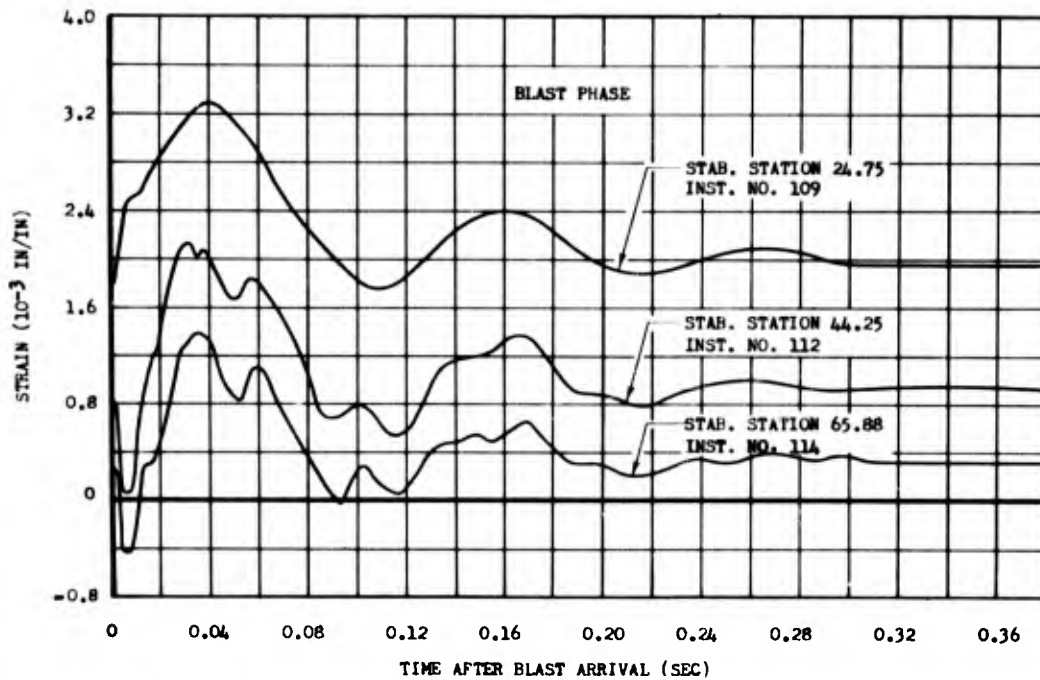
Fig. C.40 Comparison of the Rear Spar-cap Strain (Exposed Side) vs Time for Stabilizer Exposed to Both Thermal and Blast Inputs, Station 6500, Shot 10

171
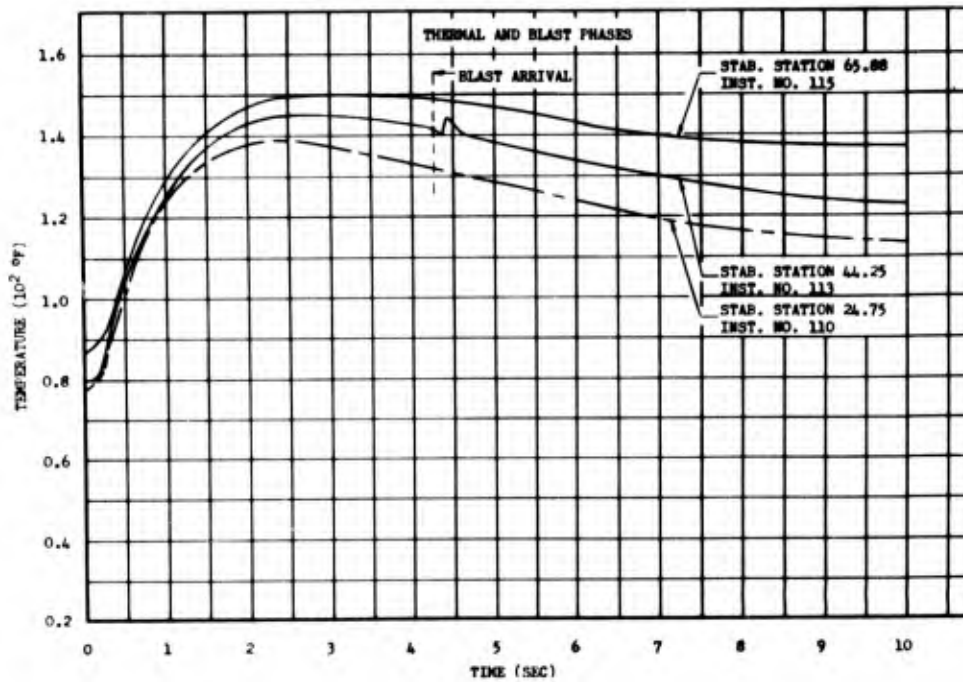
Fig. C.41 Comparison of the Rear Spar-cap Temperature (Exposed Side) vs Time for Stabilizer Exposed to Both Thermal and Blast Inputs, Station 6500, Shot 10
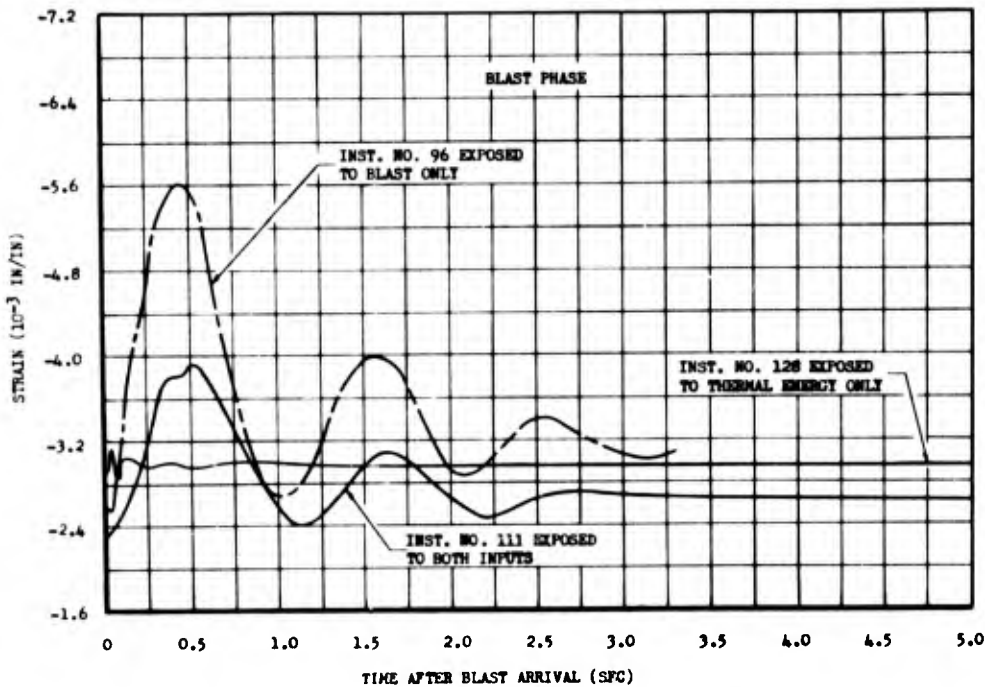
Fig. C.42 Comparison of the Rear Spar-cap Strain (Unexposed Side) vs Time at Stabilizer Station 24.75, for All Stabilizers At Station 6500, Shot 10

172
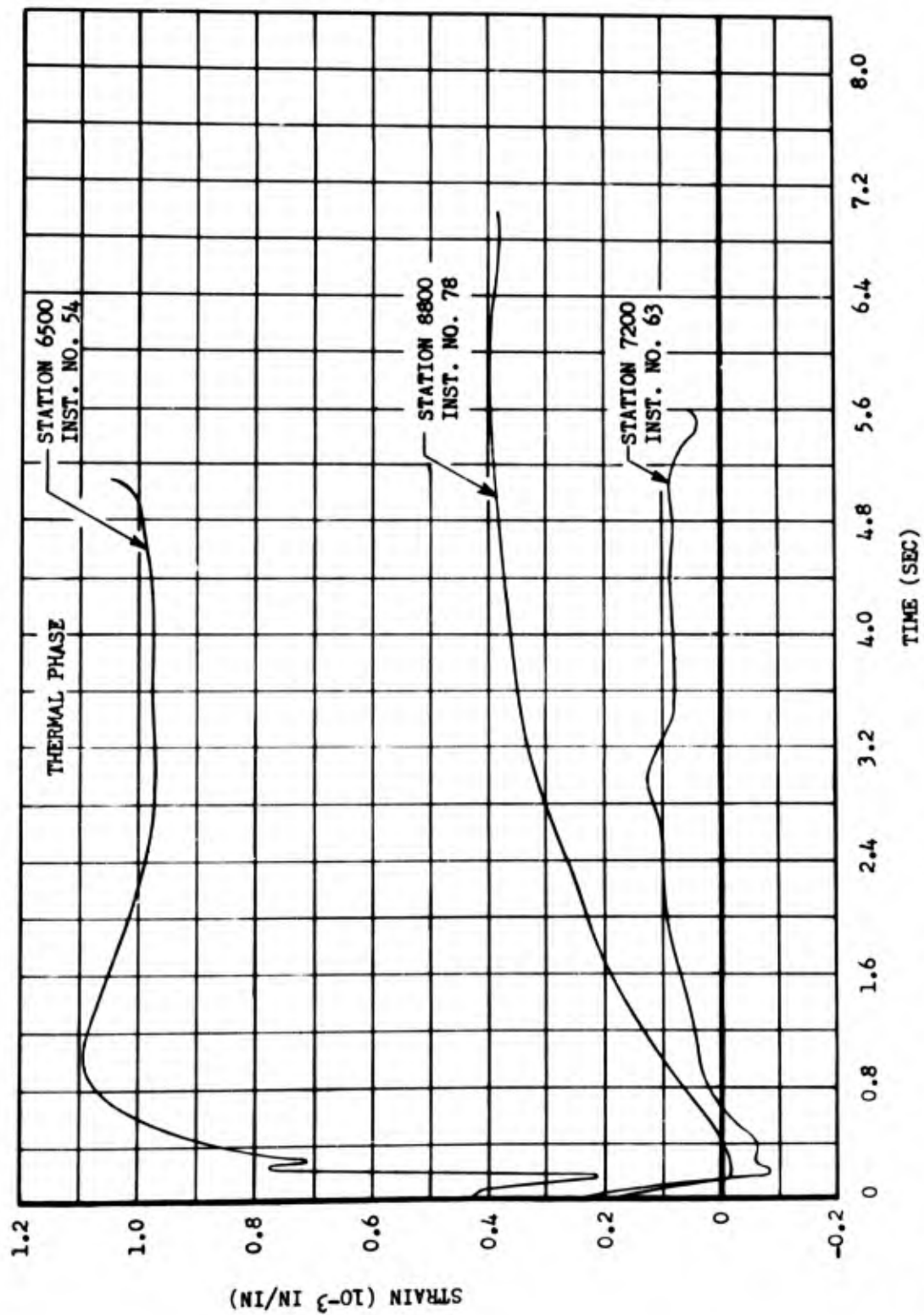
Fig. C. 43 Comparison of the Skin Strain vs Time Measurements for All Stabilizers Exposed to Thermal Energy Only, Stabilizer Station 24.75, Shot 9

173
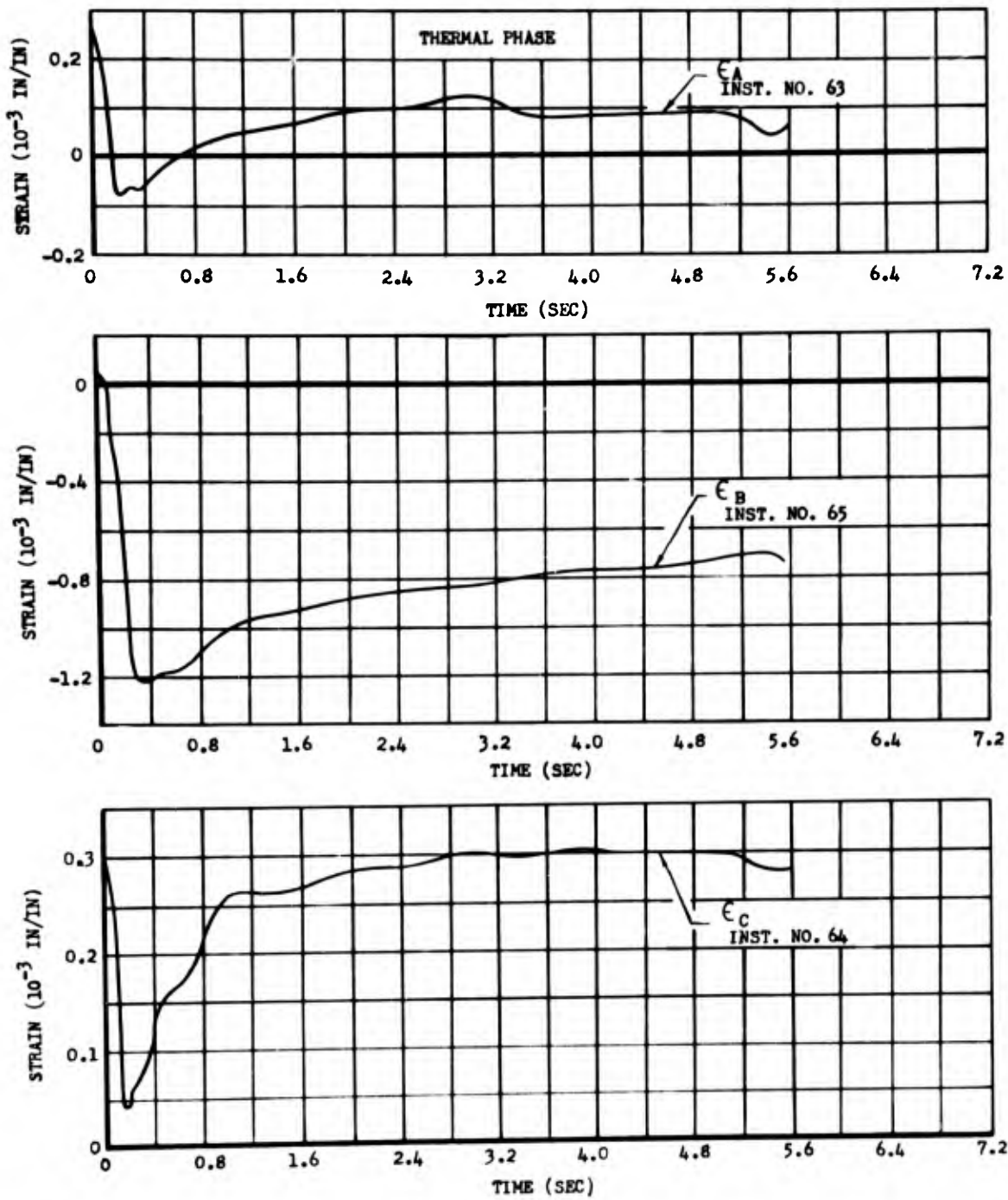
Fig. C.44 Comparison of the Skin Strain From Three Rosette Axis vs
Time for Stabilizer Exposed to Thermal Energy Only,
Stabilizer Station 24.75, Station 7200, Shot 9

174
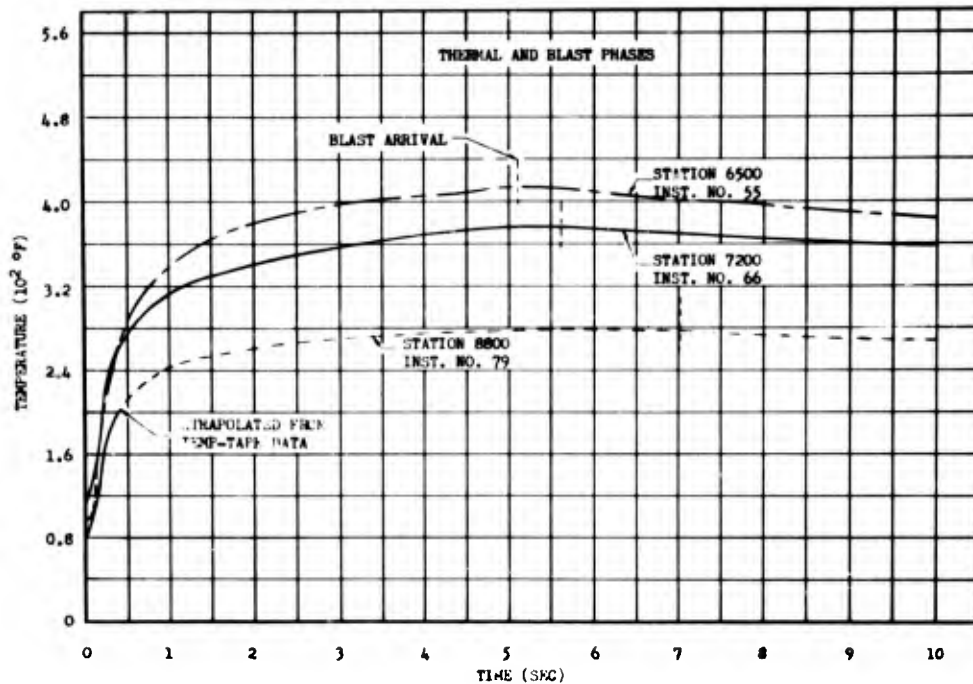
Fig. C.45 Comparison of the Skin Temperature vs Time at Stabilizer
Station 24.75 for All Stabilizers Exposed to Thermal Energy
Only, Shot 9
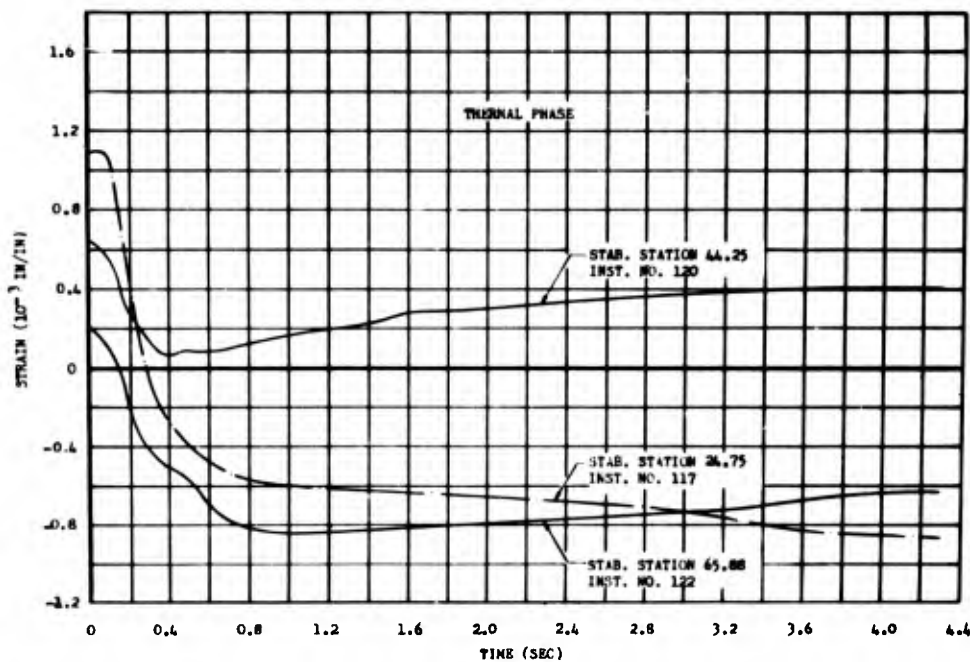
Fig. C.46 Comparison of the Skin Strain vs Time for the Stabilizer
Exposed to Thermal Energy Only, Station 6500, Shot 10

175
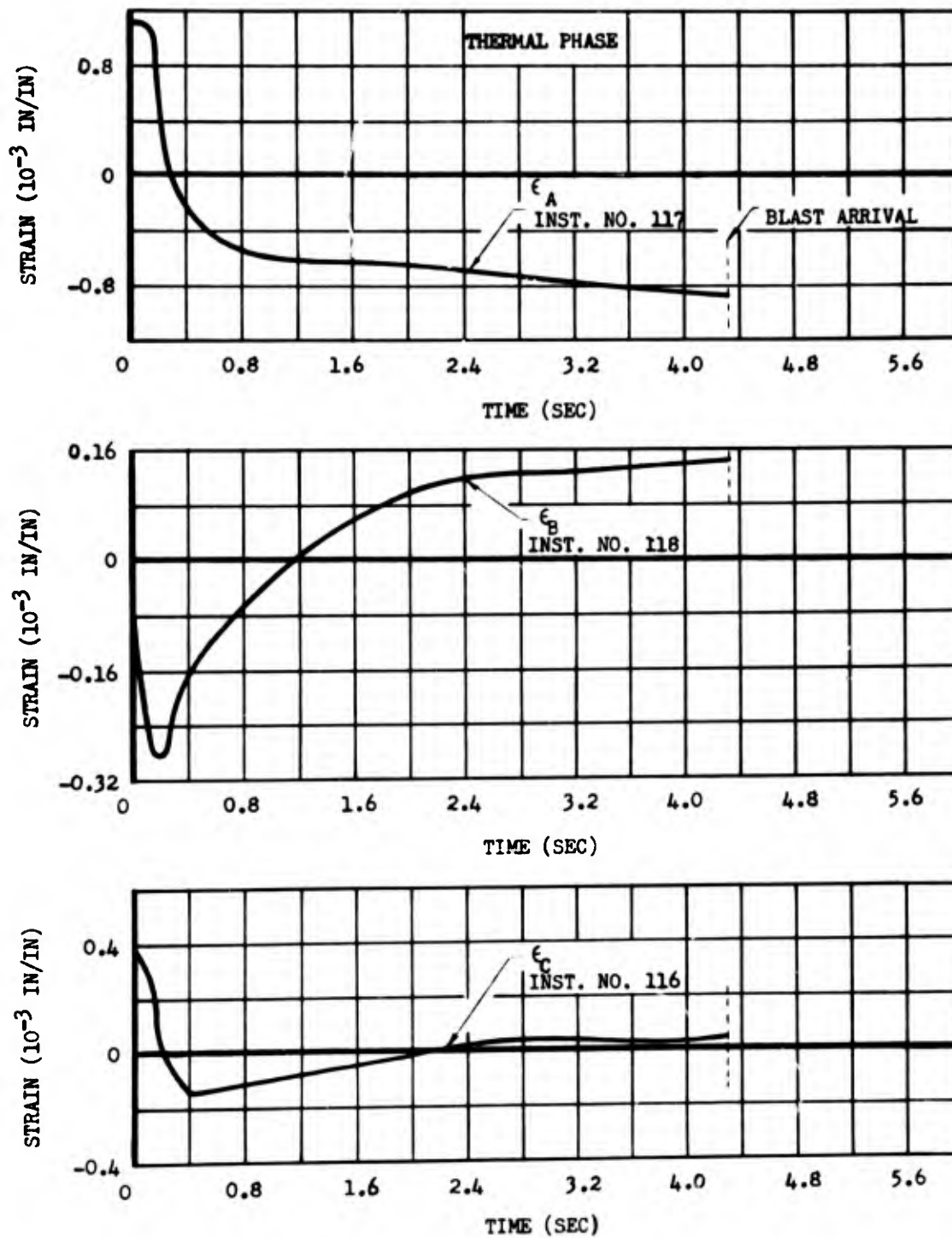
Fig. C.47 Comparison of the Skin Strain From Three Rosette Axis vs
Time From Stabilizer Exposed to Thermal Energy Only,
Stabilizer Station 24.75, Station 6500, Shot 10

176
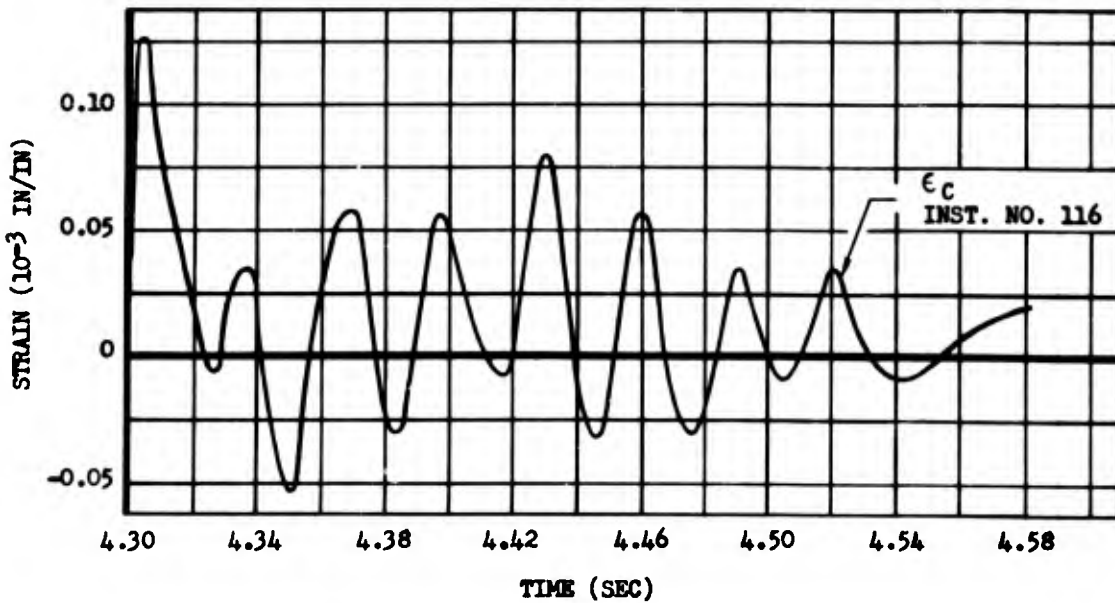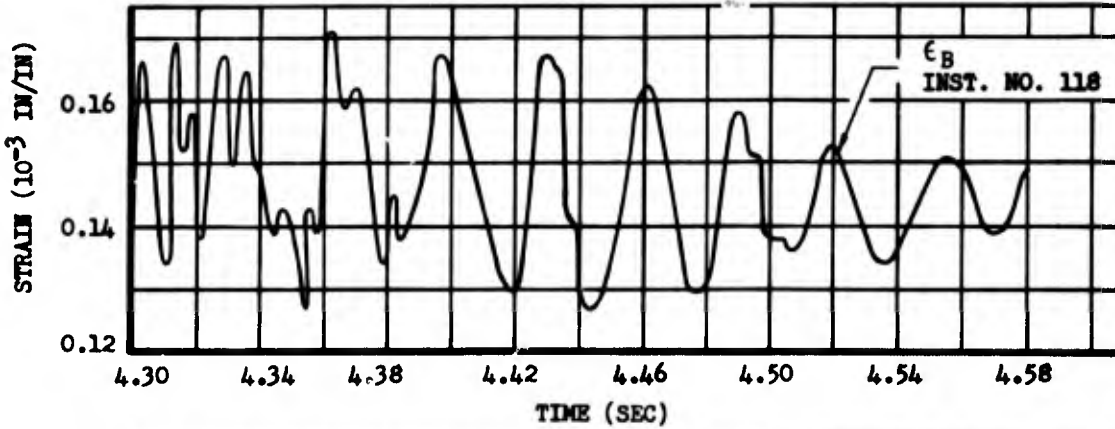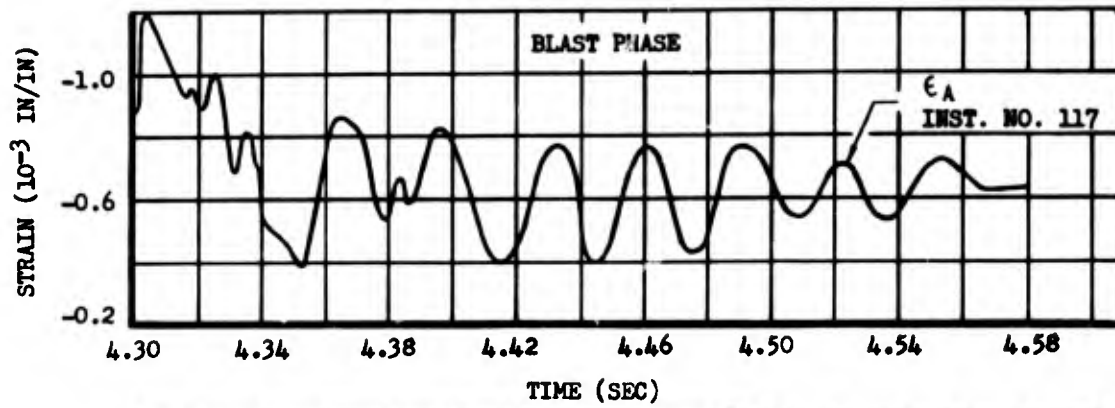
Fig. C.48 Comparison of the Skin Strain From Three Rosette Axis vs
Time From Stabilizer Exposed to Thermal Energy Only,
Stabilizer Station 24.75, Station 6500, Shot 10

177
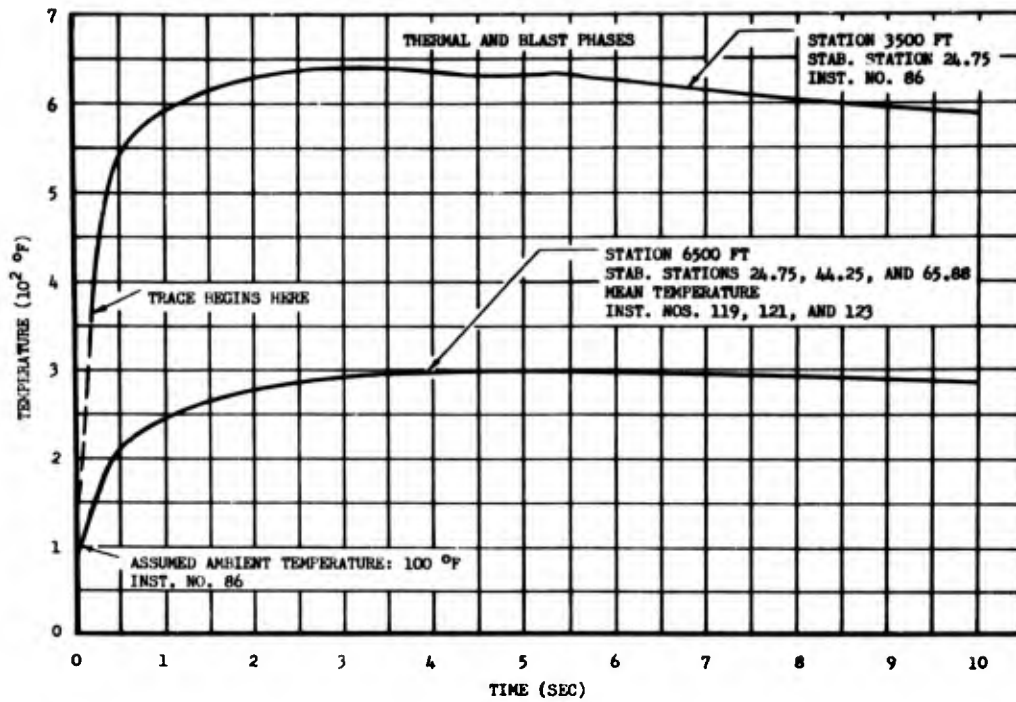
Fig. C.49 Comparison of Skin Temperature vs Time at Various Stabilizer Stations From All Stabilizers Exposed to Thermal Energy Only, Shot 10
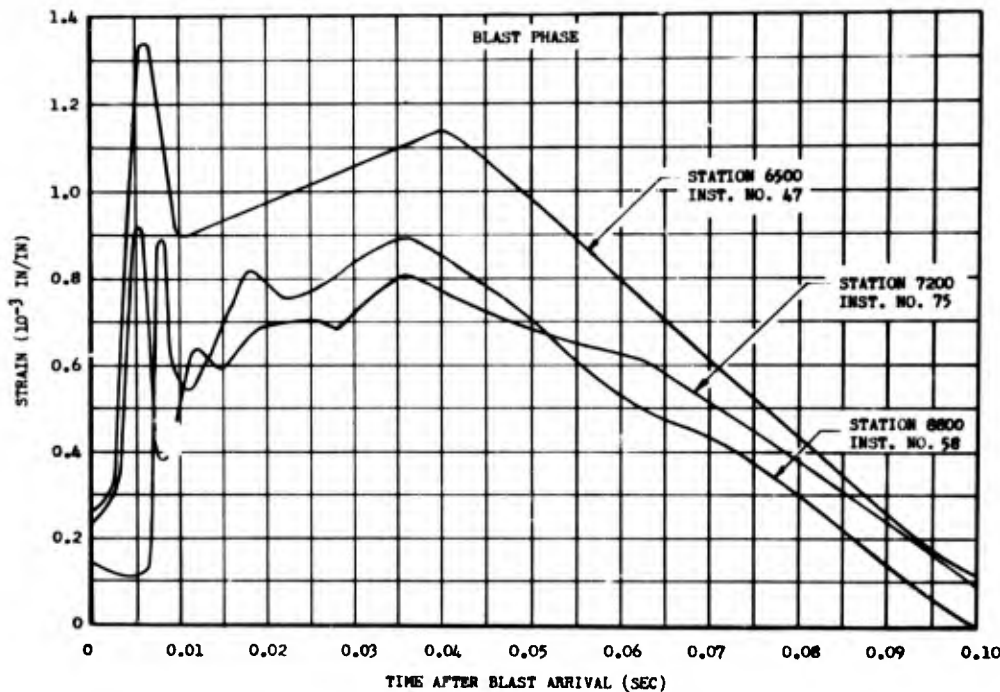
Fig. C.50 Comparison of the Skin Strain vs Time at Stabilizer Station 24.75 For All Stabilizers Exposed to Blast Only, Shot 9

178
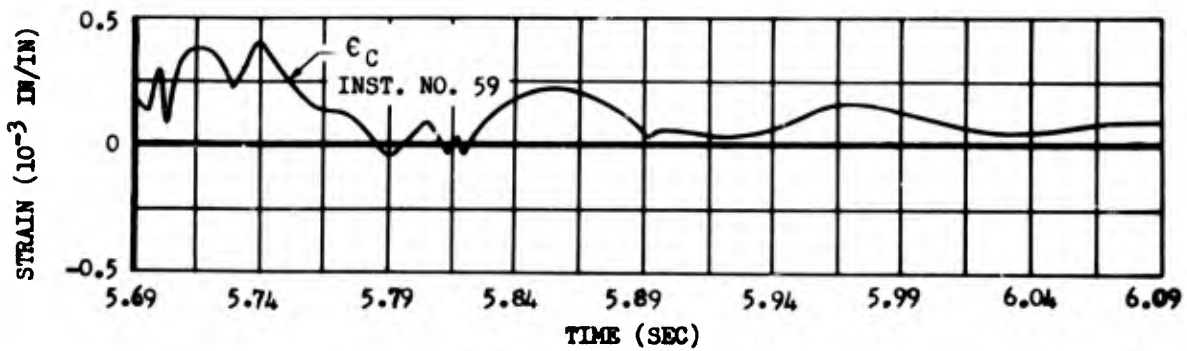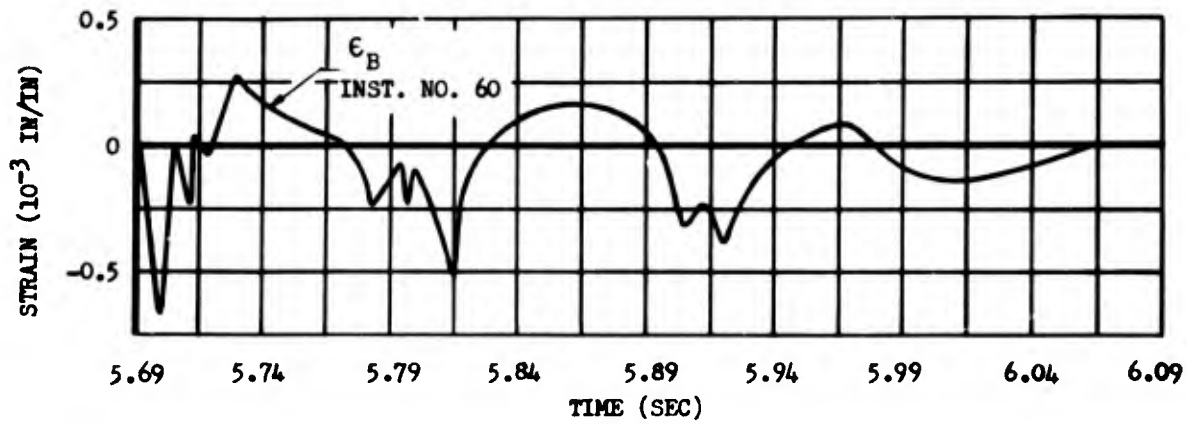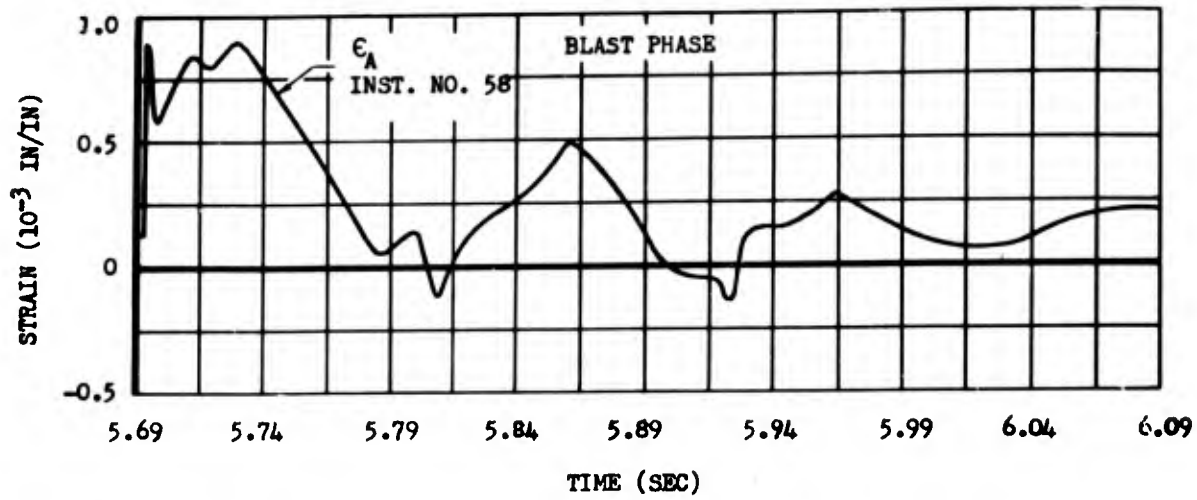
Fig. C.51 Comparison of the Skin Strain From Three Rosette Axis vs Time for Stabilizer Exposed to Blast Only, Stabilizer Station 24.75, Station 7200, Shot 9

179
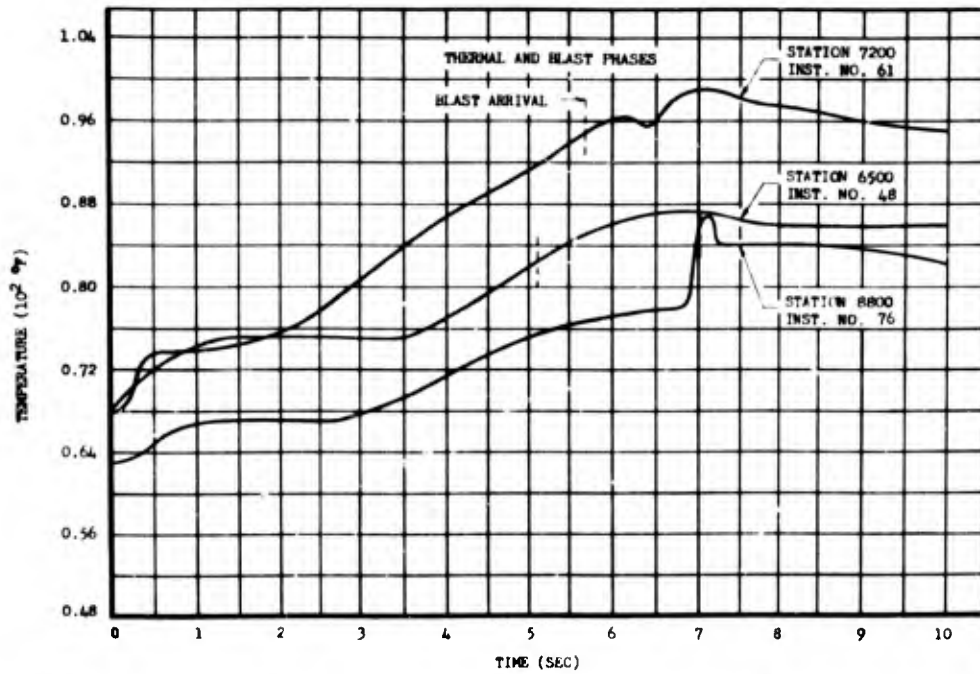
Fig. C.52 Comparison of the Skin Temperature vs Time at Stabilizer
Station 24.75 For All Stabilizers Exposed to Blast Only,
Shot 9
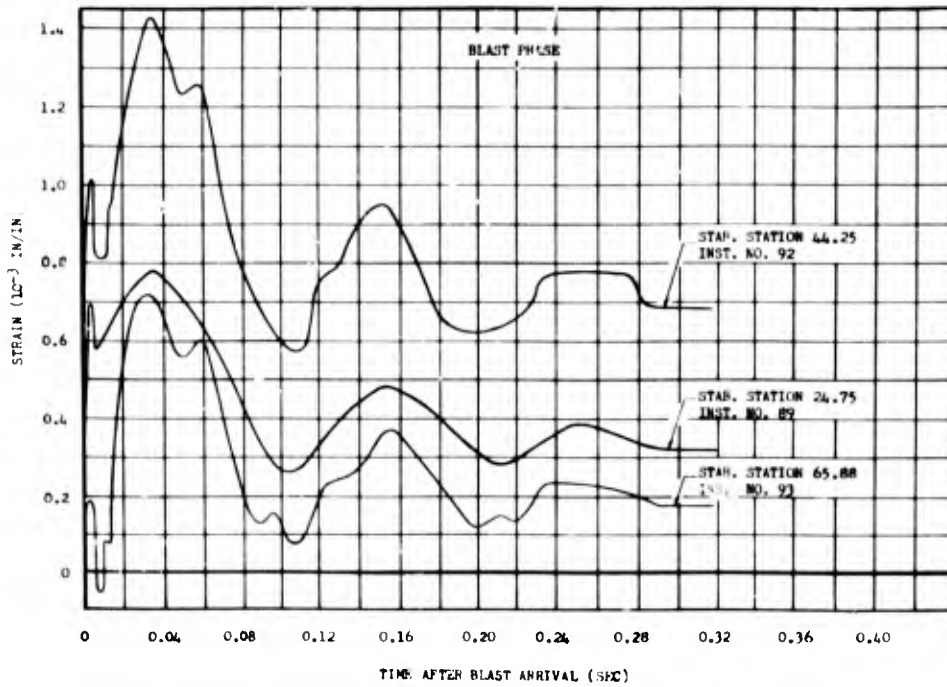
Fig. C.53 Comparison of the Skin Strain vs Time For The Stabilizer
Exposed to Blast Only, Station 6500, Shot 10

180
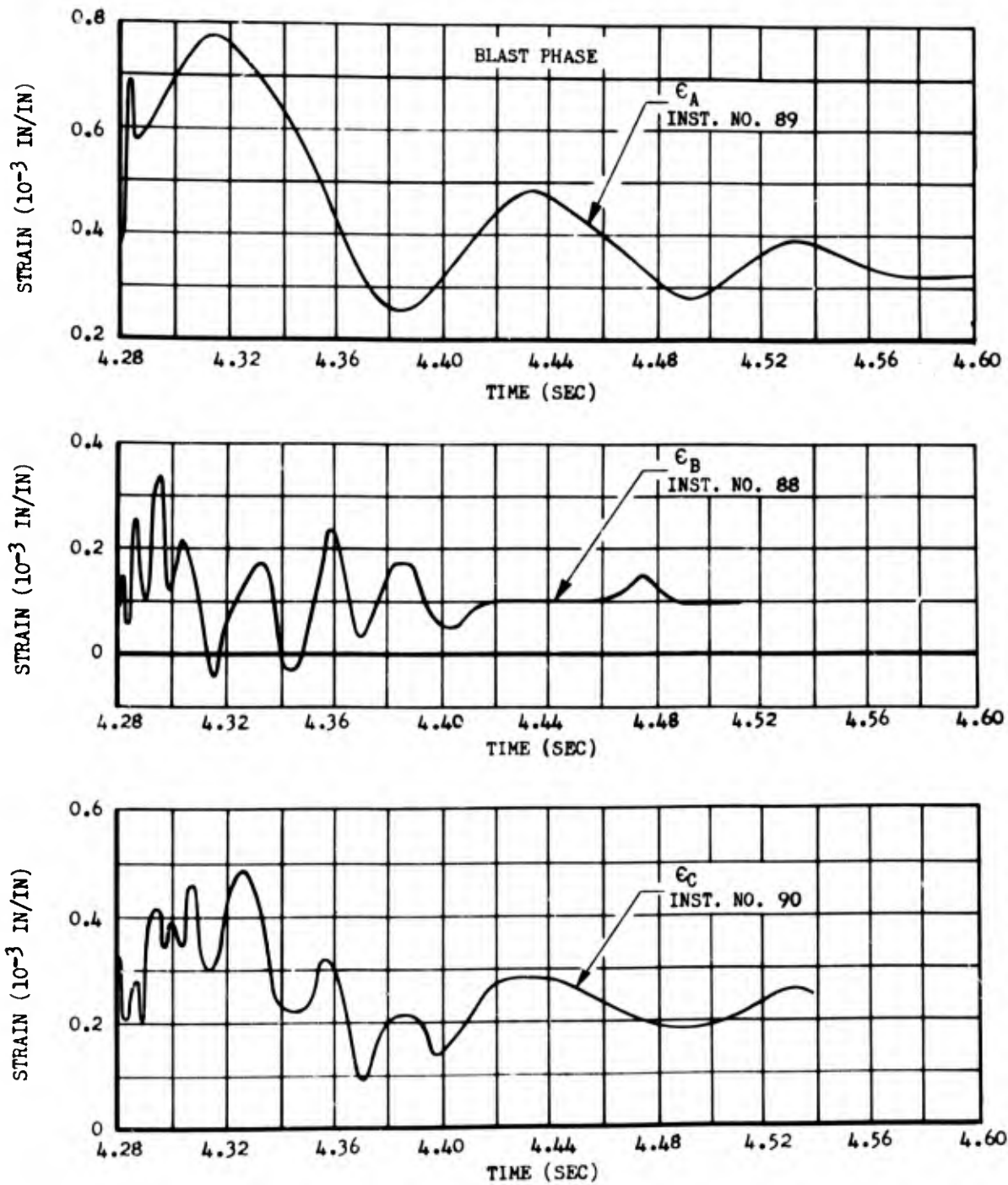
Fig. C.54 Comparison of the Skin Strain From Three Rosette Axis
vs Time for Stabilizer Exposed to Blast Only, Stabilizer
Station 24.75 Station 6500, Shot 10

181
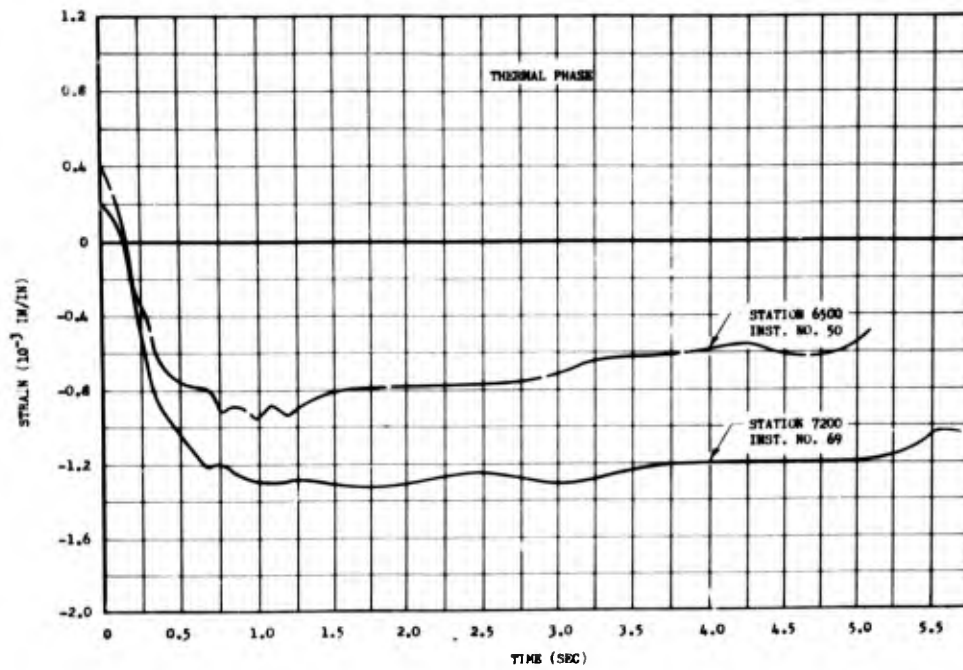
Fig. C.55 Comparison of the Skin Strain vs Time at Stabilizer Station
24.75 For All Stabilizers Exposed to Both Thermal and
Blast Inputs, Shot 9
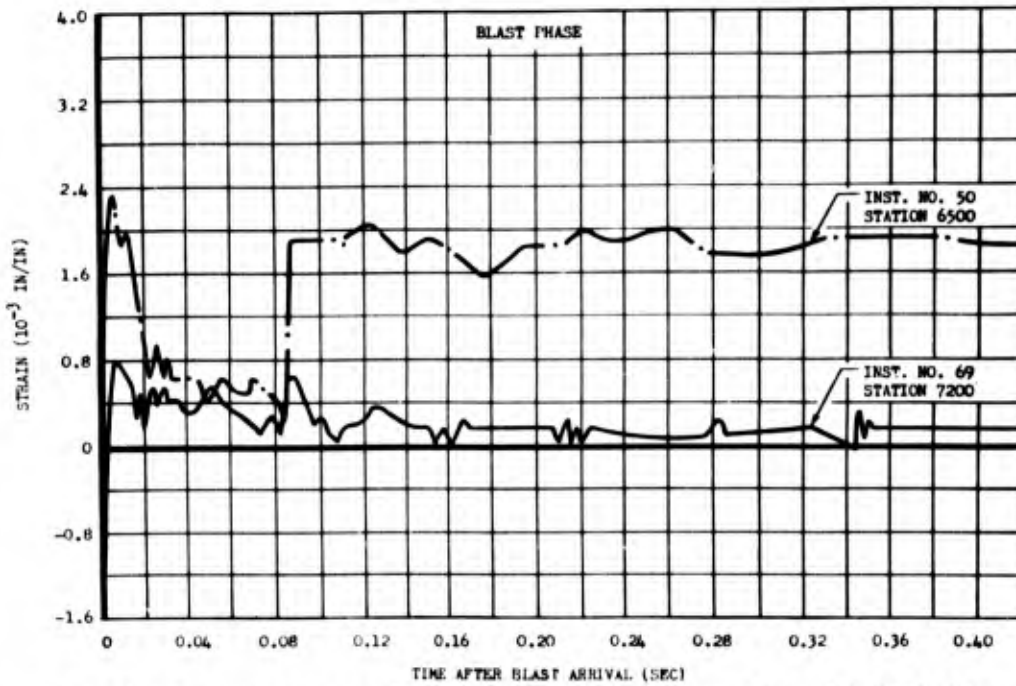
Fig. C.56 Comparison of Skin Strain vs Time For All Stabilizers
Exposed to Both Thermal and Blast Inputs, Stabilizer
Station 24.75, Shot 9

182
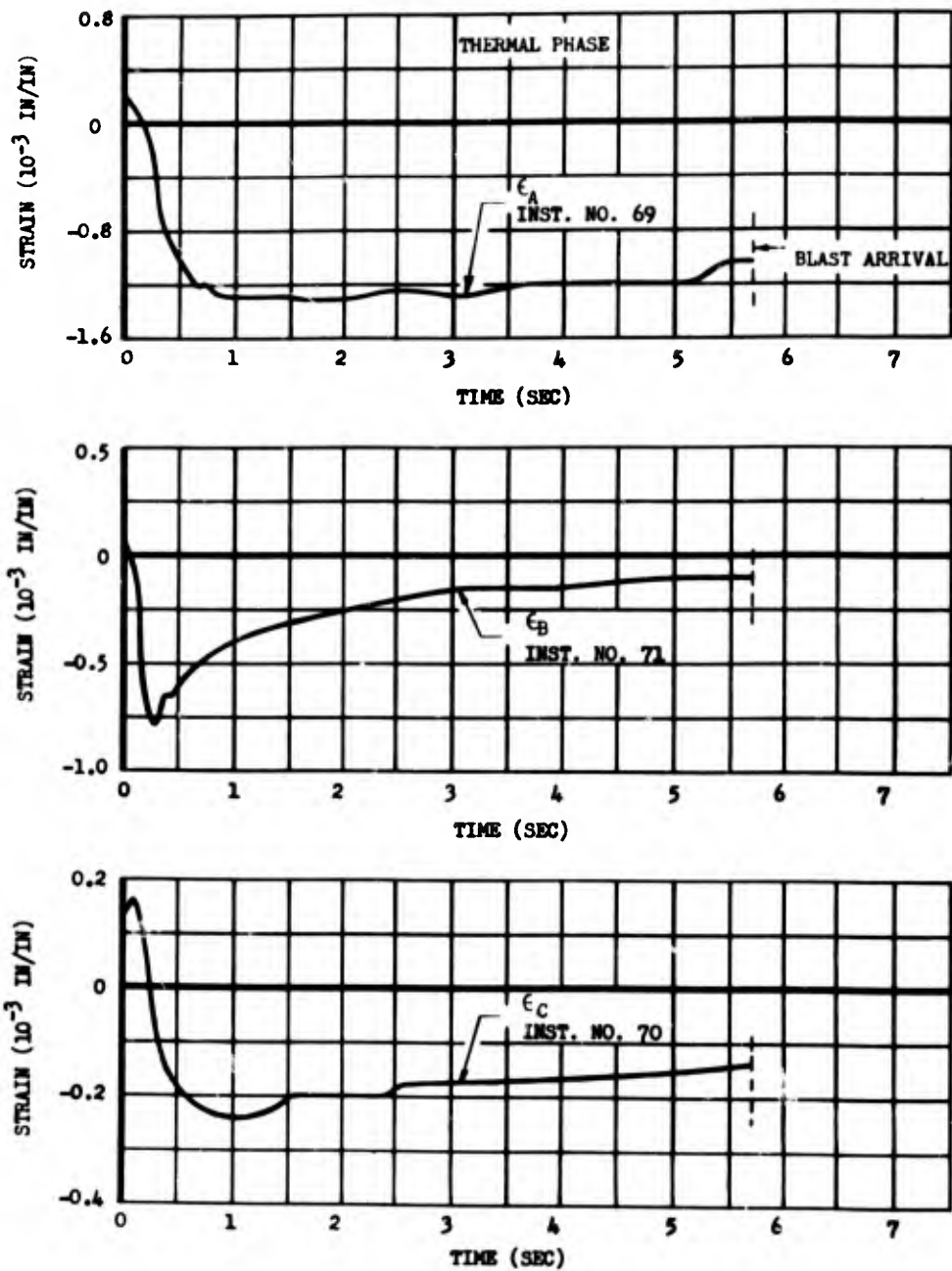
Fig. C.57 Comparison of the Skin Strain From Three Rosette Axis vs Time for Stabilizer Exposed to Both Thermal and Blast Inputs, Stabilizer Station 24.75, Shot 9, Station 7200

183
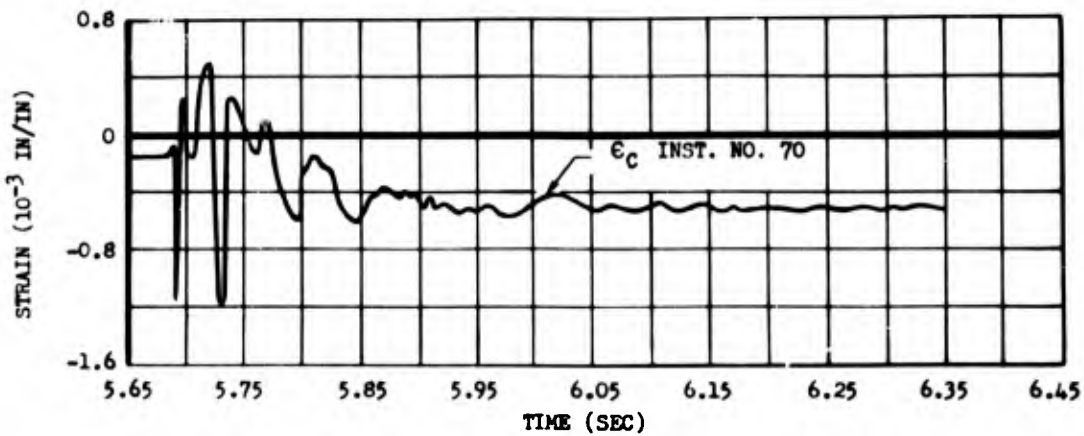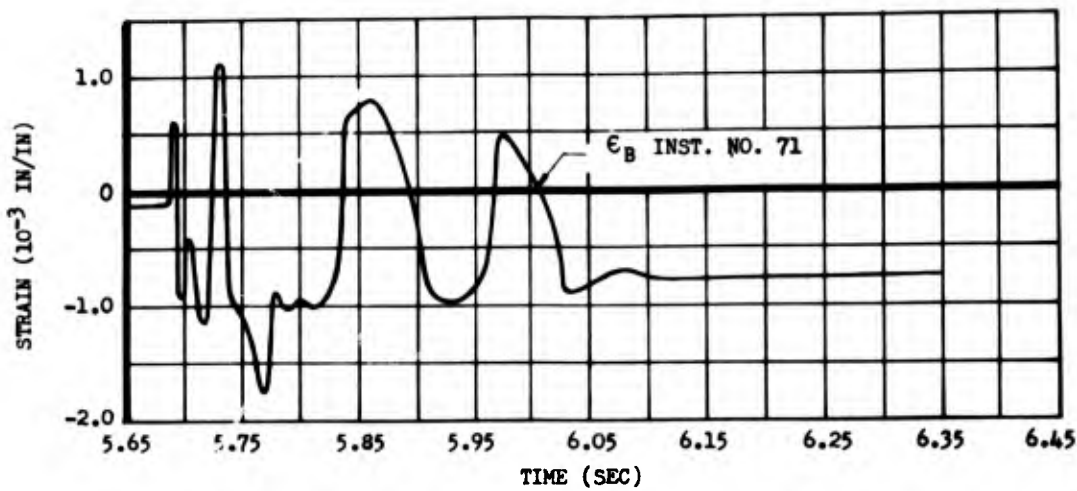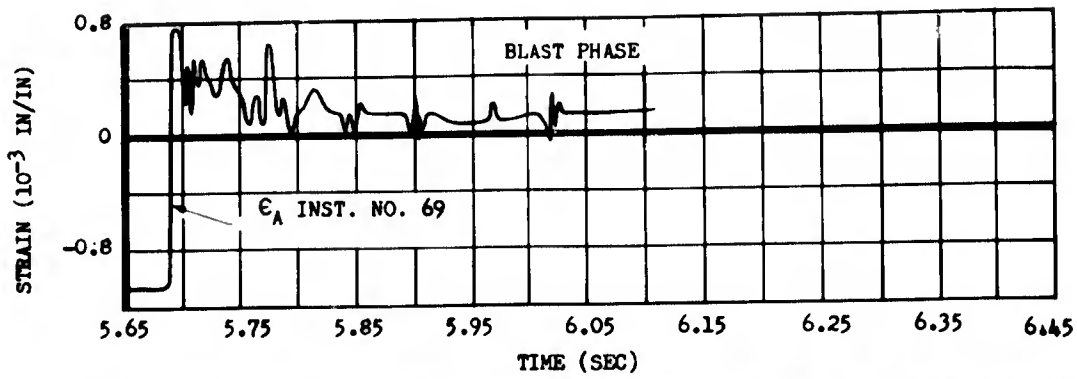
Fig. C.58 Comparison of the Skin Strain From Three Rosette Axis vs Time for Stabilizer Exposed to Both Thermal and Blast Inputs, Stabilizer Station 24.75, Shot 9, Station 7200

184
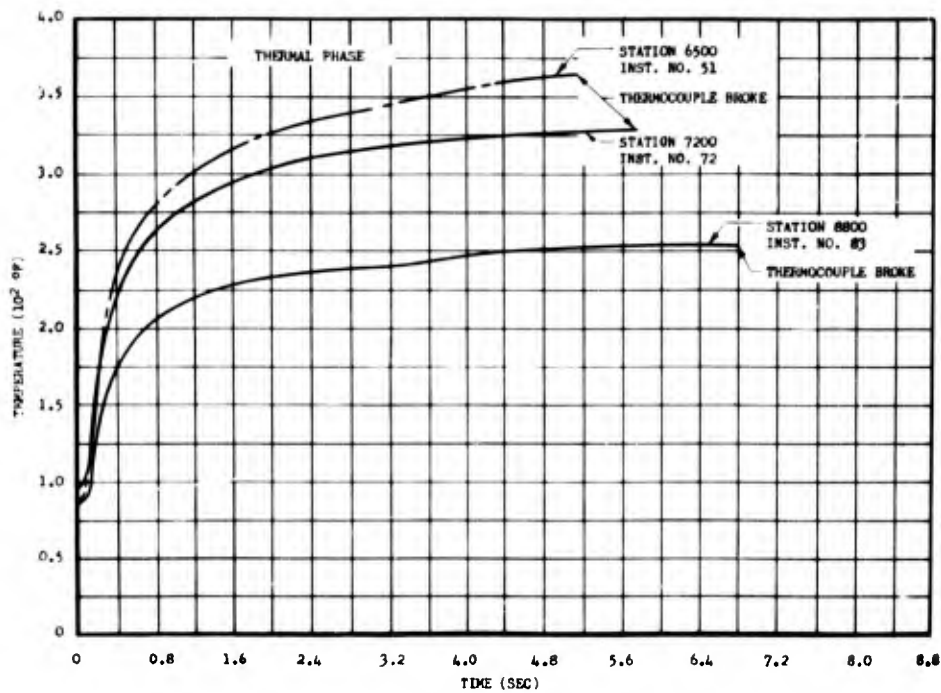
Fig. C.59 Comparison of the Skin Temperature vs Time for All
Stabilizers Exposed to Both Thermal and Blast Inputs,
Stabilizer Station 24.75, Shot 9
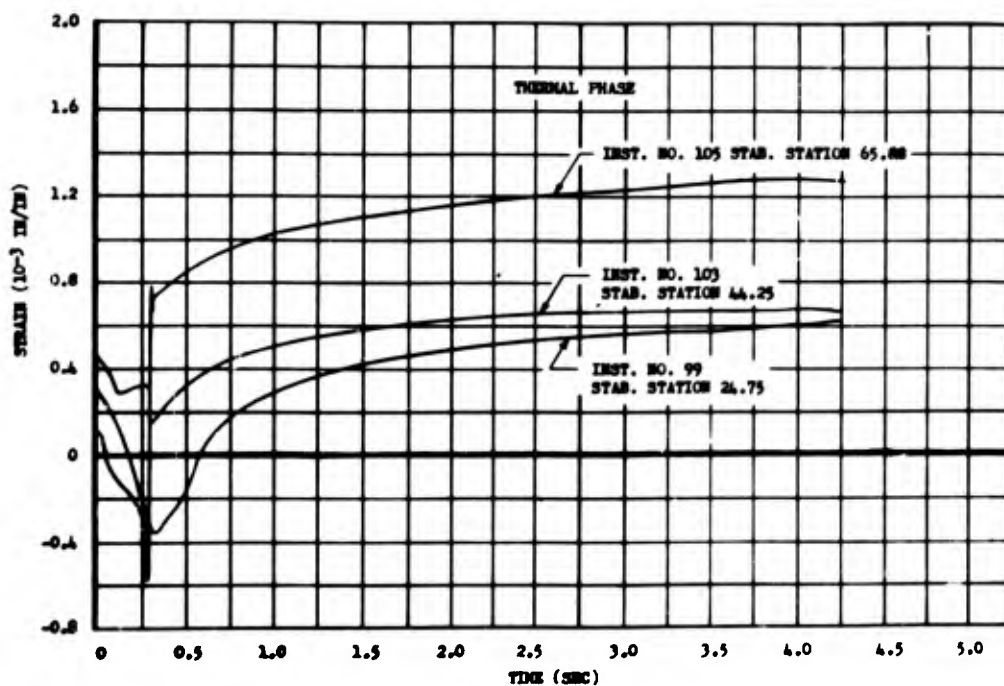
Fig. C.60 Comparison of the Skin Strain vs Time for the Stabilizer
Exposed to Both Thermal and Blast Inputs, Station 6500,
Shot 10
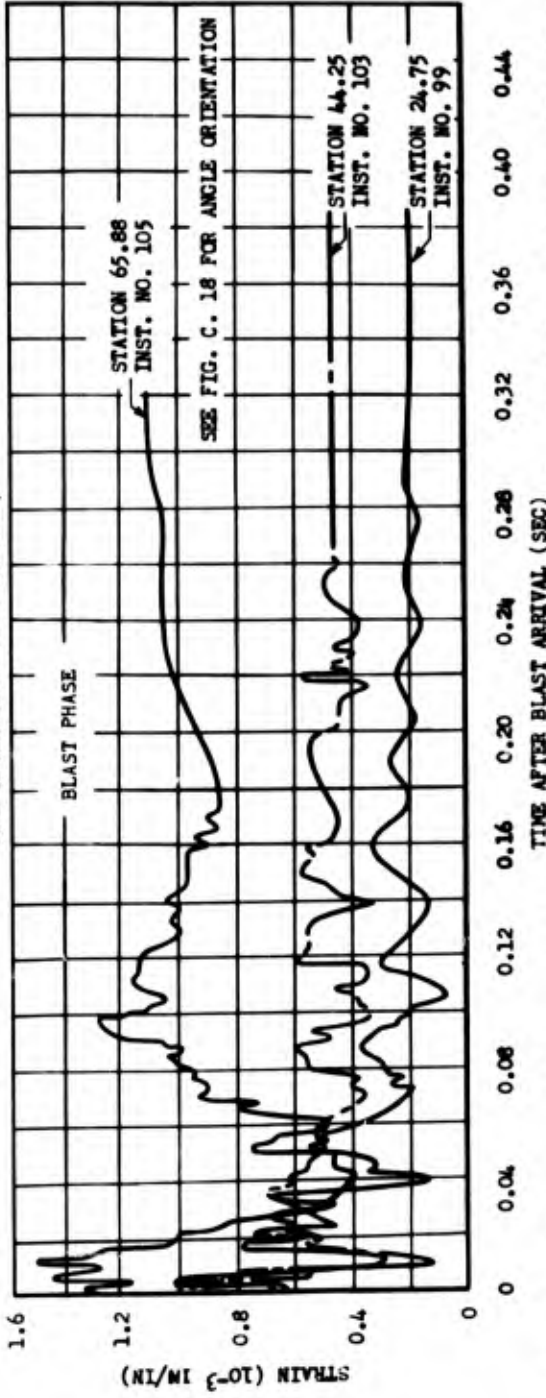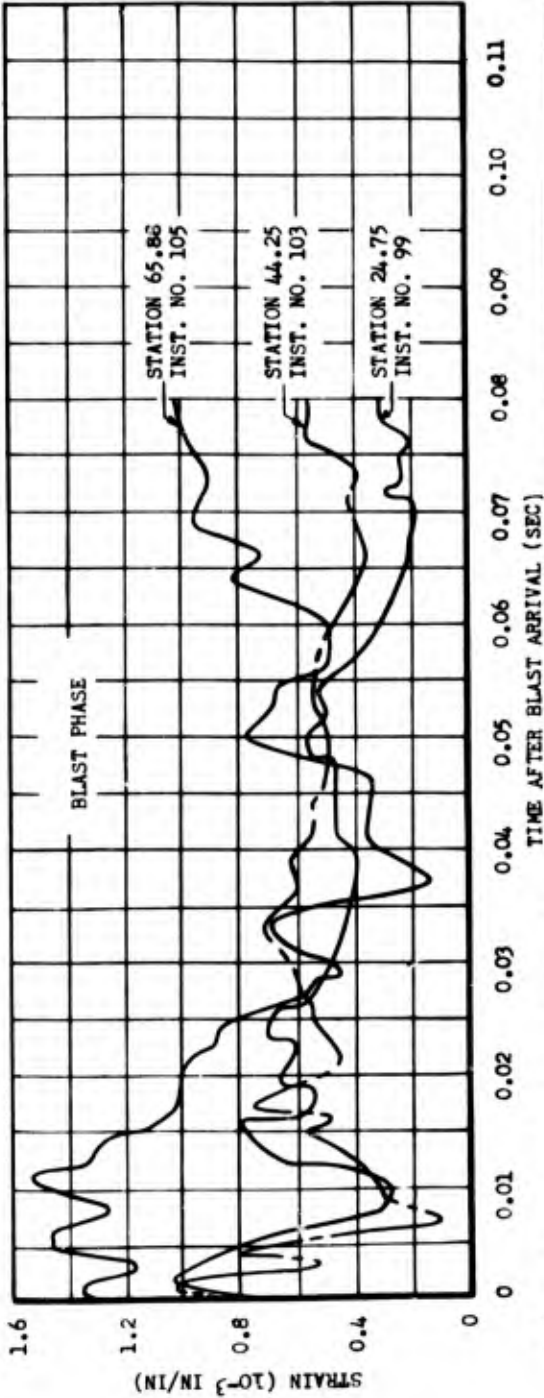
Fig. C.61 Comparison of the Skin Strain vs Time for the Stabilizer Exposed to Both Thermal and Blast Inputs, Station 6500, Shot 10

186
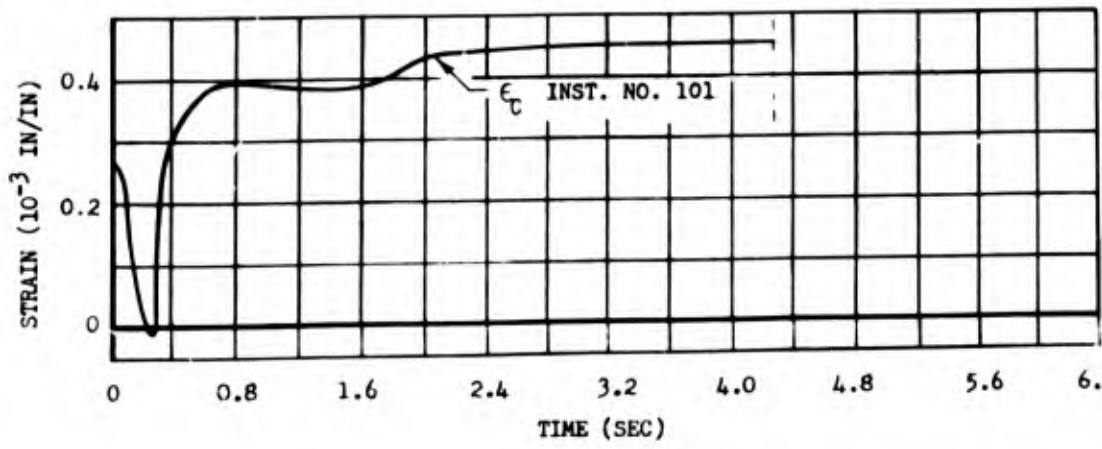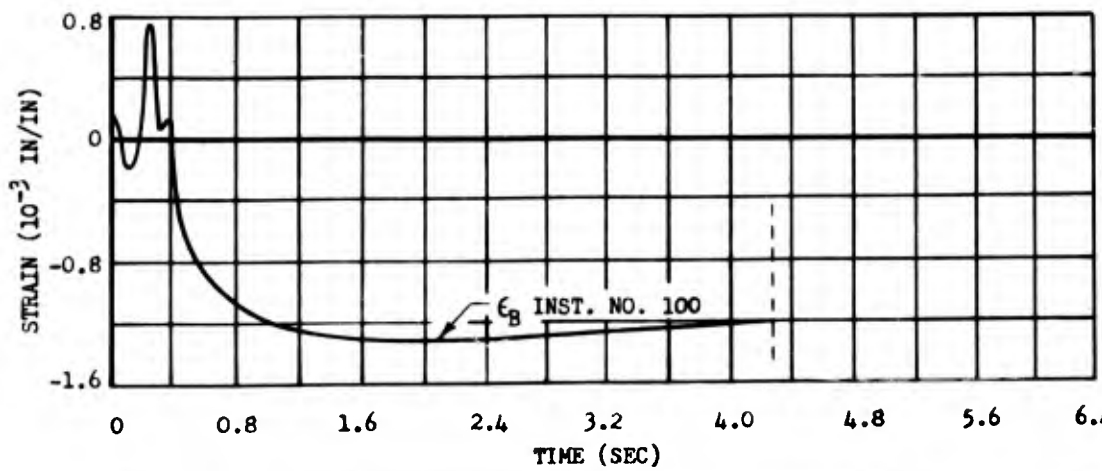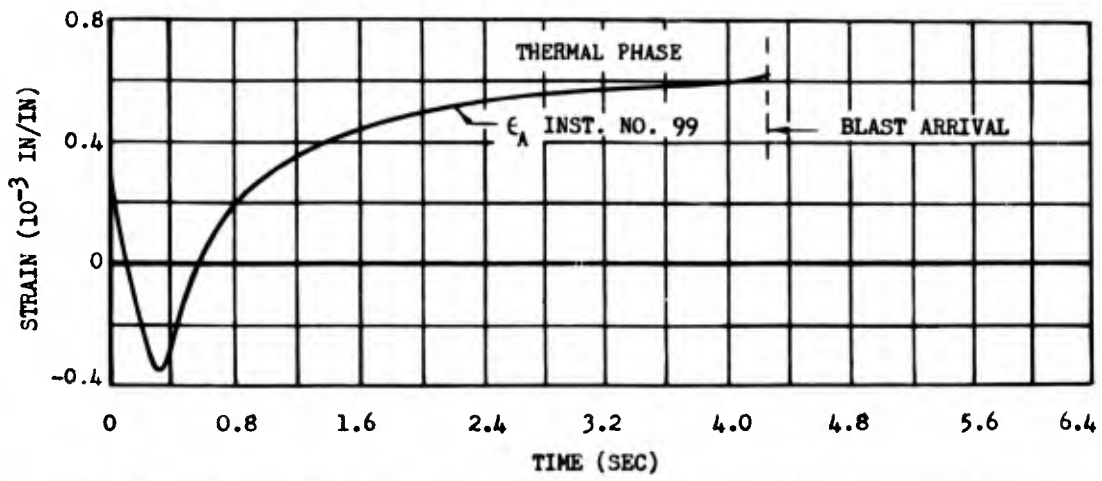
Fig. C.62 Skin Strain from Three Rosette Axis vs Time for Stabilizer
Exposed to Both Thermal and Blast Inputs, Stabilizer
Station 24.75, Station 6500, Shot 10
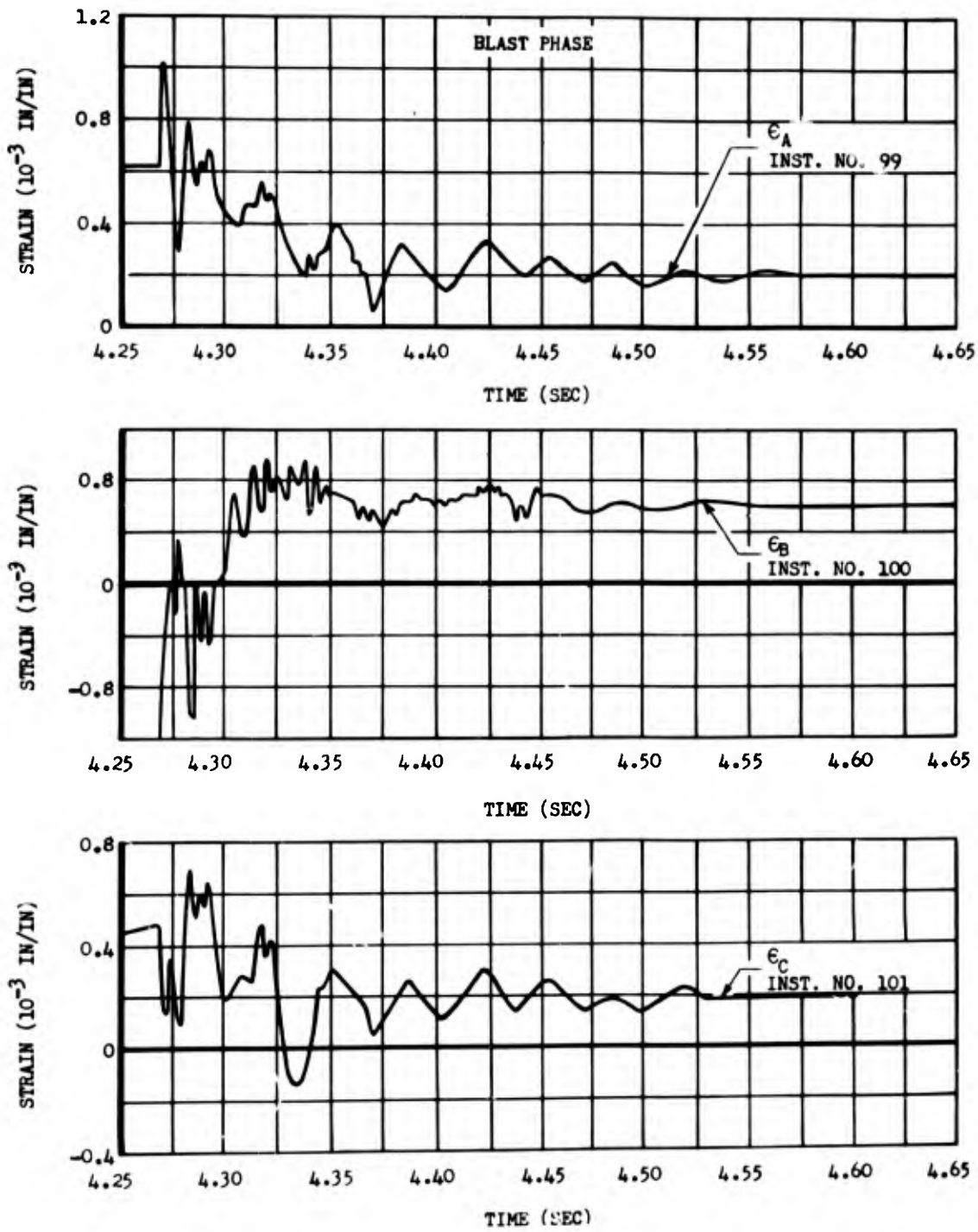
Fig. C.63 Comparison of the Skin Strain from Three Rosette Axis vs
Time for Stabilizer Exposed to Both Thermal and Blast
Inputs, Stabilizer Station 24.75, Station 6500, Shot 10

188
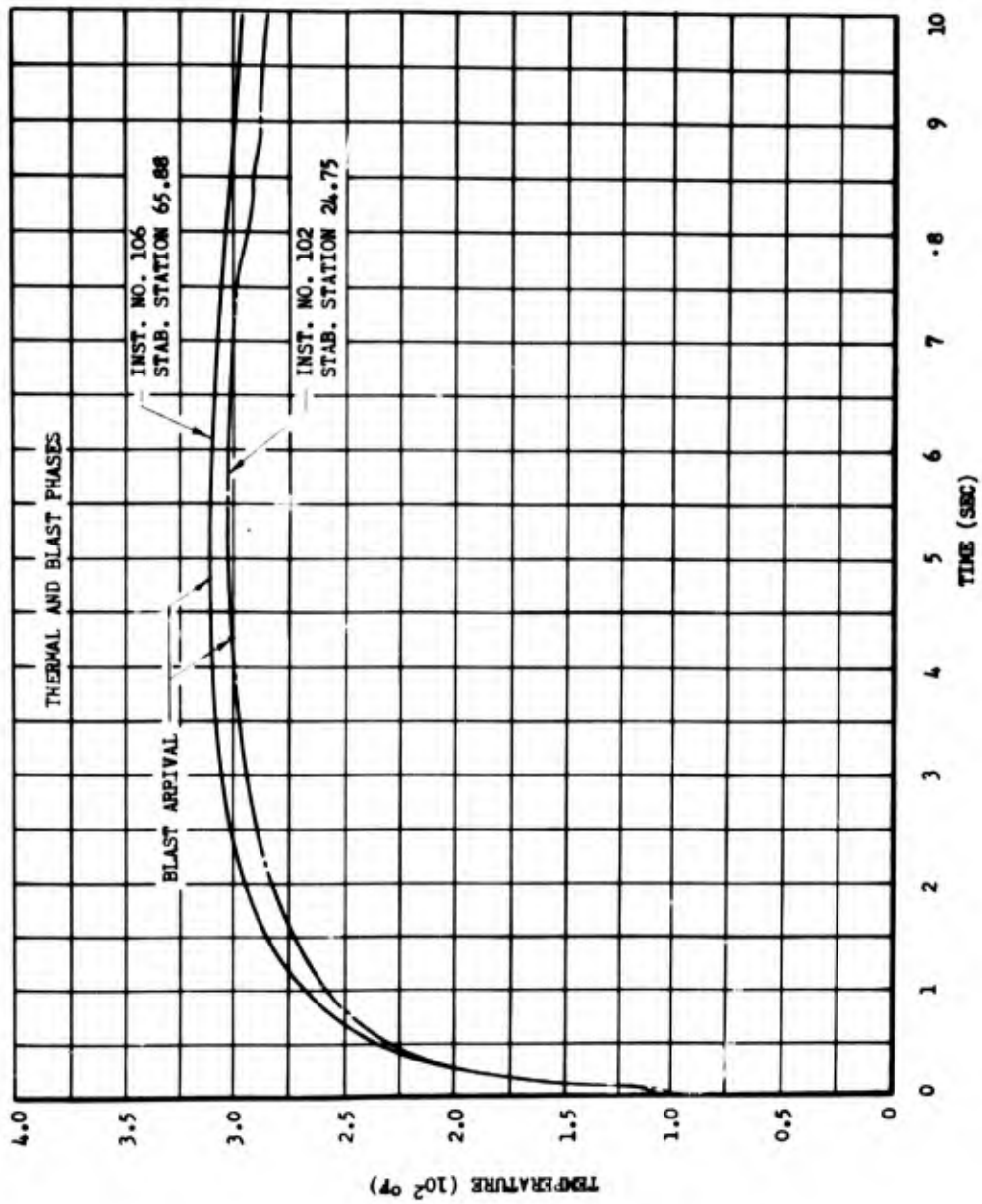
Fig. C.64 Comparison of the Skin Temperature vs Time for the Stabilizer Exposed
to Both Thermal and Blast Inputs, Station 6500, Shot 10
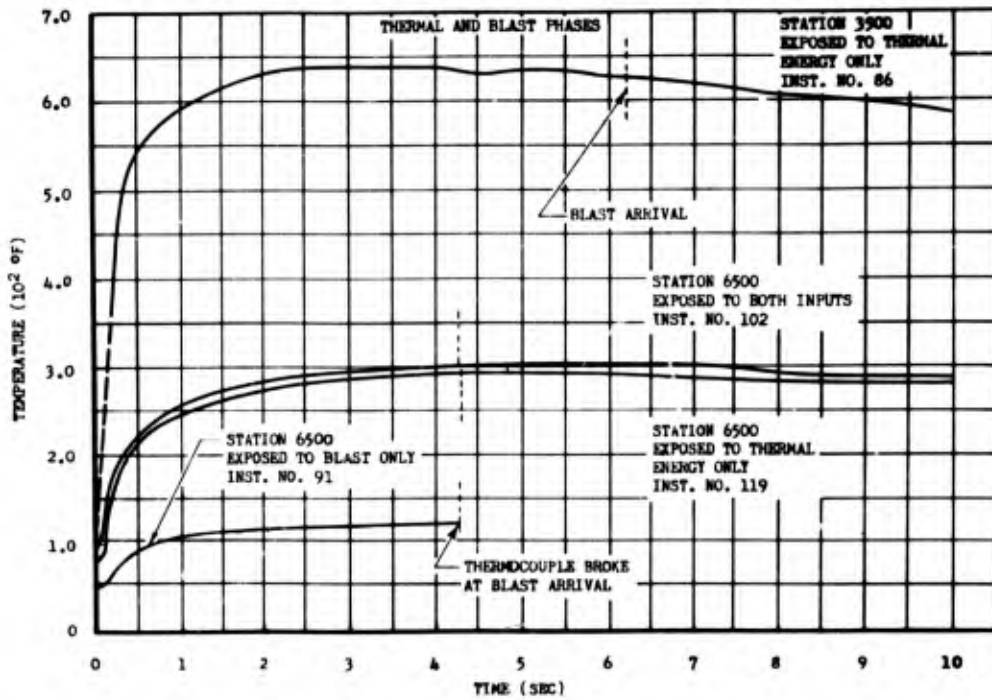
Fig. C.65 Comparison of the Skin Temperature (Inside Front Face) vs
Time for Stabilizer Exposed During Shot 10 (at Stabilizer
Station 24.75)
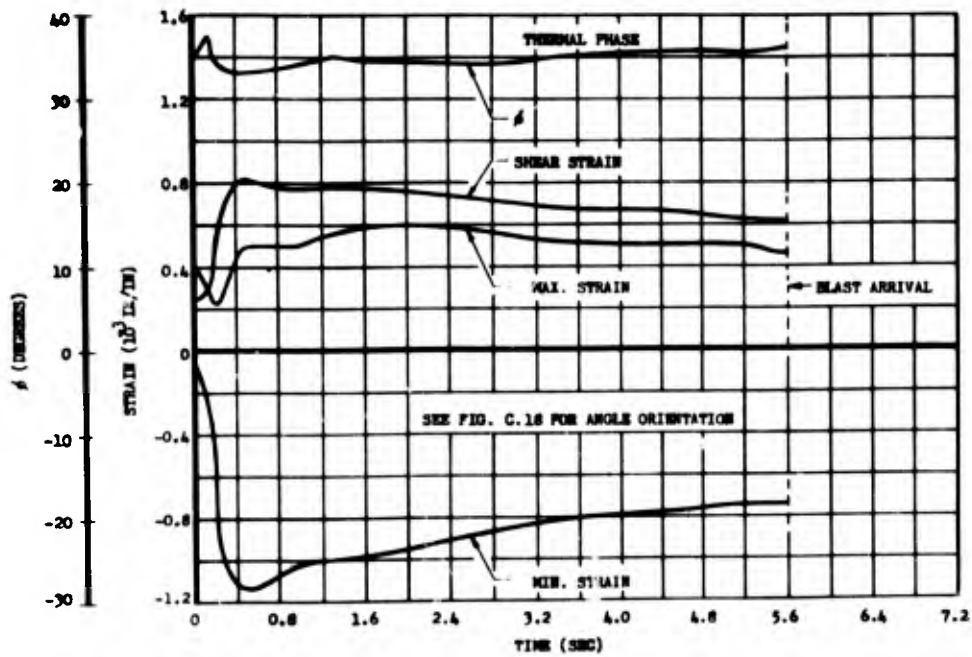
Fig. C.66 Principle Strains, Maximum Shear, and Angle of Maximum
Principle Strain vs Time from Equiangular Rosette Data,
for Stabilizer Exposed to Thermal Energy Only, Stabilizer
Station 24.75, Shot 9, Station 7200

190
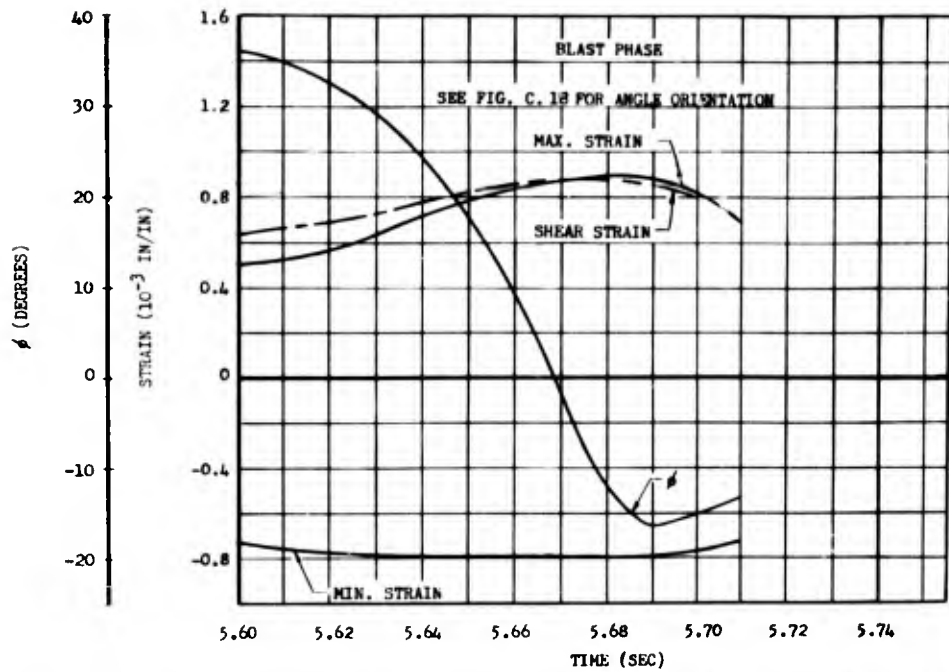
Fig. C.67 Principle Strains, Maximum Shear, and Angle of Maximum
Principle Strain vs Time from Equiangular Rosette Data,
for Stabilizer Exposed to Thermal Energy Only, Stabilizer
Station 24.75, Shot 9, Station 7200
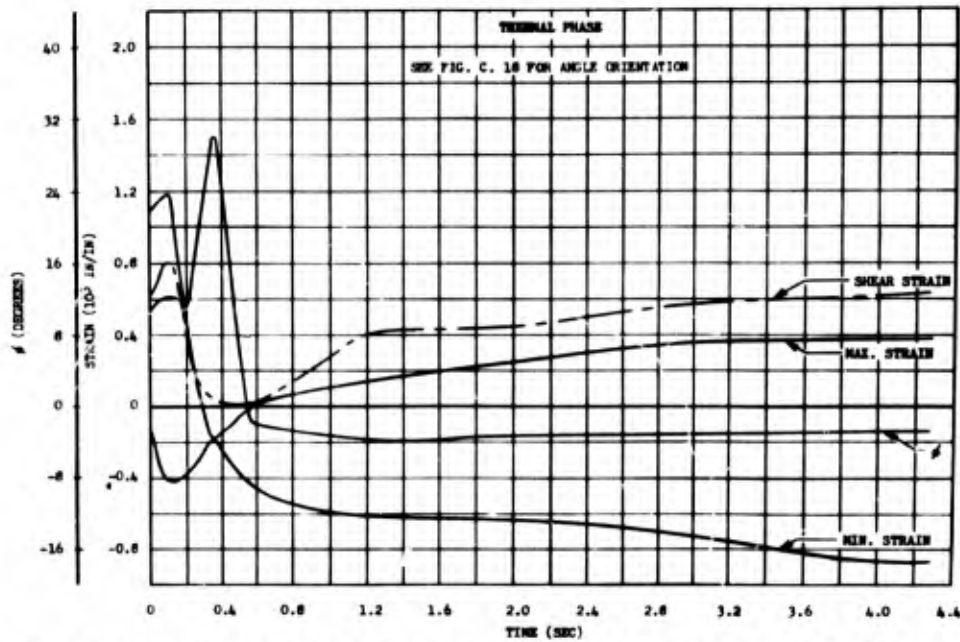
Fig. C.68 Principle Strains, Maximum Shear, and Angle of Maximum
Principle Strain vs Time from Equiangular Rosette Data,
for Stabilizer Exposed to Thermal Energy Only, Stabilizer
Station 24.75, Shot 10, Station 6500

191
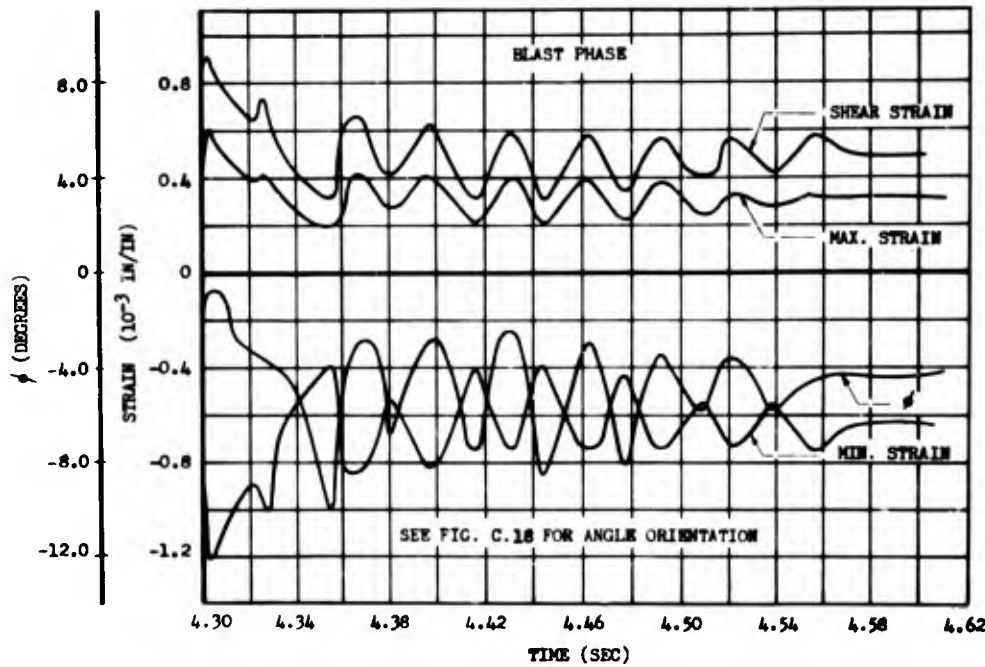
Fig. C.69 Principle Strain, Maximum Shear, and Angle of Maximum Principle Strain vs Time from Equiangular Rosette Data for Stabilizer Exposed to Thermal Energy Only, Stabilizer Station 24.75, Shot 10, Station 6500
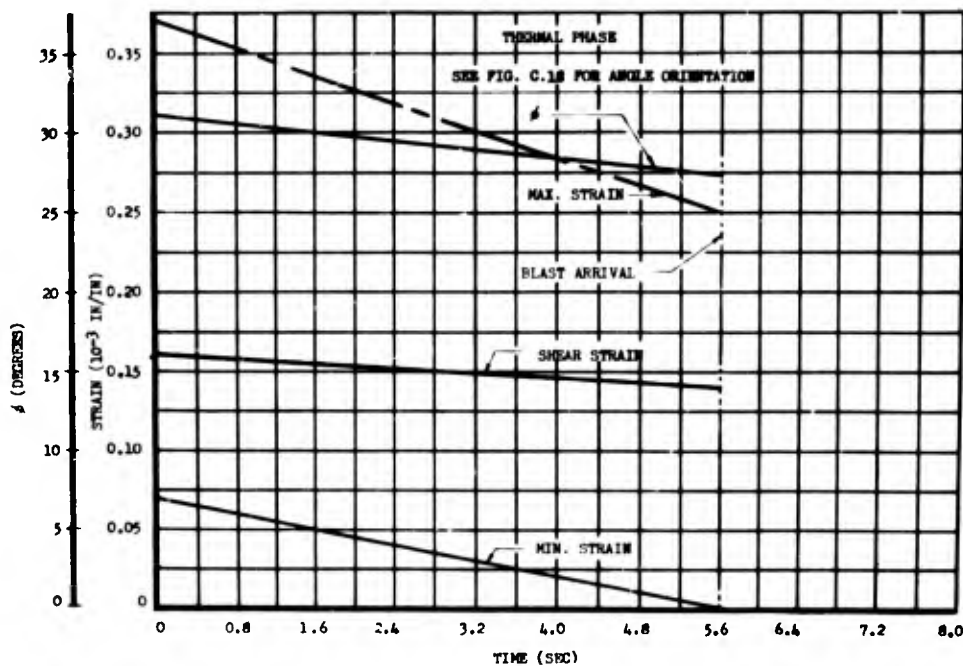
Fig. C.70 Principle Strains, Maximum Shear, and Angle of Maximum Principle Strain vs Time from Equiangular Rosette Data, for Stabilizer Exposed to Blast Only, Stabilizer Station 24.75, Shot 9, Station 7200

192
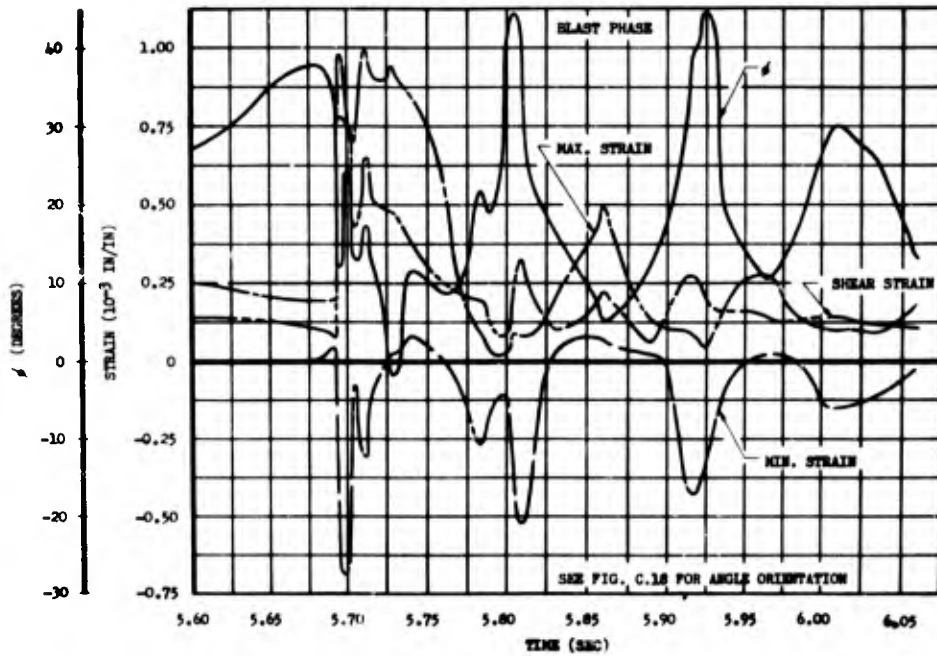
Fig. C.71 Principle Strains, Maximum Shear, and Angle of Maximum
Principle Strain vs Time from Equiangular Rosette Data,
for Stabilizer Exposed to Blast Only, Stabilizer Station 24.75
Shot 9, Station 7200
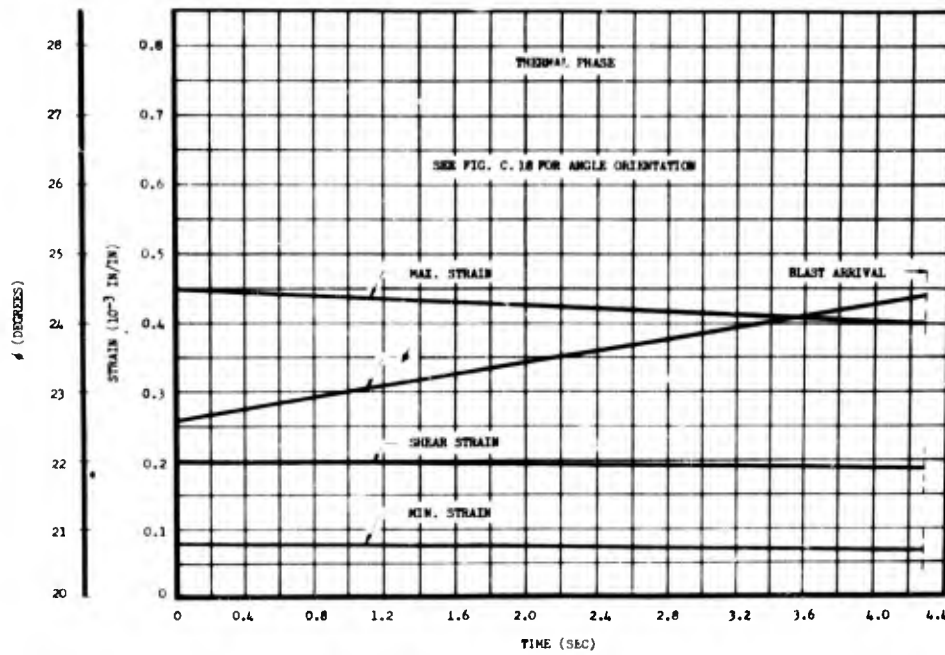
Fig. C.72 Principle Strains, Maximum Shear, and Angle of Maximum
Principle Strain vs Time from Equiangular Rosette Data,
for Stabilizer Exposed to Blast Only, Stabilizer Station 24.75
Shot 10, Station 6500
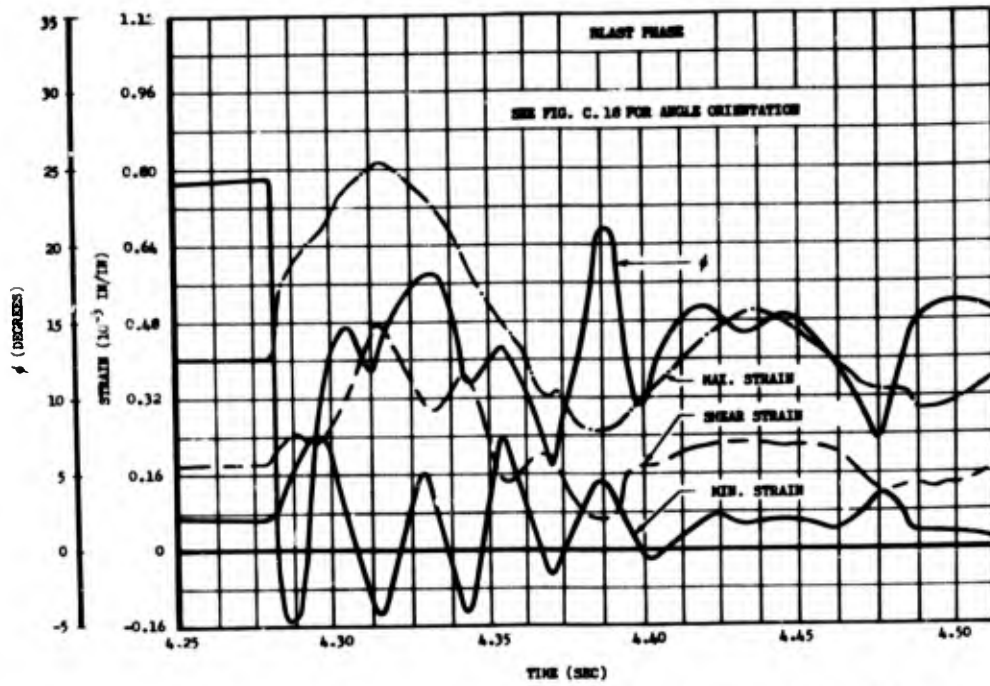
Fig. C.73 Principle Strains, Maximum Shear, and Angle of Maximum
Principle Strain vs Time from Equiangular Rosette Data,
for Stabilizer Exposed to Blast Only, Stabilizer Station
24.75, Shot 10, Station 6500
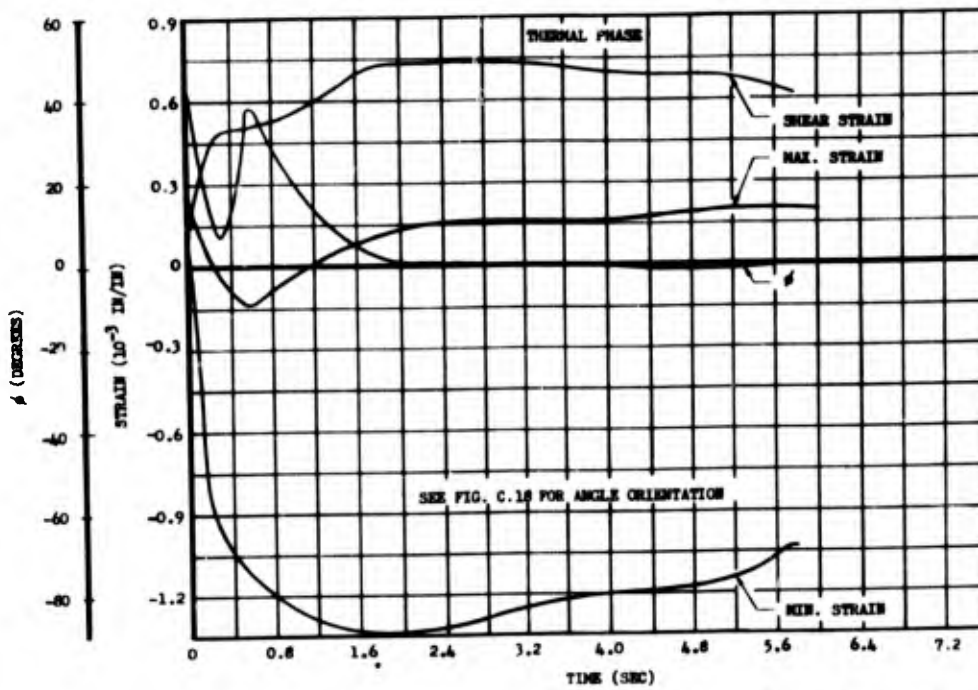
Fig. C.74 Principle Strains, Maximum Shear, and Angle of Maximum
Principle Strain vs Time from Equiangular Rosette Data,
for Stabilizer Exposed to Both Thermal and Blast Inputs,
Stabilizer Station 24.75, Shot 9, Station 7200

194
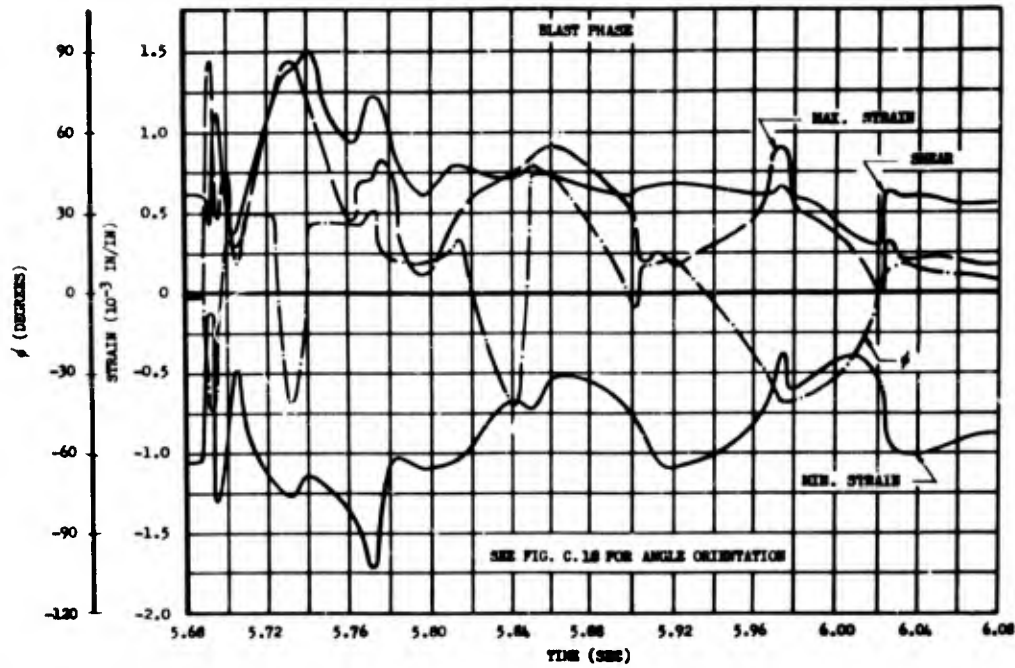
Fig. C.75 Principle Strains, Maximum Shear, and Angle of Maximum
Principle Strain vs Time from Equiangular Rosette Data,
for Stabilizer Exposed to Both Blast and Thermal Inputs,
Stabilizer Station 24.75, Shot 9, Station 7200
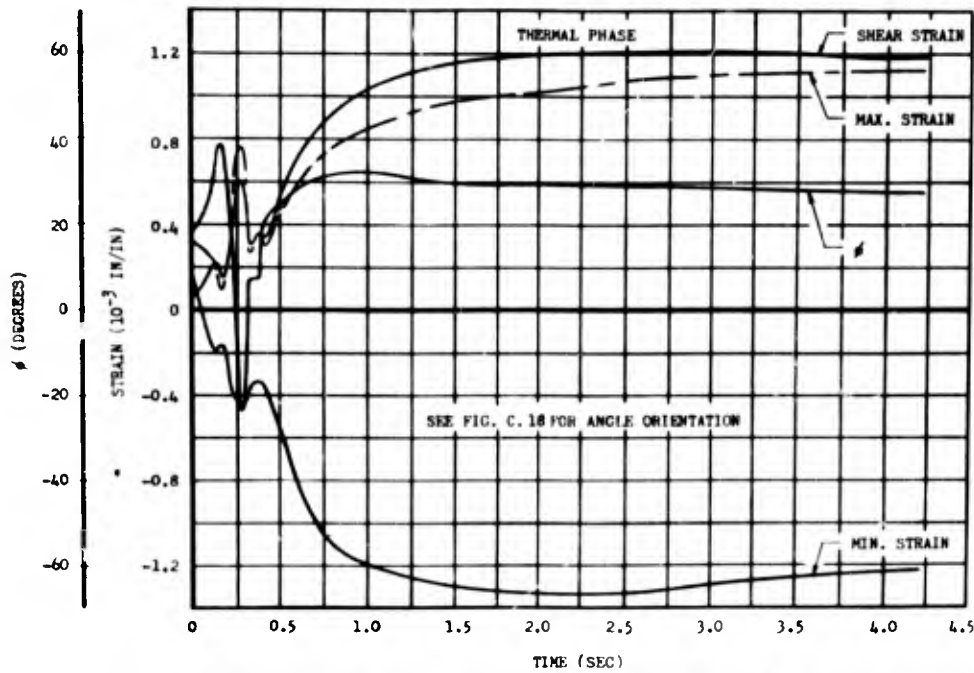
Fig. C.76 Principle Strains, Maximum Shear, and Angle of Maximum
Principle Strain vs Time from Equiangular Rosette Data,
for Stabilizer Exposed to Both Thermal and Blast Inputs,
Stabilizer Station 24.75, Shot 10, Station 6500

195
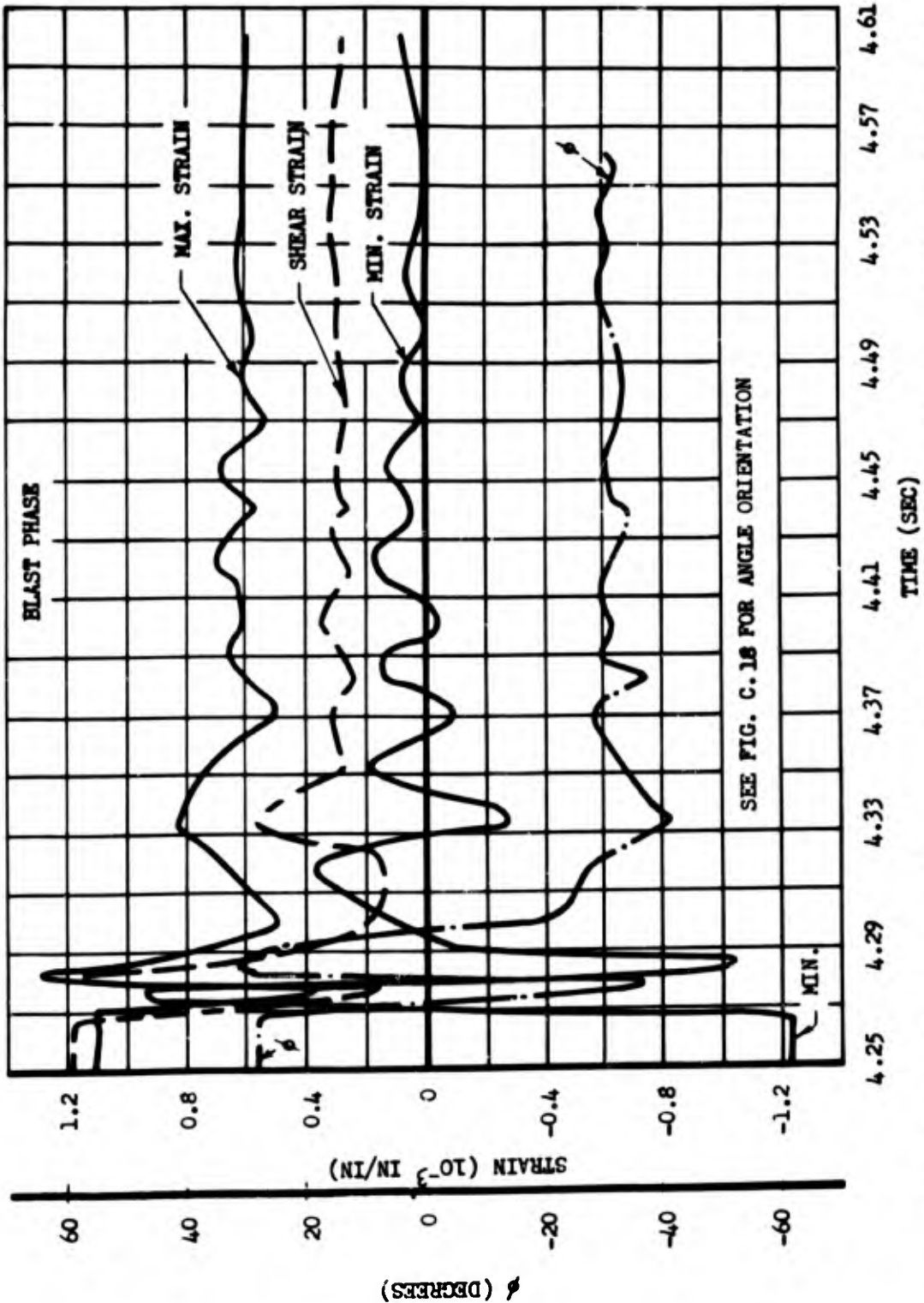
Fig. C.77 Principle Strains, Maximum Shear, and Angle of Maximum Principle Strain vs Time from Equiangular Rosette Data, for Stabilizer Exposed to Both Thermal Blast Inputs, Stabilizer Station 24.75, Shot 10, Station 6500

196
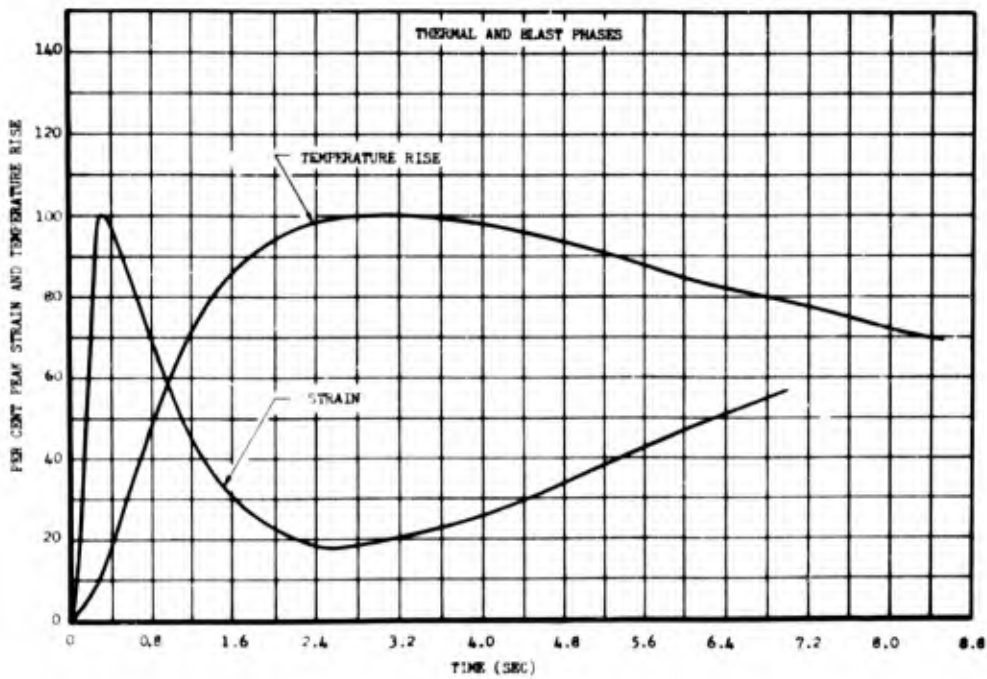
Fig. C.78 Normalized Average Rear Spar-cap Strain and Temperature
vs Time from Stabilizers Exposed to Thermal Energy Only,
Shot 9, Stabilizer Station 24.75
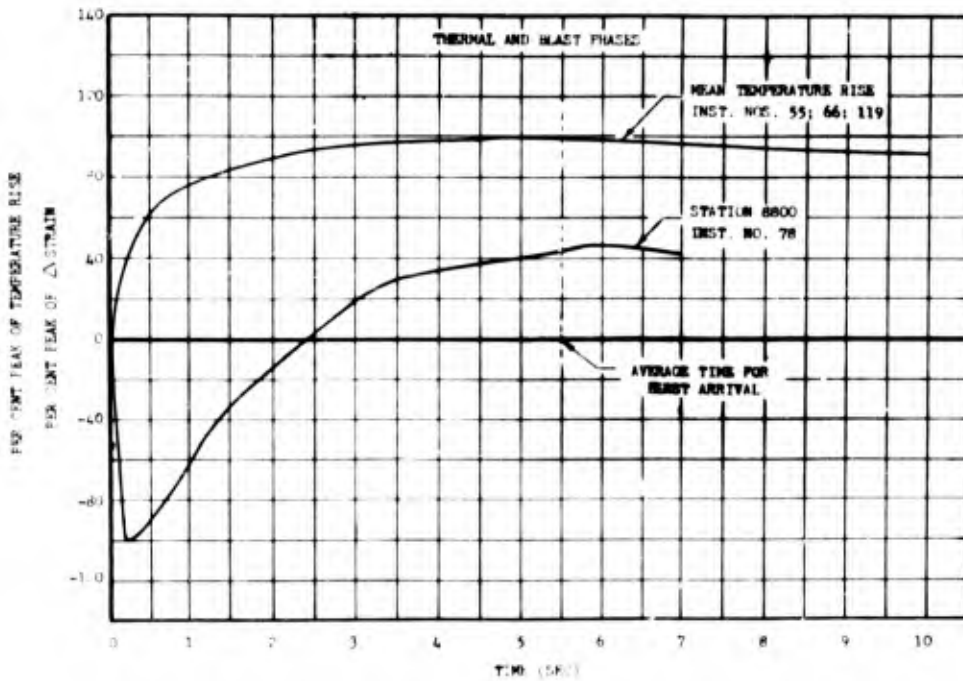
Fig. C.79 Normalized Average Skin Strain and Temperature vs Time
for Stabilizers Exposed to Thermal Energy Only, Shot 9,
Stabilizer Station 24.75

197

THERMAL AND BLAST PHASES
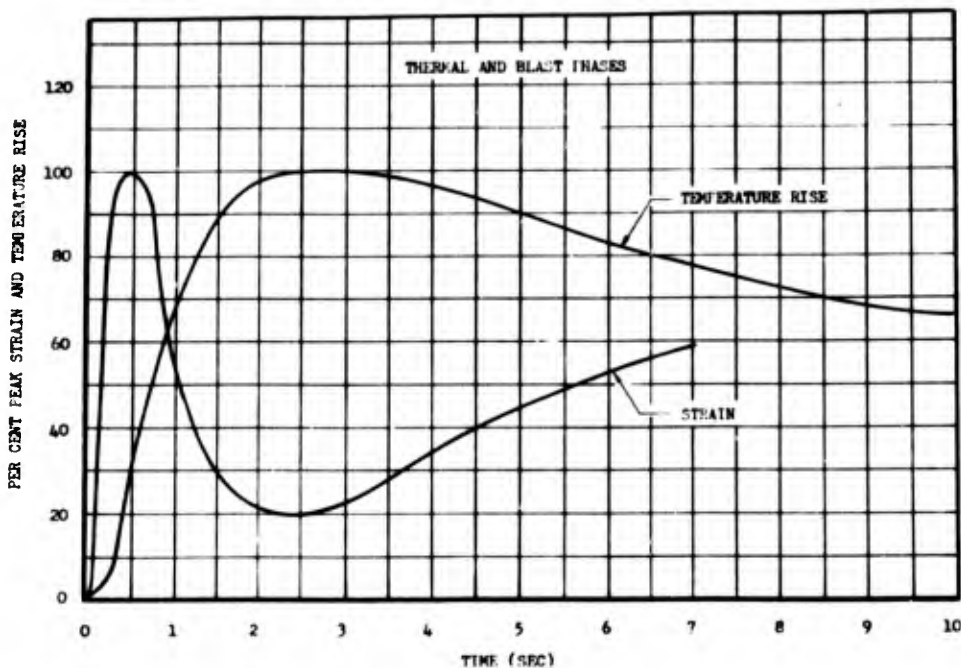
Fig. C. 80 Normalized Average Rear Spar-cap Strain and Temperature
vs Time from Stabilizers Exposed to Both Thermal and
Blast Inputs, Shot 9, Stabilizer Station 24. 75

THERMAL AND BLAST PHASES
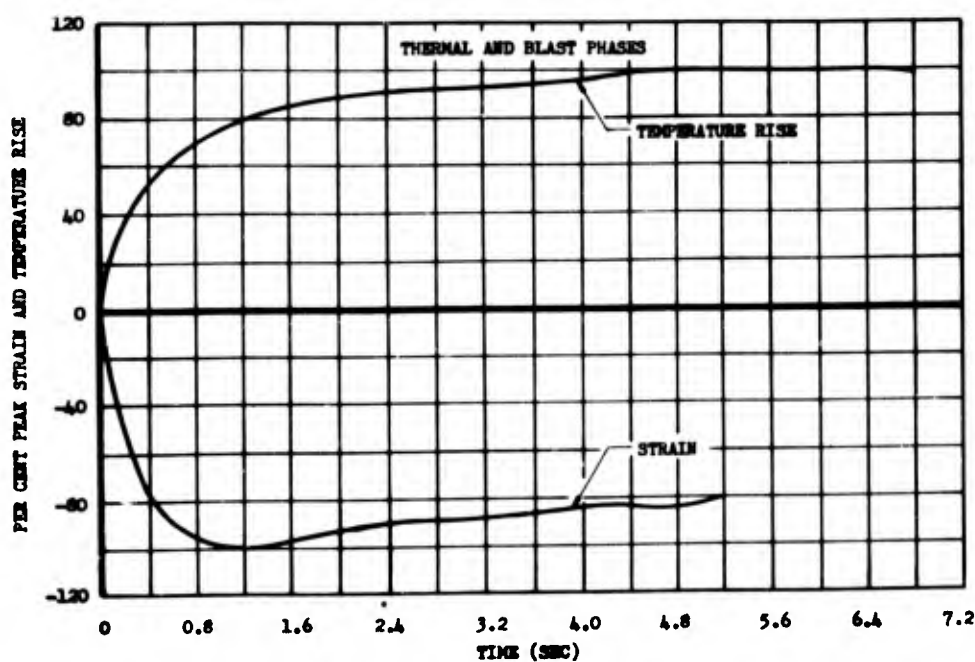
Fig. C. 81 Normalized Average Skin Strain and Temperature vs Time
for Stabilizers Exposed to Both Thermal and Blast Inputs,
Shot 9, Stabilizer Station 24. 75

198
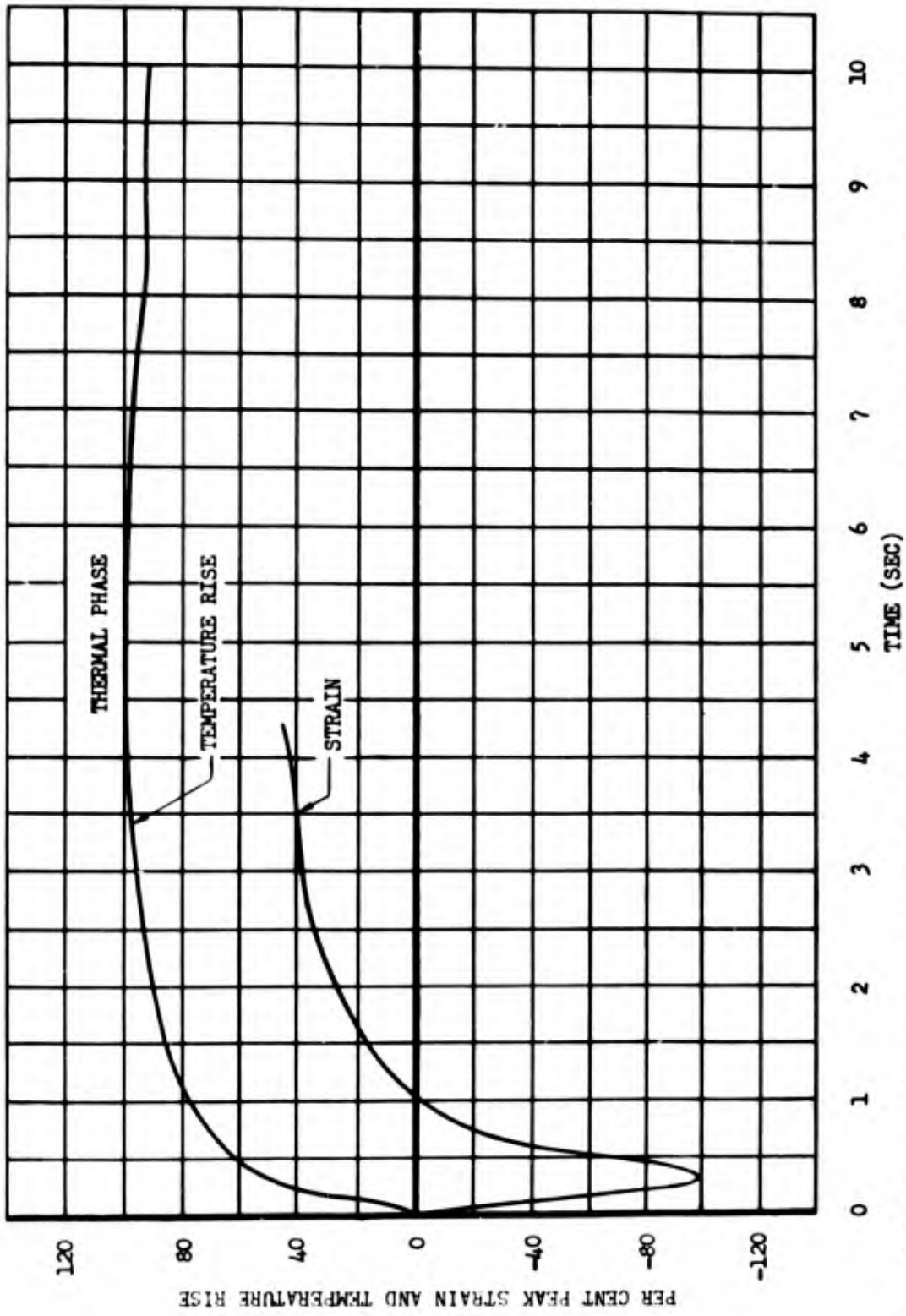
Fig. C.82 Normalized Average Skin Strain and Temperature vs Time for Stabilizers on Shot 10, Stabilizer Station 24.75

199
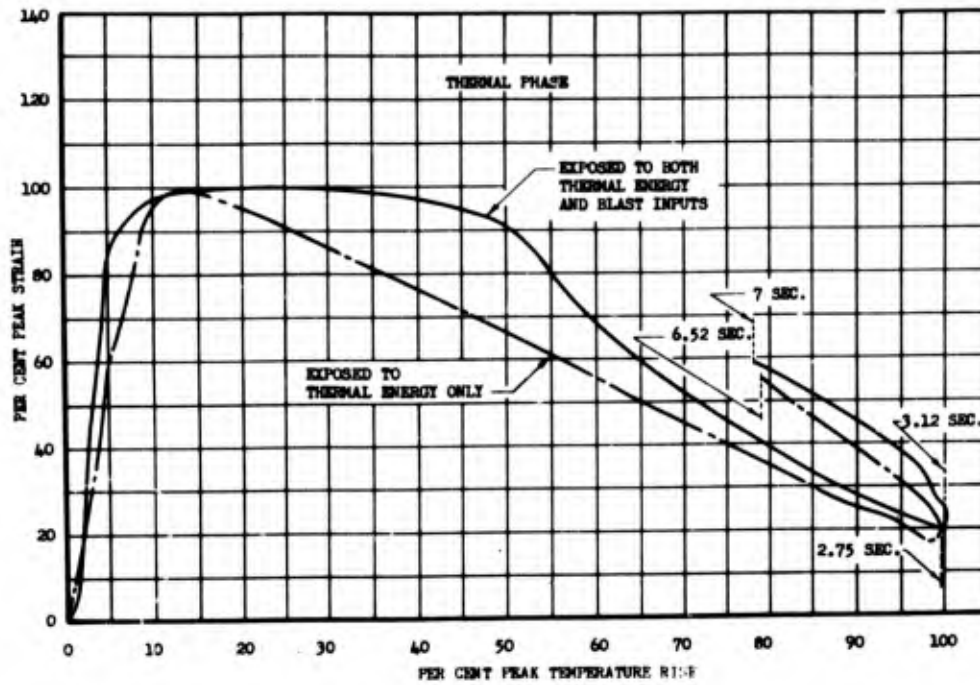
Fig. C. 83 Normalized Average Rear Spar-cap Strain vs Normalized
Average Rear Spar-cap Temperature Rise for the Stabilizers
at All Stations, Stabilizer Station 24. 75, Shot 9
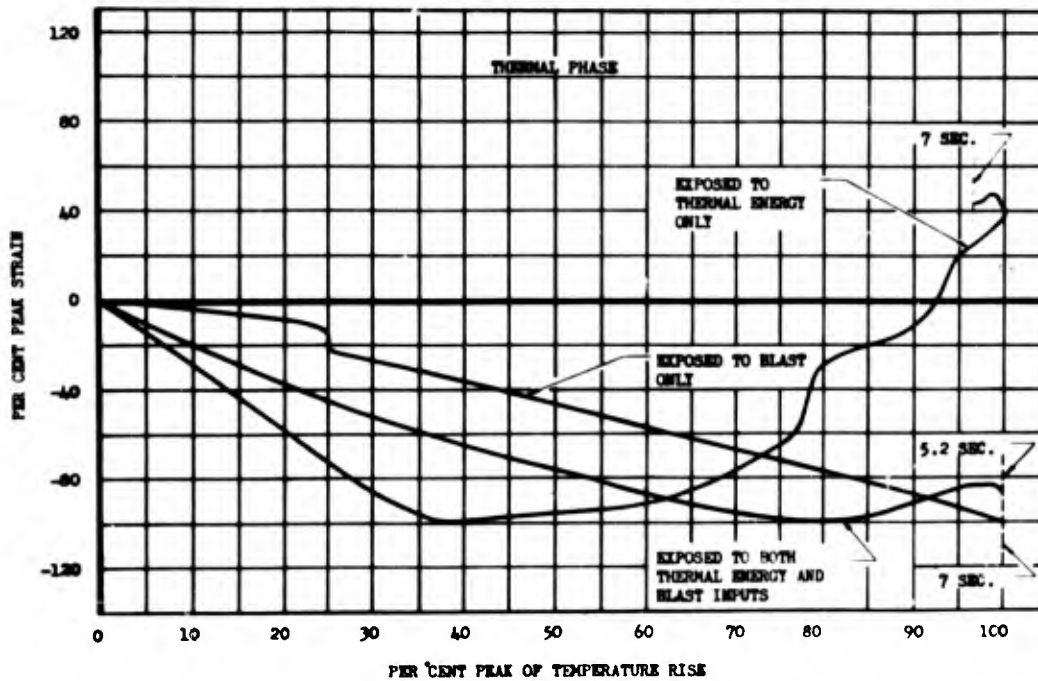
Fig. C. 84 Normalized Average Skin Strain vs Normalized Average
Skin Temperature for the Stabilizers at All Stations, Stabi-
lizer Station 24. 75, Shot 9

200
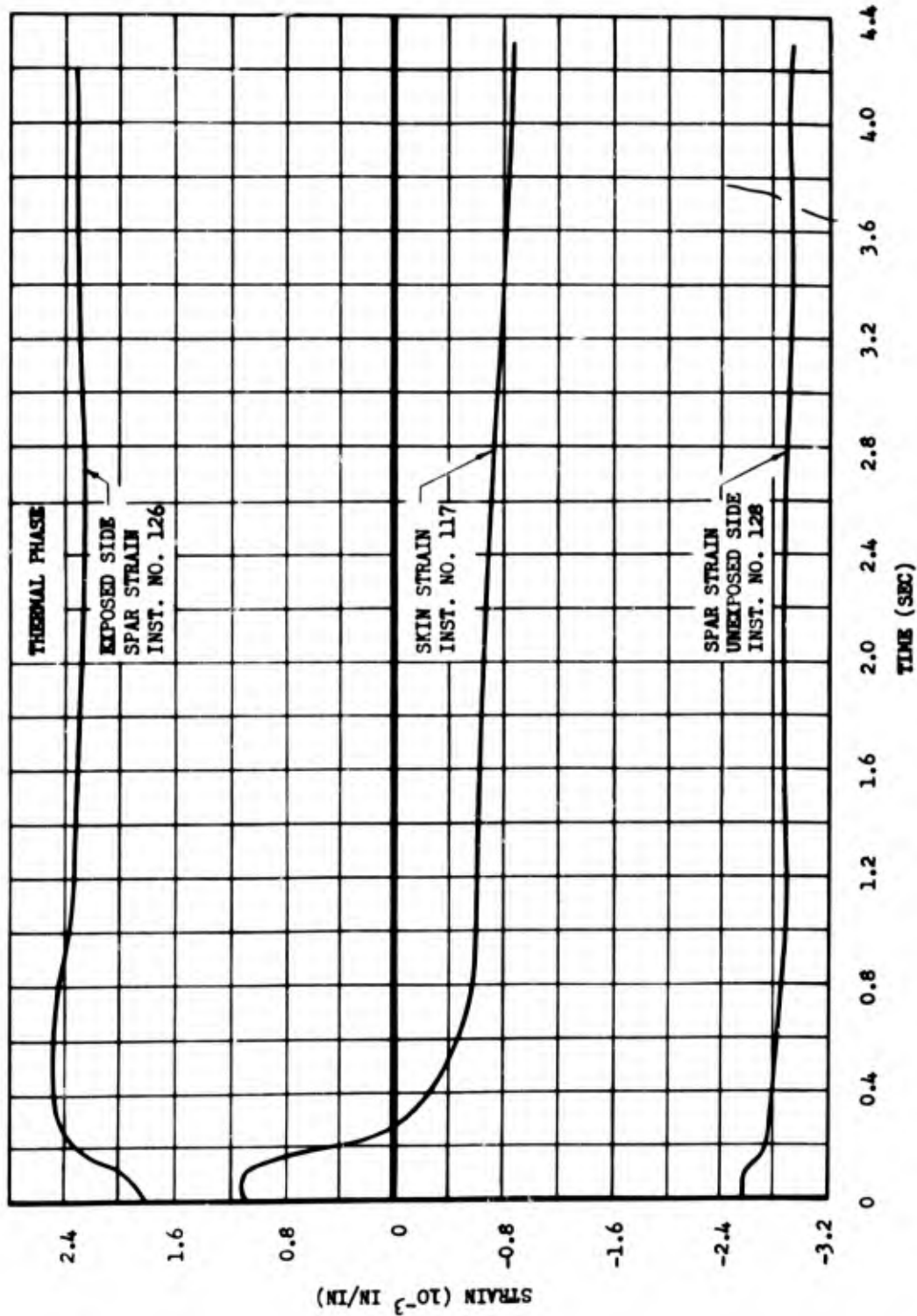
Fig. C.85 Comparison of Skin Strain and Rear Spar-cap Strain vs Time at Stabilizer Station 24.75, Exposed to Thermal Energy Only, Station 6500, Shot 10
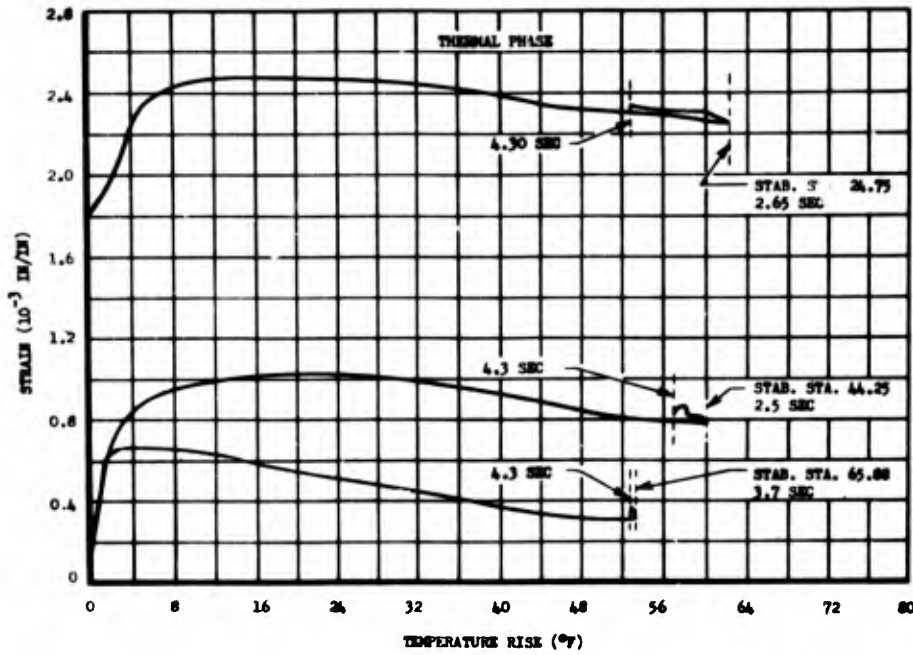
Fig. C. 86 Comparison of Rear Spar-cap Strain (Exposed Side) vs
Temperature Rise at Various Stabilizer Stations, Exposed
to Thermal Energy Only, Station 6500, Shot 10
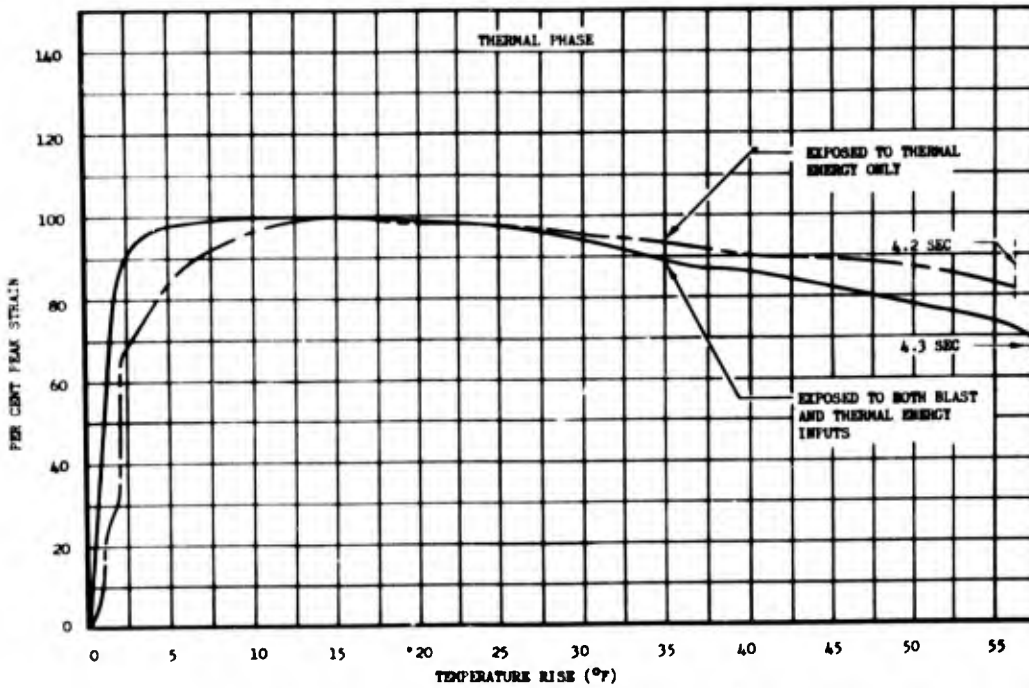
Fig. C. 87 Comparison of Normalized Front Spar Flange Strain vs
Temperature Rise from Stabilizers with Various Exposures,
Stabilizer Station 24. 75, Shot 10, Station 6500

202

APPENDIX D

MISCELLANEOUS SPECIMENS

D.1 BONDED METAL AIRCRAFT PANELS

The bonded metal aircraft panels that were used were thin metal sheets (skin), reinforced by various configurations of metal stiffeners, which were attached to the skin by structural adhesives, as opposed to rivets or other mechanical linkages. The panels used were of three different types of construction called hat, waffle, and honeycomb core, in accordance with the type of stiffener employed. The honeycomb core was bonded between two metal face sheets in a conventional sandwich configuration.

D.1.1 Procedure

Six different panel-exposure conditions were used; these are listed in Table D.1, where each type is given an abbreviated name which will be used throughout this Appendix. Details of the individual panel configurations are presented in Figs. D.1 through D.4. Partial irradiation was accomplished by shielding the border of the panel from direct thermal radiation by means of aluminum foil.

With one exception, all panel exposures were made with the specimen shielded from the effects of the blast phase by a glass-fronted steel enclosure which admitted approximately 78 per cent of the incident thermal energy. A drawing of a panel installed in a blast shield is shown in Fig. D.5. As a precaution against overturning or sliding, those blast shields located in regions of predicted 3.0 psi or greater overpressure were moored by stakes and cables. The 0.020 in. hat panel (No. 13) exposed at Station 6500 during Shot 10 for the purpose of obtaining motion pictures of the thermal and blast effects was mounted, without benefit of shielding, to a steel backplate.

Primary instrumentation on all exposed panels consisted of
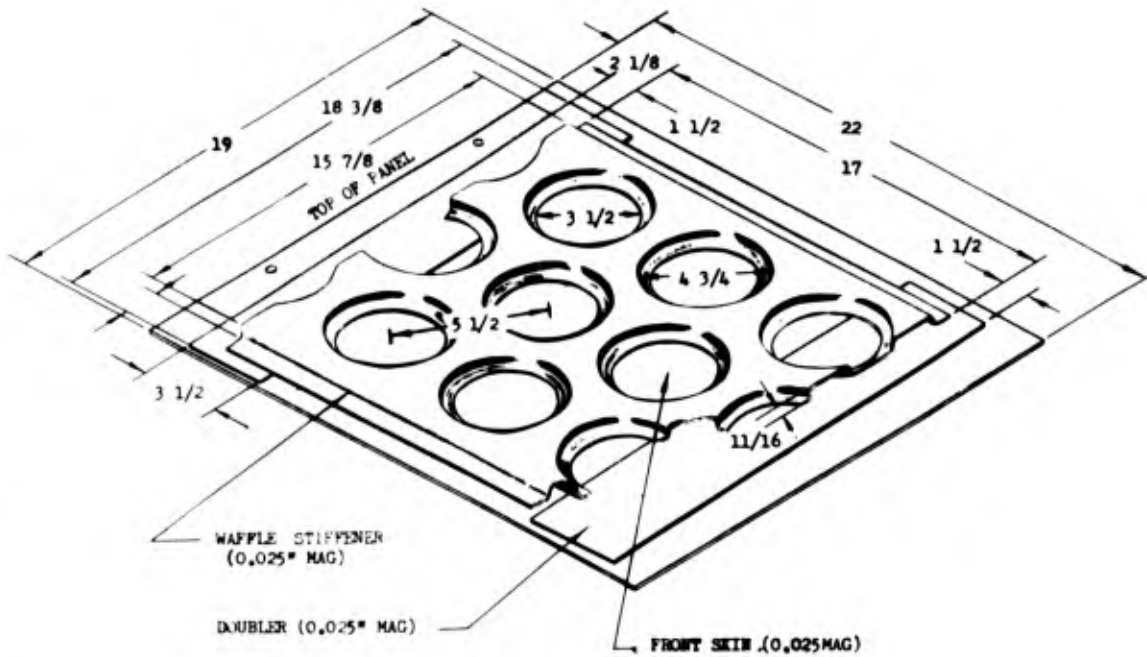
Fig. D.1 Waffle Panel
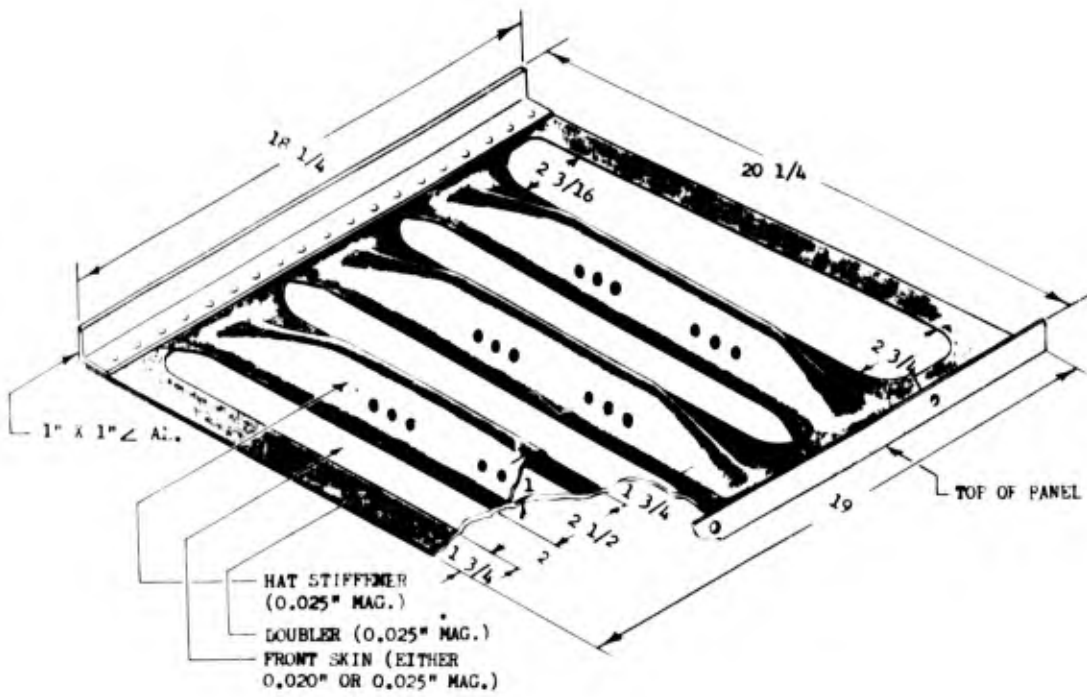
Fig. D.2 Hat Panel (Free Edge)

204
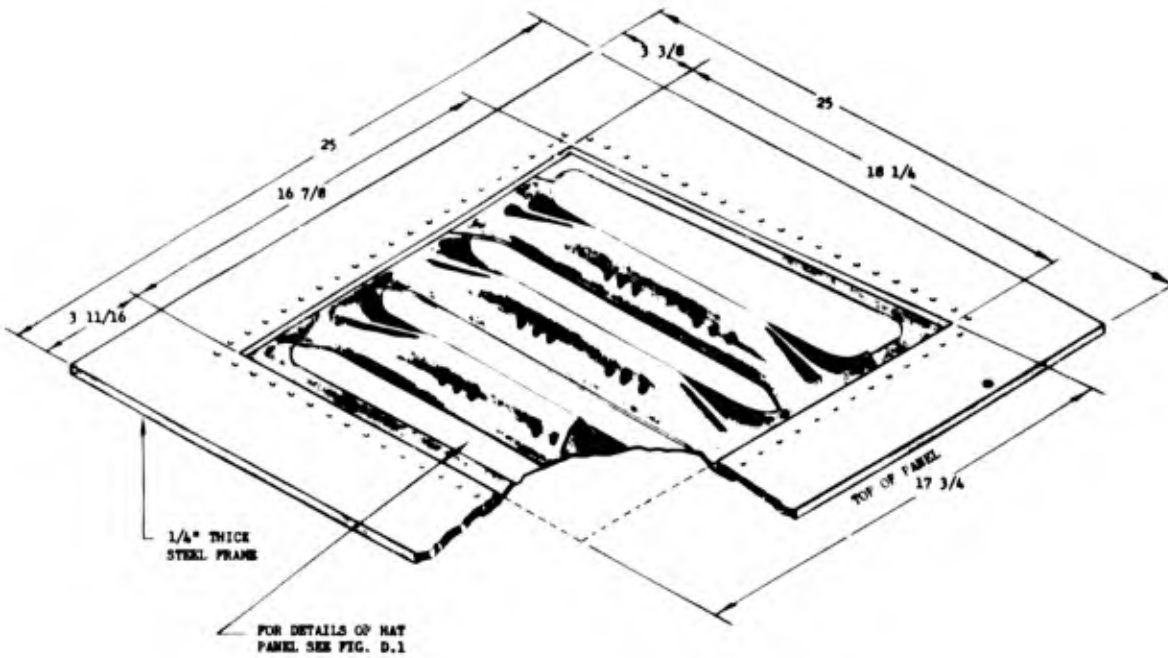
Fig. D.3 Hat Panel (Fixed Edge)

Labels in figure:
3/8
25
25
16 7/8
16 1/4
3 11/16
TOP OF PANEL
17 3/4
1/4" THICK STEEL FRAME
FOR DETAILS OF HAT PANEL SEE FIG. D.1

Fig. D.4 Honeycomb Core Panel

Labels in figure:
19"
19"
TOP OF PANEL
REAR SKIN (0.016" 24ST3)
FLANGE 1" WIDE
DOUBLER (0.032" 24ST3) 2" WIDE
RAISED SURFACE 14 3/4" SQUARE
HONEYCOMB CORE- 1/4" HEX (0.0015" 3SH FOIL) HEIGHT OF HONEYCOMB 5/8"
FRONT SKIN (0.016" 24ST3)

205
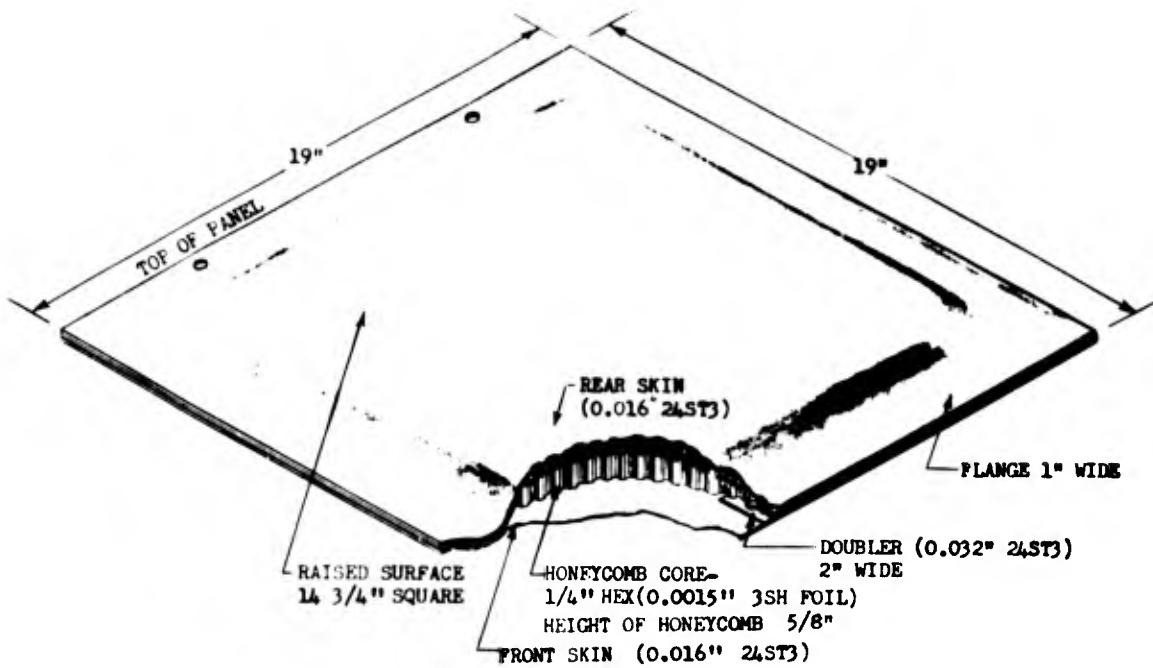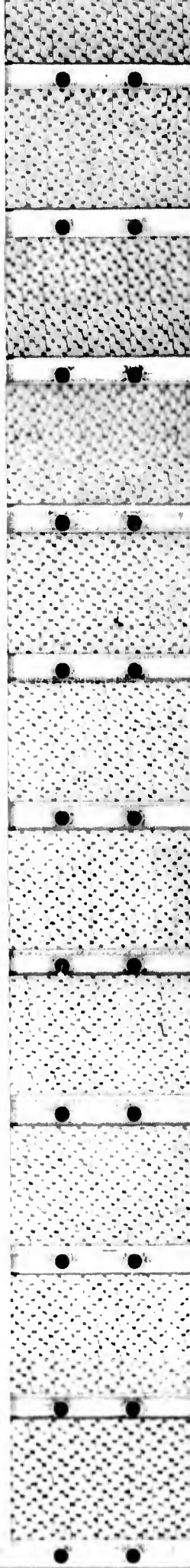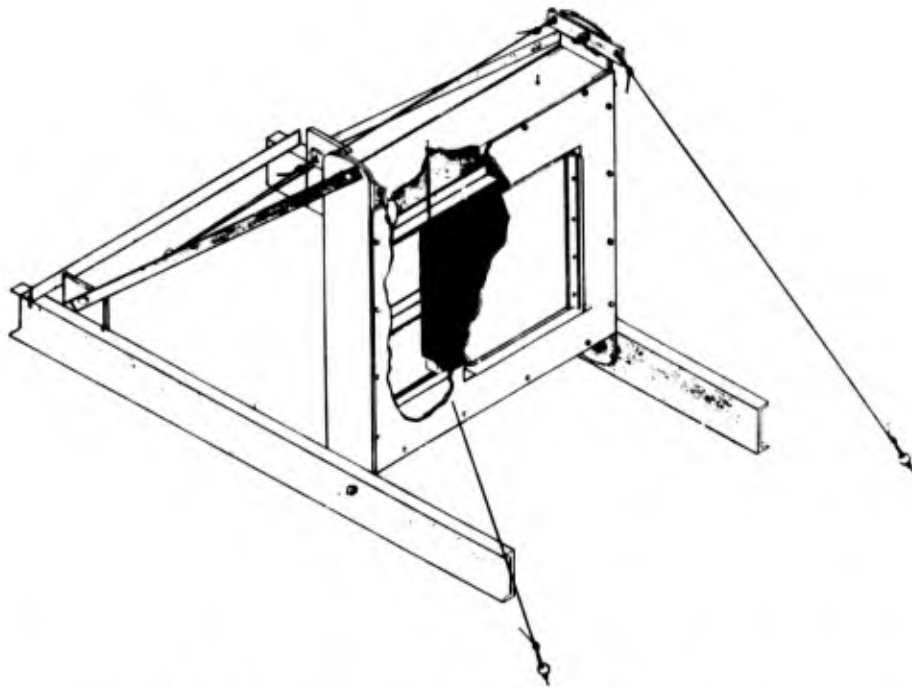
Fig. D.5 Typical Panel Installation in Blast Shield
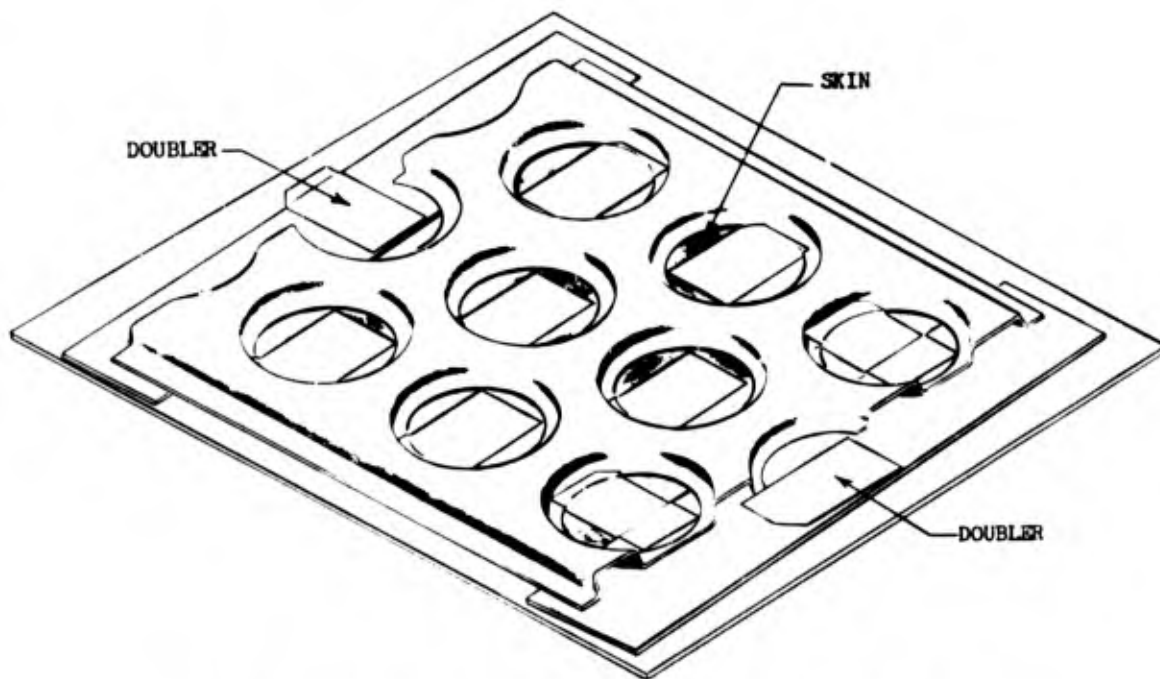
Fig. D.6 Temp-tape Installations on Waffle Panel

206
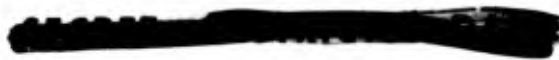
Skin Thickness (in.)	Mat.	Panel Type	Edge Condition	Irradiation	Abbreviated Nomenclature	Panel Numbers
0.025	Mag.	Waffle	Free	Total	0.025" Waffle	1 thru 7
0.020	Mag.	Hat	Free	Total	0.020" Hat	8 thru 13
0.020	Mag.	Hat	Free	12" sq. Area	0.020" Hat (Partial)	14 thru 17
0.025	Mag.	Hat	Free	Total	0.025" Hat	18 thru 23
0.025	Mag.	Hat	Fixed	Total	0.025" Hat (Fixed)	24 thru 30 and 37
0.016	Al.	Honeycomb Core	Free	Total	0.016" Honeycomb	31 thru 36

temp-tapes for peak temperature determination. Typical installations are shown in Figs. D.6, D.7, and D.8. Secondary instrumentation on six exposed panels consisted of 29 channels of strain and temperature data recorded by oscillographs. Table D.2 lists the installation numbers and pertinent information concerning each time-history channel. Figures D.9 and D.10 show the strain gage and thermocouple installations on waffle and hat panels. The installation on the honeycomb core panel consisted of two thermocouples, one each on the rear faces of the skin and of the stiffener sheet.

Control of the temperature rise was accomplished by spraying all panels with a special silicone base paint. Black paint, having an absorptivity of 0.96, was used on all panels except panel No. 1, which was painted a shade of gray, having an absorptivity of 0.82.

Figures D.11 and D.12 present the exposure programs for Shots 9 and 10, respectively.

D.1.2   Results

The results presented in this section include peak temperatures, temperature rises, descriptions of buckling damage, photographs, and time-history curves of strain and temperature.

A range of temperature rises of from approximately 140°F to greater than 525°F was realized, with damage ranging from negligible to depths of buckle of 9/64 in. Bond release was evident on one hat, two waffle, and five honeycomb core panels. Paint blistering occurred

SECTION A-A
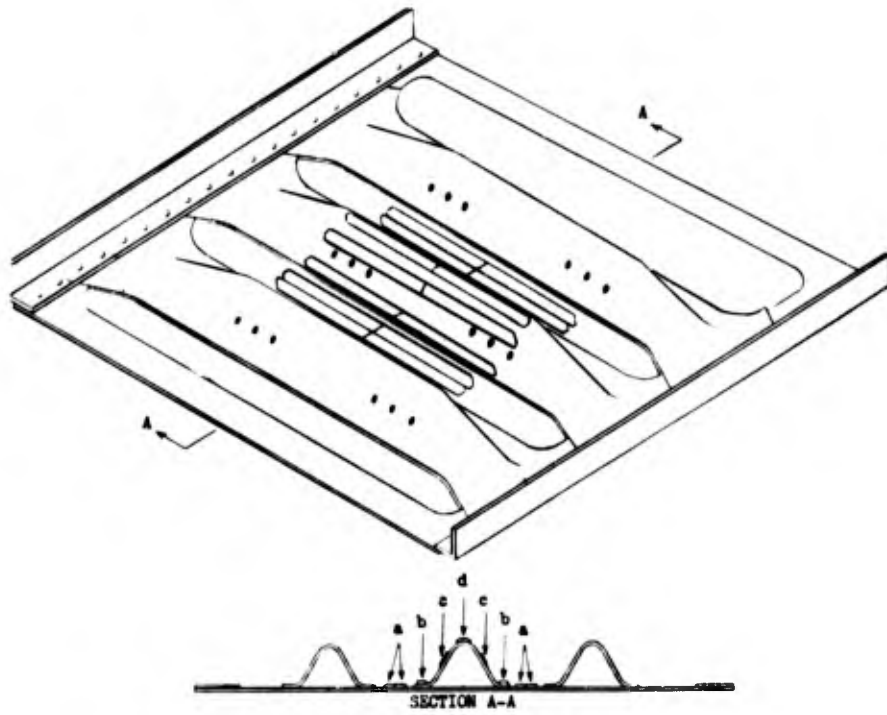
Fig. D.7 Temp-tape Installations on Hat Panel. Letters Indicate Location Code.

REAR FACE

FLANGE
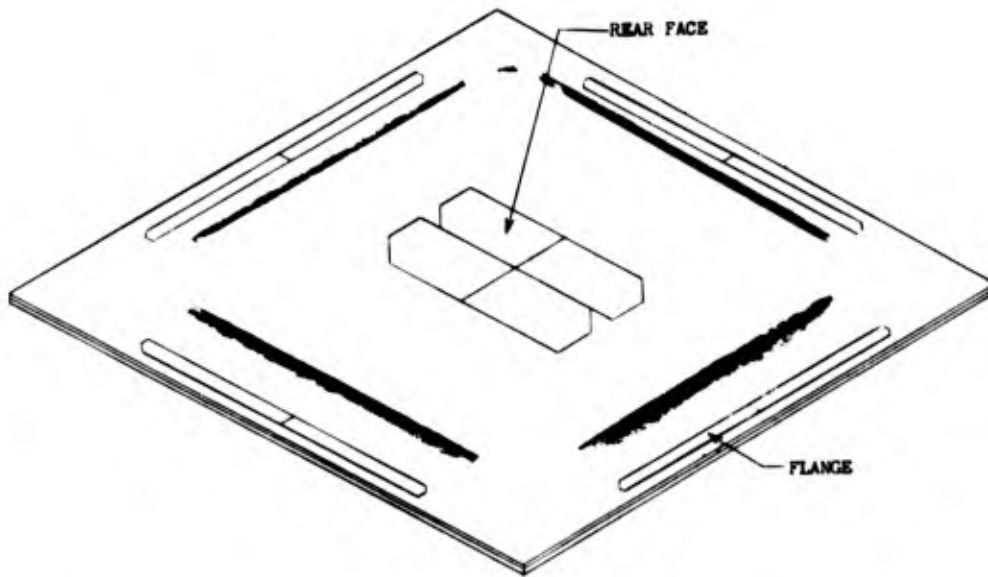
Fig. D.8 Temp-tape Installations on Honeycomb Core Panel

208

TABLE D.2 - Index to Oscillographic Instrumentation Installation
Numbers (For Bonded Metal Aircraft Panels)

Inst. No.	Quantity Measured	Location on Panel[a]	Panel Type	Panel No.	Station	Shot No.	Figure Reference
133	Strain	Center of Skin	Waffle	1	6500	9	D.20
134	Temperature	Center of Skin	Waffle	1	6500	9	D.20; D.22
135	Strain	Flange of Stiffener	Waffle	1	6500	9	D.21
136	Temperature	Flange of Stiffener	Waffle	1	6500	9	D.21; D.22
137	Temperature	Edge of Skin	Waffle	1	6500	9	D.22
138[b]	Temperature	Skin Under Stiffener	Waffle	1	6500	9	
139	Temperature	Wall of Stiffener	Waffle	1	6500	9	D.22
140	Strain	Center of Skin	Hat (Fixed)	24	7200	9	D.27
141	Temperature	Center of Skin	Hat (Fixed)	24	7200	9	D.27; D.29
142	Strain	Crest of Stiffener	Hat (Fixed)	24	7200	9	D.28
143	Temperature	Crest of Stiffener	Hat (Fixed)	24	7200	9	D.28; D.29
144	Temperature	Center of Skin, Left	Hat (Fixed)	24	7200	9	D.29
145	Strain	Center of Skin	Hat	18	7200	9	D.24
146	Temperature	Center of Skin	Hat	18	7200	9	D.24; D.26
147	Strain	Crest of Stiffener	Hat	18	7200	9	D.25
148	Temperature	Crest of Stiffener	Hat	18	7200	9	D.25; D.26
149	Temperature	Front Skin	Honeycomb	36	7200	10	D.31
150	Temperature	Rear Skin	Honeycomb	36	7200	10	D.31
151	Temperature	Top of Stiffener	Waffle	7	7200	10	D.23
152	Temperature	Top of Stiffener	Waffle	7	7200	10	D.23
153	Temperature	Skin Under Stiffener	Waffle	7	7200	10	D.23
154	Temperature	Flange of Stiffener	Waffle	7	7200	10	D.23
155	Temperature	Edge of Skin	Waffle	7	7200	10	D.23
156	Temperature	Center of Skin	Waffle	7	7200	10	D.23
157	Temperature	Skin Under Stiffener	Hat (Fixed)	30	7200	10	D.30
158	Temperature	Wall of Stiffener	Hat (Fixed)	30	7200	10	D.30
159	Temperature	Flange of Stiffener	Hat (Fixed)	30	7200	10	D.30
160	Temperature	Edge of Skin	Hat (Fixed)	30	7200	10	D.30
161	Temperature	Center of Skin	Hat (Fixed)	30	7200	10	D.30
180 181	Mean Thermal Energy[c]				6500	9	D.22
183 185	Mean Thermal Energy[c]				7200	9	D.26; D.29
193 194	Mean Thermal Energy[c]				7200	10	D.23; D.30 D.31

a Refer to Figures D.9 and D.10
b Channel Invalid (Trace Returned to M.Z.)
c Corrected for 1/2" Glass Attenuation and Incidence Angle Due to Bombing Error

209

THERMOCOUPLE & STRAIN GAGE INSTRUMENTATION
STATION 6500, SHOT 9
(PANEL NO. 1)

NOTE: NUMBERS REFER TO
INSTALLATION NUMBERS
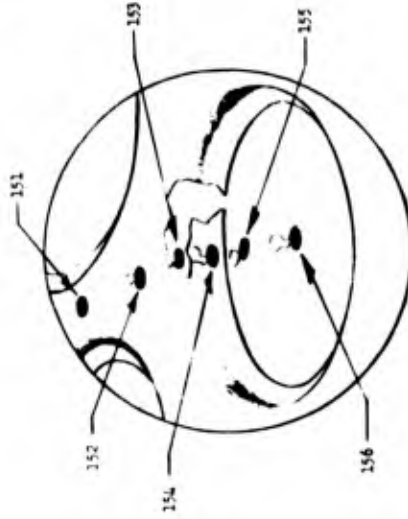
THERMOCOUPLE INSTRUMENTATION
STATION 7200, SHOT 10
(PANEL NO. 7)

WAFFLE PANEL INDICATING
INSTRUMENTED PORTION

Fig. D.9 Thermocouple and Strain Gage Installation Locations on Waffle Panels, Shot 9 and Shot 10

PANEL NO. 30

FIXED EDGE, STATION 7200, SHOT 10

PANEL NO. 28

FIXED EDGE, STATION 7200, SHOT 9

TOP EDGE OF PANEL

HAT PANEL INDICATING
INSTRUMENTED PORTION

NOTE: NUMBERS REFER TO
INSTALLATION NUMBERS

PANEL NO. 18

FREE EDGES, STATION 7200, SHOT 9
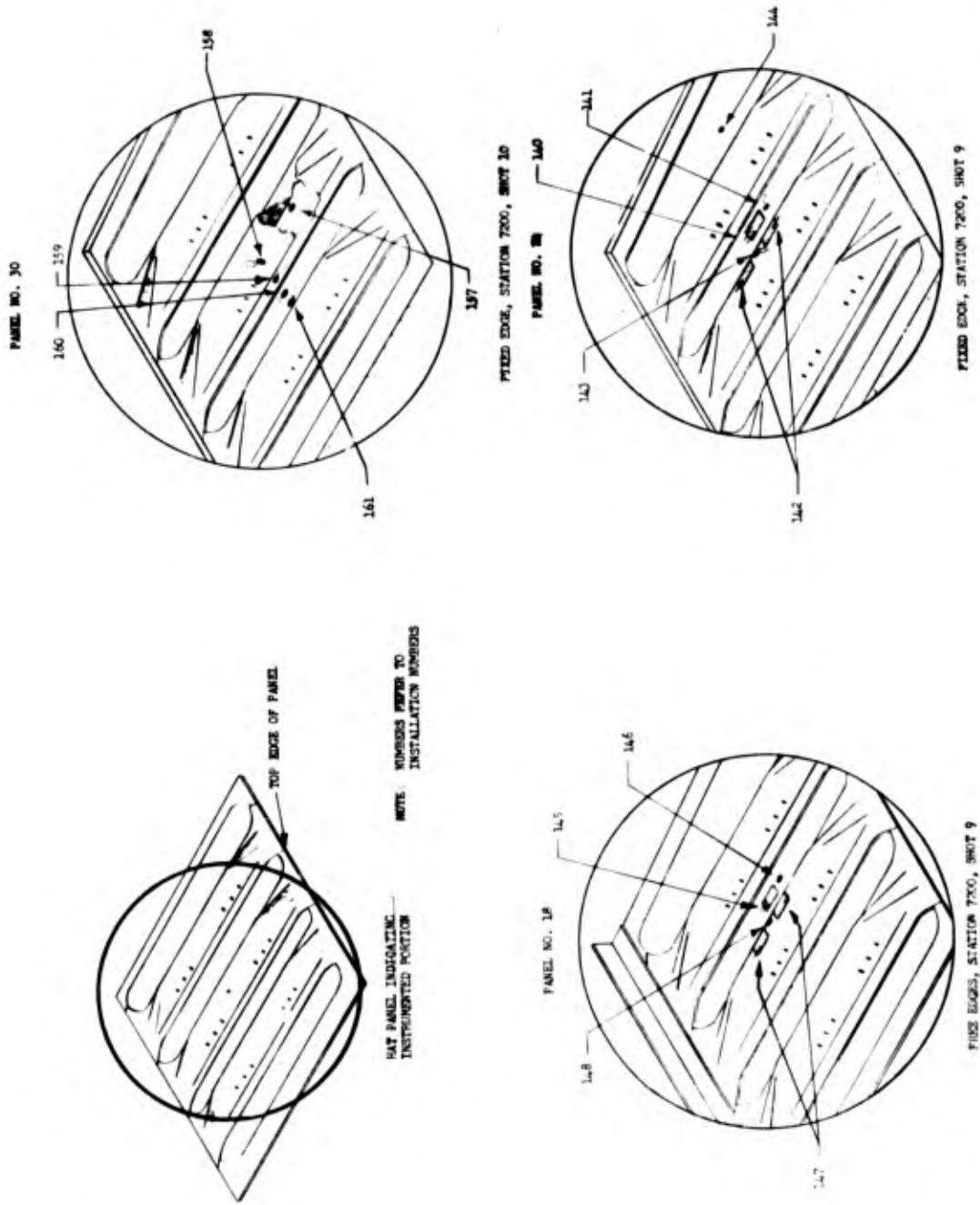
Fig. D.10 Thermocouple and Strain Gage Installation Locations on Hat Panels, Shot 9 and Shot 10

211

PANEL	PANEL NO.	EXPECTED TEMPERATURE RISE (°F)
0.025" WAFFLE	1*	550
	2	500
	3	400
	4	300
0.020" HAT	8	500
	9	400
	10	300
0.020" HAT (PARTIAL)	14	400
	15	300
0.025" HAT	18*	515
	19	500
	20	400
	21	300
0.025" HAT (FIXED)	24*	515
	25	500
	26	400
	27	300
0.016" HONEYCOMB	31	550

* OSCILLOGRAPHICALLY INSTRUMENTED
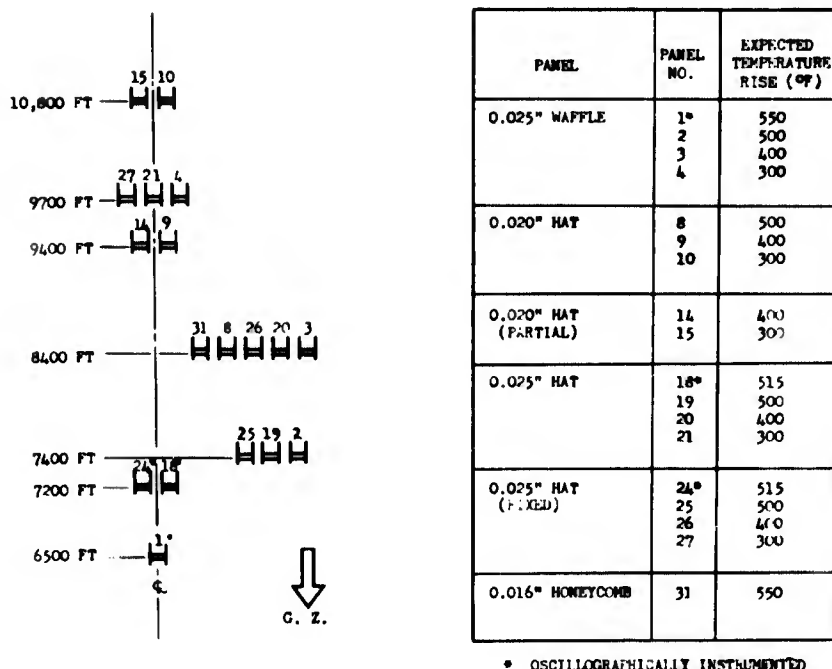
Fig. D. 11   Schematic Diagram of Bonded Metal Aircraft Panel Program for Shot 9

PANEL	PANEL NO.	EXPECTED TEMPERATURE RISE (°F)
0.025" WAFFLE	5	550
	6	450
	7*	200
0.020" HAT	11	500
	12	400
	13**	350
0.020" HAT (PARTIAL)	16	500
	17	400
0.025" HAT	22	500
	23	400
0.025" HAT (FIXED)	28	500
	29	400
	30*	200
0.016" HONEYCOMB	32	750
	33	625
	34	500
	35	400
	36*	300

** EXPOSED TO BOTH THERMAL AND BLAST
* OSCILLOGRAPHICALLY INSTRUMENTED
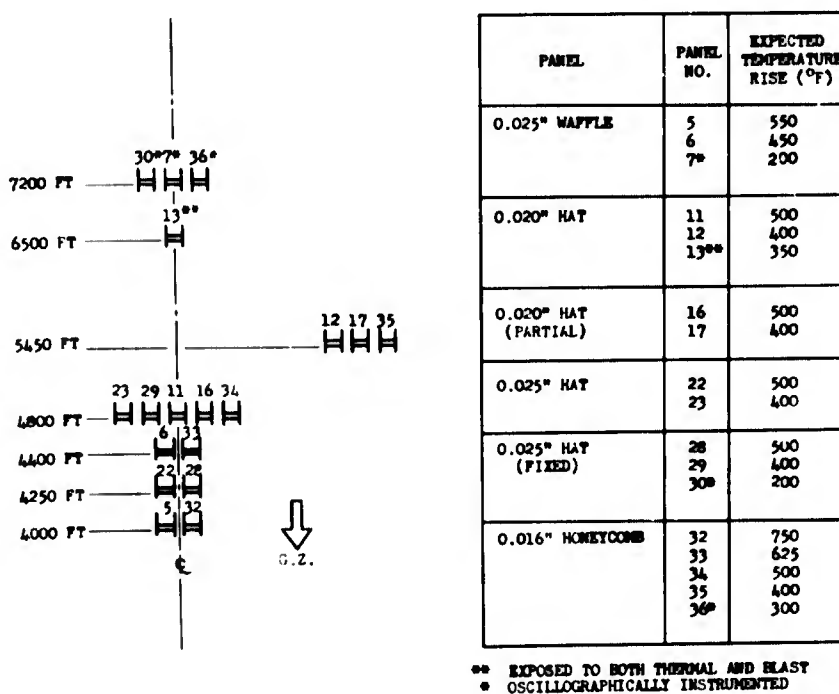
Fig. D. 12   Schematic Diagram of Bonded Metal Aircraft Program for Shot 10

212

on panels No. 5, 6, 16, 28, and 32.

Buckling damage reported herein is a measured value of the maximum depth of buckle, defined as the greatest vertical distance from any one trough of a buckle to the adjacent crest as shown in Fig. D. 13. The measurements of buckle depth for free edge hat and waffle

MAXIMUM DEPTH OF BUCKLE

FRONT SKIN OF BUCKLED PANEL
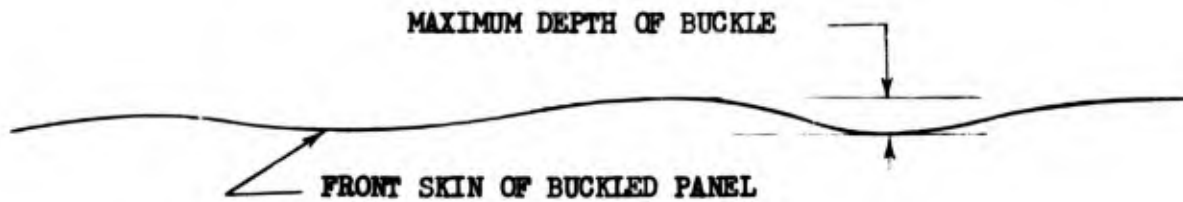
Fig. D. 13 Illustration of Maximum Depth of Buckle

panels were confined to the center portion of the panel to eliminate the effect of bending and warping of the unsupported edges.

Peak temperature and inspection results are presented in Tables D. 3, D. 4, D. 5, and D. 6, and photographs showing typical damage are given in Figs. D. 14 through D. 19. Time-history data are given in Figs. D. 20 through D. 31.

D. 1. 3   Discussion

Three response characteristics of bonded metal panels, i.e., buckling, bond release, and temperature distribution, are considered in this duscussion section.

D. 1. 3. 1   Panel Buckling

Waffle panel deformation was characterized by an outward buckling of the circular skin areas not enclosed by the stiffener and a general inward bowing of the entire panel. Hat panel buckling was somewhat similar to that of the waffle panels. Sketches of typical panel deformations are presented in Figs. D. 32 and D. 33 for free edge and fixed edge hat panels, respectively. On those hat panels which exper-

AFTER EXPOSURE

BEFORE EXPOSURE
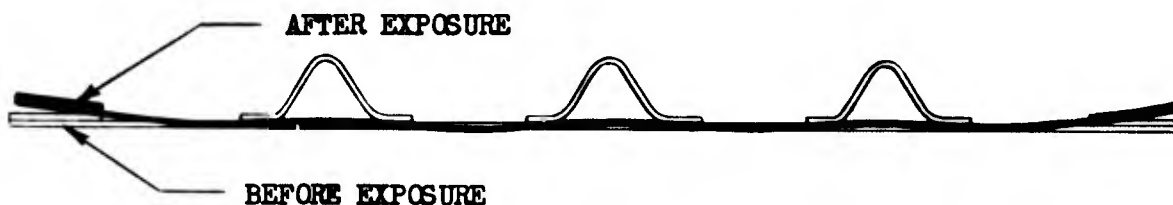
Fig. D. 32 Typical Deformation of Hat Panels, Free Edge

ienced the higher temperatures, ripples were found superimposed on the buckles. No definite pattern of buckling of the honeycomb panels could be determined, except that the buckles occurred only on the area

213

TABLE D.3 - Summary of Temperatures and Damage Sustained by
Waffle Panels

Panel Number	1	2	3	4	5	6	7
Thermal Energy Incident on Panel (cal/sq cm)	11.5	9.0	6.8	5.1	18.5	15.7	6.1
Ground Range (ft)	6500	7400	8400	9700	4000	4400	7200
Shot No.	9	9	9	9	10	10	10
Peak Temperature (°F)							
Skin	370	377-423	331-363	265-287	540-635	517-539	340
Doubler	144-170	171-178	144-170	144-170	232-252	195-224	144-170
Temperature Rise* (°F)							
Skin	246	257-303	211-243	145-167	420-514	397-419	221
Doubler	24-50	51-58	24-50	24-50	112-132	75-104	24-50
Bond Release	No	No	No	No	Yes	Yes	No
Maximum Depth of Buckle (in.)	1/32	1/32	None	None	1/4	9/64	1/64
Maximum Bow of Panel (in.)	1/16 (In)	None	1/32 (In)	None	1/4 (In)	9/64 (In)	None

* Assumed Ambient Temperature - 120°F

TABLE D.4 - Summary of Temperatures and Damage Sustained by
Honeycomb Core Panels

Panel Number	31	32	33	34	35	36
Thermal Energy Incident on Panel (cal/sq cm)	6.8	18.5	15.7	13.4	10.6	6.1
Ground Range (ft)	8400	4000	4400	4800	5450	7200
Shot No.	9	10	10	10	10	10
Peak Temperature (°F)						
Rear Skin	171-177	232-252	171-177	195-224	171-177	160
Flange	144-170	232-252	195-224	171-177	171-177	144-170
Temperature Rise[a] (°F)						
Front Skin [b]	212	575	487	415	328	188
Front Skin [c]	224-244	426-492	224-244	303-399	224-244	188
Rear Skin	68-74	129-149	68-74	92-121	68-74	57
Flange	41-67	129-149	92-121	68-74	68-74	41-67
Bond Release	No	Yes	Yes	Yes	Yes	Yes
Front Skin (%)	0	90	90	15	5	35
Flange (%)	0	15	20	0	20	0
Maximum Depth of Buckle (in.)	1/64	1/16	3/64	3/64	1/32	1/32
Maximum Bow of Panel (in.)		3/32 (In)	1/16 (In)	3/64 (In)	1/16 (In)	1/32 (In)

(a) Assumed Ambient Temperature - 103°F for rear face and flange, and 117°F for front face
(b) Assumed proportional to incident thermal energy (See data for Panel No. 36)
(c) Assumed 3.3 times rear face temperature rise (See data for Panel No. 36)

TABLE D.5 - Summary of Temperatures and Damage Sustained by the 0.020 in. Hat Panels

	Total Irradiation						Partial Irradiation			
Panel Number	8	9	10	11	12	13	14	15	16	17
Thermal Energy Incident on Panel (cal/sq cm)	6.8	5.5	4.4	13.4	10.6	9.8	5.5	4.4	13.4	10.6
Ground Range (ft)	8400	9400	10,800	4800	5450	6500	9400	10,800	4800	5450
Shot Number	9	9	9	10	10	10	9	9	10	10
Peak Temperature (°F) Location a * (Skin)	377-423	288-308	265-287	540-635	488-514	488-514	288-308	253-264	540-634	465-487
b	253-264	232-252	195-231	377-423	288-308	288-308	232-252	178-194	377-423	265-287
c	195-224	171-177	171-177	265-287	195-224	253-264	144-170	144-170	225-231	195-224
d	195-224	171-177	171-177	195-224	195-224	253-264	144-170	144-170	225-231	195-224
Temperature Rise (°F) Location a * (Skin)	247-293	158-178	135-157	430-524	378-404	378-404	158-178	123-134	430-524	355-377
b	123-134	102-122	65-101	267-313	178-198	178-198	102-122	48-64	267-313	155-177
c	65-94	41-47	41-47	155-177	85-114	143-154	14-40	14-40	115-121	85-114
d	65-94	41-47	41-47	85-114	85-114	143-154	14-40	14-40	115-121	85-114
Bond Release	No	No	No	No	No	No	No	No	No	No
Maximum Depth of Buckle (in.)	1/32	1/32	1/64	3/32	5/64	3/16	1/32	1/32	7/64	3/32
Maximum Over-all Bow of Panel (in)	1/32 (in)	1/64 (in)	None	1/8 (in)	1/16 (in)	7/64 (in)	None	None	1/8 (in)	1/16 (in)

Assumed Ambient Temperature - 130°F for Shot 9, and 110°F for Shot 10
* See Fig. D.7

TABLE D.6 - Summary of Temperatures and Damage Sustained by 0.025 in. Hat Panels

	Free Edge									Fixed Edge				
Panel Number	18	19	20	21	22	23	24	25	26	27	28	29	30	37
Thermal Energy Incident on Panel (cal/sq cm)	9.6	9.0	6.8	5.1	17.0	13.4	9.6	9.0	6.8	5.1	17.0	13.4	6.1	26
Ground Range (ft)	7200	7600	8400	9700	4250	4800	7200	7600	8400	9700	4250	4800	7200	4700
Shot Number	9	9	9	9	10	10	9	9	9	9	10	10	10	5
Peak Temperatures (°F) Location a * (Skin)	395	377-423	288-308	265-287	635	488-514	392	442-464	288-308	265-287	540-634	488-514	300	635
b	253-265	253-265	232-252	232-252	177-252	309-514	265-287	253-265	232-252	195-231	377-423	288-308	220	424-441
c	232-252	232-252	195-224	171-177	288-308	265-287	232-252	232-252	171-177	171-177	265-287	253-264	198	265-287
d	235	232-252	195-224	178-194	288-308	253-264	248	232-252	171-177	171-177	265-287	232-252	225-252	265-287
Temperature Rise (°F) Location a * (Skin)	270	247-293	158-178	135-157	525	378-404	257	312-334	157-178	135-157	430-524	378-404	188	590
b	123-135	123-135	102-122	102-122	267-313	199-220	135-157	123-135	102-122	65-101	267-313	178-198	109	379-396
c	102-122	102-122	65-94	41-47	178-198	155-177	102-122	102-122	41-47	41-47	155-177	143-154	86	220-242
d	113	102-122	65-94	48-64	178-198	143-154	112	102-122	41-47	41-47	155-177	122-142	115-142	220-242
Bond Release	No	No	No	No	Yes	No	No	No	No	No	No	No	No	Yes
Maximum Depth of Buckle (in.)	3/64	3/64	1/32	1/64	5/32	7/64	3/32	7/64	1/8	3/32	1/8	7/64	3/32	7/64
Maximum Over-all Bow of Panel (in.)	1/64 (in)	1/32 (in)	None (in)	None (in)	3/16 (in)	5/64 (in)	1/16 (in)	1/16 (out)	3/64 (out)	1/16 (out)	7/64 (out)	1/16 (out)	1/32 (in)	1/16 (in)

Assumed Ambient Temperature - 130°F for Shot 9, 110°F for Shot 10
* See Fig. D.7

1/32" Buckle Depth, Panel No. 2

1/4" Buckle Depth, Panel No. 5
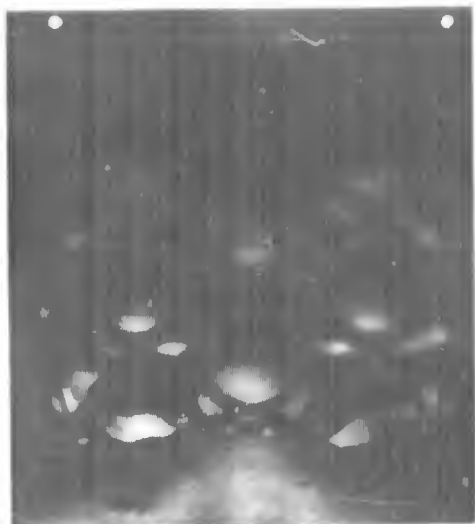
9/64" Buckle Depth, Panel No. 6

Bond Release, Panel No. 5

Fig. D.14 Typical Thermal Damage to Waffle Panels
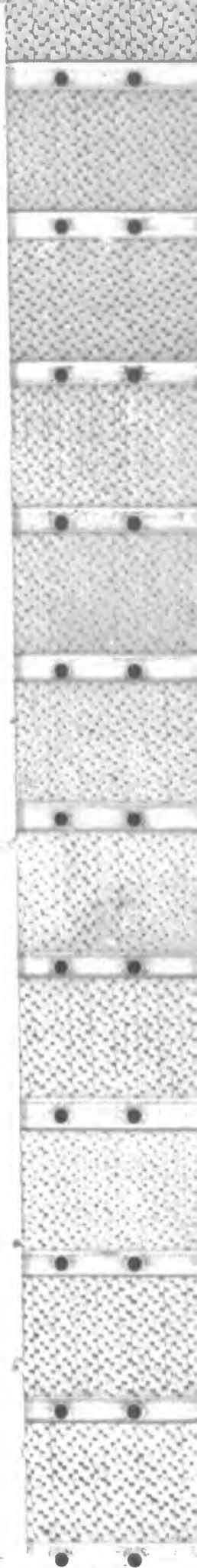
1/32" Buckle Depth, Panel No. 36
(Typical of Panels No. 31 and 36)
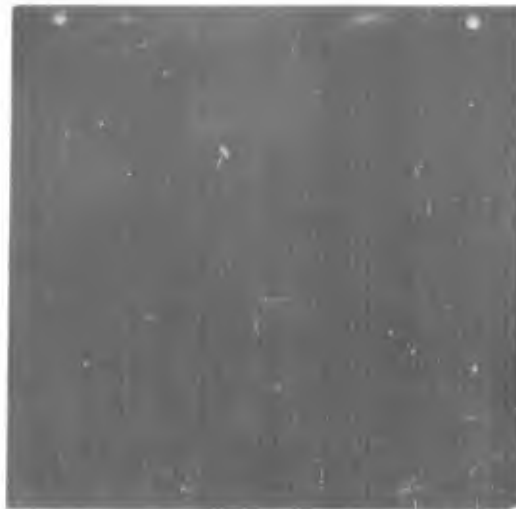
3/64" Buckle Depth, Panel No. 34

Front Face Bond Release, Panel
No. 32
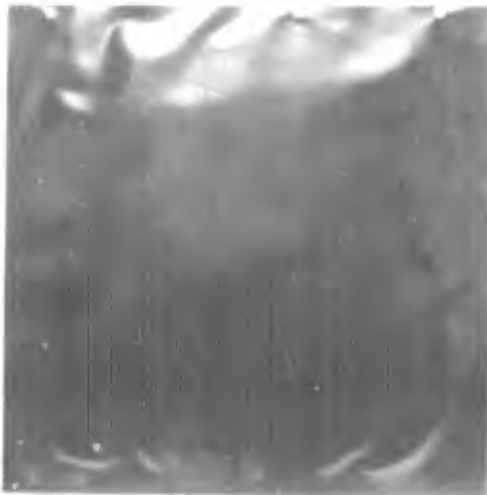
1/16" Buckle Depth, Panel No. 32
(Typical of Panels No. 32 and 33)

Periphery Bond Release, Panel
No. 35

Fig. D. 15   Typical Thermal Damage to Honeycomb Core Panels

217

1/32" Buckle Depth, Panel No. 8   3/32" Buckle Depth, Panel No. 11
(Typical of Panels No. 8 and 9)
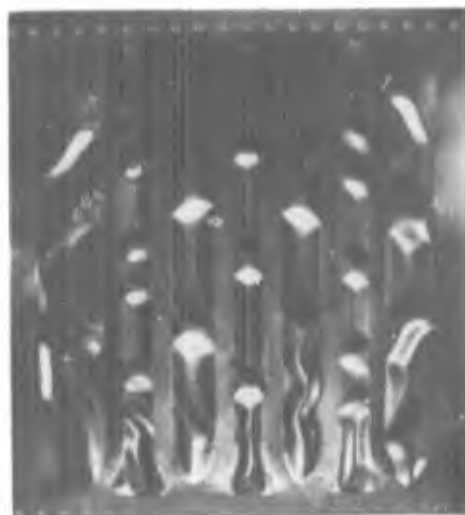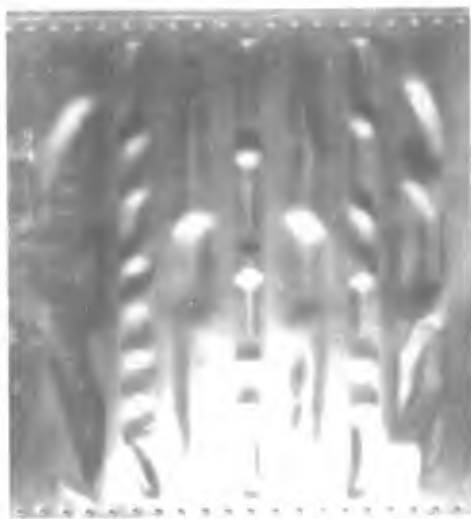
5/64" Buckle Depth, Panel No. 12   Thermal and Blast Damage, 3/16"
                                     Buckle Depth, Panel No. 13
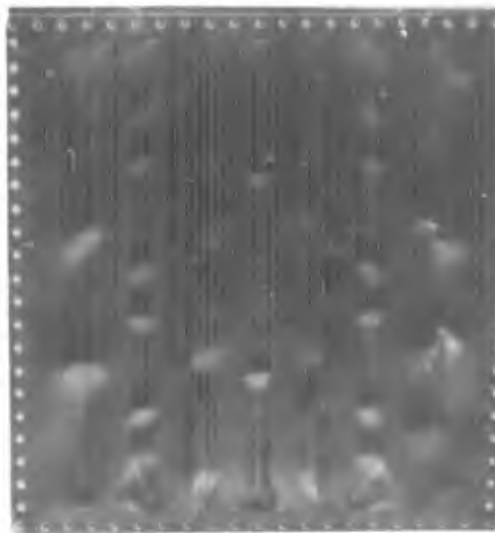
Fig. D.16   Typical Thermal Damage to 0.020 in. Hat Panels, Free
            Edges

218
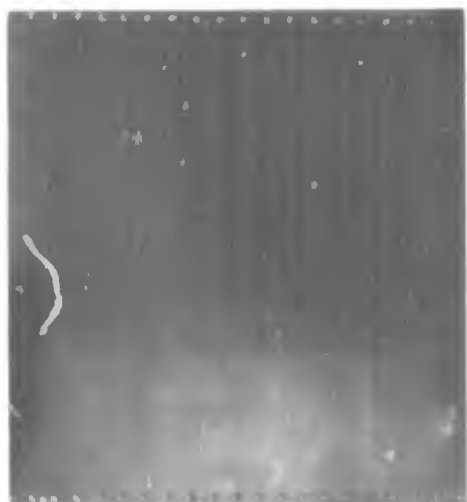
1/32" Buckle Depth, Panel No. 15   3/32" Buckle Depth, Panel No. 17

7/64" Buckle Depth, Panel No. 16

Fig. D. 17   Typical Thermal Damage to 0. 020 in. Hat Panels, Free
Edges, Partially Irradiated

219
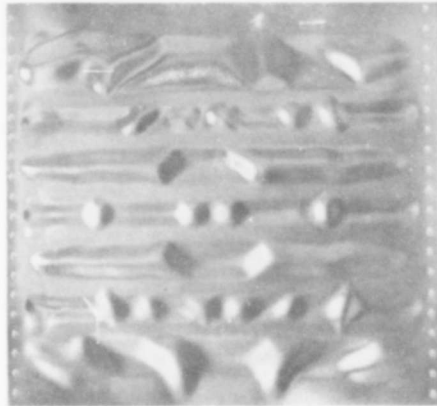
3/64" Buckle Depth, Panel No. 18
(Typical of Panels No. 18 and 19)

5/32" Buckle Depth, Panel No. 22
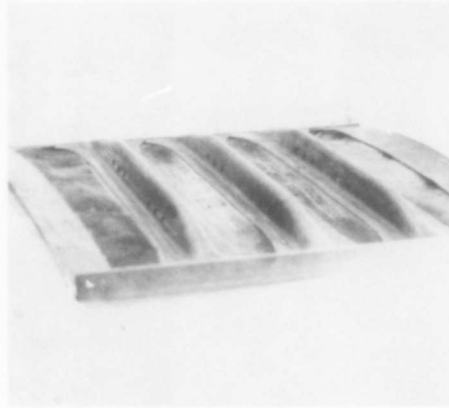
7/64" Buckle Depth, Panel No. 23

Bond Release, Panel No. 22

Fig. D.18   Typical Thermal Damage to 0.025 in. Hat Panels, Free
Edges

220
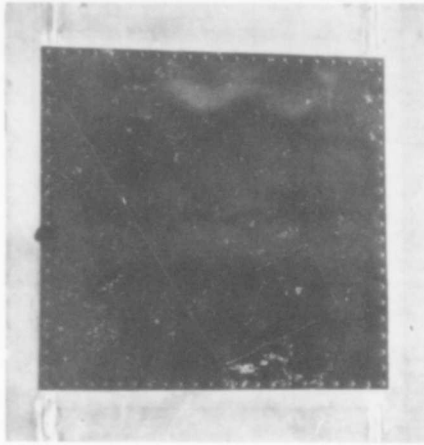
3/32" Buckle Depth, Panel No. 24   7/64" Buckle Depth, Panel No. 29
(Typical of Panels No. 24, 25, 26,
27, 30)
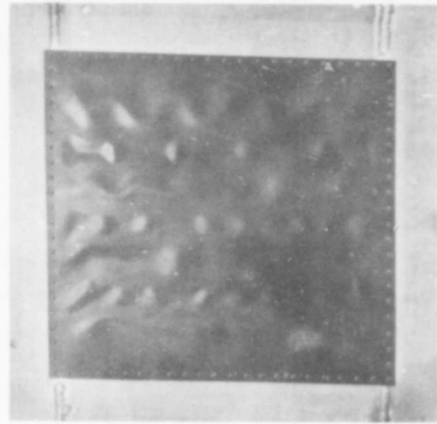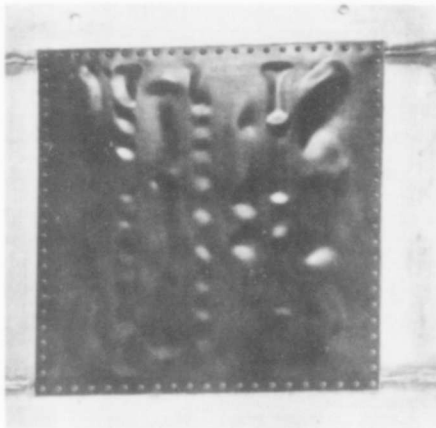
1/8" Buckle Depth, Panel No. 28   Bond Release, Panel No. 37
(Typical of Panels No. 28 and 37)
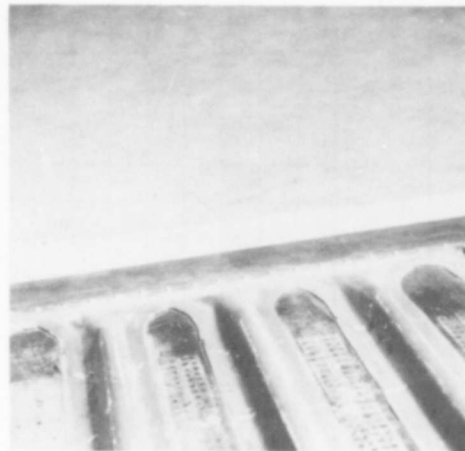
Fig. D.19 Typical Thermal Damage to 0.025 in. Hat Panels, Fixed
Edges

221
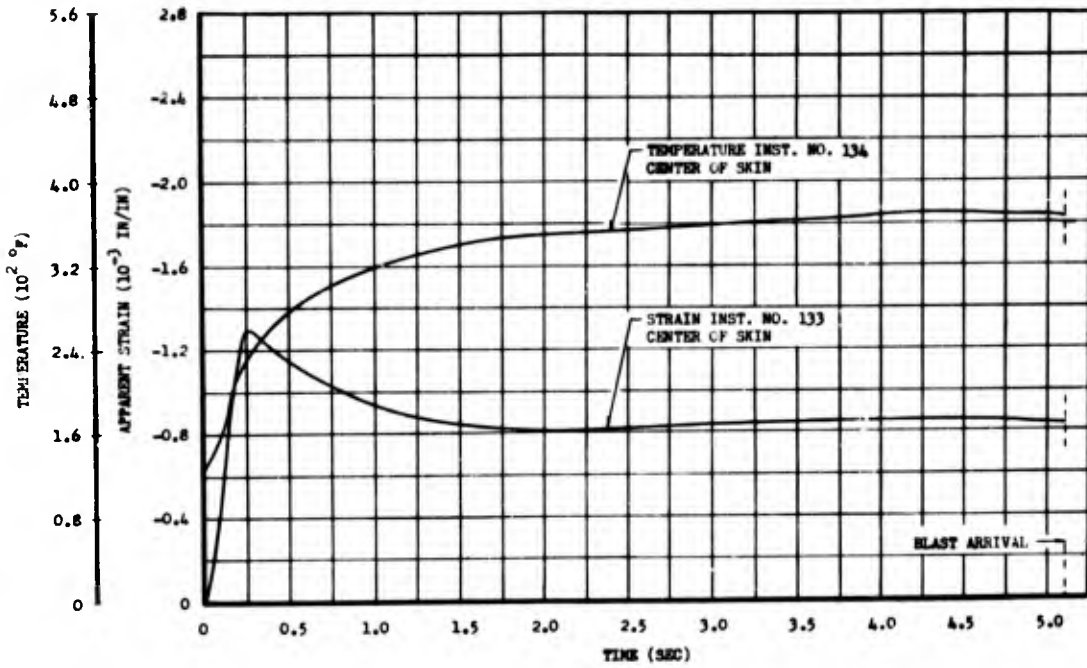
Fig. D.20 Comparison of the Strain-time and Temperature-time Data
for the Center of the Skin of Waffle Panel No. 1, Station
6500, Shot 9 (See Fig. D.9)
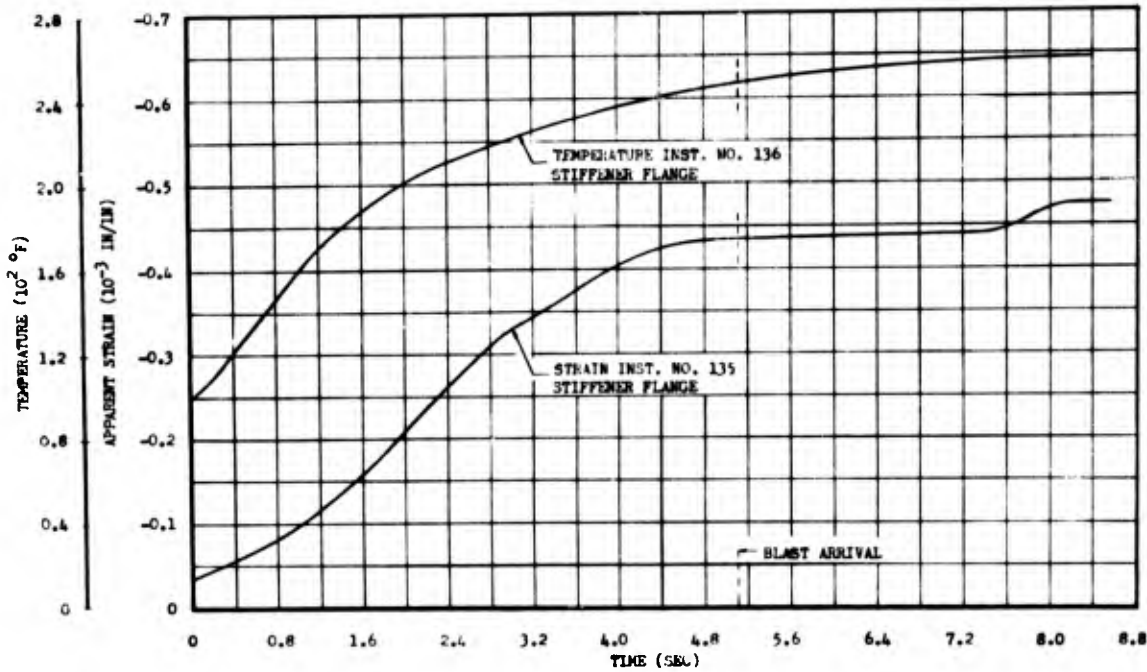
Fig. D.21 Comparison of the Strain-time and Temperature-time Data
for the Stiffener Flange of Waffle Panel No. 1, Station
6500, Shot 9 (See Fig. D.9)

222
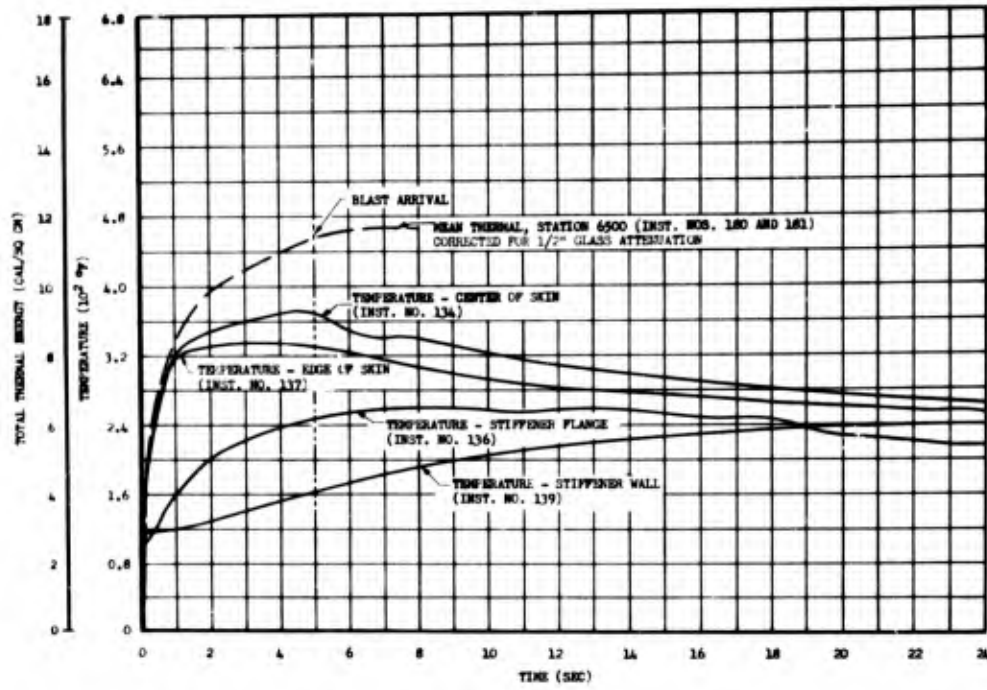
Fig. D.22   Comparison of the Temperature-time Data for Waffle Panel
No. 1, Station 6500, Shot 9 (See Fig. D.9)
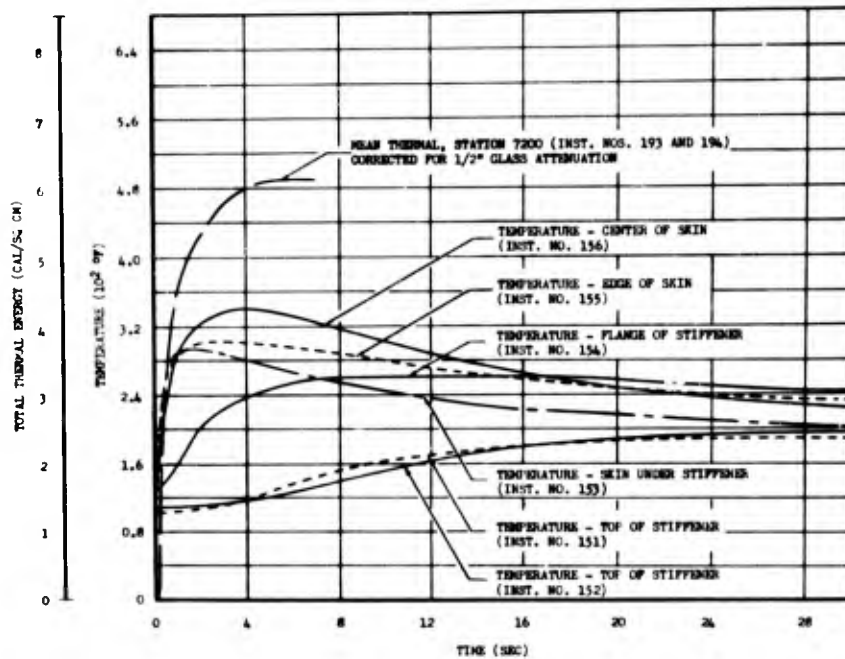
Fig. D.23   Comparison of the Temperature-time Data for Waffle Panel
No. 7, Station 7200, Shot 10 (See Fig. D.9)

223
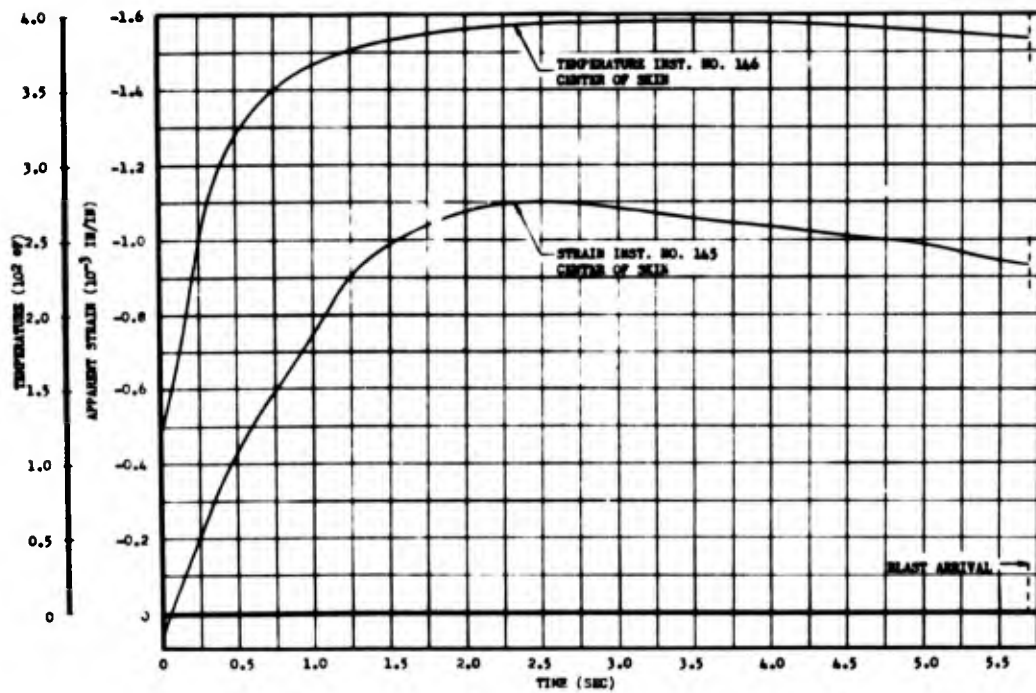
Fig. D.24 Comparison of the Strain-time and Temperature-time Data
for the Center of the Skin of Panel No. 18, 0.025 in. Hat,
Station 7200, Shot 9 (See Fig. D.10)
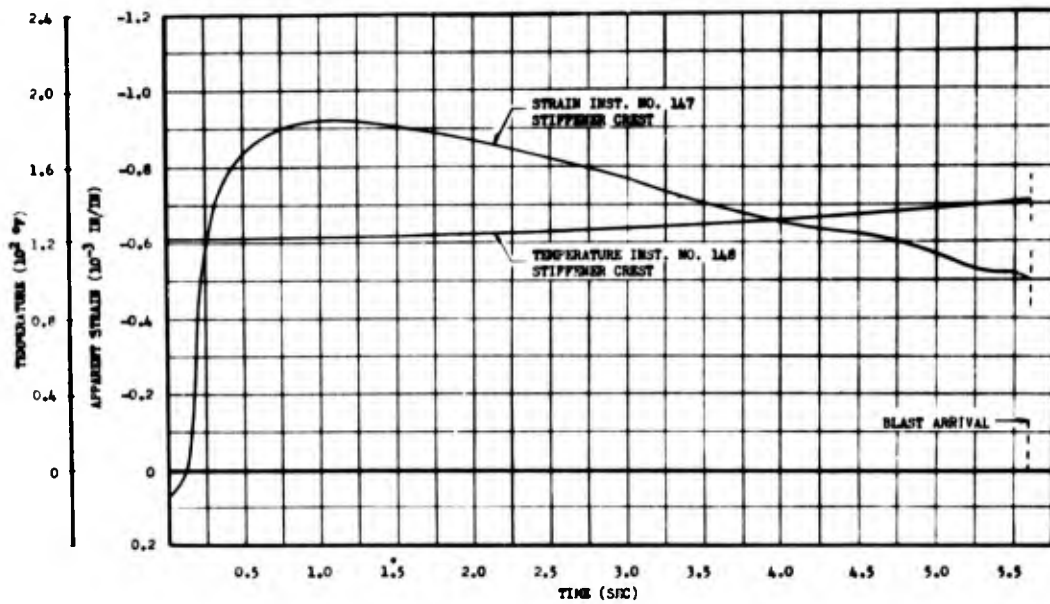
Fig. D.25 Comparison of the Strain-time and Temperature-time Data
for the Stiffener Crest of Panel No. 18, 0.025 in. Hat,
Station 7200, Shot 9 (See Fig. D.10)

224
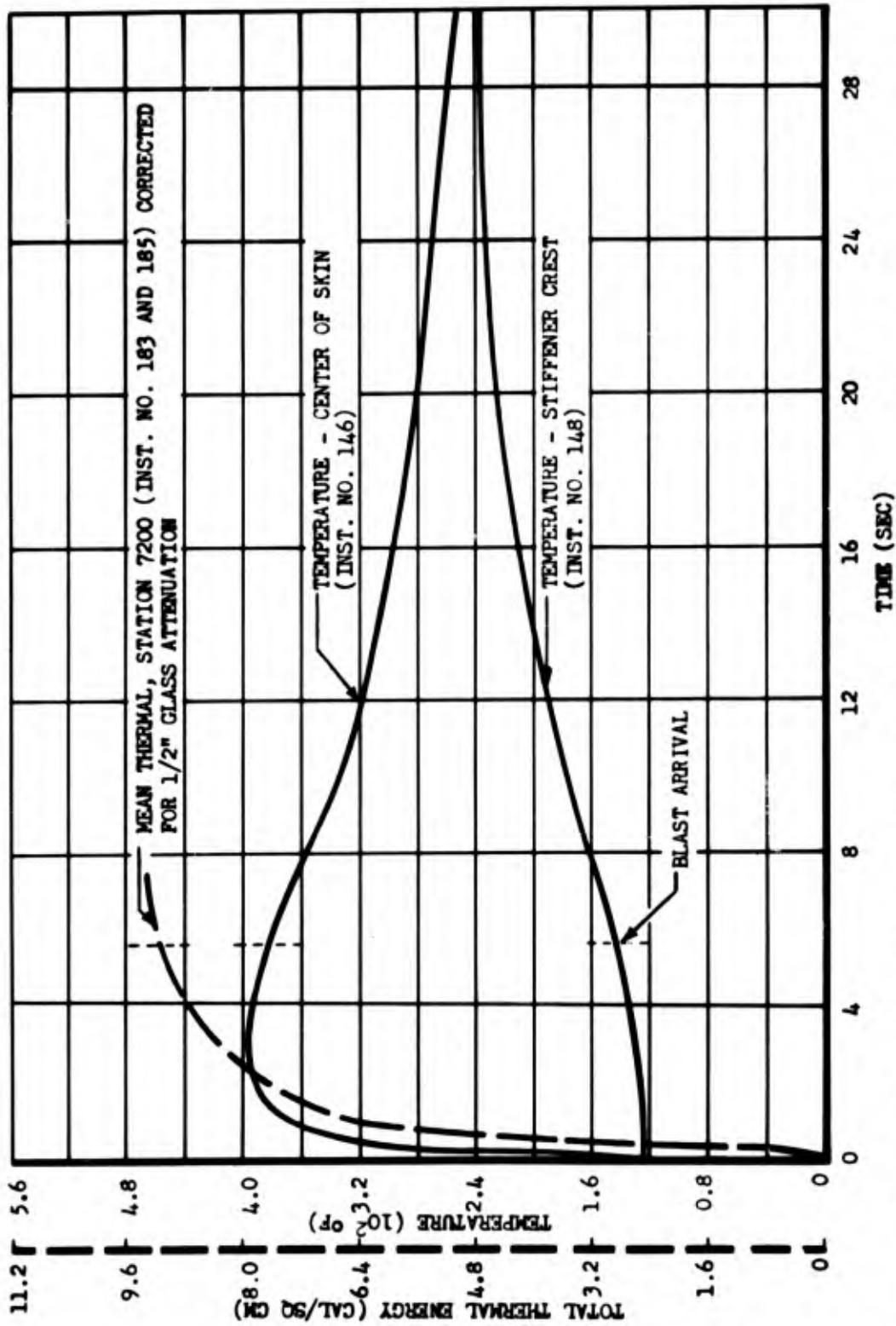
Fig. D.26 Comparison of the Temperature-time Data for Panel No. 18, 0.025 in Hat, Station 7200. Shot 9 (See Fig. D.10)
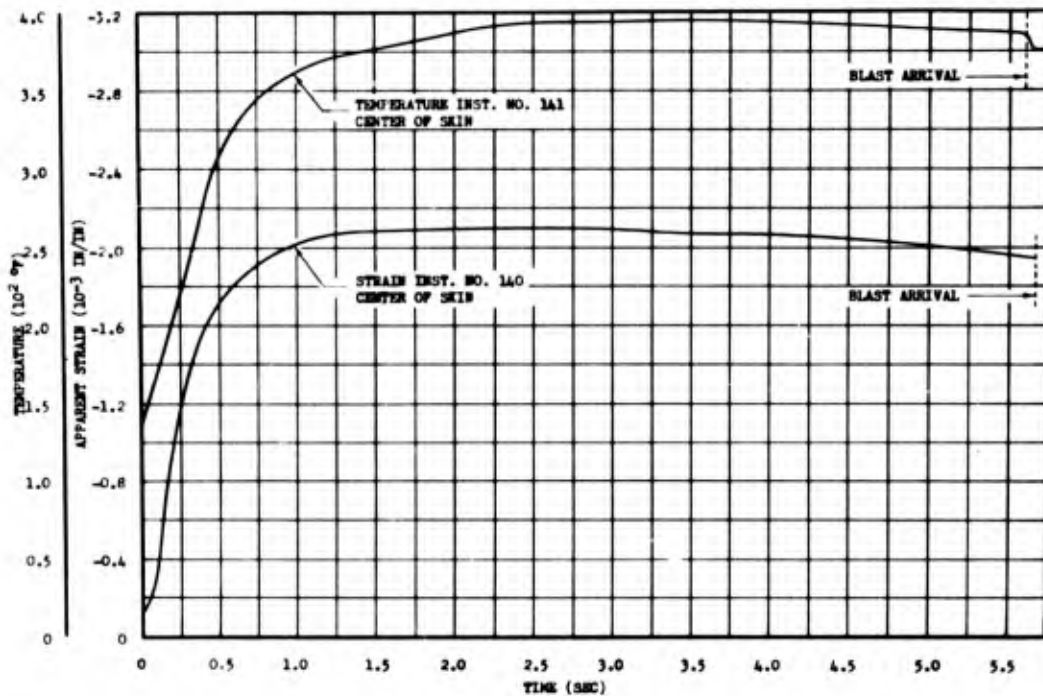
Fig. D.27 Comparison of the Strain-time and Temperature-time Data
for the Center of the Skin of Panel No. 24, 0.025 in. Fixed
Edge Hat, Station 7200, Shot 9 (See Fig. D.10)
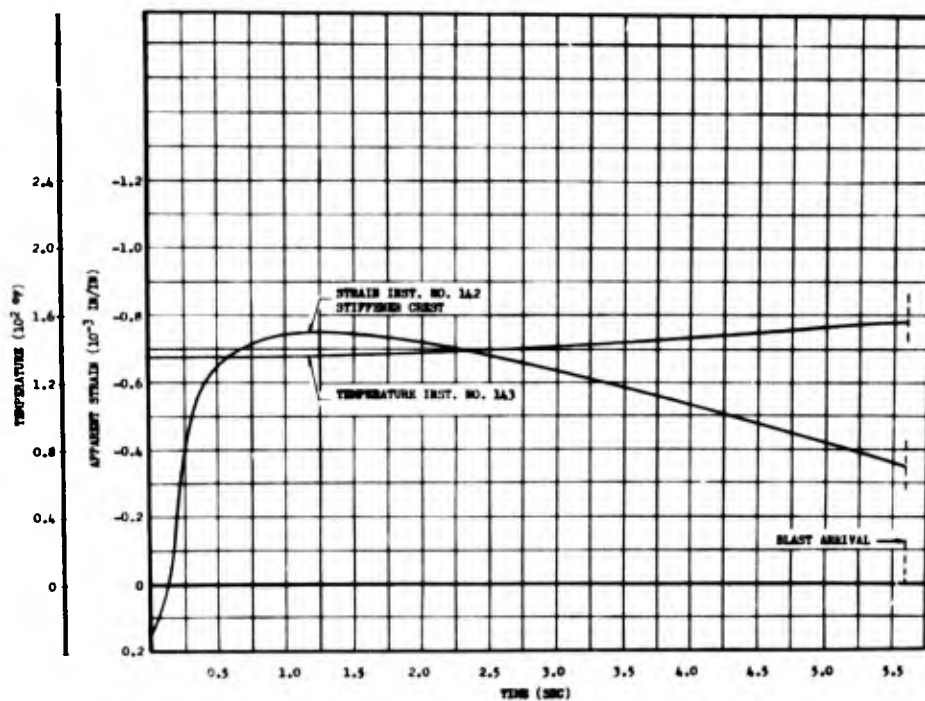
Fig. D.28 Comparison of the Strain-time and Temperature-time Data
for the Stiffener Crest of Panel No. 24, 0.025 in. Fixed
Edge Hat, Station 7200, Shot 9 (See Fig. D.10)

226
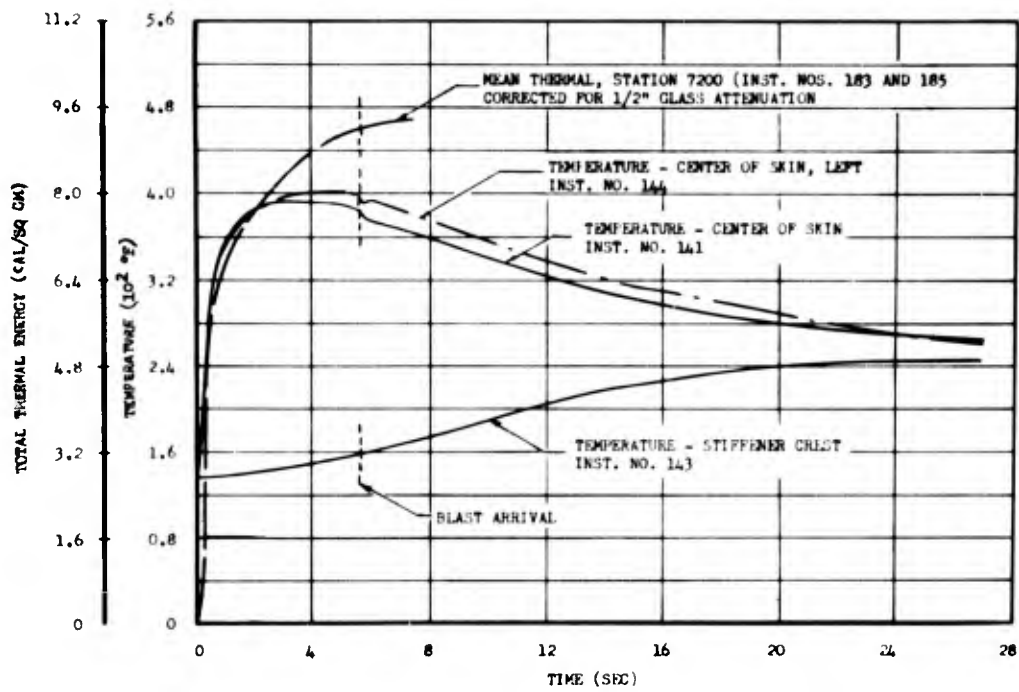
Fig. D.29 Comparison of the Temperature-time Data for Panel No. 24, 0.025 in. Fixed Edge Hat, Station 7200, Shot 9 (See Fig. D.10)
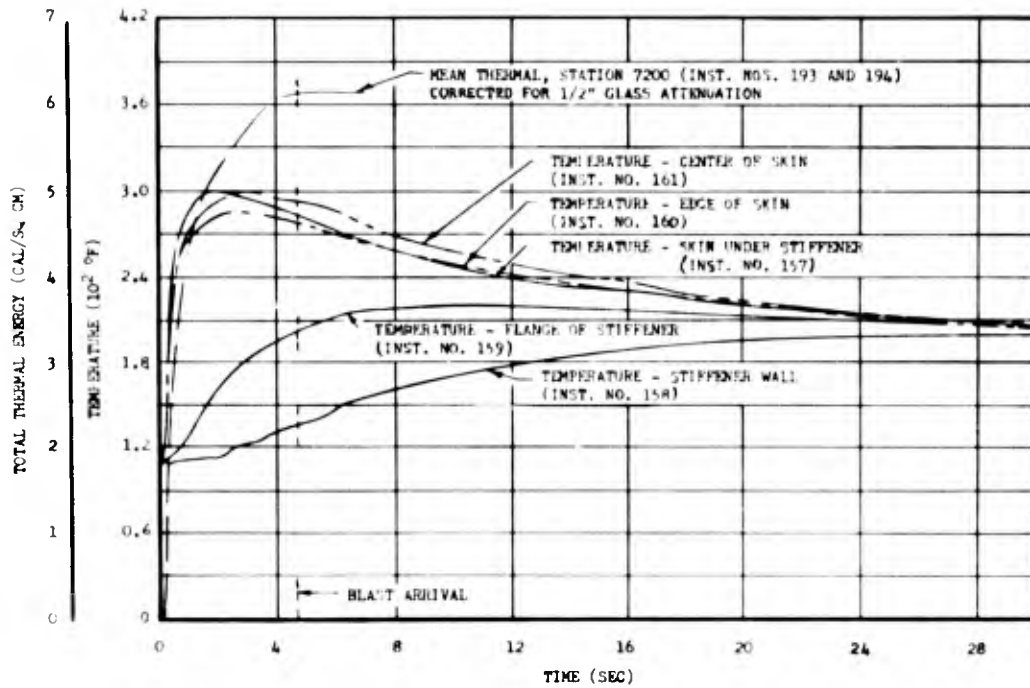
Fig. D.30 Comparison of the Temperature-time Data for Panel No. 30, 0.025 in. Fixed Edge Hat, Station 7200, Shot 10 (See Fig. D.10)

227
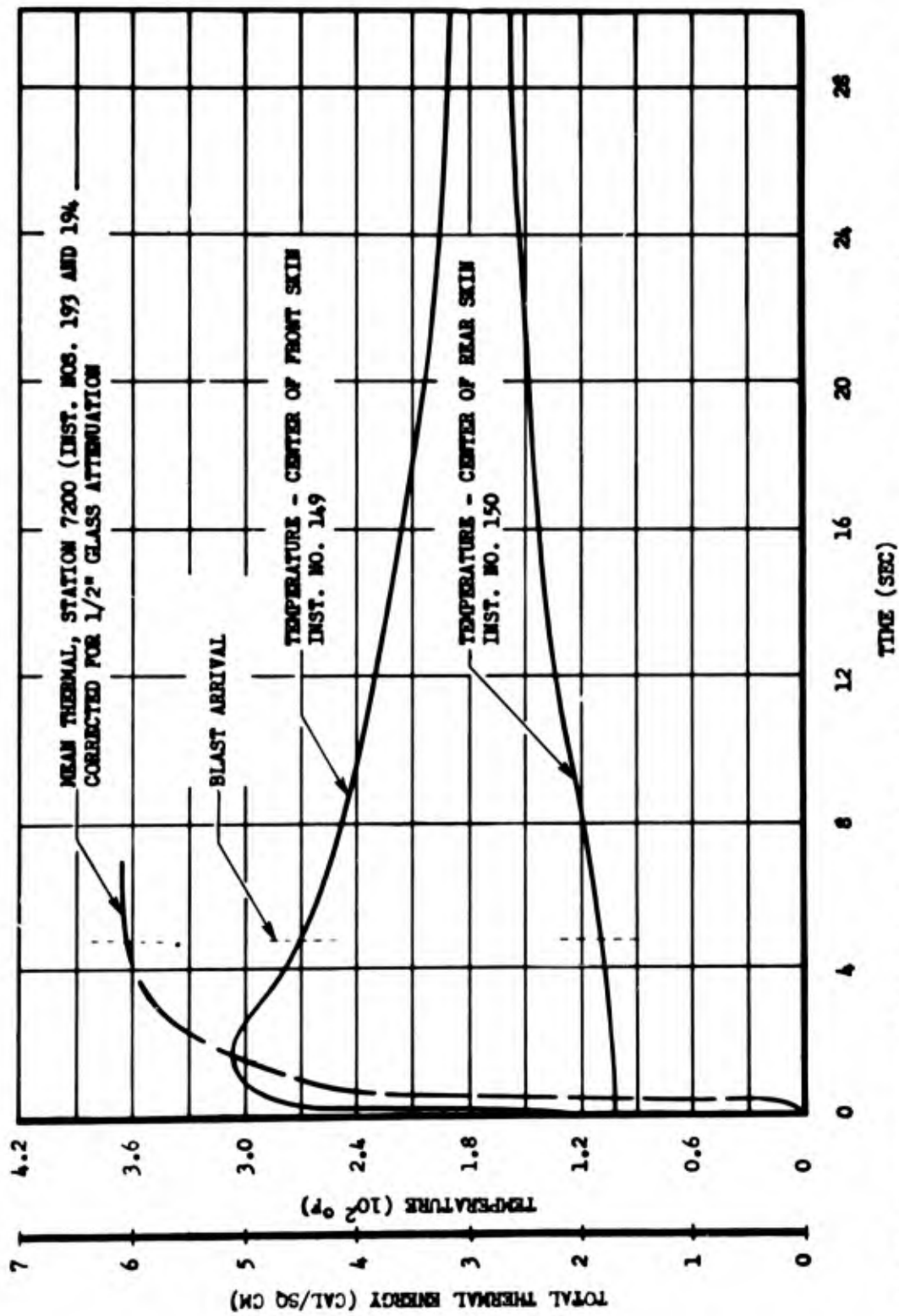
Fig. D.31 Comparison of the Front and Rear Face Temperature-time Data for Honeycomb Core Panel No. 36, Station 7200, Shot 10

near the periphery of the honeycomb core.

Graphs of maximum depth of buckle versus skin temperature rise for the four parameters of panel type, skin thickness, edge condi-

Fig. D.33   Typical Deformation of Hat Panels, Fixed Edge

tion, and area of irradiation are presented in Figs. D.34, D.35, D.36, and D.37, respectively.   The point of inflection on the curves for hat panels may indicate a temperature rise beyond which the smaller secondary "ripples" were formed on top of the larger primary buckles.

With an initial (ambient) temperature of about $100^{\circ}F$, permanent skin buckling was initiated at temperature rises of about $50^{\circ}F$ for 0.020 in. hat (partial) and 0.025 in. hat (fixed) panels, about $100^{\circ}F$ for 0.020 in. hat, 0.025 in. hat, and 0.016 in. honeycomb panels, and about $200^{\circ}F$ for 0.025 in. waffle panels.   Figure D.34 indicates that, although permanent buckling was initiated at a higher temperature for the waffles than for the hat or honeycomb panels, the buckle depth increased rapidly with increasing temperature and at higher temperature rises was greater than either of the other type panels.

The skin thickness of the hat panels appeared to have little effect on the maximum depth of buckle at lower temperature rises; however, at relatively higher temperatures as shown in Fig. D.35, the 0.025 in. hat panels experienced slightly greater depths of buckle than the 0.020 in. hat panels.

The parameter of edge condition, as illustrated in Fig. D.36, had a pronounced effect at lower temperature rises and somewhat less effect at higher temperatures.

For a given skin temperature rise, partial irradiation appeared to cause a somewhat larger depth of buckle than total irradiation on 0.020 in. hat panels, as shown in Fig. D.37.

D.1.3.2   Bond Release

Bond release on the hat and waffle panels on the area near the edges of the panels occurred at lower temperatures than those required to cause bond release on the center portion of the panels.   On waffle and hat panels, bond release apparently occurred first under the doublers, then under the portion of the stiffener near the edges of the panel, and then under the remaining portion of the stiffener, in order

229
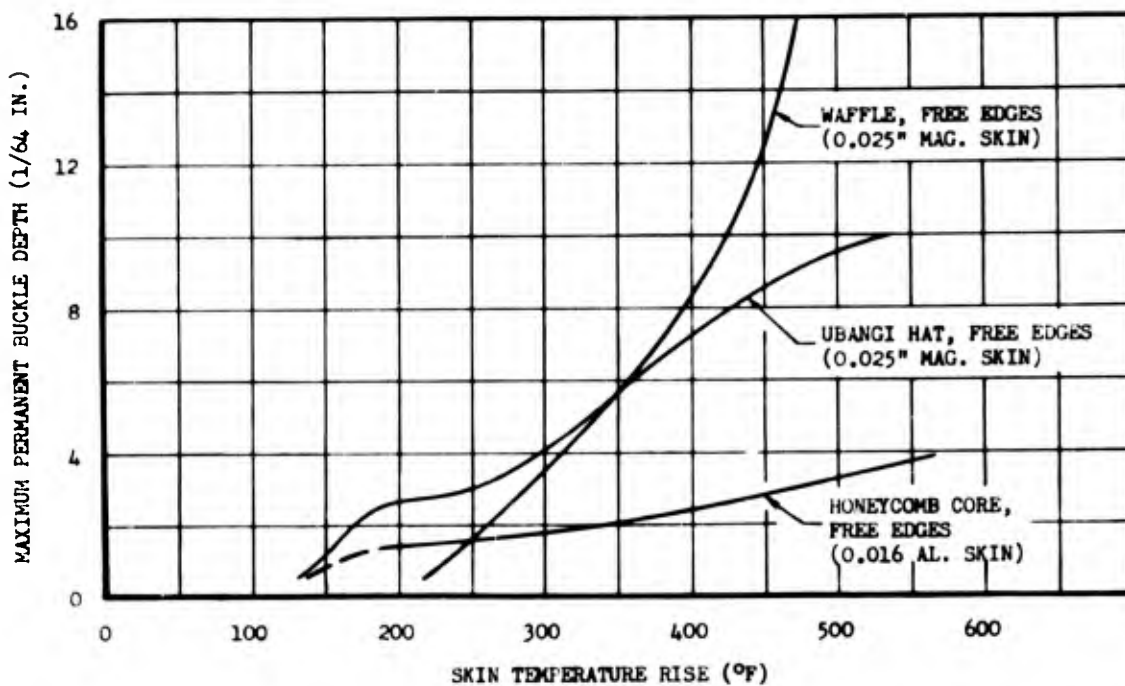
Fig. D.34 Vulnerability of Bonded Metal Aircraft Panels to Permanent
Skin Buckling as a Function of Skin Temperature Rise for
the "Panel Type" Parameter
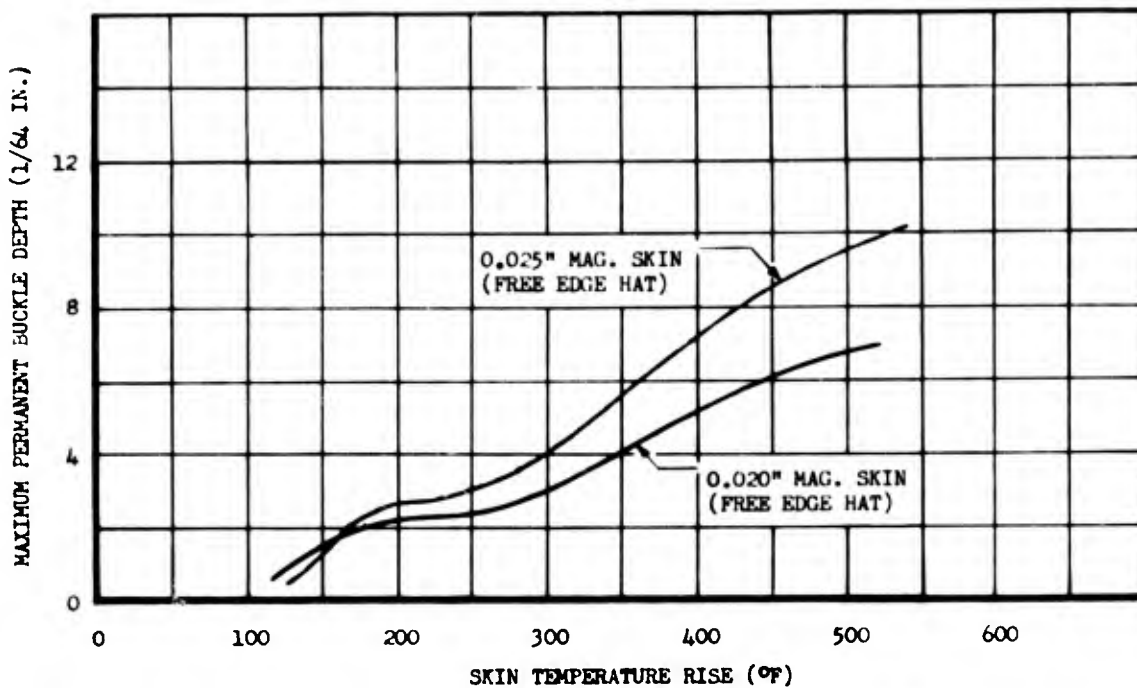
Fig. D.35 Vulnerability of Bonded Metal Aircraft Panels to Permanent
Skin Buckling as a Function of Skin Temperature Rise for
the "Skin Thickness" Parameter

230
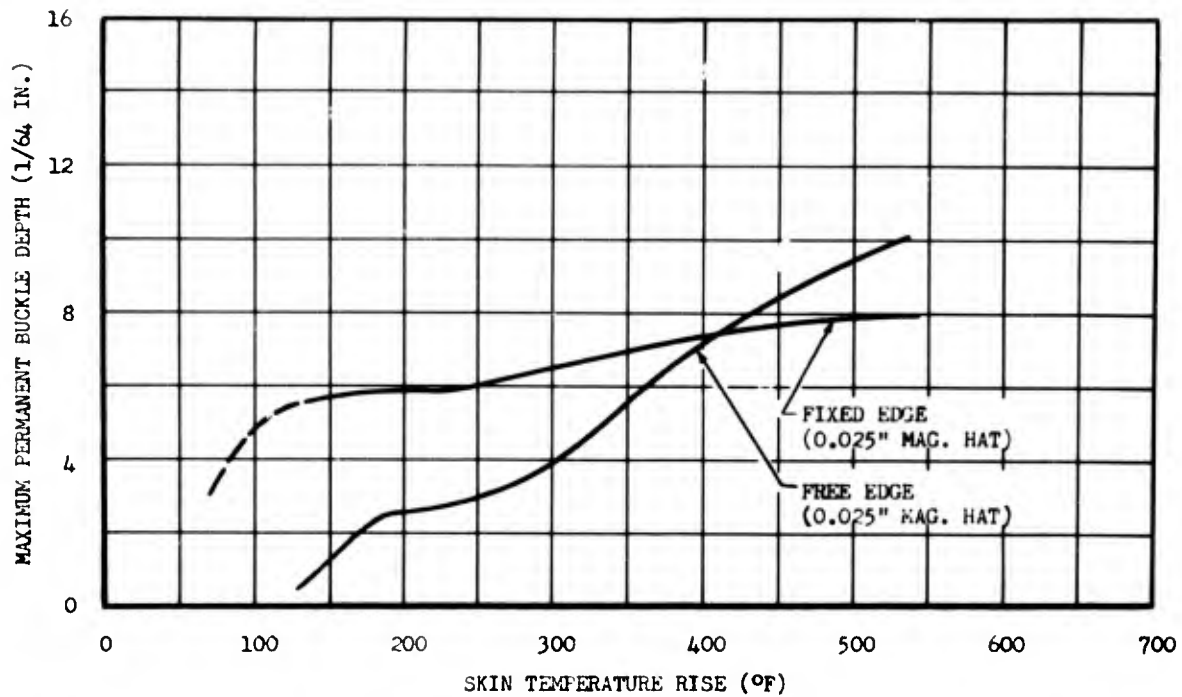
Fig. D.36 Vulnerability of Bonded Metal Aircraft Panels to Permanent Skin Buckling as a Function of Skin Temperature Rise for the "Edge Condition" Parameter
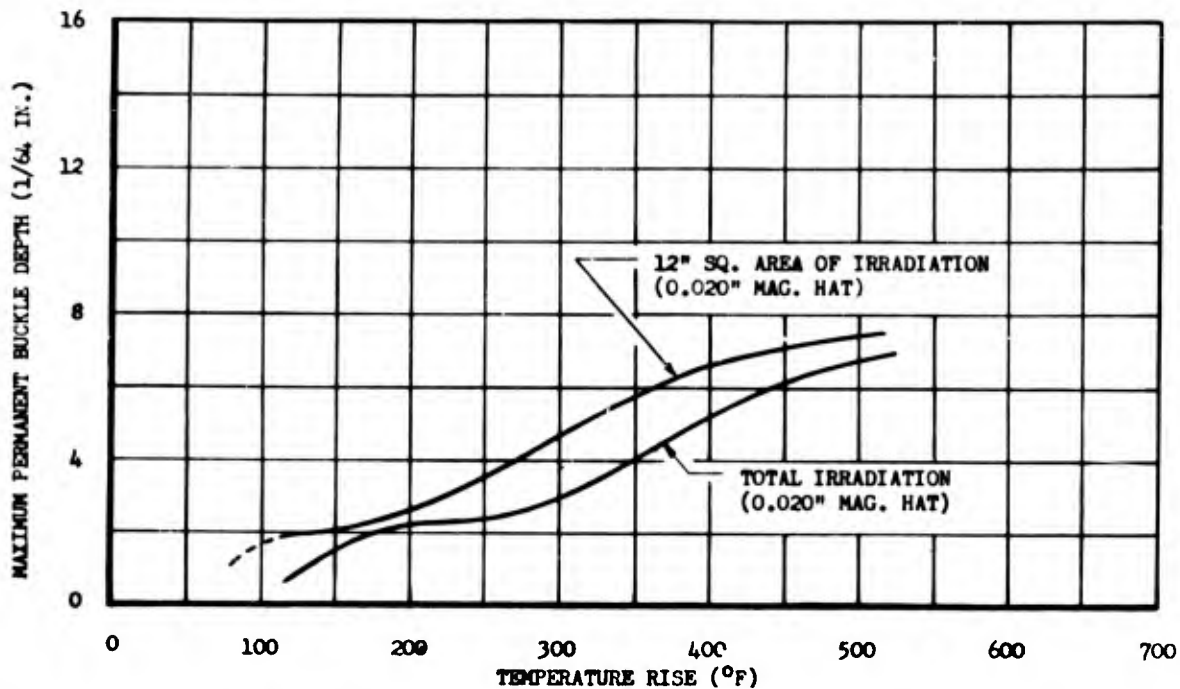
Fig. D.37 Vulnerability of Bonded Metal Aircraft Panels to Permanent Skin Buckling as a Function of Skin Temperature Rise for the "Area of Irradiation" Parameter

231

of increasing temperature. On honeycomb panels, releasing of bond between the skin and the honeycomb core occurred at lower temperatures than those required to cause releasing of the bond between the doubler and the skin. There were insufficient data to fix accurately the threshold or the degree of bond release for the various panel types.

Hat panels were the most resistant to bond release of any of the types of panels tested. Temperatures in the range of from 540°F to 634°F* were sustained by hat panels with no apparent bond release. At temperatures greater than 635°F, bond release occurred near the ends of the hat stiffeners on panel No. 22, and over nearly the entire area of bond panel No. 37.

Bond release of waffle panels did not occur at temperatures up to 423°F but did occur near the edges of panels No. 6 and 5 in temperature ranges of from 517°F to 539°F and from 540°F to 634°F, respectively.

Honeycomb core panels were the least resistant to bond release. Separation of the skin from the honeycomb core occurred at temperatures as low as 300°F. Release of about 20 per cent of the doubler length was observed on panel No. 35 at a temperature of about 445°F. Approximately 90 per cent separation of the skin from the core
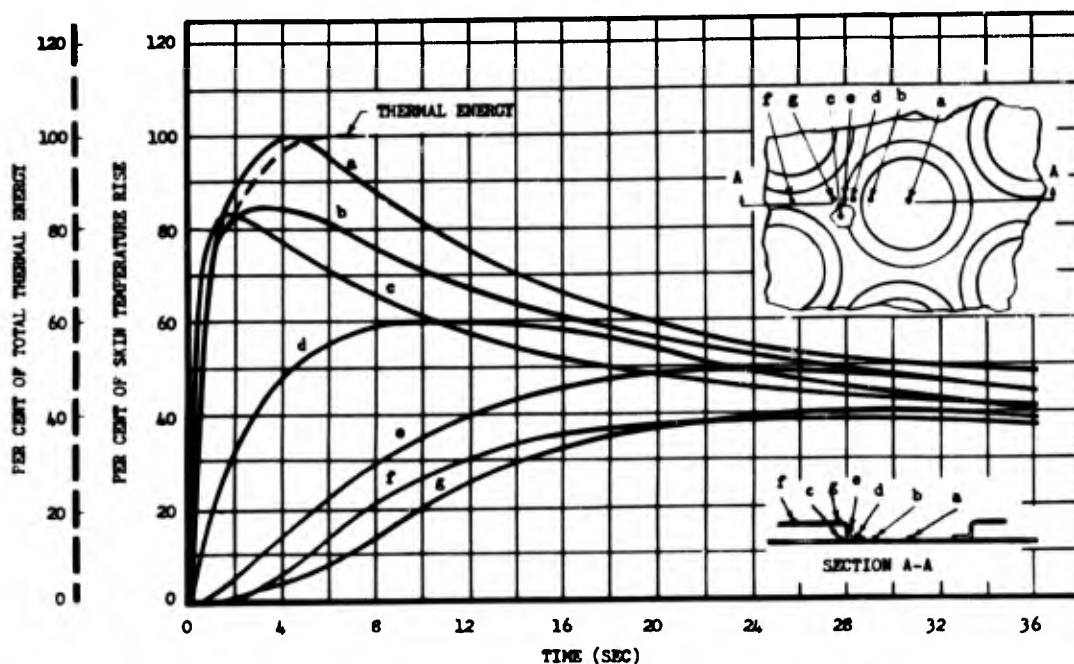
Fig. D.38 Relative Temperature Rise Distribution as a Function of
Time for Various Locations on Waffle Type Aircraft Panels

---

* All temperatures given in this section are total or peak readings.
Tables D.3, D.4, D.5, and D.6 give temperature rises and ambient temperatures as well as peak temperatures.

232
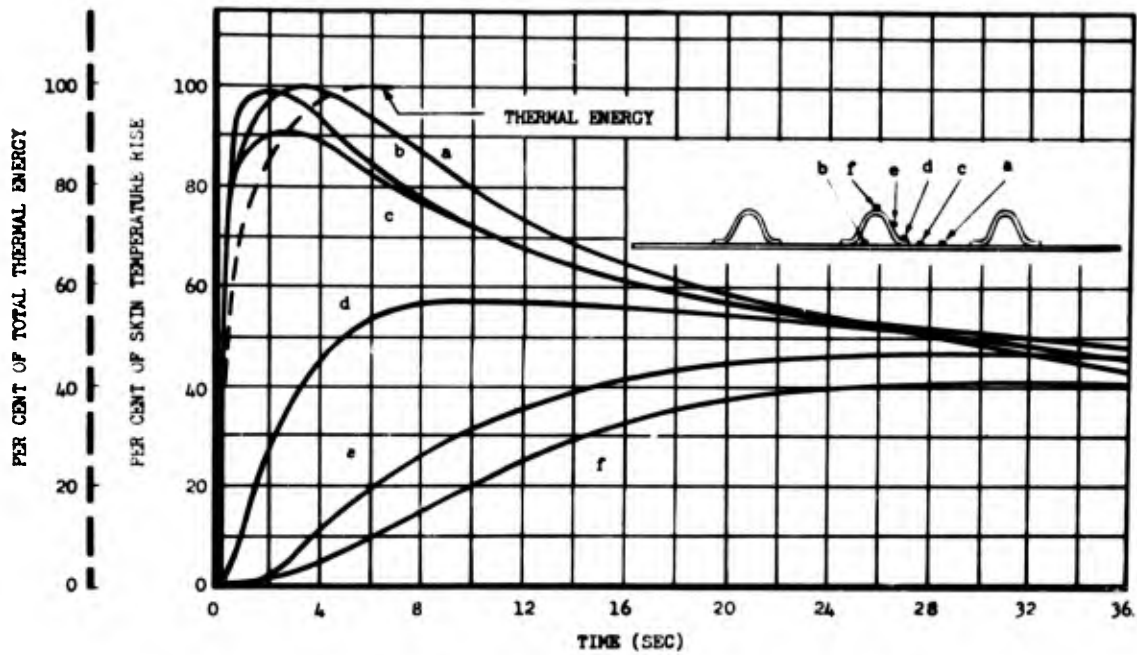
Fig. D. 39   Relative Temperature Rise Distribution as a Function of Time for Various Locations on Hat Type Aircraft Panels
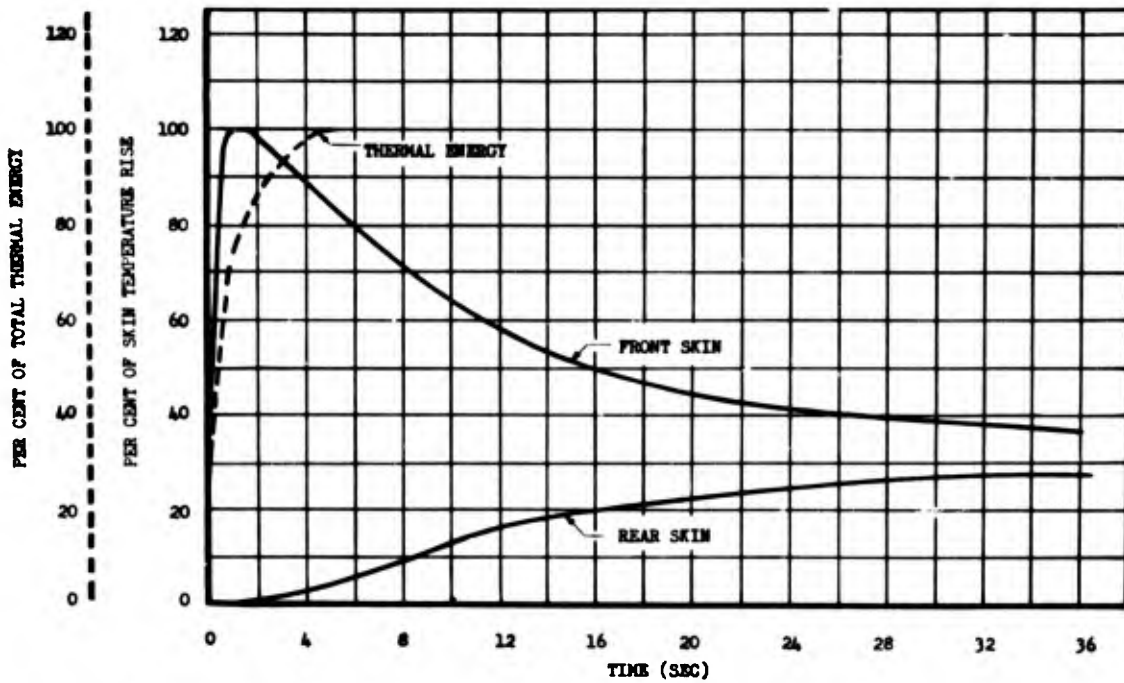
Fig. D. 40   Relative Temperature Rise Distribution as a Function of Time for the Front and Rear Faces of Honeycomb Core Type Aircraft Panel

233

occurred on panels No. 32 and 33 which experienced temperatures of 575°F and 487°F, respectively.

D.1.3.3   Temperature Distribution

All time-history temperature data of bonded metal panels were normalized to per cent of skin temperature rise for each location on each type of panel and are presented in Figs. D.38, D.39, and D.40. If more than one data curve was available for a given location, the average of the curves is shown.

D.2   B-36 COMPONENTS

Certain components salvaged from B-36 aircraft that had been damaged in a windstorm were exposed as test specimens during the UPSHOT-KNOTHOLE operation. It was deemed advisable to include in the program a B-36 horizontal stabilizer and elevator assembly and a B-36 wing section, since the data obtained from tests of these two components could lend valuable support to the solution of several problems currently being investigated.

D.2.1   Procedure

The stabilizer and elevator specimen, Fig. D.41 consisted of
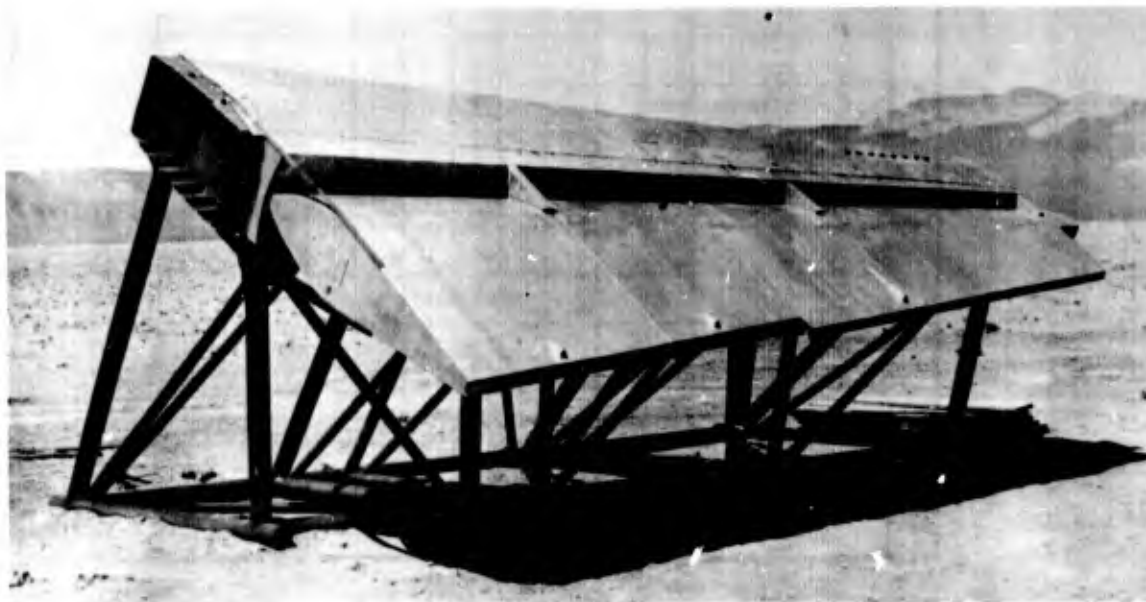
Fig. D.41   B-36 Stabilizer and Elevator Assembly Prior to Shot 9, Range 13,000 ft

that portion of the left-hand stabilizer and elevator assembly between Stations 50 and 372, excluding both the leading edge of the stabilizer and the trim and servo tabs of the elevator. The repair work required prior to the test consisted of the installation of plywood bulkheads at Station 372 on both the stabilizer and elevator to seal the interiors and the replacement of 10 access doors and 7 skin panels on the elevator surface. Although a mixture of panel types would not normally be used on an elevator in service, the 7 skin panels were replaced by panels with closed end hat stiffeners, whereas the original panels were all of the type utilizing open end hat stiffeners. This offered the possibility of gathering data on both types of panels in one test. Of the 7 panels replaced, 2 were on the upper unexposed surface of the elevator and 5 were on the lower, exposed surface. These 5 panels are Nos. 7, 8, 10, 11, and 14 in Fig. D.42.

The wing section used was a 26 ft section of the left wing outer panel extending from Station 855 (Bulkhead 25.5) to Station 1170 (Bulkhead 35), as shown in Fig. D.43. The aileron and the leading edge were not included. Both ends of the section were sealed with fitted plywood bulkheads as shown for the outboard end in Fig. D.44.

D.2.1.1   Stabilizer and Elevator Assembly

The stabilizer and elevator assembly was mounted on a jig, as shown in Fig. D.41, in such a way that the blast incidence would approximate that realized during a bombing run. To accomplish this, the assembly was positioned with the spar horizontal and normal to a line from ground zero to the specimen and with the chord making a 30° angle with the ground. The lower surface faced upward with the leading edge directed away from ground zero. The elevator was attached to the stabilizer at the three conventional hinge points with chord lines coinciding and was restricted in rotation by four steel angles bolted to the upper surfaces of the elevator and to the jig. The stabilizer and elevator assembly was mounted by the addition of 2 in. by 2 in. steel angles installed vertically on the rear spar of the stabilizer and then bolted to the jig. This method also strengthened the spar, since spar shear was thereby transferred to the mounting jig. The height of the assembly was such that the lowest point of the elevator was approximately 3 ft above the ground. The jig, consisting of a welded construction using 8 in. steel pipe, was designed in three sections for ease in transportation, and was bolted together at the test site before mounting the stabilizer and elevator in place.

The specimen was first exposed on Shot 9 at a ground range of 13,000 ft and an expected overpressure of 1.8 psi based on the predicted yield. As anticipated, little or no damage was suffered; consequently, it was planned to move the entire assembly and mount into a

235
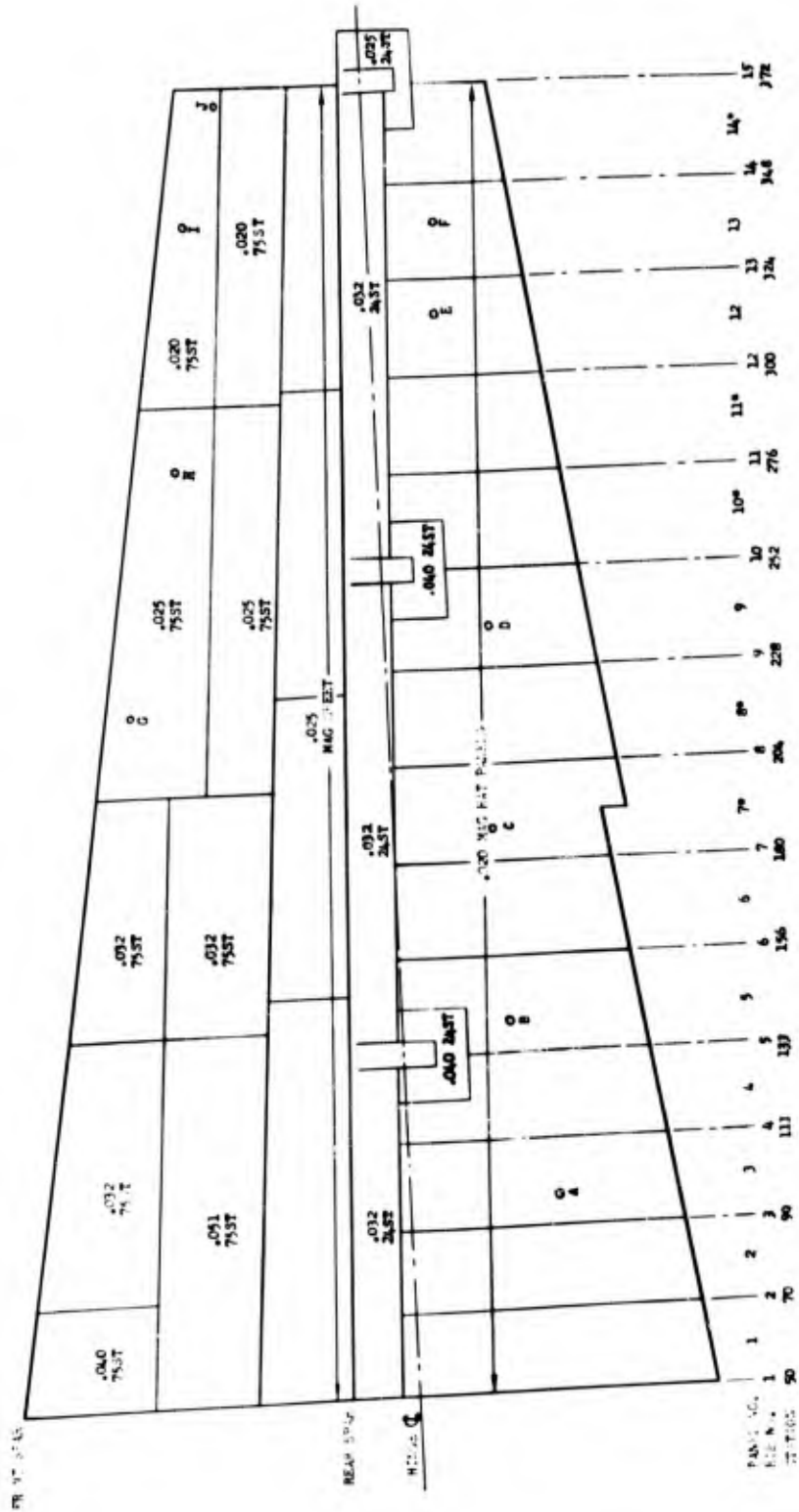
Fig. D.42 Skin and Plating Diagram of B-36 Left Horizontal Stabilizer and Elevator Assembly, Lower Surface, Presenting Peak Temperatures (Temp-tape Data), Range 13,000 ft, Shot 9, and Range 5300 ft, Shot 10
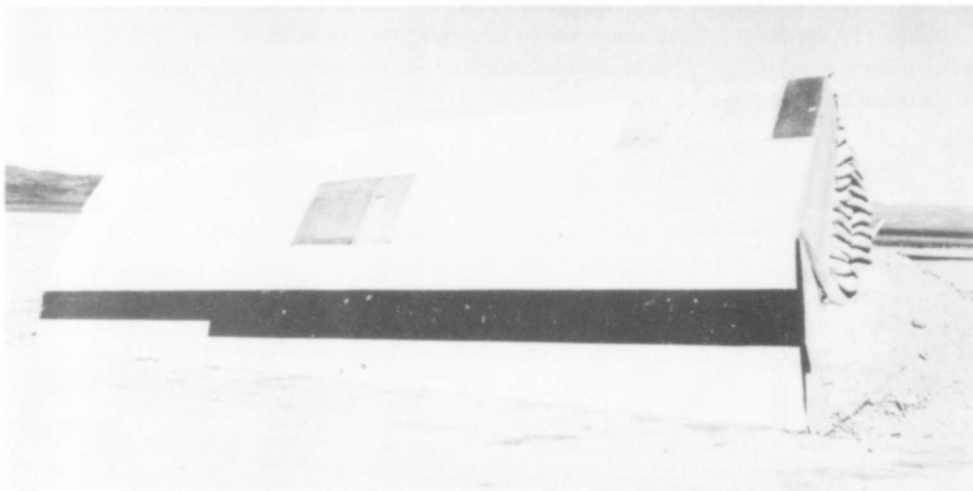
Fig. D. 43 B-36 Left Wing Outer Panel Prior to Shot 9, Range 4800 ft

Fig. D. 44 B-36 Wing Section Prior to Shot 9, Range 4800 ft, Showing
Plywood Bulkhead at Outboard Extremity

237

region of higher overpressure for Shot 10. The stabilized area at ground range 5300 ft was chosen for its location on Shot 10, since it offered a predicted overpressure of approximately 2.9 psi, as well as the camera coverage originally set up for other test articles on Shot 9. Immobility at this location was achieved by the use of four tie-downs consisting of 3/8 in. steel cable anchored to poured concrete deadmen as shown in Fig. D.45.

Fig. D.45 B-36 Stabilizer and Elevator Assembly Prior to Shot 10, Range 5300 ft

The instrumentation for both shots consisted of temp-tapes to record peak temperatures of various skin panels.

D.2.1.2 B-36 Wing Section

The wing section was mounted with the chord normal to the incident radiation, the main spar resting on the ground and the lower surface facing ground zero. The wing was supported in the rear by an embankment of earth and was held in place by 1/4 in. diameter steel cables guying the structure to two concrete deadmen poured outside and to the rear of each end of the section. Some degree of stabilization of dust was achieved by the use of sodium tetrasilicate stabilizing compound over an area 35 ft wide and approximately 20 ft in front of the specimen.

The only exposure planned for the B-36 wing section was in Shot 9 at a ground range of 4800 ft. The overpressure, based on the predicted yield, was to be approximately 8 psi and the thermal input expected was 28 cal/sq cm. These inputs were expected to be critical for a skin thickness of 0.091 in., which was approximately the median of the various thicknesses which ranged from 0.040 in. to 0.156 in. In an attempt to achieve varying peak temperatures for the same skin thickness, the skins were painted white, gray, and black, as shown in Fig. D.46.
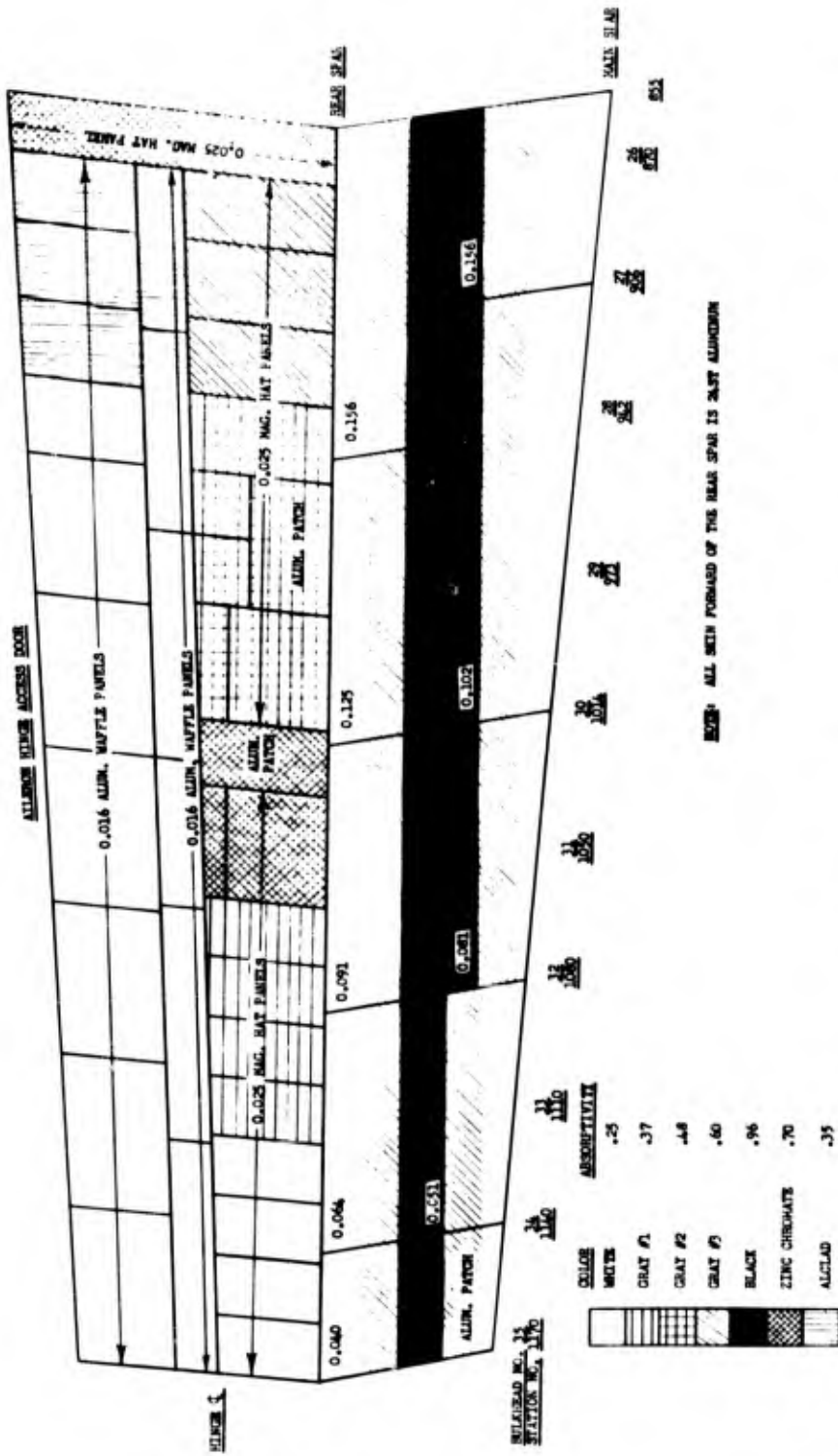
Fig. D.46 Skin and Plating Diagram of B-36 Left Wing Outer Panel, Lower Surface, Portraying Absorptivity Pattern, Range 4800 ft, Shot 9

In view of the primary objective in exposing the B-36 wing section, that of thermal blast coupling studies, temp-tape instrumentation was far more extensive than it was with the stabilizer and elevator assembly. Each of the wing panel absorptivity configurations was instrumented.

Since heavy damage was expected to all but the thickest skins, no detailed listing of minor preshot damage was compiled.

D.2.2   Results

The results contained herein consist of peak temperature data obtained from the B-36 components and a visual assessment of the damage sustained.

D.2.2.1   Stabilizer and Elevator Assembly

Temp-tape locations and readings for the stabilizer and elevator assembly are as recorded in Fig. D.42. Elevator panel and rib numbers are also designated in this figure.

The assembly, on Shot 9, was subjected to inputs of 3.3 cal/sq cm and 1.2 psi at an actual ground range of 13,585 ft. Damage was very light, consisting primarily of slight dishing of elevator panels No. 5, 6, and 7 to depths of 1/8 in., 3/16 in., and 1/8 in., respectively. The entire assembly was considered serviceable.

The true ground range for Shot 10 was 5350 ft and the inputs were 14.4 cal/sq cm and 3.2 psi. The damage sustained during Shot 10 is as follows:

1. Elevator:

a. Ribs 2, 3, 5, 6, 7, 10, and 11 were buckled aft of the spar. The buckling of the ribs was a maximum about half way between the spar and the trailing edge. At this point the ribs were crushed from 3/4 to 1 1/2 in. The deformation was located chiefly on the lower surface with only slight effects on the upper surface.

b. The upper surface skin panels showed no deformation other than that which accompanied the rib buckling.

c. The lower surface skin panels, except Nos. 1 and 9, were dished in with a center deflection of 1/4 to 1/2 in.

d. All lower surface skin panels showed evidence of thermal damage. The areas between the stiffeners were scorched and the skin was bowed in from 1/16 to 1/8 in.

e. The access doors in panels 3 and 5 were blown off. The fasteners of the access door in panel 9 were opened but the door remained on the elevator. One of the two fasteners of the access door on panel 13 was opened.

240

f. The two 1/2 in. bolts which attached the stiffening angle on the elevator to the jig, Station 133, were sheared as shown in Fig. D.47.

2. Stabilizer:

a. All stabilizer bulkheads except the one at Station 50 failed. The severity of damage varied but each bulkhead exhibited at least one of the following characteristic failures:

(1) Structural member buckled, twisted or torn.

(2) Rivets sheared or pulled out.

(3) Gussets or connections torn loose.

b. The bulkhead at Station 226 and 252 were damaged to a greater degree than the others. The central vertical members and the forward diagonals of the rib trusses sheared from the lower chord and pierced the lower surface skin and the front spar. The lower surface skin was very noticeably caved inward in this region.

Fig. D.47 B-36 Stabilizer Assembly, Range 5300 ft (3.2 psi), Shot 10, Showing Sheared Bolts on Mounting Jig

c. The upper and lower skins were generally wrinkled. The wrinkles ran mostly spanwise but followed no general pattern. The skin panel on the lower surface, forward of the rear spar, from Station 252 to 372, was dished in about 1/2 in. between the stringers.

d. The trailing edge skin was torn from upper to lower surface at Stations 100 and 170. The paint on the lower half of the trailing edge was scorched but showed no thermal buckling.

In general, the stabilizer and elevator assembly during Shot 10 was damaged beyond economical repair. Figures D.48 thru D.53 show general postshot conditions.

D.2.2.2   B-36 Wing Section

The B-36 wing section was exposed on Shot 9 only, where the inputs experienced were 23 cal/sq cm and 5.7 psi. The true ground range was 5459 ft from actual ground zero.

The complete results of the temp-tape instrumentation of the B-36 wing panel are given in Fig. D.54. The temperatures listed
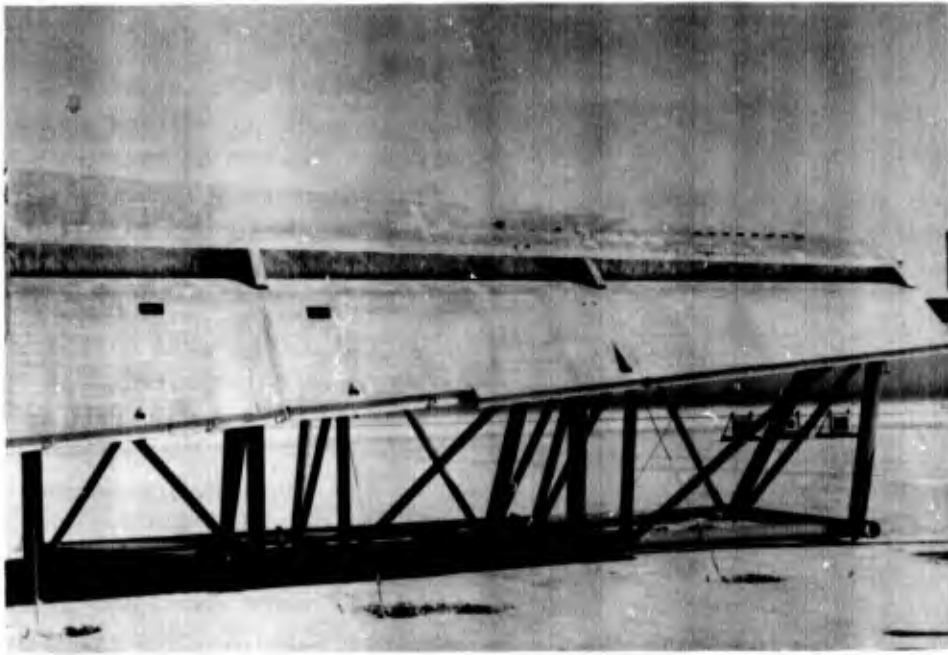
Fig. D.48 B-36 Stabilizer Assembly, Range 5300 ft (3.2 psi), Shot 10
Showing Over-all View of Elevator Skin Buckling
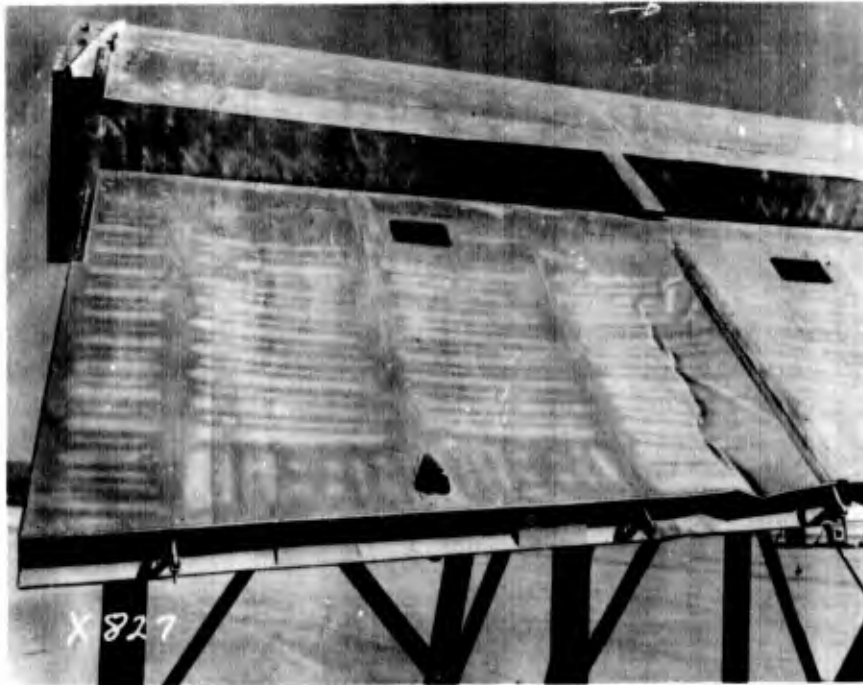
Fig. D.49 B-36 Stabilizer Assembly, Range 5300 ft (3.2 psi), Shot 10
Showing Elevator Skin Damage, Station 50 to Station 133

242
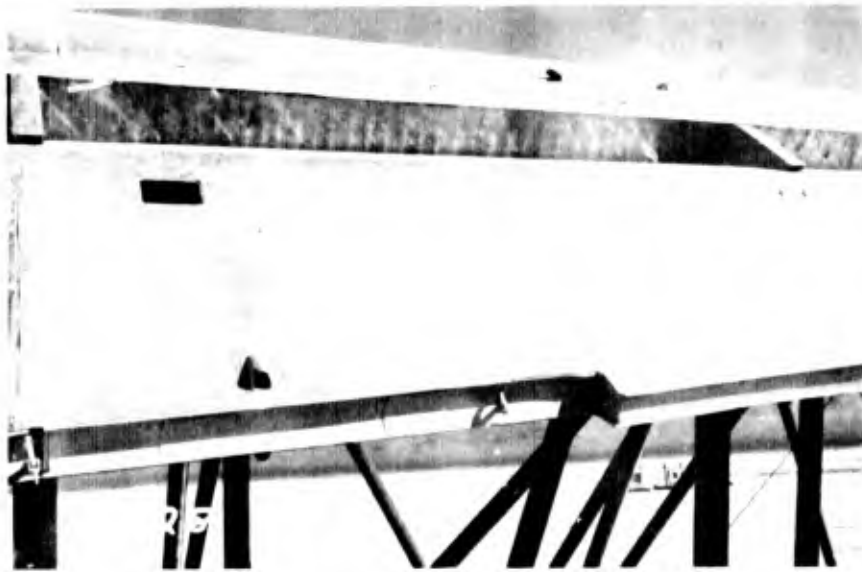
Fig. D.50 B-36 Stabilizer Assembly, Range 5300 ft (3.2 psi), Shot 10,
Showing Elevator Skin Damage, Station 133 to Station 252
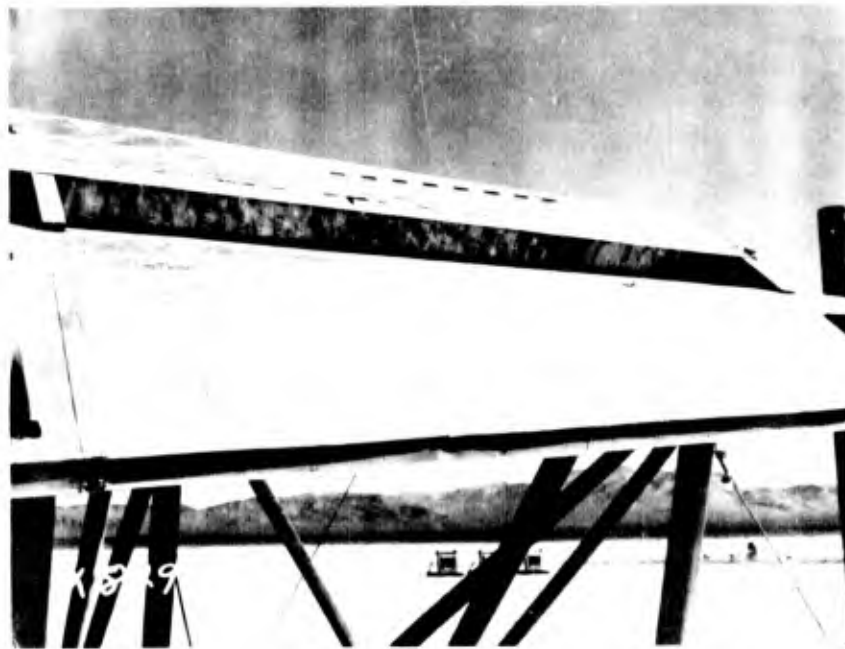
Fig. D.51 B-36 Stabilizer Assembly, Range 5300 ft (3.2 psi), Shot 10,
Showing Elevator Skin Damage, Station 252 to Station 372
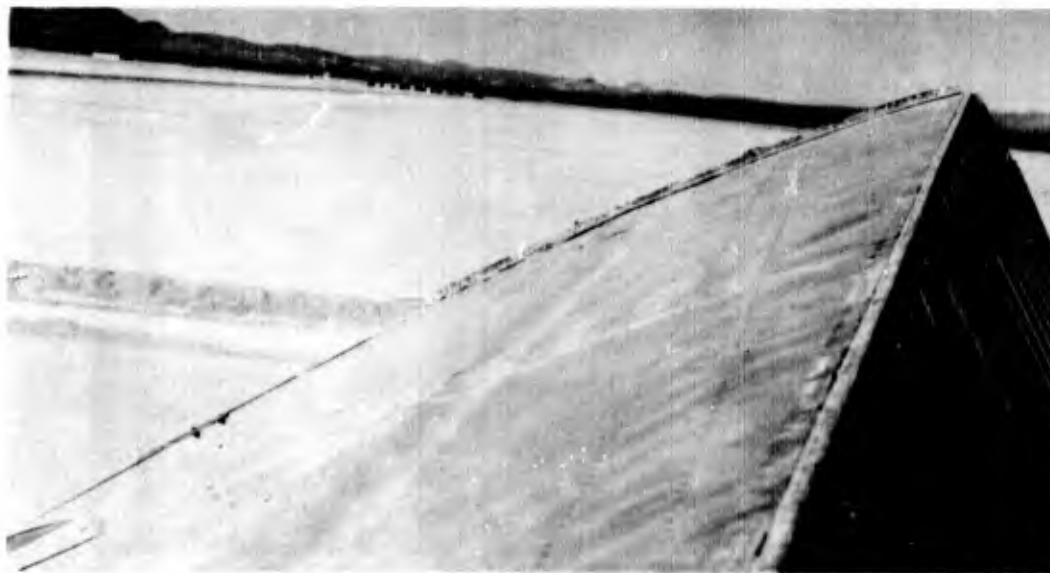
Fig. D.52 B-36 Stabilizer Assembly, Range 5300 ft (3.2 psi), Shot 10,
Showing Typical Skin Buckling on Stabilizer Looking Inboard
Toward Station 50
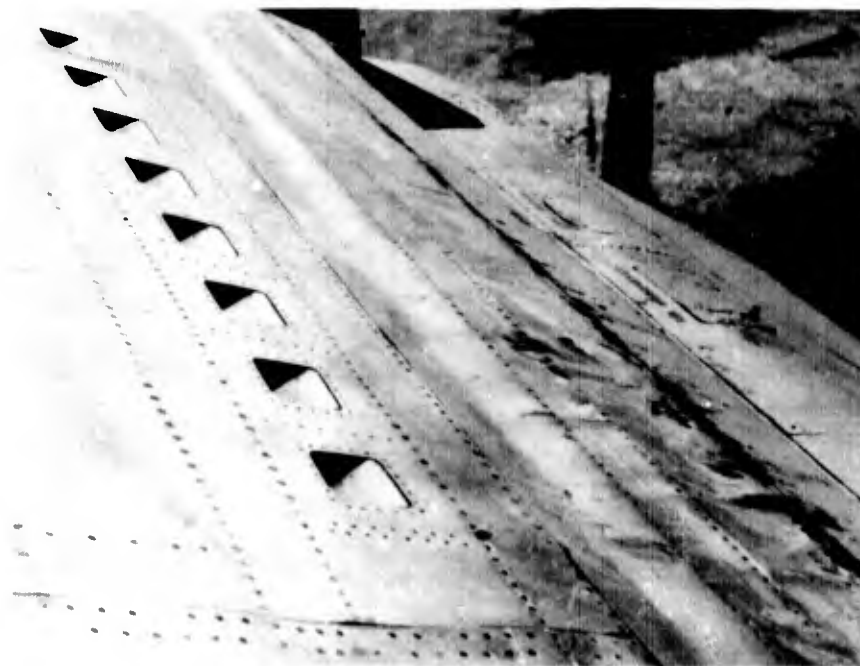
Fig. D.53 B-36 Stabilizer Assembly, Range 5300 ft (3.2 psi), Shot 10,
Showing Typical Skin Buckling on Stabilizer Looking Out-
board Toward Station 372

Fig. D.54 Minimum Values of Peak Temperature Ranges (Temp-tape Data) on B-36 Left Wing Outer Panel, Lower Surface, Range 4800 ft, Shot 9

NOTE: "a" INDICATES TEMP-TAPE DESTROYED

245
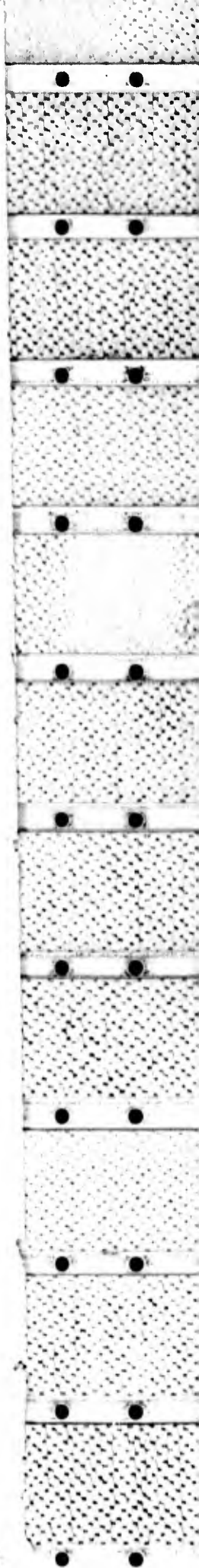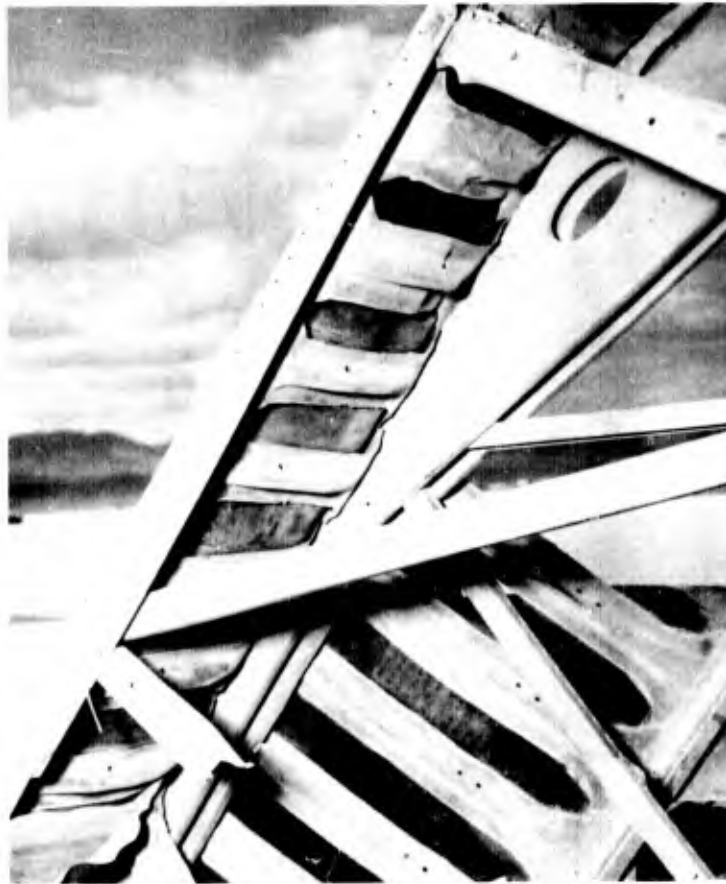
Fig. D.55 B-36 Wing Section, Range 4800 ft (5.7 psi), Shot 9, Close-
up View of Hat Panels Along Inboard End. Note bond failures.

Fig. D.56 B-36 Wing Section Range 4800 ft (5.7 psi), Shot 9, Showing
General Damage

Fig. D.58   B-36 Wing Section Range 4800 ft (5.7 psi), Shot 9, Close-up View of Interior of Wing at Outboard Extremity

Fig. D.57   B-36 Wing Section Range 4800 ft (5.7 psi), Shot 9, Showing General Skin Damage at Outboard Extremity

are the melting points of the various pigments and constitute the mini-mum temperatures of ranges which bracket the peak temperatures as discussed in Appendix A. Except in certain anomalous cases, peak skin temperatures are at least as high as the temperatures given in the figure.

A visual damage assessment of the B-36 wing panel revealed the following:

1. The aileron hinge access door was torn completely off the main structure.

2. The 0.016 in. aluminum waffle panels comprising the aileron hinge access door showed serious thermal and blast damage.

3. Some of the 0.025 in. magnesium hat panels were also torn loose from the structure and showed more serious thermal damage than did the aluminum panels. In some cases, complete separation of the bond occurred, as shown in Fig. D.55.

4. All of the diagonals in the interspar bulkhead trusses, except those of the pod bulkheads at Station 1007.25 and 1020.75, failed by buckling or shearing of rivets or both.

5. The 0.040, 0.051, and 0.064 in. thick interspar skins on the lower surface were dished in and torn. There was no evidence of dish-ing in the thicker skin other than that allowed by the bulkhead failures.

6. A slight buckling occurred in the webbing of the rear and front spars.

Postshot condition of the wing panel is shown in Figs. D.55 to D.59.
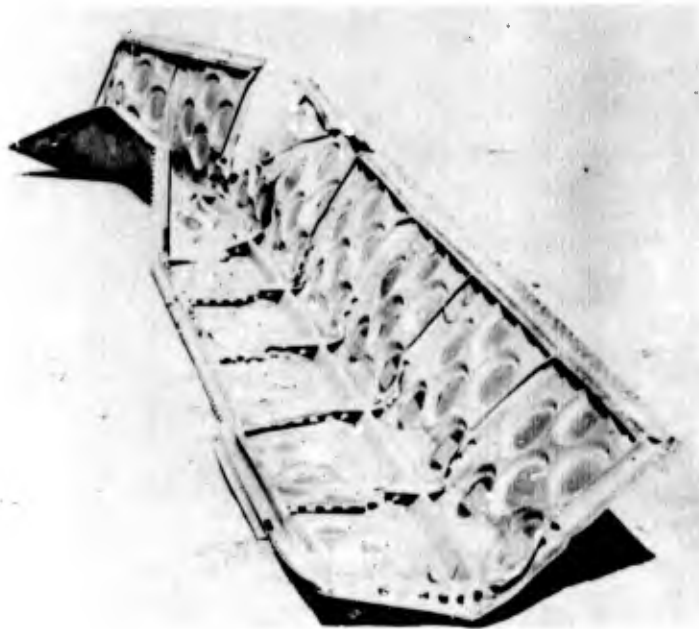
Fig. D.59 B-36 Wing Section, Range 4800 ft (5.7 psi), Shot 9, View of Under Side of Aileron Hinge Access Door

D.2.3   Discussion

The thermal inputs to the stabilizer and elevator assembly, as given in Section D.2.2.1, are based on range only and the incidence angles due to the orientations of the plane of the specimen during Shots 9 and 10 have not been considered. Since the assembly was positioned on the jig with the normal making an angle of 60° with the ground, the incidence angles, especially that for Shot 10, were large and, consequently, were of major import. The incidence angles for Shots 9 and 10 are given in Tables E.3 and E.4 and the corresponding total thermal energies normally incident upon the surface were 0.97 and 8.3 cal/sq cm, respectively. These values apply only to those areas which are parallel to the plane of the main spar and the chord. The angle of 16° 40' formed by the upper and lower plane surfaces of the elevator add a further correction to the incidence angle and must be included in a precise analysis of the damage to the elevator skin panels.

The threshold value for critical overpressure damage to the stabilizer and elevator assembly evidently lies between 1.2 and 2 psi, the values experienced on Shots 9 and 10, respectively.

Although every effort was made to maintain the B-36 wing in a dust-free condition so that values of absorptivity would be known, it is apparent upon studying the temp-tape readings that the intended values of absorptivity were not realized. An analysis of the temp-tape data indicated a general trend of absorptivities toward a mean value of 0.5, because, perhaps, of the presence of dust on the specimen. That is to say, absorptivities less than 0.5 tended to be increased, whereas those greater than 0.5 tended to be dimished.

The internal failure of the bulkheads could place in doubt any conclusions drawn from a correlation of panel damage and overpressure since the panel reaction to the same overpressure in the absence of internal damage cannot be predicted.

D.3   CONTROL SURFACE COVERINGS

It was reported by Project 3.1 of the TUMBLER-SNAPPER operation that one of the most vulnerable components of bomber aircraft, when exposed to nuclear detonations in either a tail-in or side-in orientation, was the fabric covering on the movable control surfaces. The thermal phase was highly destructive, some fabric coverings being burned completely through during the initial second of exposure at inputs of 6 to 7 cal/sq cm. Consequently, any attempt to decrease the over-all vulnerability of the aircraft must include a modification of the control surface coverings to the extent that their thermal resistance would be greatly increased.

D.3.1 Procedure

Test panels of various type control surface coverings were fabricated to simulate the installation of such coverings on aircraft movable control surfaces. All panels consisted of light aluminum channel frames over which the various coverings were stretched and then conditioned by the use of dope and/or enamel. Table D.7 lists the various panels, their composition, conditioning, and code letters. The magnesium sheet and fabric panels were 18 in. square and the aluminum foil panels were 20 in. square.

A typical test rack, devised for supporting the panels, is shown in Fig. D.60. The uprights were supported by 1/8 in. steel

Fig. D.60 Typical Display of Control Surface Covering Panels

guy ropes secured to aircraft mooring stakes. The test panels were fastened to wires, stretched between the uprights, by means of clips at the top and side of each panel.

The thermal input levels at which the panels were displayed were based on the predicted yield and chosen with the expectation that the threshold value for critical damage to each type of panel would be bracketed. Ground ranges used on Shot 9 were 4000, 5500, 7000, and 10,000 ft, with respective predicted thermal inputs of 38, 23, 15, and 7.5 cal/sq cm. The results of the Shot 9 exposure led to the choice of 5500, 6000, 6500, and 7000 ft as ground ranges for Shot 10, with thermal inputs of 12.5, 10.5, 8.8 and 7.5 cal/sq cm, respectively. Tables D.8 and D.9 lists the number and types of panels exposed during Shots 9 and 10.

D.3.2 Results

The complete results of Shots 9 and 10 are presented in Table D.10. The division between critical and non-critical damage was somewhat arbitrarily set as the threshold of deformation to the test panel.

TABLE D.7 - Composition and Conditioning of Control Surface Covering Panels

Code	Cotton Cloth	Orlon Cloth	Clear Dope 2 Brush Coats	Clear Dope Spray Coats 2	Clear Dope Spray Coats 4	Aluminising Dope 6 os/gal 2 Spray Coats	Aluminising Dope 8 os/gal 2 Spray Coats	Aluminising Dope 8 os/gal 4 Spray Coats	White Enamel MIL-E-7729 1 Coat	White Enamel MIL-E-7729 2 Coats	Adhesive MIL-C-4003 Plus 1 Mil Aluminum Foil	Varnish MIL-V-1693 With 20 os Alum/gal
A	X*		X	X		X						
B	X		X	X			X					
C	X		X					X				
D	X		X	X		X						X
E.	X		X	X			X		X			
F	X		X	X		X					X	
G	X		X	X				X	X			
H		X	X	X								
I		X	X	X		X						
J	X		X	X				X		X		
K		X	X	X			X		X			
L		X	X	X				X	X			
N	X		X		X							

M — Vacuumized aluminum cloth with enough clear dope to stretch cloth tight

Hg — 0.020 magnesium sheet with an aluminised finish

Pw — Aluminum foil - weathered for 4 months

ECF — Enamel covered foil

ECFw — Enamel covered foil - weathered for 4 months

* Indicates the material and treatment of the given test panel

TABLE D. 8 - Number and Type of Control Surface Covering Test
Panels Exposed on Shot 9

Type of Panel	Range (ft)			
	4000	5500	7000	10,000
A	2	2	2	2
B	3	3	3	4
C	3	3	3	3
D	2	2	2	2
E	3	3	3	3
F	2	2	2	2
G	3	3	3	3
J	2	2	2	2
L	1	1	1	
Mg	4	4	4	4

TABLE D. 9 - Number and Type of Control Surface Covering Test
Panels Exposed on Shot 10

Type of Panel	Range (ft)			
	5500	6000	6500	7000
A	2	2	2	1
B	2	2	2	2
C	2	2	2	3
D	2	2	2	2
E	2	2	2	3
F	2	2	2	2
G	2	2	2	3
H	1	2	2	1
I	1	2	2	1
J	2	2	2	2
K	1	2	2	1
L		1	1	
M		1	1	
N	1	1	2	1
Mg	4	2	2	3
F_w		1		
ECF	1	2	2	1
ECF_w		1	1	

252

Severe blistering and flaking of the enamel and dope coverings may or may not be critical, depending partially upon the strength of the exposed cloth and the condition of the remaining coats of dope.

The total thermal input data were taken from Tables E. 4 and E. 5. No correction for incidence angle was attempted, because considerable sagging of the panels existed throughout the array; the panels nearest the uprights were normal to a line from the intended burst point, whereas those in the center were more nearly vertical.

Typical damage sustained by the test panels is shown in Fig. D. 61 through Fig. D. 63.

Fig. D. 61 Typical Postshot Condition of Control Surface Covering Test Panel Array

D. 3. 3   Discussion

In general, the fabric panels were much less resistant to thermal radiation than were the magnesium sheet and aluminum foil panels. Although the use of white enamel did tend to increase their resistance, the fabric panels in no case showed superiority to the others.

Curves showing percentage of damage versus thermal inputs for various panels were prepared from the data of Table D. 10 and are presented in Fig. D. 64. For the purpose of clarity, only those portions of some curves are presented where they cross the "critical damage" or "50 per cent destroyed" line. Thermal inputs required for critical damage to each type of panel can be read directly from the curves.

D. 4   AIRCRAFT UNDERCARRIAGE COMPONENTS

Various aircraft undercarriage components including tires,

A   Type ECF 6500 ft Shot 10 0%

B   Type ECF 6000 ft Shot 10 10%

C   Type F 5500 ft Shot 10 20%

D   Type Mg 5500 ft Shot 9 30%

E   Type Mg 4000 ft Shot 9 60%

F   Type G 7000 ft Shot 9 70%

Fig. D.62   Typical Damage to Control Surface Covering Panels Giving
Type of Panel, Range, Shot, and Per Cent Destruction

254
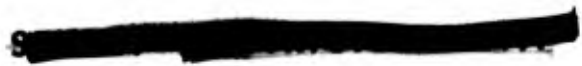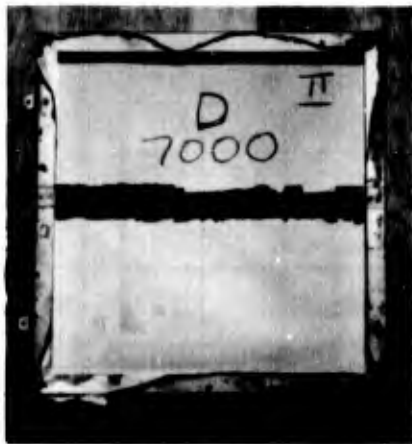
A Type D 7000 ft Shot 10 80%

B Type B 10,000 ft Shot 9 80%

C Type B 7000 ft Shot 10 90%
   (Front)

D Type B 7000 ft Shot 10 90%
   (Rear)

E Type M 6000 ft Shot 10 100%
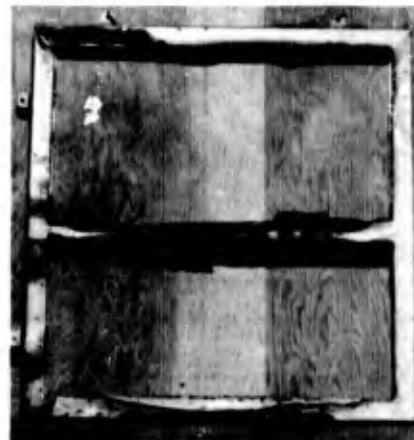
F Unidentified 100%

Fig. D.63   Typical Damage to Control Surface Covering Panels Giving
Type of Panel, Range, Shot, and Per Cent Destruction

255
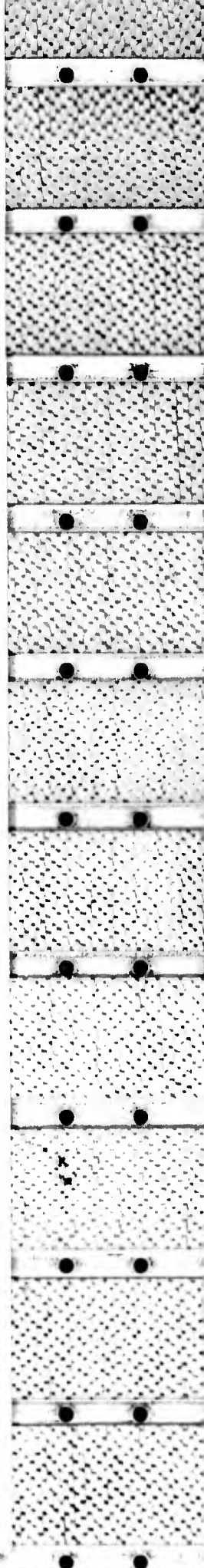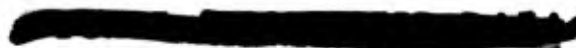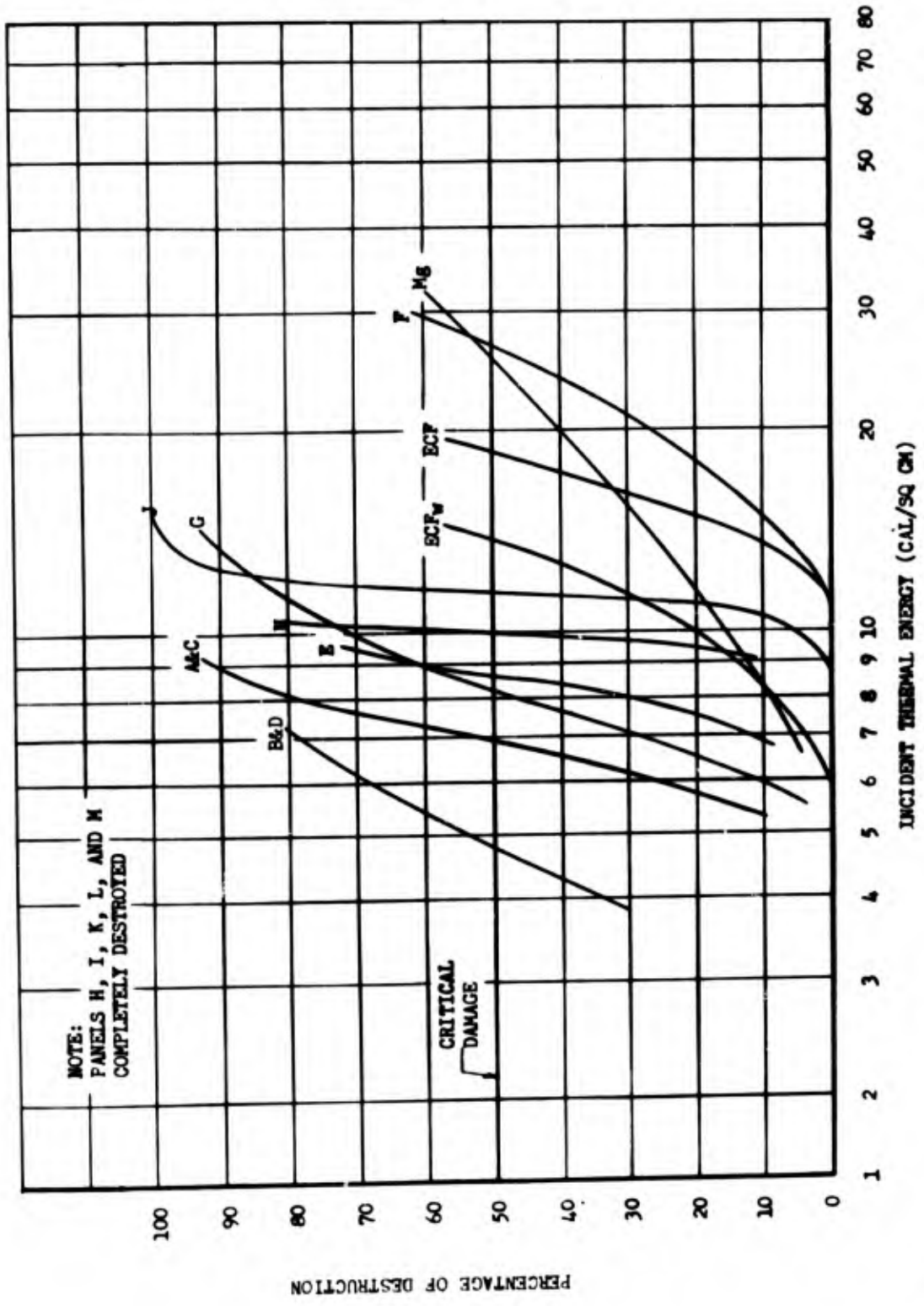
Fig. D. 64 Percentage of Destruction Versus Thermal Input Plotted from Data Contained in Table D.10

256

TABLE D.10 - Percentage of Destruction to Control Surface Coverings

Q-input (cal/sq cm)	Shot No.	Intended Range Ft	Actual Range Ft	Type of Panel																	
				A	B	C	D	E	F	G	H	I	J	K	L	M	N	Mg	Pv	ECP	ECPv
29.0	9	4000	4662	100	100	100	100	100	60	100			100		100			60			
18.8	9	5500	6148	100	100	100	100	100	20	100			100		100			30			
13.3	10	5500	5552	100	100	100	100	80	20	80	100	100	90	100			90	30		10	
13.0	9	7000	7620	80	90	100	100	100	20	70			100		100			30			
11.3	10	6000	6042	90	100	100	100	80	10	80	100	100	0	100	100	100	80	20	20	10	30
9.8	10	6500	6542	100	90	100	100	80	0	80	100	100	0	100	100	100	100	20		0	10
8.4	10	7000	7046	80	80	90	80	10	10	70	100	100	0	100			20	10		0	
6.2	9	10000	10612	20	80	10	70	10	10	0			0					0			

Legend

Critical Damage

100 Completely destroyed

90 Front face and part of rear face burnt out

80 Front face burnt out, rear face undamaged or scorched

70 Part of front face burned out

60 Curled at edges or deformed

Non-critical Damage

40 Severely blistered and flaked

30 Moderately blistered and/or flaked

20 Lightly blistered and/or scorched

10 Scorched

0 No damage

wheels, brakes, and hydraulic equipment were exposed to relatively high thermal inputs during Shot 7. The Mechanical Branch, Aircraft Laboratory (WADC) selected and procured the test articles to be exposed and also determined their deployment

D.4.1 Procedure

The aircraft undercarriage components exposed consisted basically of two types, rubber components and hydraulic components, mounted on 4 ft sq steel panels. A typical rubber components panel consisted of a tire, a wheel, and various related rubber samples, including several segments of disc brake linings. The hydraulic components panels consisted of electromechanical and hydraulic actuators and their related equipment. Photographs of a typical rubber components and hydraulic components panel are shown in Fig. D.65 and D.66, respectively. The accumulators on the hydraulic panels were pre-charged with air to 1000 psi and then with hydraulic fluid to approximately 3000 psi. The test panels were mounted normal to the line of direct thermal radiation, anchored with rods driven in the ground, and supported by a backfill of earth, as shown in Fig. D.67.

In order to determine effective exposure levels for the undercarriage components, three test samples were set out on Shot 5 in the T-2 area, covering a wide range of thermal inputs. The test samples were 1 in. by 4 in. strips of rubber tread stock, 1/4 in. thick, bolted to steel plates. The plates were welded to a tripod-like mount which was driven in the ground about 2 ft, as shown in Fig. D.68. The test samples were placed at ground ranges of 1180, 1650, and 2320 ft, corresponding to the respective unattenuated thermal inputs of 800, 400, and 200 cal/sq cm based on the predicted yield. The two samples closest to ground zero could not be located after the test and the back plate of the one that was recovered had been bent in the center. The tread rubber showed evidence of considerable sand blasting, and the heat had so overcured the rubber that it had taken the shape of the bent backing plate. Because of a lower-than-predicted yield the unattenuated thermal input at this range was only about 160 cal/sq cm; however, this figure should be somewhat smaller because of dust attenuation.

On the basis of the data obtained from the single test sample, one each rubber components panel and hydraulic components, panel were positioned at ranges of 1920, 2800, 3460, and 5000 ft during Shot 7, where the unattenuated thermal inputs were calculated to be 300, 150, 100, and 50 cal/sq cm, respectively. All panels were located on a line extended outward from ground zero at an azimuth of 100°.

Two temp-tapes were installed on the unexposed side of each of the test panels in order to record the peak temperature sustained by the 3/32 in. sheet steel to which the components were affixed.
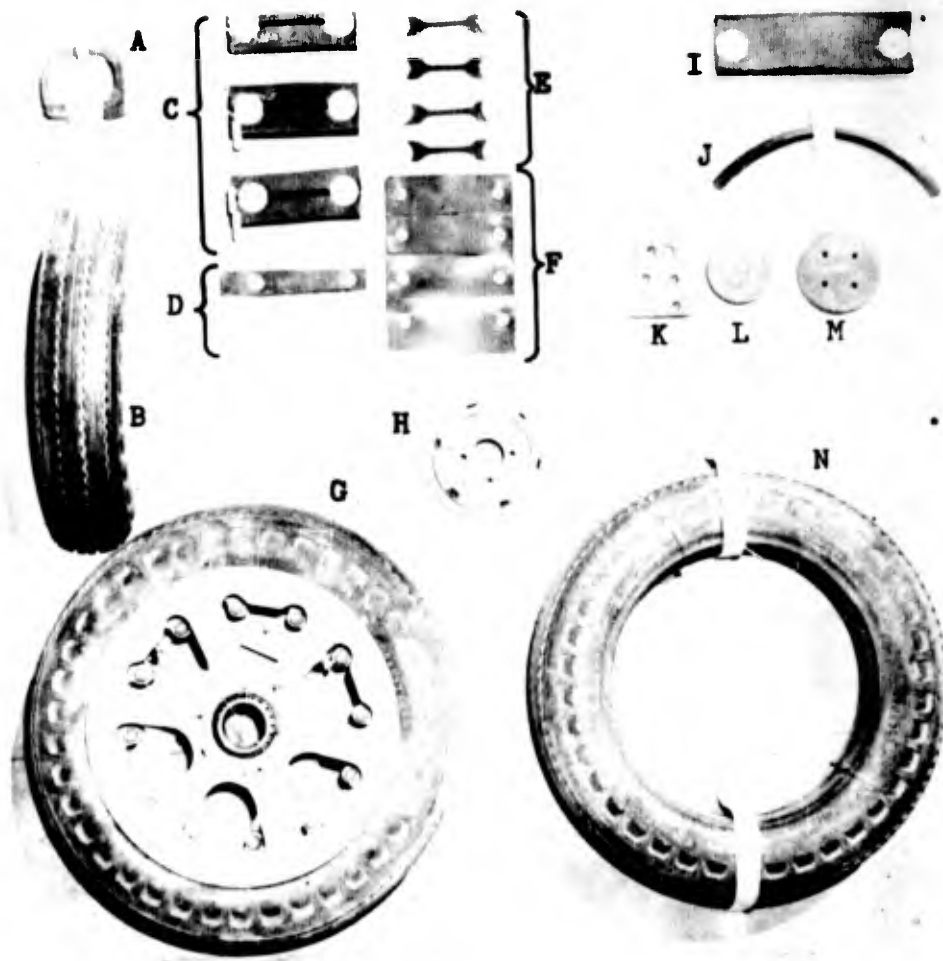
A, B   - Section cf 20 x 4.4 Type VII Casing
C   - Low Temperature Carcass Test Specimens
D, E, F - Test Samples - Representative Tread Stocks
G   - Mounted and Inflated 20 x 4.4 Tire and Wheel Assembly
H   - Small Expander Tube Brake Assembly
I   - Section of Brake Expander Tube
J   - Disc Type Brake Hydraulic Seal
K, L, M - Segments of Disc Brake Linings
N   - 20 x 4.4 10 P.R. Casing

In addition to the above an assortment of experimental
hydraulic "O" rings was displayed on Panel #2 Range
2800 ft.

Fig. D.65 Typical Array of Rubber Components Specimens

259
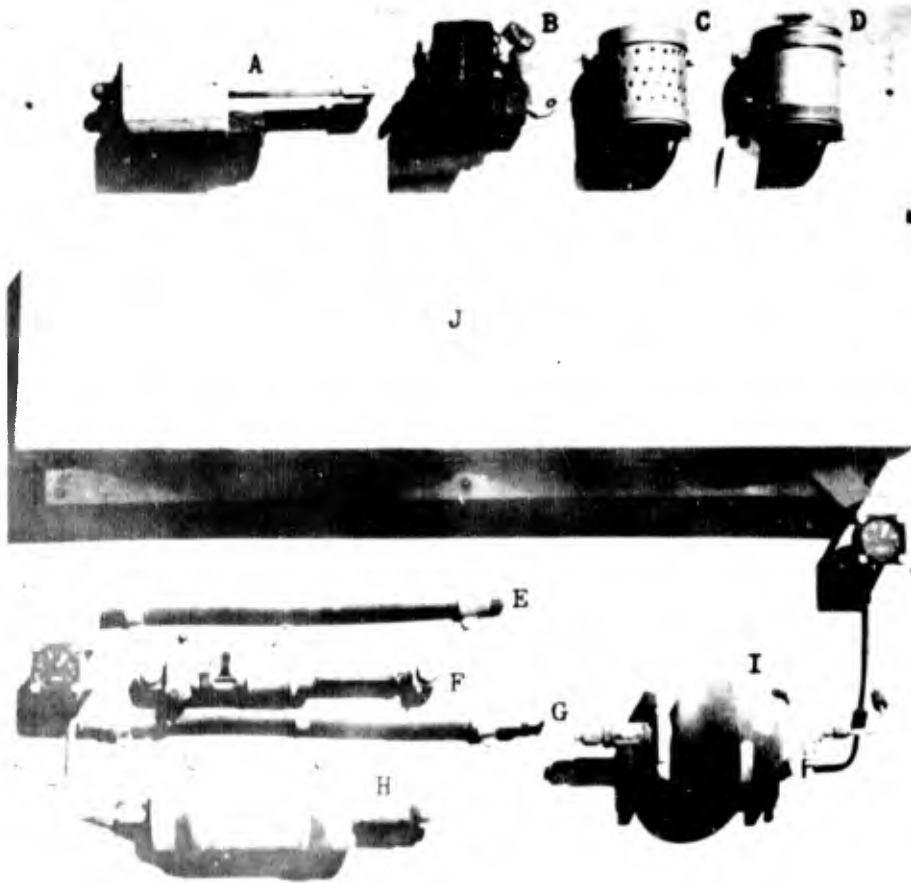
A – Electromechanical Linear Actuator*
B – Electromechanical Rotary Actuator**
C – Can of Packings (dry)
D – Can of Packings (submerged in hydraulic fluid)
E – Medium Pressure Hydraulic Hose
F – Hydraulic Actuator
G – High Pressure Hydraulic Hose
H – Cylindrical Accumulator
I – Spherical Accumulator
J – Hose Samples Similar to Items E and G (Shielded
    by aluminum cover)

  * This item was displayed on Panel #1 Range 1920 ft
    and Panel #2 Range 2800 ft only
 ** This item was displayed on Panel #1 Range 1920 ft
    only

Fig. D.66 Typical Array of Hydraulic Components Specimens
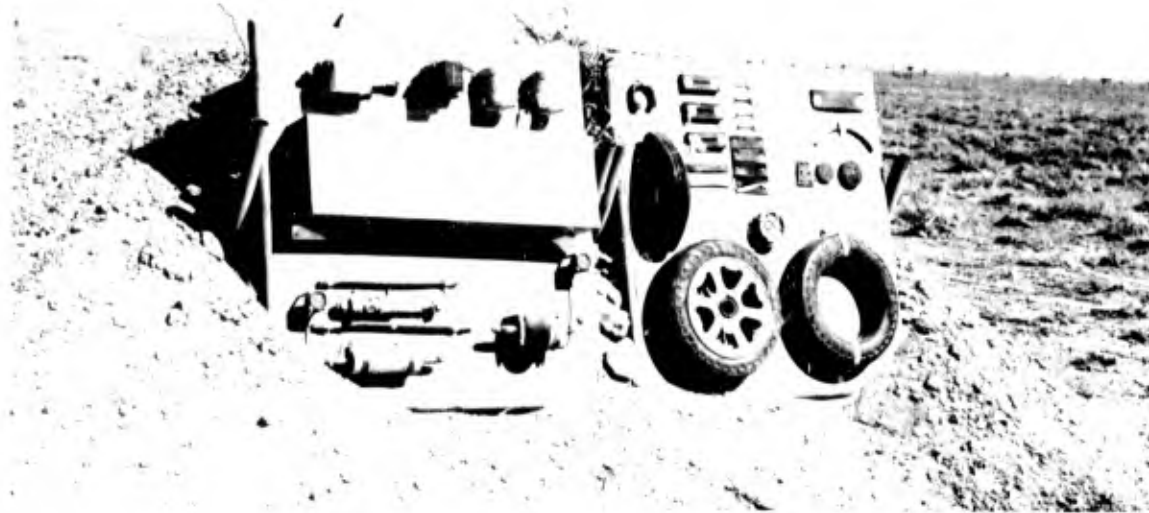
Fig. D.67 Typical Arrangement of Aircraft Undercarriage Component
Panels Prior to Shot 7

Fig. D.68 Rubber Probe Sample and Support, Prior to Shot 5

D.4.2   Results

The four ranges at which the panels were exposed provided a satisfactory test, since the majority of the foremost specimen were damaged beyond use, whereas the rear specimens were generally serviceable, although noticeably affected.   Typical postshot photographs of the test panels appear in Fig. D.69 and D.70.   On the basis of the reported yield of Shot 7, the theoretical unattenuated thermal inputs for the given exposure ranges were calculated to be 360, 160, 110, and 48 cal/sq cm.   However, in view of probable dust attenuation, more realistic values of the thermal inputs experienced by the specimens were calculated from the peak temperature data and are presented in para. D.4.3 where a discussion of the thermal inputs is presented.

Detailed damage regarding the serviceability of most of the rubber specimens cannot be presented in this report because laboratory tests to determine the depth of deterioration have not been concluded at this writing.   However, a visual damage analysis of the rubber components panels conducted at the test site revealed the following:

1.   Panel No. 1, Range 1920 ft

This panel showed considerable evidence of damage from flying stones or other objects.   The tire casing and the casing sector as well as two low temperature strips were missing from the board and were not recovered.   The pressure in the mounted tire had dropped from 95 to 65 psi.   All of the rubber test strips were recovered, and appeared to be no longer serviceable.   The surfaces of the thicker specimens appeared badly deteriorated.

2.   Panel No. 2, Range 2800 ft

This panel exhibited only minor physical damage.   The unmounted complete casing was missing from the panel.   The pressure in the mounted casing had dropped from 100 to 55 psi.   All rubber samples were recovered and exhibited only minor physical damage from sand blasting although considerable thermal damage was still in evidence. All of the silicone and synthetic hydraulic "O" rings, which were exposed on this panel only, were recovered for laboratory tests.

3.   Panel No. 3, 3460 ft

This panel appeared unaffected by the blast but again the thermal effect was quite apparent.   The effects of sand blasting was more noticeable than on Panel No. 2.   The casing sector was missing from the panel.   All rubber samples were recovered for analysis.

4.   Panel No. 4, 5000 ft

This panel was in good condition with only minor evidence of sand blasting.   All items were in place and recovered for analysis.   Of particular interest was the fact that the 15 per cent stretch samples exhibited near-normal retraction upon release.   Retraction of the stretch samples was not noticeable on the more forward panels.

262
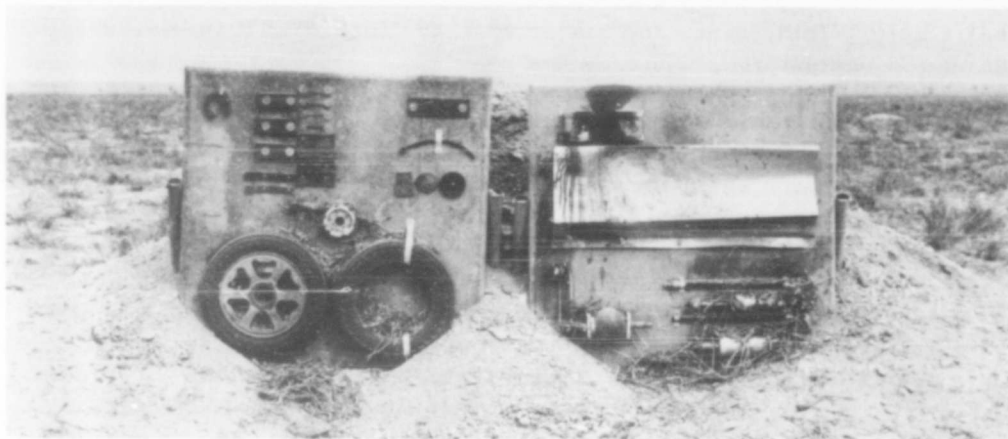
Fig. D. 69   Aircraft Undercarriage Component Panels, Range 3460 ft, Shot 7
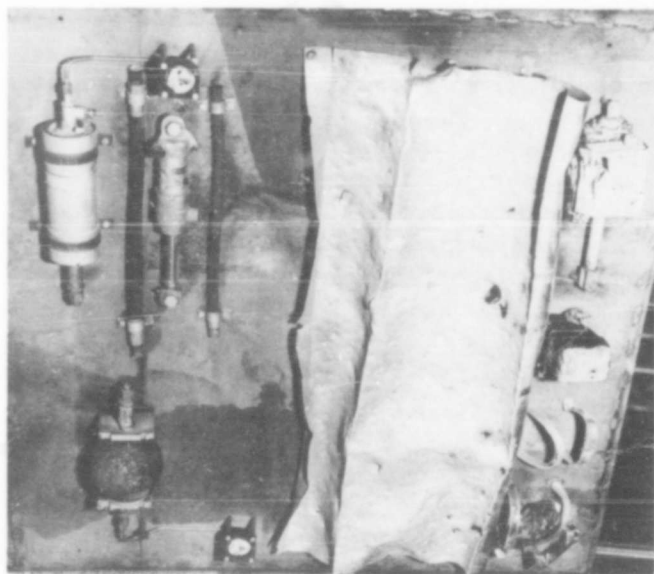
Fig. D. 70   Close-up of Hydraulic Components Panel, Range 1920 ft, Shot 7

263

All specimens exposed on the hydraulic components panels have been subjected to either laboratory tests or inspections and the results thereof are more reasonably presented according to article rather than range. The final results regarding the hydraulic specimens are:

1. Electromechanical Linear Actuator, Item A of Fig. D.66

The electromechanical linear actuator at Range 1920 ft was not serviceable. The screwjack was bent and the limit switch box suffered critical damage, viz., defective wiring, deformed and punctured case, and bent brackets. The motor and gearing performed satisfactorily during laboratory tests. The actuator at Range 2800 ft was found to be serviceable although the limit switch box was again bent and the paint showed evidence of considerable sand blasting.

2. Electromechanical Rotary Actuator, Item B of Fig. D.66

The electromechanical rotary actuator was serviceable although visibly affected. The paint on the limit switch box was badly chipped and the box was deformed and punctured. Nothing inside the limit switch box was damaged.

3. Hydraulic Packings, Item C and D of Fig. D.66

All of the packings from Panel No. 1 were lost; the can of dry packing was blown open and the entire can of submerged packings was missing. All other specimens, both dry and submerged, were recovered and were proven completely serviceable by laboratory tests.

4. Medium and High Pressure Hydraulic Hose, Items E and G of Fig. D.66

All specimens were recovered and found to be satisfactory. No difference was apparent between the exposed specimens and those shielded by the aluminum cover.

5. Hydraulic Actuator, Item F of Fig. D.66

Laboratory inspections and tests showed that the hydraulic actuators from the forward three panels were not serviceable. The piston rods were either bent or so badly pitted that the seals could no longer hold the pressure. The actuator at the most remote range was serviceable.

6. Cylindrical and Spherical Accumulators, Items H and I of Fig. D.66

All of the accumulators were found to be serviceable under laboratory inspections; however, a failure occurred in every case in that no pressure remained in the accumulators because of broken hydraulic lines or faulty check valves. A visual inspection at the test site revealed that all of the accumulator gages at the forward three ranges were badly damaged and unreadable; the fourth set of gages showed some pressure remaining in the accumulators but even this had been relieved by the time the laboratory inspection was conducted.

D.4.3 Discussion

Since the primary objective of this test was to determine the effect of thermal radiation on aircraft undercarriage components, the knowledge of the precise values of the thermal inputs at each range would be highly desirable; however, because of the dust which is raised up during the thermal phase, it is exceedingly difficult to calculate accurate values of the incident thermal energy. Certain minimum limits may be placed on the total thermal energy incident on each set of panels from analysis of the peak temperatures attained by the steel panels themselves. The peak temperature data are not entirely re-liable in that some variation occurred among the readings of the four temp-tapes at each range; however, probable peak temperatures for each range were obtained by plotting and averaging the maximum and minimum values indicated by the temp-tapes and are presented in Table D.11. The incident thermal energy may be calculated from the

TABLE D.11 - Input Data for Undercarriage Components Test Panels

Range (ft)	Peak Max. ($^\circ$F)	Temp. Min. ($^\circ$F)	Probable Temp. Change* ($^\circ$F)	Theoretical Unattenuated Thermal Energy (cal/sq cm)	Peak Over-pressure (psi)
1920	252	232	196	360	27
2800	252	232	180	160	13
3460	194	171	136	110	9.4
4000	170	144	96	48	5.0

* Assumed Ambient Temperature = 54°F

formula

$$Q = 0.17 \, \Delta T \qquad\qquad D.1$$

where Q is the incident thermal energy (cal/sq cm) and ΔT is the tem-perature rise ($^\circ$F). The value 0.17 was determined by the type (steel), thickness (0.94 in.), and assumed absorptivity (0.7) of the material used in the construction of the panels. Assuming the ΔT values given in Table D.11 the incident thermal energies received by the panels, as calculated from formula D.1, would be 33.3, 30.6, 23.1, and 16.3 cal/sq cm for the ranges of 1920, 2800, 3460, and 4000 ft respectively.

265

It is possible however, that the specimens were actually subjected to even higher inputs than these, for the panels were backfilled with earth, offering the possibility of a heat sink and a reduction in the peak temperature otherwise attainable. Likewise, dust accumulation on the surface of the panels may have lowered the absorptivity (see para. D. 2. 3) resulting in an increase in the thermal energy required to produce the measured temperature rises. However, even allowing for these indeterminant factors, it is apparent upon a comparison of the calculated values to the theoretical values of thermal inputs that relatively high attenuation factors were encountered due to dust and to the burning and smoking of ground litter as well as the undercarriage components themselves. It is also possible, however, that the specimens were subjected to higher inputs than those calculated from the temp-tape data. The fact that the panels were backfilled with earth offered the possibility of a heat sink which would reduce the peak temperature sustained by the panels and thus the actual thermal energy would be greater than that calculated from formula D. 1. Likewise, dust accumulation on the surface of the panels may have lowered the absorptivity (see para D. 2. 3) resulting in an increase in the thermal energy required to produce the measured temperature rise. In view of these conditions and the possibility of others, the calculated total thermal energies incident upon the specimens at the various ranges are presented as minimum values in Table D. 11.

APPENDIX E

INPUT MEASUREMENTS

E.1 GENERAL

Because of the nature of the program of Project 8.1 during Shots 9 and 10, input measurements of overpressure and thermal energy were desired on the same time base as the response measurements. In addition, these input measurements were desired at various ranges during Shots 3, 5, 6, and 7; however, no oscillographic instrumentation was available and it was necessary to rely upon calculated inputs or if available, data which could be procured from other organizations. The term "input" as used herein shall be taken to mean the peak-value or time-history measurement of blast overpressure (lb/sq in.), total thermal energy (cal/sq cm), or gamma radiation dosage (Roentgens) effects of a nuclear explosion at a given range.

E.2 PROCEDURE

Time-history input measurements of blast overpressure and incident thermal energy were made at each of the four Project 8.1 instrumentation stations during both Shots 9 and 10. Thermal energy measurements were also made behind the glass in each of stabilizer blast shields, and gamma radiation dosage measurements were taken both outside and inside the instrumentation shelter during each shot. The deployment of each of the input measuring devices for Shot 9 and Shot 10 is shown in Fig. E.1 and E.2, respectively.

An installation number was assigned to each channel of oscillographic information obtained and also to each "cigarette case" dosimeter. A list of the installations pertinent to this section, including the location and description of the quantity measured is given in Tables E.1 and E.2.
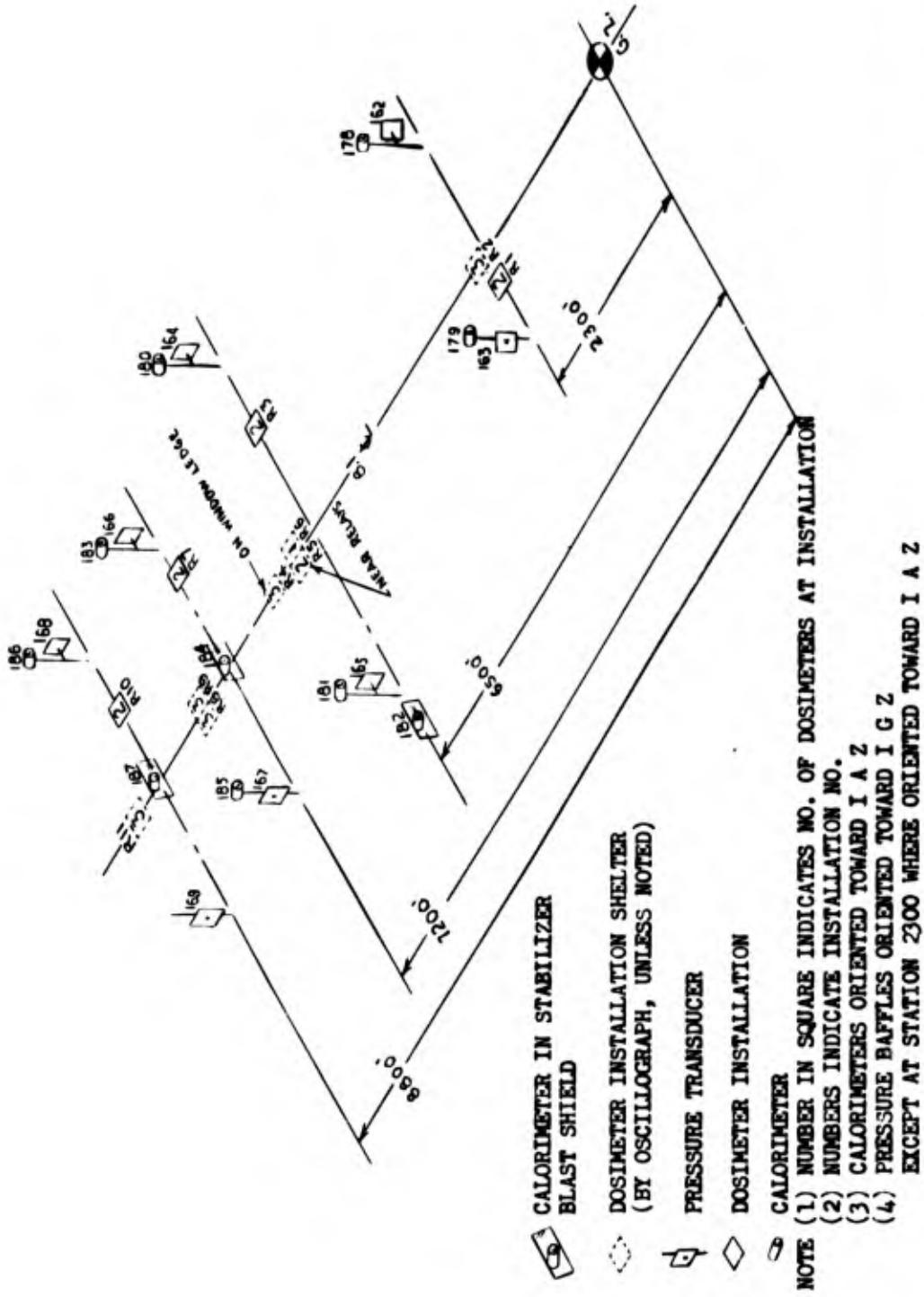
Fig. E.1 Deployment of Pressure Transducers, Calorimeters, and Dosimeters for Shot 9

CALORIMETER IN STABILIZER
BLAST SHIELD

DOSIMETER INSTALLATION SHELTER
(BY OSCILLOGRAPH, UNLESS NOTED)

PRESSURE TRANSDUCER

DOSIMETER INSTALLATION

CALORIMETER

NOTE (1) NUMBER IN SQUARE INDICATES NO. OF DOSIMETERS AT INSTALLATION
(2) NUMBERS INDICATE INSTALLATION NO.
(3) CALORIMETERS ORIENTED TOWARD I A Z
(4) PRESSURE BAFFLES ORIENTED TOWARD I G Z
EXCEPT AT STATION 2300 WHERE ORIENTED TOWARD I A Z

Fig. E.2 Deployment of Pressure Transducers, Calorimeters, and Dosimeters for Shot 10

DOSIMETER IN STABILIZER
BLAST SHIELD

DOSIMETER INSTALLATION SHELTER
(BY OSCILLOGRAPH, UNLESS NOTED)

PRESSURE TRANSDUCER

DOSIMETER INSTALLATION

CALORIMETER

NOTE (1) NUMBERS IN SQUARE INDICATES NO. OF DOSIMETERS AT INSTALLATION
(2) NUMBERS INDICATE INSTALLATION NO.
(3) CALORIMETERS ORIENTED TOWARD I A Z
(4) PRESSURE BAFFLES ORIENTED TOWARD I G Z

TABLE E. 1 - Index to Oscillographic Instrumentation Installation
Numbers

Inst. No.	Quantity	Station	Shot No.	Figure Reference
162	Overpressure	2300	9	
163	Overpressure	2300	9	E. 5
164	Overpressure	6500	9	
165	Overpressure	6500	9	E. 6
166	Overpressure	7200	9	
167	Overpressure	7200	9	E. 6
168	Overpressure	8800	9	
169	Overpressure	8800	9	E. 6
170	Overpressure	2300	10	
171	Overpressure	2300	10	E. 7
172	Overpressure	6500	10	
173	Overpressure	6500	10	E. 8
174	Overpressure	7200	10	
175	Overpressure	7200	10	E. 8
176	Overpressure	8800	10	E. 8
177	Overpressure	8800	10	
178	Total Thermal Energy	2300	9	E. 11
179	Total Thermal Energy	2300	9	E. 11
180	Total Thermal Energy	6500	9	E. 11
181	Total Thermal Energy	6500	9	E. 11
182	Total Thermal Energy (Inside Blast Shield)	6500	9	
183	Total Thermal Energy	7200	9	E. 11
184	Total Thermal Energy (Inside Blast Shield)	7200	9	
185	Total Thermal Energy	7200	9	E. 11
186	Total Thermal Energy	8800	9	E. 11
187	Total Thermal Energy (Inside Blast Shield)	8800	9	
188	Total Thermal Energy	2300	10	E. 12
189	Total Thermal Energy	2300	10	E. 12
190	Total Thermal Energy	6500	10	E. 12
191	Total Thermal Energy	6500	10	E. 12
192	Total Thermal Energy (Inside Blast Shield)	6500	10	
193	Total Thermal Energy	7200	10	E. 12
194	Total Thermal Energy	7200	10	E. 12
195	Total Thermal Energy	8800	10	E. 12
196	Total Thermal Energy	8800	10	E. 12

TABLE E.2 - Index to Installation Numbers for "Cigarette Case"
Dosimeters

Inst. No.	Station	Shot No.	Location
R1	2300	9	Outside
R2	2300	9	Inside, by Oscill. No. 1
R3	6500	9	Outside
R4	6500	9	Inside, by Oscill. No. 2
R5	6500	9	Inside, by Oscill. No. 3
R6	6500	9	Inside, by Window
R7	7200	9	Outside
R8	7200	9	Inside, by Oscill. No. 4
R9	7200	9	Inside, by Oscill. No. 5
R10	8800	9	Outside
R11	8800	9	Inside, by Oscill. No. 6
R12	2300	10	Outside
R13	2300	10	Inside, by Oscill. No. 1 (Nearest to GZ)
R14	2300	10	Inside, by Oscill. No. 7 (Greatest distance from GZ)
R15	2300	10	In Entrance to Shelter
R16	6500	10	Outside
R17	6500	10	Inside, by Oscill. No. 3
R18	6500	10	Inside by Oscill. No. 5
R19	7200	10	Outside
R20	7200	10	Inside, by Oscill. No. 4
R21	8800	10	Outside
R22	8800	10	Inside, by Oscill. No. 6

E.2.1 Blast Overpressure

Two different transducer types, one a Statham, Model P-6
orifice type, and the other a Consolidated Engineering Corporation
(CEC), Model 4-310 diaphragm type, were used at each of the four
Project 8.1 instrument stations during Shots 9 and 10, except at Station
8800 during Shot 10 where two Statham transducers were employed.
Details of the pressure transducers and their calibration is given in
Appendix A.

The pressure transducers were mounted 4 ft above the ground
in the center of square aluminum baffles, which were oriented edge-on
toward intended ground zero except at Station 2300, Shot 9 where they

271

were oriented edge-on toward intended air zero because it was not expected that the mach stem would form at this close range. A photograph of this arrangement is shown in Fig. E.3.

E.2.2 Total Thermal Energy

Total thermal energy measurements were made using two NRDL disc type calorimeters at each of the four Project 8.1 instrumentation stations during Shots 9 and 10, except at Station 8800 during Shot 9 where only one was used. In addition to this, one calorimeter was placed inside the stabilizer at Station 6500, 7200, and 8800 during Shot 9 and at Station 6500 during Shot 10 in order to measure the total thermal energy received by the stabilizers shielded from the blast, and to determine the transmission characteristics of the "Herculite" plate glass. The calorimeters were mounted 5 ft above the ground on the same pipe used for mounting the pressure transducers as shown in Fig. E.3. The calorimeters were oriented toward intended air zero. Details of the NRDL calorimeter are given in Appendix A.

Fig. E.3 Typical Pressure Transducer, Calorimeter, and Dosimeter Installation

E.2.3 Gamma Radiation Dosage

Gamma radiation dosage measurements were made using "cigarette case" dosimeters, supplied by the Signal Corp Engineering Laboratories (SCEL). A sketch of the "cigarette case" dosimeter is shown in Fig. E.4. The dosimeters were positioned both outside and inside of each of the four Project 8.1 instrumentation shelters during both Shots 9 and 10 in order to determine the dosage received by the oscillograph magazine and the amount of attenuation of gamma radiation afforded by the instrument shelter. Two dosimeters were located outside the shelter and three for each oscillograph inside the shelter for each station and each shot.

272

Fig. E. 4 "Cigarette Case" Dosimeter

Labels in figure: BAKELITE, FILM BADGE, LEAD CONTAINER, LEAD STRIP, PLASTIC CIGARETTE CASE
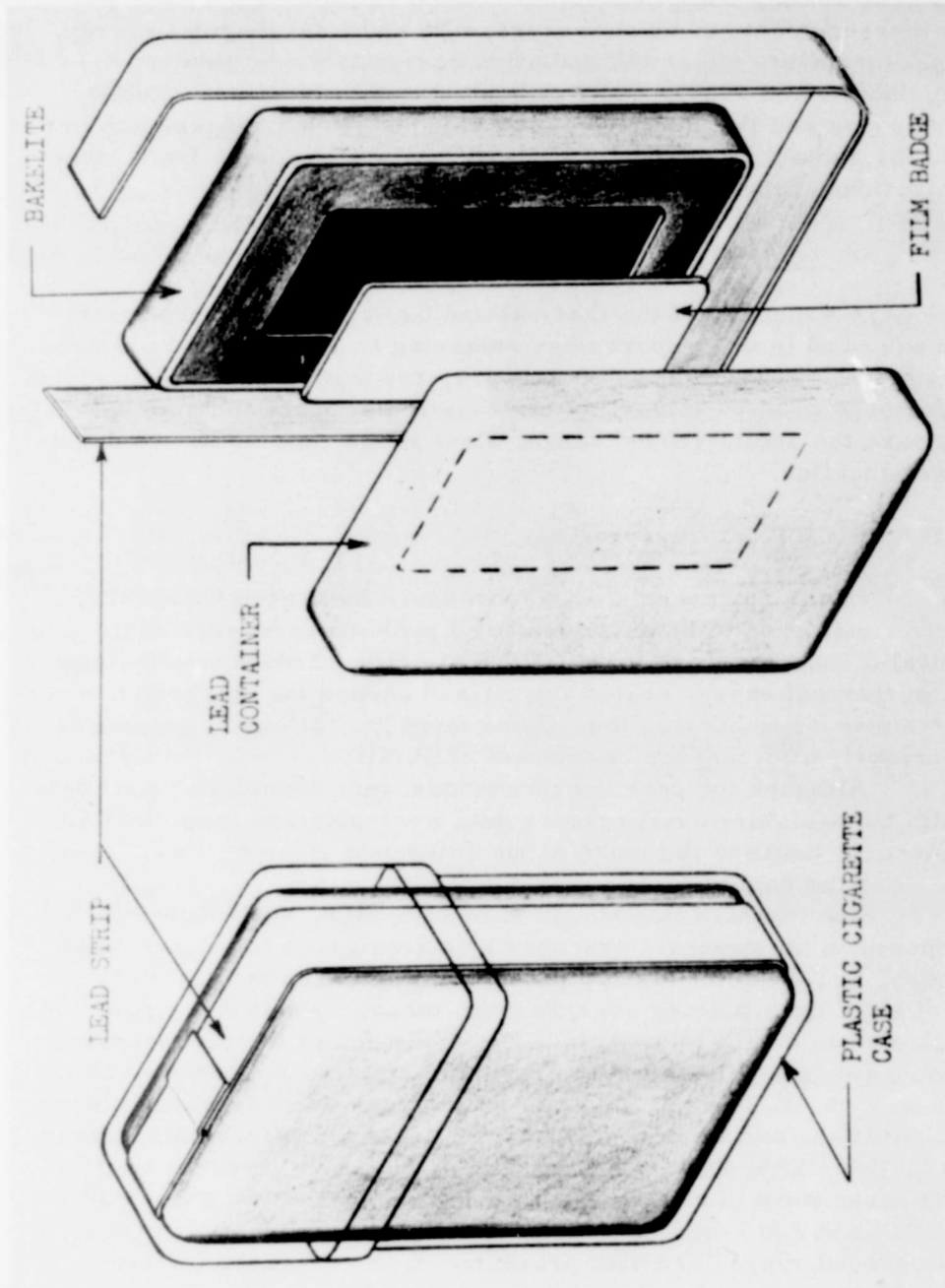
E.3   RESULTS

The results compiled herein consist of time-history and peak value measurements of blast overpressure and total thermal energy, and measurements of gamma radiation dosage taken by Project 8.1 during Shots 9 and 10. In addition, calculated peak values of blast overpressure and thermal energy for various ground ranges, are presented for Shots 3, 5, 6, and 7, unless data are available from other organizations, in which case the latter are presented.

E.3.1   Shots 9 and 10

A summary of the thermal and blast input measurements which are used in this report when referring to any particular station or range is given in Tables E.3 and E.4, respectively, for Shots 9 and 10. Included in these tables, in addition to the inputs and nominal range, are the actual ground range, slant range, and incidence angle for each location.

E.3.1.1   Blast Overpressure

Of the 16 channels of overpressure measurements made, 14 were considered to have yielded valid peak overpressure data. The two invalid channels were installations at Station 2300 where the high value of thermal energy heated the air and caused the diaphragm of the CEC transducer to buckle, thus giving false indications of pressures and seriously affecting the instrument calibration.

Although the peak overpressures were considered good data, no valid time-history overpressure data were obtained from the CEC transducers, because the leaks to the reference sides of the differential gages were too rapid.

The Statham transducer at Station 8800, Shot 10 (Inst. 177) was opened to atmospheric pressure by a small hole for experimental purposes, and the time-history portion of this curve is invalid. A total of eight time-history overpressure measurements were good, one at each station during both shots. A comparison of the overpressure-time data for Shot 9 is shown in Figs. E.5 and E.6 and for Shot 10 is shown in Figs. E.7 and E.8. A list of the peak overpressure, positive phase duration, and time of shock arrival data for each installation is given in Table E.5, from which curves of peak overpressure versus ground range were plotted for Shot 9 and Shot 10 and are presented in Figs. E.9 and E.10, respectively. The blast line data on overpressure versus ground range, are also presented in these figures for comparison.

The point of inflection at about 0.05 sec on the overpressure-

TABLE E.3 - Exposure Sites, Locations and Inputs, Shot 9

INTENDED GROUND RANGE (FT)	TOTAL THERMAL ENERGY (CAL/SQ CM)	PEAK OVERPRESSURE (LBS/SQ IN.)	ACTUAL GROUND RANGE (FT)	ACTUAL SLANT RANGE (FT)	DISTANCE FROM CENTER LINE[a] (FT)	INCIDENCE ANGLE[b] (DEG) VERTICAL SPECIMENS	TILTED SPECIMENS
2300 - STATION	49.5	12.0	2936	3808	0		11.1
4000 - CONTROL SURFACE COVERING PANELS	29.0	7.1	4662	5254	400	28.2	
4800 - B-36 WING PANEL	23.1	5.7	5459	5973	498		5.8
5500 - CONTROL SURFACE COVERING PANELS	18.8	4.8	6148	6608	480	22.1	
6500 - STATION	14.8	3.9	7098	7500	0	19.5	4.9
7000 - CONTROL SURFACE COVERING PANELS	13.0	3.4	7620	7996	300	18.1	
7200 - STATION	12.3	3.4	7796	8163	0	17.8	4.4
7400 - AIRCRAFT PANELS	11.6	3.2	8010	8368	200		4.2
8400 - AIRCRAFT PANELS	8.8	2.6	9005	9325	200		3.8
8800 - STATION	8.0	2.4	9391	9699	0	14.9	3.7(c)
9400 - AIRCRAFT PANELS	7.1	2.1	9990	10280	0		3.5
9700 - AIRCRAFT PANELS	6.6	2.0	10290	10571	0		3.4
10000 - CONTROL SURFACE COVERING PANELS	6.2	1.9	10612	10885	400	13.2	
10800 - AIRCRAFT PANELS	5.3	1.7	11388	11643	0		3.1
13000 - B-36 STABILIZER	3.3	1.2	13585	13800	0		49.9

a LEFT OF PROJECT 8.1 LINE (FACING IGZ)
b ANGLE BETWEEN THE NORMAL TO THE SPECIMEN AND THE LINE OF DIRECT RADIATION
c INCIDENCE ANGLE TO STABILIZER SHIELDED FROM BLAST IS 5.0°

TABLE E.4 - Exposure Sites, Locations and Inputs, Shot 10

INTENDED GROUND RANGE (FT)	TOTAL THERMAL ENERGY (CAL/SQ CM)	PEAK OVERPRESSURE (LBS/SQ IN.)	ACTUAL GROUND RANGE (FT)	ACTUAL SLANT RANGE (FT)	DISTANCE FROM CENTER LINE[a] (FT)	INCIDENCE ANGLE[b] (DEG) VERTICAL SPECIMENS	TILTED SPECIMENS
2300 - STATION	53.7	9.2	2340	2398	0		3.8
3500 - T-28 STABILIZER	29.6	6.2	3552	3591	171		3.5
4000 - AIRCRAFT PANELS	23.8	5.1	4036	4072	0		2.3
4250 - AIRCRAFT PANELS	21.6	4.6	4288	4320	0		2.1
4400 - AIRCRAFT PANELS	20.2	4.4	4438	4469	0		2.0
4800 - AIRCRAFT PANELS	17.2	3.8	4838	4866	0		1.9
5300 - B-36 STABILIZER	14.4	3.2	5350	5376	290		54.5
5450 - AIRCRAFT PANELS	13.6	3.0	5498	5523	285		1.6
5500 - CONTROL SURFACE COVERING PANELS	13.3	2.9	5552	5576	510	5.6	1.6
6000 - CONTROL SURFACE COVERING PANELS	11.3	2.5	6042	6065	200	5.2	1.5
6500 - STATION	9.8	2.2	6537	6558	0	4.8	1.4(c)
6500 - CONTROL SURFACE COVERING PANELS	9.8	2.2	6542	6563	200	4.8	1.4
7000 - CONTROL SURFACE COVERING PANELS	8.4	1.9	7046	7065	400	4.4	1.3
7200 - STATION	7.8	1.8	7237	7256	0		1.3
8800 - STATION	5.1	1.4	8836	8852	0		1.0

a LEFT OF PROJECT 8.1 LINE (FACING IGZ)
b ANGLE BETWEEN THE NORMAL TO THE SPECIMEN AND THE LINE OF DIRECT RADIATION
c INCIDENCE ANGLE TO STABILIZER SHIELDED FROM BLAST IS 13.5°
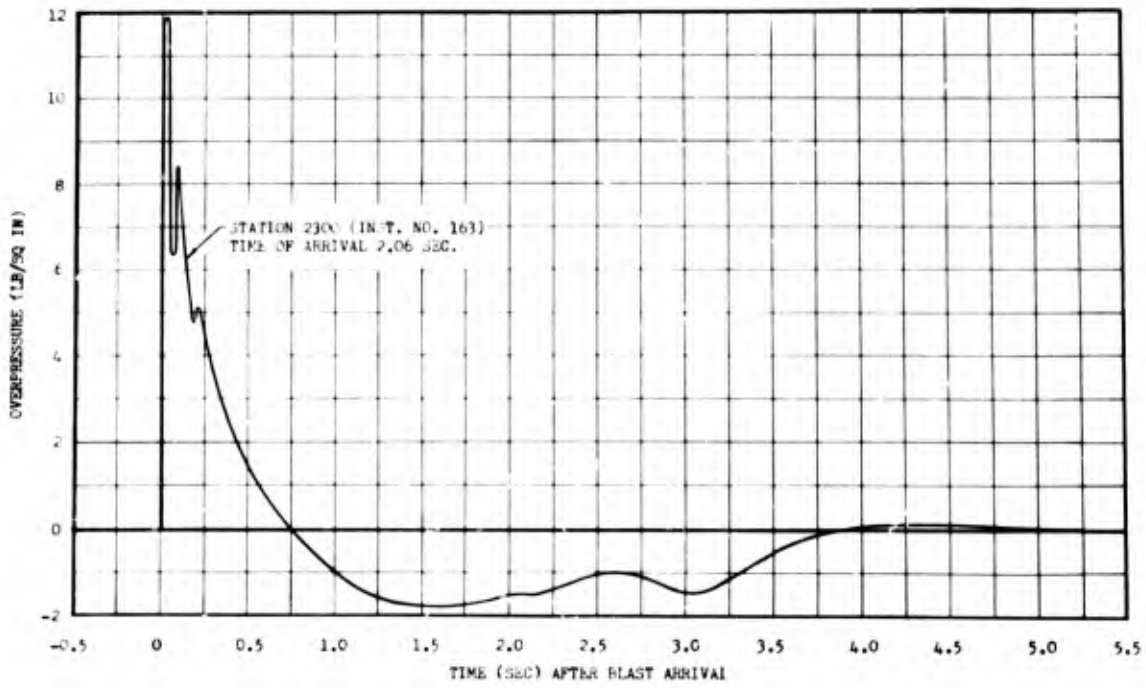
Fig. E.5 Variation of Overpressure with Time at Station 2300, Shot 9
(See Fig. E.6)
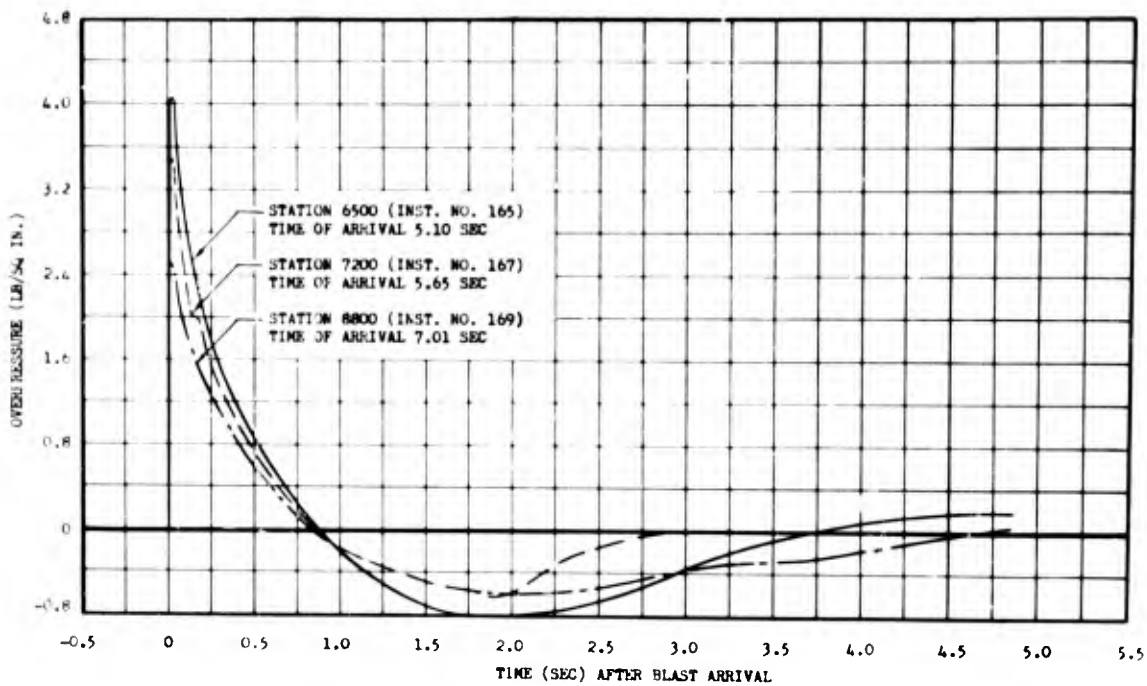
Fig. E.6 Variation of Overpressure with Time for Stations 6500, 7200,
and 8800, Shot 9 (See Fig. E.5)

276
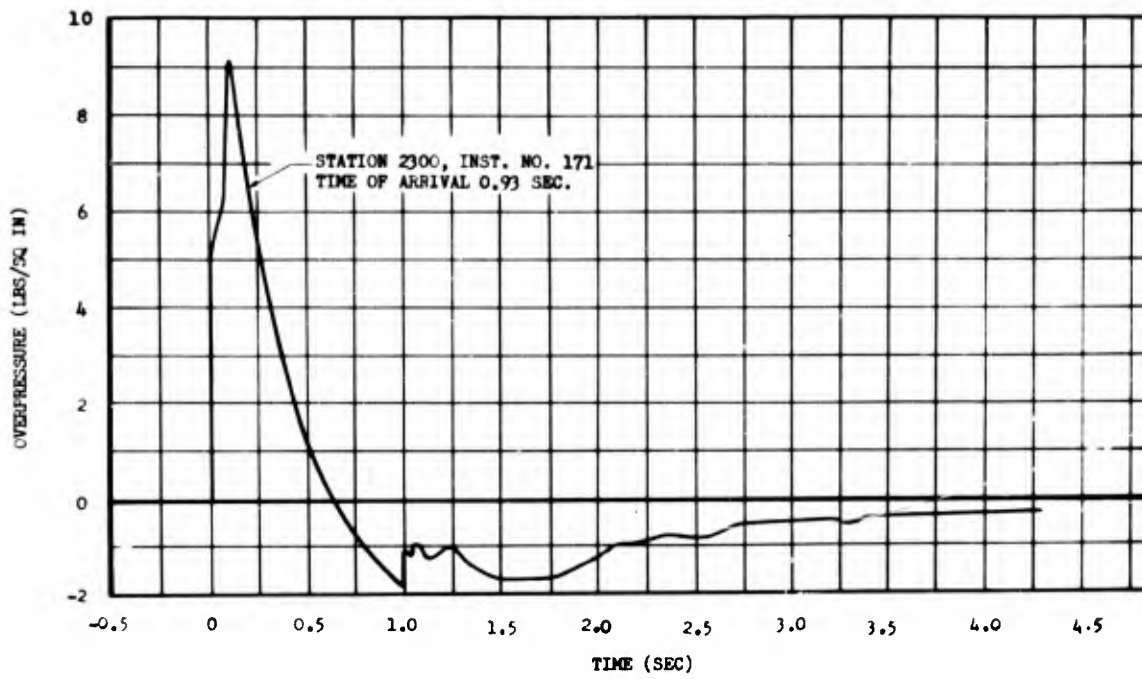
Fig. E.7 Variation of Overpressure with Time for Station 2300, Shot
10 (See Fig. E.8)
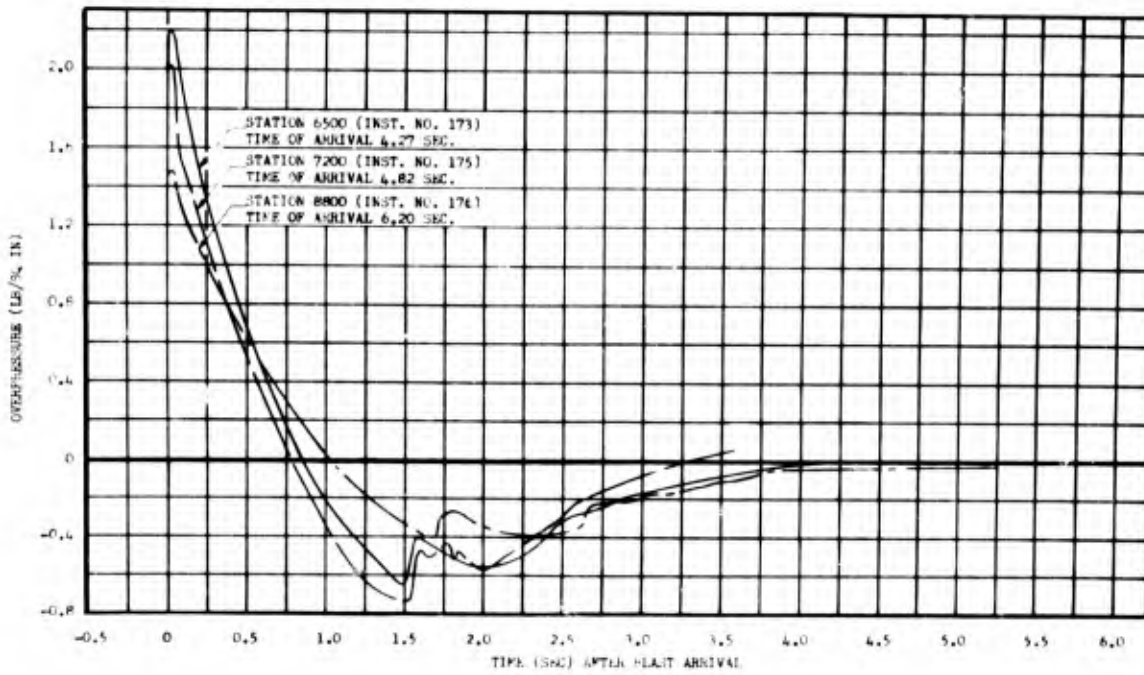
Fig. E.8 Variation of Overpressure with Time for Stations 6500, 7200,
and 8800, Shot 10 (See Fig. E.7)

277
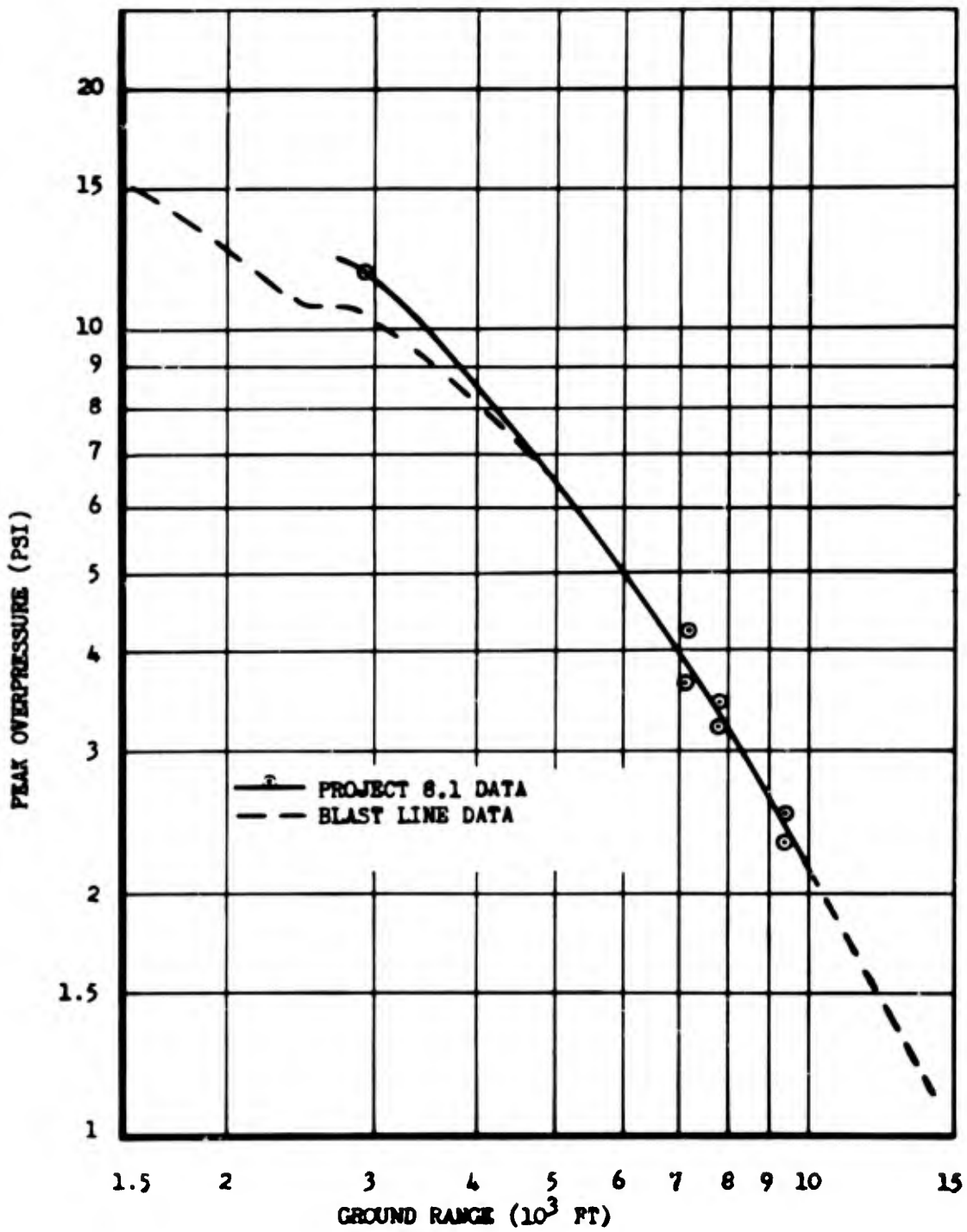
Fig. E.9 Variation of Peak Overpressure with Ground Range Along
the Project 8.1 Line, Shot 9

278
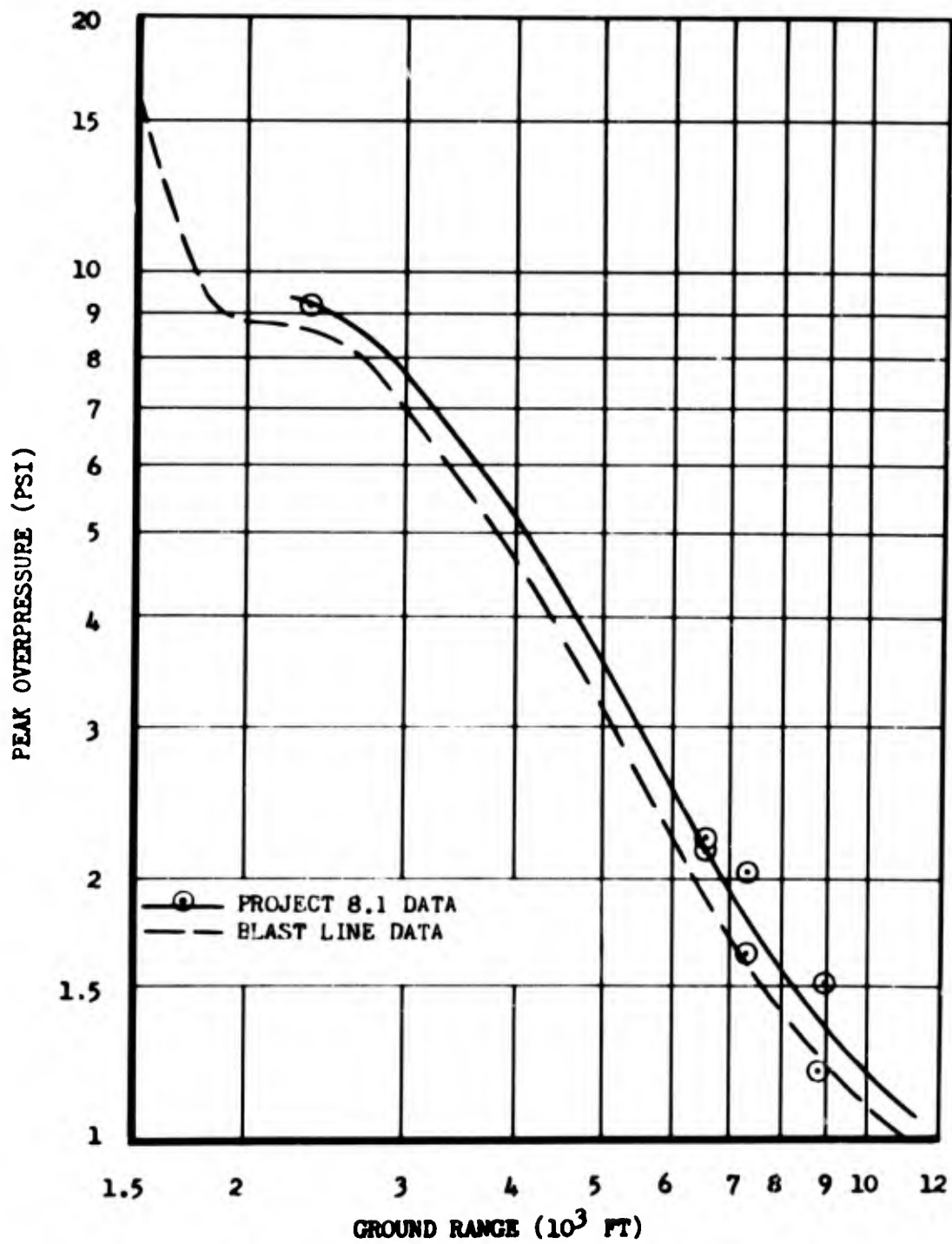
Fig. E. 10 Variation of Peak Overpressure with Ground Range Along
the Project 8.1 Line, Shot 10

279

TABLE E.5 - Summary of Peak Overpressure, Positive Phase Duration, and Time of Arrival for Shots 9 and 10

Shot No.	Station	Actual Ground Range (ft)	Peak Overpressure (lb/sq in.)	Positive Phase Duration (sec)	Time of Shock Arrival (sec)	Inst. No.
9	2300	2936	11.98	0.76	2.06	163
	6500	7098	3.65		5.10	164
			4.24	0.85	5.10	165
	7200	7796	3.22		5.65	166
			3.48	0.79	5.65	167
	8800	9391	2.33		7.01	168
			2.51	0.93	7.01	169
10	2300	2340	9.27	0.62	0.93	171
	6500	6537	2.15		4.27	172
			2.22	0.86	4.27	173
	7200	7237	1.65		4.82	174
			2.04	0.77	4.82	175
	8800	8836	1.51	1.03	6.20	176
			1.20		6.20	177

time curve for Station 2300, Shot 10, shown in Fig. E.7, probably indicates the presence of a precursor wave at this station. A peculiarity of the blast phase overpressure at all stations during Shot 10 was a sharp rise in overpressure during the negative phase at about the time the minimum overpressure occurred (see Figs. E.7 and E.8).

There appears to be a limit total thermal energy level above which the CEC diaphragm type transducer cannot be used because of severe buckling of the diaphragm. There are insufficient data to fix this threshold thermal energy; however, it probably lies in the range between 15 and 50 cal/sq cm.

E.3.1.2   Total Thermal Energy

Each of the 19 channels of total thermal energy measurements which were attempted yielded valid data. All thermal data were corrected for heat dissipation of the disc, for 8 per cent quartz window attenuation, and for incidence angle due to bombing error. A comparison of the mean total thermal energy at each station for Shot 9 is shown in Fig. E.11 and for Shot 10 in Fig. E.12. A list of the total thermal energy received at each installation is given in Table E.6.

280
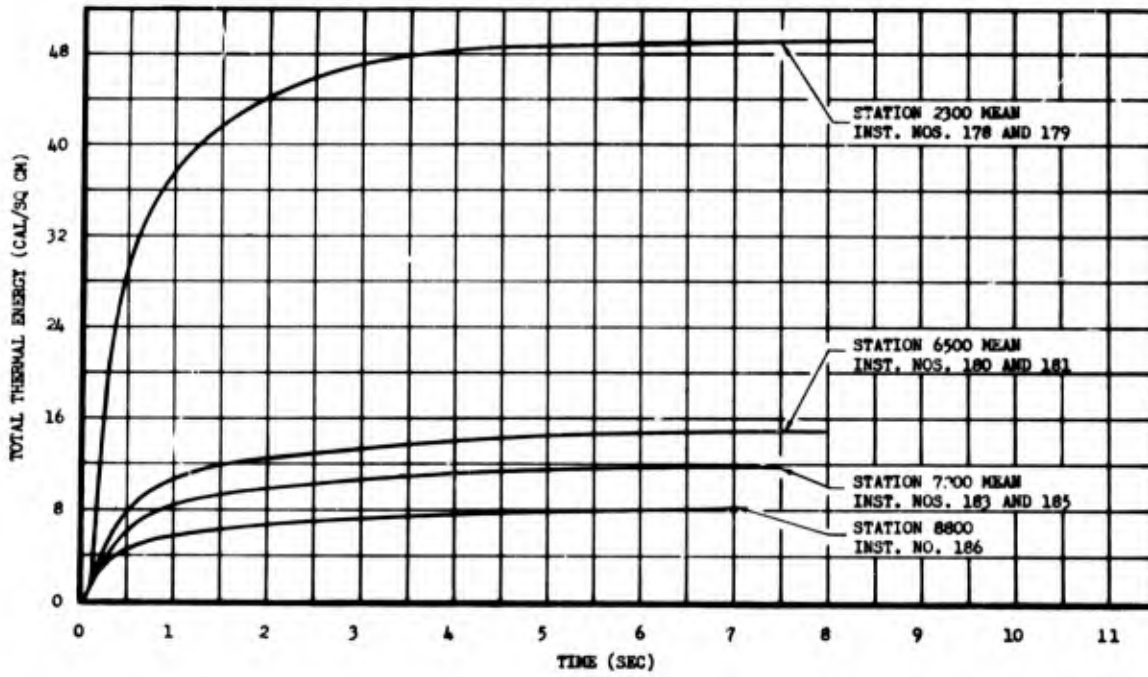
Fig. E.11 Comparison of the Thermal Energy-time Data at Stations
2300, 6500, 7200, and 8800 for Shot 9
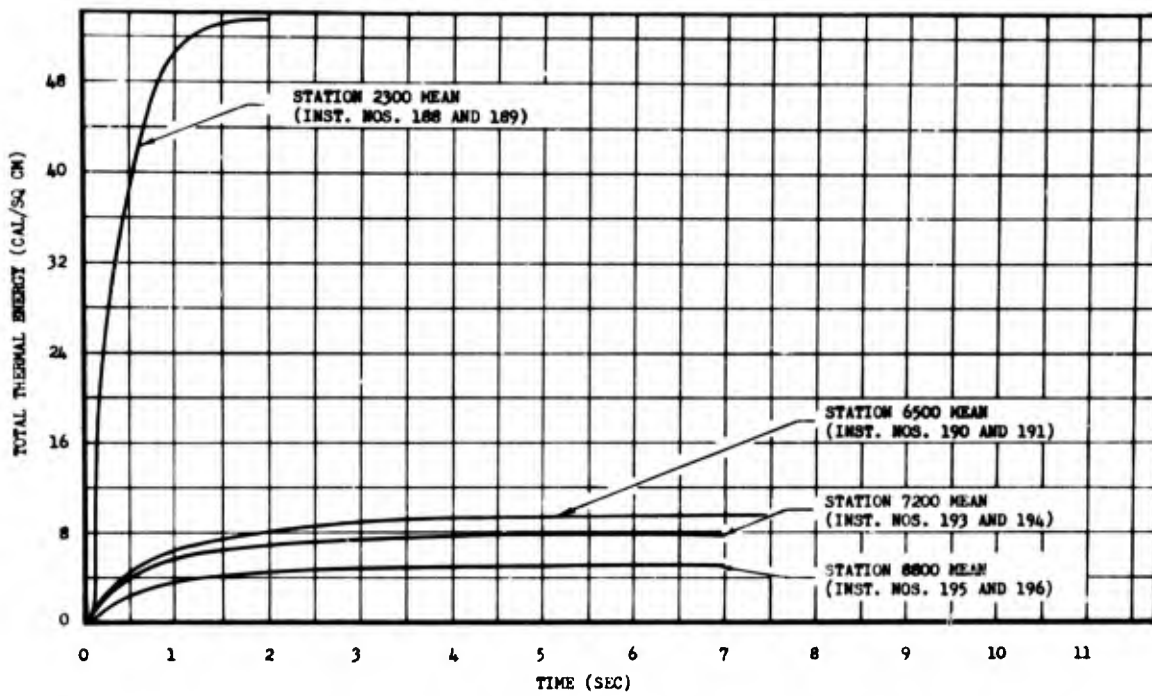
Fig. E.12 Comparison of the Thermal Energy-time Data at Stations
2300, 6500, 7200, and 8800 for Shot 10

281

TABLE E.6 - Measured Total Thermal Energy Data for Shots 9 and 10

Station	Actual Ground Range (ft)	Thermal Energy (cal/sq in.)	Inst. No.
Shot 9			
2300	2936	50.8	178
		47.4	179
6500	7098	15.8	180
		14.0	181
		10.4*	182
7200	7796	12.36	183
		8.74*	184
		11.62	185
8800	9391	8.3	186
		6.22*	187
Shot 10			
2300	2340	55.0	188
		52.2	189
6500	6537	9.86	190
		8.72	191
		6.74*	192
7200	7237	7.61	193
		7.93	194
8800	8836	4.96	195
		5.25	196

* Measurement made behind glass in stabilizer blast shield

The variation of total thermal energy with ground range for Shot 9 and Shot 10 is shown in Figs. E.13 and E.14, respectively.

A summary of the glass transmission values calculated from the thermal energy measurements made at the stations and behind the glass of the blast shields at the stations is given in Table E.7. The data on glass transmission are discussed in Appendix F.1.

E.3.1.3   Gamma Radiation Dosage

A summary of the radiation dosage data obtained during Shots 9 and 10, including the apparent attenuation afforded by the instrument shelters calculated from these data, is shown in Table E.8. The radiation dosage data for Shot 9 and Shot 10 are shown in Fig. E.15.

The 140 roentgens and 108 roentgens of gamma radiation
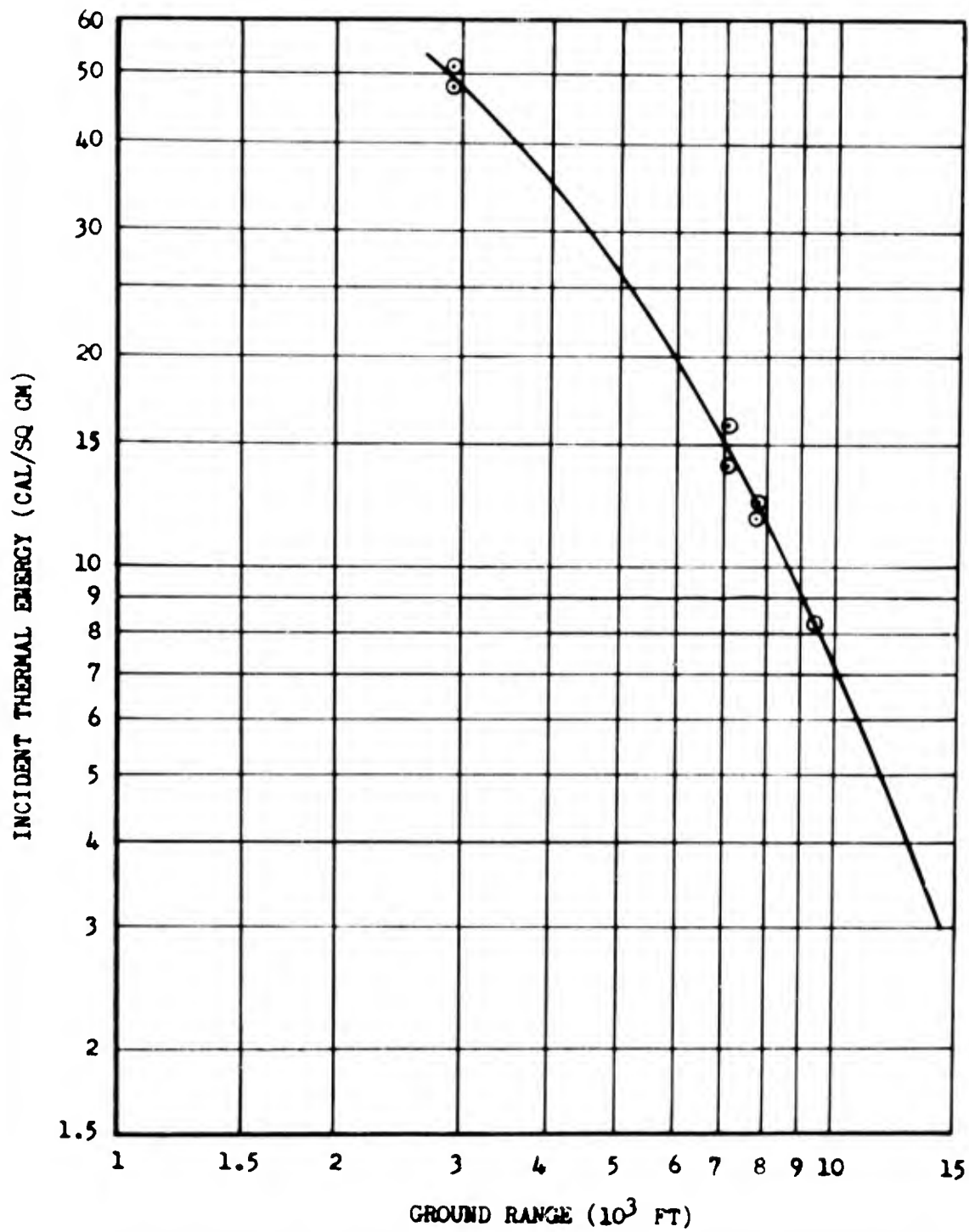
Fig. E.13 Variation of Total Thermal Energy with Ground Range Along
the Project 8.1a Line, Shot 9
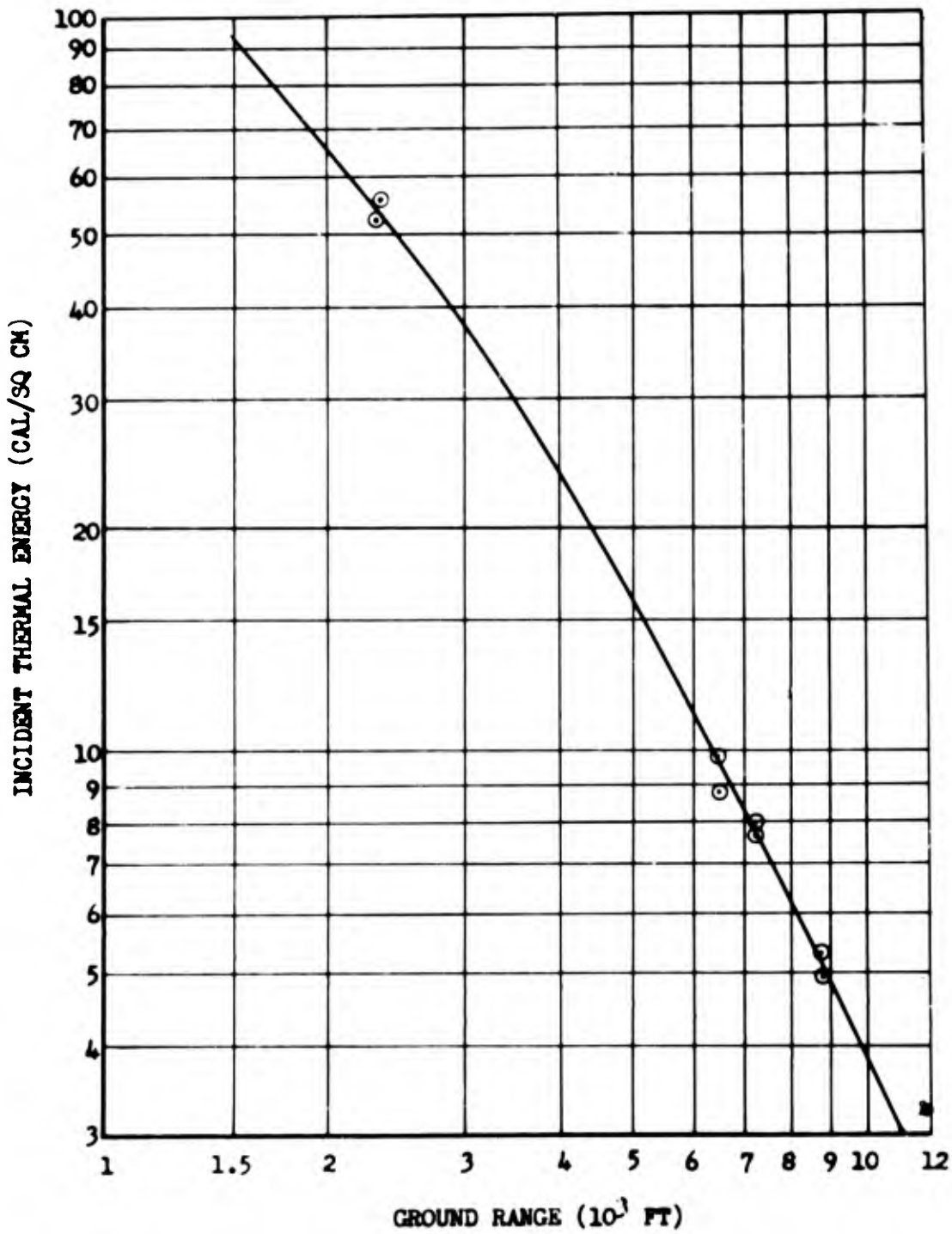
Fig. E.14 Variation of Total Thermal Energy with Ground Range
Along the Project 8.1a Line, Shot 10

284
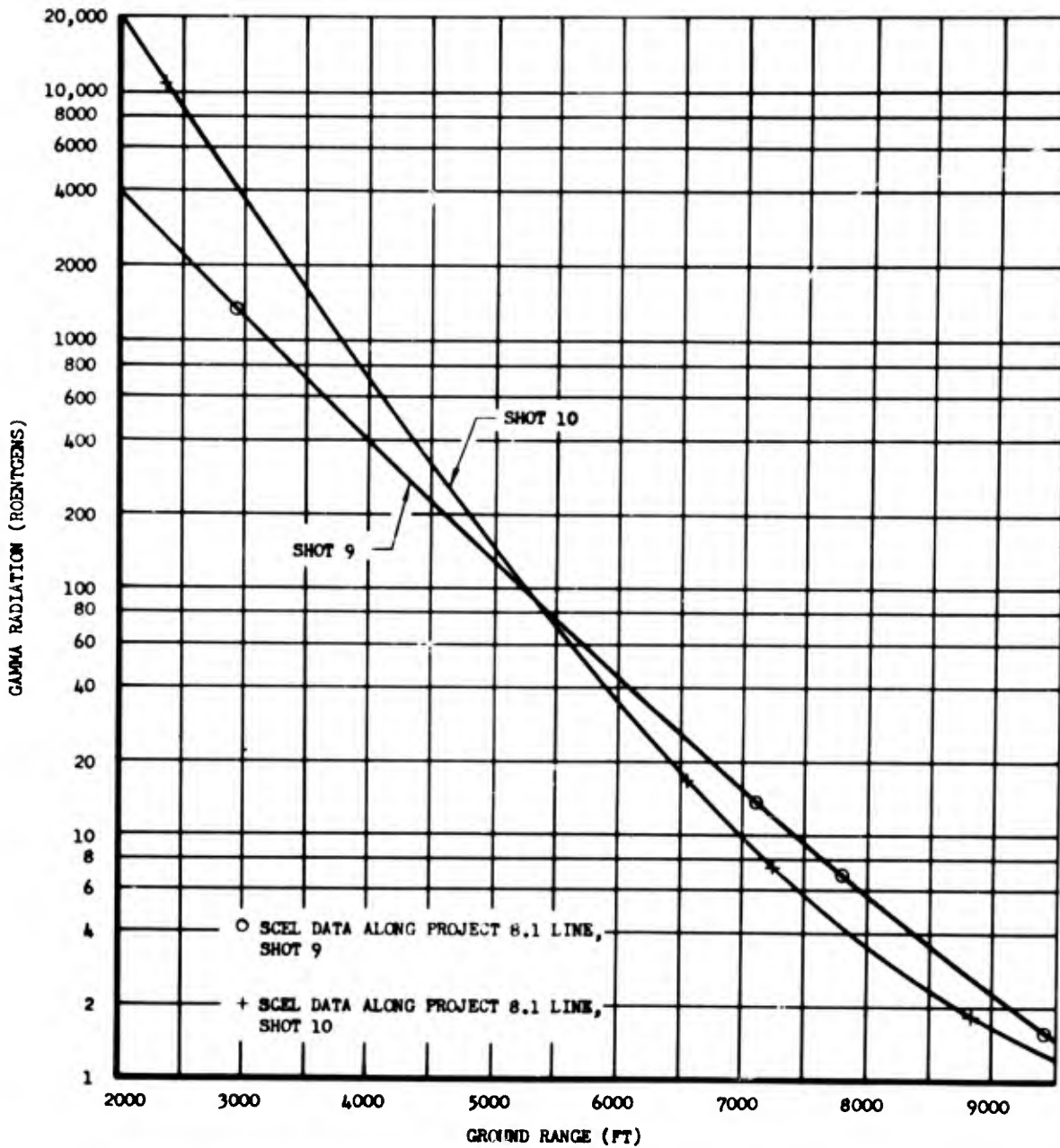
Fig. E. 15 Variation of Gamma Radiation Dosage with Ground Range
for Shot 9 and Shot 10

285

TABLE E.7 - Thermal Energy Data Behind Glass, Shots 9 and 10

Station	Shot No.	Glass Thickness (in.)	Measured Thermal (cal/sq cm)		Apparent Transmission (%)
			Behind Glass	At Station	
6500	9	7/8	10.4	15.8	65.8
				14.0	74.3
7200	9	3/4	8.74	12.36	70.7
				11.62	75.1
8800	9	3/4	6.22	8.30	75.0
6500	10	3/4	6.74	9.86	68.3
				8.72	77.2

TABLE E.8 - Radiation Dosage Data, Shots 9 and 10

Station	Shot No.	Actual Ground Range (ft)	Inst. No.	Radiation Dosage (Roentgens)		Apparent Attenuation (%)
				Outside Shelter	Inside Shelter	
2300	9	2936	R1	1375		
			R2		1.20	99.9
6500	9	7098	R3	13.5		
			R4		0.2	98.5
			R5		0.06	99.6
			R6		0.14	99.0
7200	9	7796	R7	7.0		
			R8		0.14	98
			R9		0.2	97.1
8800	9	9391	R10	1.56		
			R11		0	100
2300	10	2340	R12	10750		
			R13		140	98.7
			R14		108	99.0
			R15		67	99.4
6500	10	6537	R16	16.5		
			R17		0.41	97.5
			R18		0.97	94.1
7200	10	7237	R19	0.74		
			R20		0.33	55.5
8800	10	8836	R21	1.88		
			R22		0.15	92.0

286

dosage received by oscillographs number 1 and 7, respectively, at Station 2300 during Shot 10 were sufficient to cause severe fogging of the oscillograph records; however, no data were lost because of this fogging. Only 67 roentgens (Inst. R15) were received in the entrance hatch.

E.3.2   Shots 3, 5, 6, and 7

Peak overpressure and total thermal energy inputs were calculated by scaling from data from other nuclear explosions and/or normalized input curves. A summary of the calculated peak overpressure and total thermal energy data for each range used by Project 8.1a during Shots 3, 5, 6, and 7 is given in Table E.9. The total thermal energy measurements were corrected for atmospheric attenuation; however, no correction for dust attenuation was attempted. A discussion of this dust attenuation is given in para. D.4.3.

TABLE E.9 - Summary of Calculated Inputs at the Exposure Sites for Shots 3, 5, 6, and 7

Shot No.	Specimen	Ground Range (ft)	Peak Overpressure (lb/sq in.)	Total Thermal Energy [a] (cal/sq cm)
3	Panel Blast Shield	1850	2.0[b]	2.1
	Panel Blast Shield	2440	1.4[b]	1.2
	Panel Blast Shield	2620	1.3[b]	1.0
5	Rubber Sample	1180	34	500
	Rubber Sample	1650	24	260
	Rubber Sample	2320	12	130
	Panel Blast Shield	3500	6.6	54
	Panel Blast Shield	3900	5.4	43
	Panel Blast Shield	4460	4.3	32
	Stabilizer Blast Shield	4700	4.0	29
6	Panel Blast Shield	550	9.4	26
	Panel Blast Shield	800	4.9	10
	Panel Blast Shield	1100	3.2	6.1
7	Undercarriage Components	1920	27	360
	Undercarriage Components	2800	13	160
	Undercarriage Components	3460	9.4	110
	Undercarriage Components	5000	5.0	48

(a) Corrected for Atmospheric Attenuation but not Dust Attenuation
(b) SRI Preliminary Data

APPENDIX F

BLAST SHIELDING AND ABSORPTIVITY CONTROL

F. 1   TRANSPARENT MEDIA

The requirements regarding some of the data sought during UPSHOT-KNOTHOLE necessitated the shielding of certain specimens from the blast phase of a nuclear detonation while permitting them to absorb as much of the thermal energy as possible. In essence, the problem was to find suitable materials and structural configurations strong enough to withstand blast effects associated with overpressures up to 6 psi while possessing sufficiently high transmission coefficients so that the thermal requirements could be fulfilled.

F. 1. 1   Strength Characteristics

Two types of media were considered: viz., glass and "Plexiglas." Subsequent to a preliminary investigation into the physical characteristics of these media, the possibility of using annealed glass for this application was discarded in favor of tempered glass which is far more shock resistant. Tests had been performed by the Ballistic Research Laboratories, Aberdeen Proving Ground, Aberdeen, Md., and the shock resisting properties of "Herculite" (trade name for a tempered glass manufactured by the Pittsburgh Plate Glass Co.) and "Plexiglas" were found to be about equal. However, because of its low modulus of elasticity (4 to 6 x 10^5 psi), "Plexiglas" could bend and be blown out of its frame, at the overpressures to which it would be subjected, unless it were securely clamped. However, "Plexiglas" offers the distinct advantage that, when it fails, it does not disintegrate or dice as does tempered glass. The tests conducted at Aberdeen included the exposure of 1/4 in. by 16 in. by 16 in. panels of "Herculite" to various overpressures within a 2 ft shock tube. The glass panels were mounted in a frame with each edge clamped against a 1/4 in. edge

288

support using rubber gasket material for cushioning between the glass and the frame. Under these conditions, it was found that the panels generally failed at overpressures in the range of from 7 to 8 psi, although the data spread was greater. With the assumption that the stresses set up in the material are proportional to the reflected pressure, estimated thicknesses were calculated from the formula

$$s = \Delta P_r K \left(\frac{b}{L}\right)^{2*}$$ F. 1

where:

s = working stress (psi)
ΔP_r = reflected pressure (psi)
K = constant determined by aspect ratio and edge condition (numeric)
b = 1/2 unsupported width (in.)
L = thickness (in.)

If the breaking load is substituted in the above equation, "s" becomes the modulus of rupture. Therefore, an approximation of the modulus of rupture can be obtained by solving equation F. 1, using the 7 psi value for breaking load and assuming freely supported edges. The reflected pressure, ΔP_r, for 7 psi is equal to 16.6 psi, and for an aspect ratio of unity, K is equal to 1.15; then

$$s = 16.6 \, (1.15) \left(\frac{7.75}{0.25}\right)^2$$

and

$$s = 18,350 \text{ psi}$$

The 18,350 psi value does not represent the actual modulus of rupture of the glass because of the unaccounted-for influences such as dynamic overswing, the shock resistance of the rubber gasket and stress concentrations caused by surface irregularities. Consequently, a safety factor will be included to allow for these indeterminate conditions and the apparent modulus of 18,350 psi will be used for computations to determine glass panel thicknesses.

Since the heat treating processes involved in the production of "Herculite" cause high compression stresses to exist on the surfaces and adjacent layers, with balancing tension stresses within the core of the plate, the manufacturer warns that the glass is highly vulnerable to surface scratches and blows by sharp objects. Consequently, it was

---

* Timoshenko - Strength of Materials, Volume II, Chapter 3

felt that some type of protection might be required, especially during the blast phase of a nuclear detonation. Other potential dangers are present in this application of tempered glass because of the absorption, within the surface layers, of the energy contained in radiation of those wave lengths for which the glass has a low transmittance. Failure could occur as a result of this in either of two ways, both of which arise from a temperature change on the surface caused by the absorption of energy: first, the compression stresses on the surface could be relieved causing a stress unbalance throughout the glass, and second, sharp discontinuties in the surface stresses could occur at the boundaries of areas shielded by the mounting clamps. A possible solution to the preceding problems was the use of a thin sheet of "Plexiglas" as a shield over the glass which would act as an absorbing medium for the previously mentioned radiation during the thermal phase and as a shield against light flying objects during the blast phase. The shielding effect afforded by the thin "Plexiglas" sheet was investigated on shots prior to those during which the glass would be used for the basic test program.

F.1.2   Transmission Characteristics

Curves showing per cent transmission versus wave length were obtained from the manufacturers of "Herculite" and "Plexiglas", and the transmission factors for the two media were computed, assuming that the spectrum of the fireball was the same as that for solar radiation reaching the earth. Maximum economy and ease of handling limited the plate thicknesses to 3/4 in. or, at most, 7/8 in.; hence, transmission factors for heavy panels were based on these thicknesses and yielded the values of 78 per cent and 76 per cent for 3/4 and 7/8 in. "Herculite", respectively, and 60 per cent for 3/4 in. thick "Plexiglas." The transmission of 1/2 in. "Herculite" was calculated to be 82 per cent. It was necessary to allow some loss because of dust accumulation on the surface, and consequently, in all computations, 75 per cent was taken as the total transmission of all glass panels. The relatively low transmission factor for "Plexiglas" led to the decision that it would be used in the test program only in the event that glass proved to be unsatisfactory during preliminary test exposures.

F.1.3   Uses and Sizes

The specimens requiring blast shielding in order to acquire the desired data were the bonded metal panels and some of the T-28 horizontal stabilizer and elevator assemblies.

The blast shield for the bonded metal panels, described in Section D.1, required glass panels 20 in. sq. Taking the modulus of rupture for the tempered glass to be 18,350 psi, formula F.1 yields a

minimum thickness of 0.27 in. for an overpressure of 6 psi, deducting
1/2 in. from the span for all-around edge support. A thickness of 1/2
in. was chosen for use in these blast shields to allow a factor of safety
for the indeterminate variables of dynamic overswing, edge fixity, sur-
face irregularities, etc.

The extreme size of the stabilizer blast shield, described in
Appendix C, required the use of a series of glass panels rather than a
single large one, and a consideration of available production sizes and
conveniences of handling led to the decision that four panels would be
used. The over-all dimensions of each panel were 24 in. by 66 in.
Once more subtracting 1/2 in. from the span edge support for edge
support all around, formula F.1 yields a minimum thickness of 0.53
in. for a peak overpressure of 6 psi. For Station 6500 during Shot 9,
7/8 in. panels were chosen to provide a safety factor, whereas 3/4 in.
panels were used in all the remaining stabilizer blast shields at ranges
greater than 6500 ft.

F.1.4   Mounting Devices

The methods of mounting the glass panels in the blast shields
are shown in Fig. F.1 and Fig. F.2. The clamping arrangements
which are shown existed along two edges only in each case. For the
bonded metal panel blast shields, the clamps were along the vertical
edges, and for the stabilizer blast shields they were placed along the
horizontal edges. Any additional strength in the glass resulting from
the clamps was considered as an additional safety factor, since the
value for K used in formula F.1 was for plates with free edges. Lead
tape which was obtained from the Minnesota Mining and Manufacturing
Co. was used as a cushion. It was 0.008 in. thick with an adhesive
backing, and three layers were applied to each edge. In addition to the
tape, a wooden shim was used on the bonded metal panel blast shields
to take up any irregularities in the clamping device on the front plate.

F.1.5   Exposures and Results

Prior to the actual test program, blast shields of both types
were exposed to overpressures comparable to those expected during
the test program to determine, in general, the reaction of the complete
blast shield and, in particular, the shock-resistance of the glass and
"Plexiglas." In no case during the test program was there any glass
failure due to overpressure alone, although a short crack across one
corner was observed on two "Plexiglas" panels. Two glass panels in
the small blast shields were broken; however, this was attributed to
flying debris. The glass, on occasions, was found to be pitted but, in
general, appeared to be completely serviceable for the test program.

291
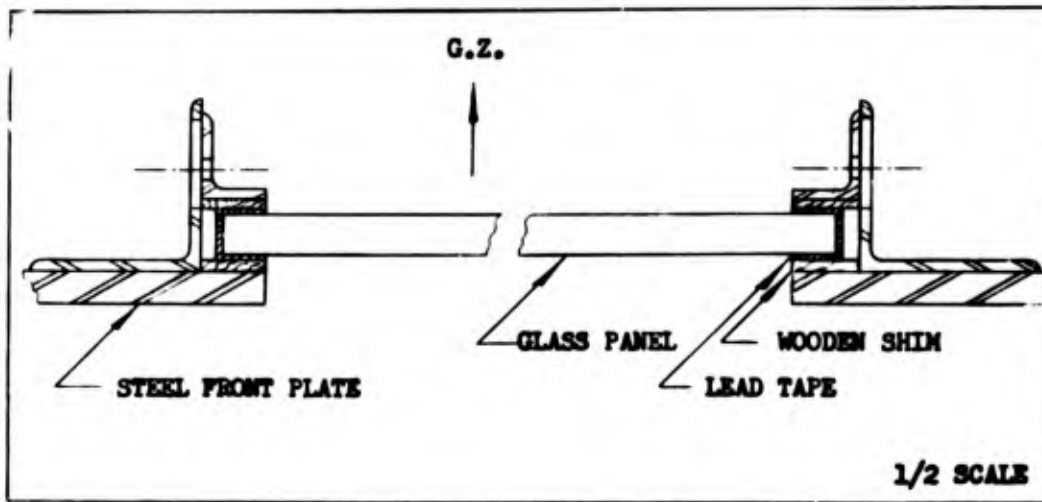
Fig. F. 1 Glass Clamps for Bonded Metal Panel Blast Shield
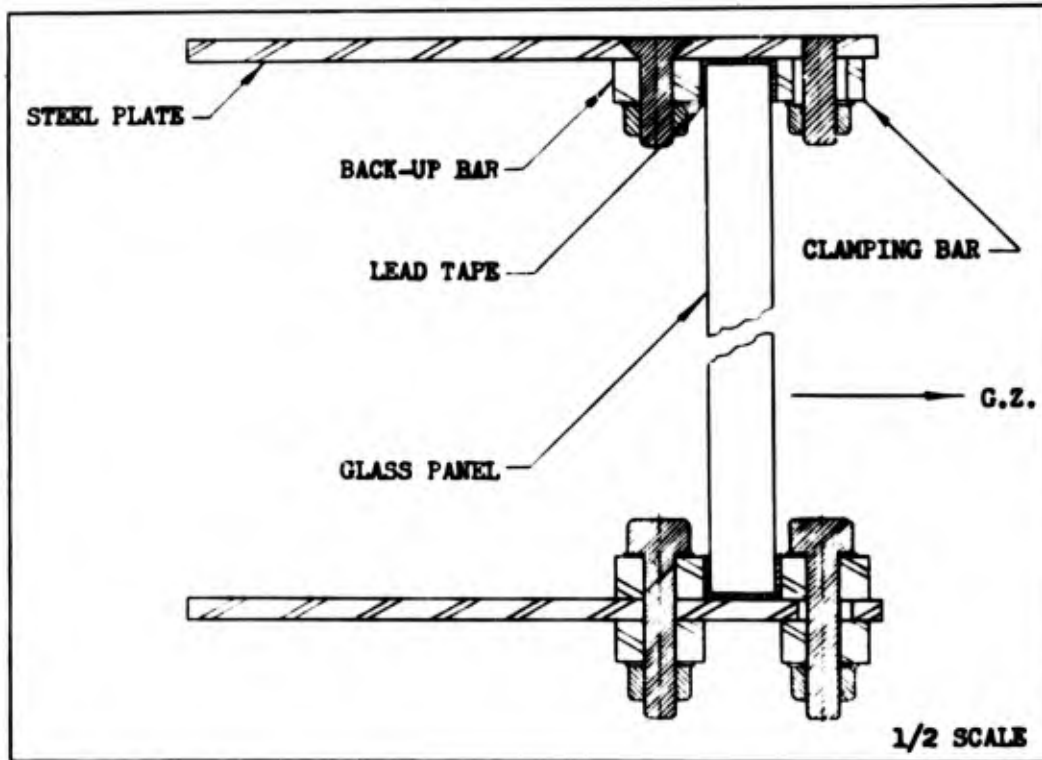
Fig. F. 2 Glass Clamps for Stabilizer Blast Shield

The "Plexiglas" panels and the thermal-shock shielding for glass were found to accumulate an excessive amount of dust, probably due to an electrostatic charge being generated on the surface during the cleaning process. Another objectionable feature of the thermal-shock shield was that it suffered severe deformation due to heat; however, this occurred only at inputs much higher than those expected during the actual tests.

Table F.1 lists the highest peak overpressures successfully

TABLE F.1 - Peak Overpressures Experienced by "Herculite" Panels Without Failure

Size (in.)	Shot No.	Ground Range (ft)	(Psi)	No. of Panels Exposed
3/8 x 20 x 20	5	3500	6.6	1
1/2 x 20 x 20	10	4038	5.1	2
3/4 x 24 x 66	5	4700	4.0	3
7/8 x 24 x 66	10	3552	6.2	4

withstood by glass panels of various sizes throughout the entire operation. It is not to be construed that these are the maximum overpressures that could be withstood by the panels.

Thermal measurements for the three exposures of 3/4 in. glass in the stabilizer blast shields yield an average total transmission factor of 74.7 per cent with a maximum deviation from the mean of approximately 2 1/2 per cent. The single exposure of 7/8 in. glass indicated a transmission factor of 70.7 per cent. No accurate thermal measurements were made within the bonded metal panel blast shields, so that the transmission factor for the 1/2 in. panels is not accurately known. However, the difference between the measured transmission and the calculated transmission of the 3/4 in. and 7/8 in. glass indicated that dust accumulation on the surface decreases the transmission to about 4 per cent below the calculated value; hence, an estimated total transmission factor for the 1/2 in. glass may be taken as 78 per cent.

F.2   ABSORPTIVITY CONTROL

Early in the planning stage of the operation it became evident that the absorptivity of the surfaces of most of the specimens would have to be controlled in order that the desired temperature rises and corresponding stresses could be attained with some degree of accuracy. A preliminary investigation revealed that a silicone base paint would

293

probably have a sufficiently high resistance to heat for this application and that the various absorptivities could be achieved by varying the ratio of white and black paints in a mixture of the two.

Several samples of black and white silicone base paints were prepared by the Lowe Brothers Paint Co., Dayton, Ohio. The samples were mixed to their standard paint formulas, but included a silicone base and sufficient inert ingredients to decrease the gloss. Preliminary investigations regarding the application of silicone paint to the specimen revealed that excessive smoking occurred during exposure to radiant heat energy on those samples which had not been subjected to a drying and baking process. Consequently, whenever possible, all painted samples and specimens were required to undergo a prescribed method of application. Each article was given one spray coat of a mixture of four parts silicone paint thinned with one part xylene and was placed in an oven at room temperature. The oven temperature was raised linearly to 275°F in 1/2 hr and was maintained at this temperature for an additional 2 1/2 hr before cooling. Oven tests were also performed on painted panels, and the resistance of the paint to high temperatures was established for conditions of slow heating. Later, a test was conducted under rapid heating conditions at the Naval Materials Laboratory, Brooklyn, N.Y., where black and white specimens were subjected to a thermal flux of 20 cal/sq cm/sec for 4 sec each. No blistering or flaking of the paint was visible and, although a slight smoking of the black sample was observed, it was concluded that this paint would be satisfactory for inputs up to this value.

In preparation for the first absorptivity tests, several small aluminum plates were painted various shades of gray, obtained by increasing, in 10 per cent increments, the percentage by weight of white paint in the mixture. The tests consisted of comparing the rates of temperature rise in the plates, caused by their exposure to a carbon arc. The only practical result obtained from the test was the knowledge that the absorptivity did not change linearly with the percentage of white paint but was greatly affected by the addition of the first increment of black paint to the mixture and was changed by progressively smaller amounts for each additional increment. Another set of 2 in. sq panels which included more shades in the region where the absorptivity was changing rapidly was prepared and presented to the Materials Laboratory, WADC, for actual calibration tests. Using a spectrophotometer, absorptivity measurements as a function of wave length were made on each sample from 0.4 microns to 4.2 microns. These data were then converted to total absorptivity, using the spectrum of solar radiation reaching the earth as a standard. This spectrum approximates that of a fireball and was used throughout the program as its equivalent. The complete calibration resulted in a curve of absorptivity as a function of per cent white paint as shown in Fig. F.3. The

use of the curve involves, first, the calculation of the absorptivity required to obtain a particular temperature rise in a given specimen
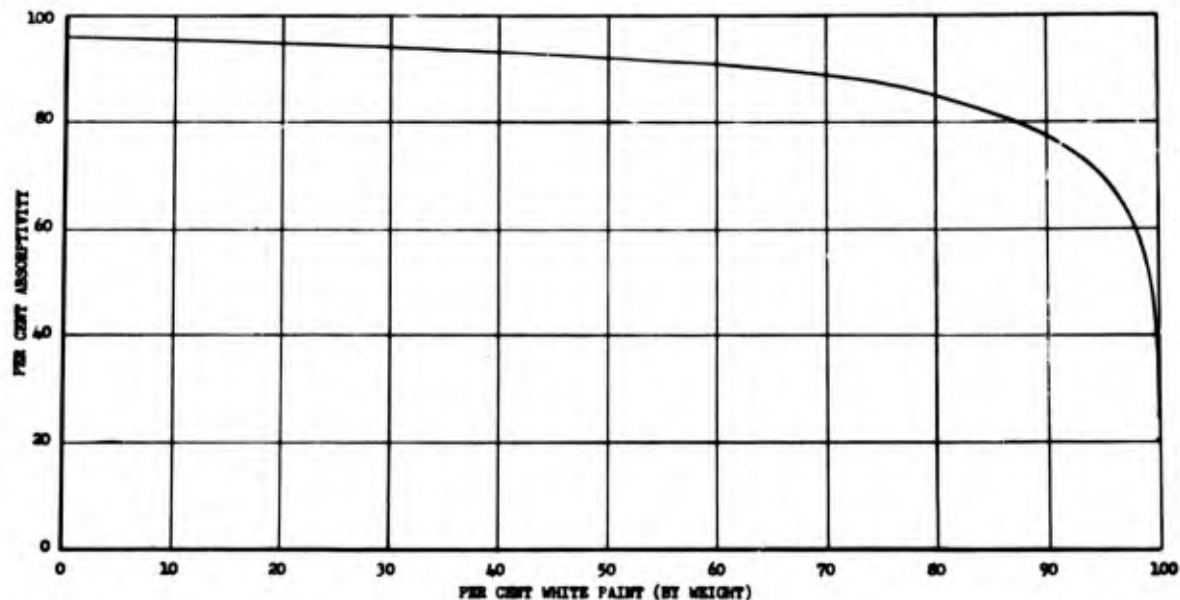
Fig. F.3 Curve Showing Variation of Absorptivity with Per Cent of White Paint in a Mixture of Black and White Silicone Base Paints

under predicted input conditions and, second, the determination of the proper mixture of paint to achieve this absorptivity.

The actual exposure of painted specimens during UPSHOT-KNOTHOLE revealed some disadvantages associated with the use of silicone paint. Although the paint did not rub off when dry, it was soluble in acetone, even after the baking process, and hence could be cleaned only with water; likewise, the painted surfaces were highly vulnerable to surface scratches, and extreme care was required in their handling. A greater limitation exists in that under the unique conditions of a nuclear detonation, the paint is not as resistant to thermal inputs as could be desired. Discoloration, scorching, and blistering are likely to occur in either of two ways, viz., through excessively high total thermal energy for thick specimens, or through excessive peak temperatures of thin specimens. The light colored tension ties and box beams at Station 2300 ft were scorched and discolored under a thermal input of 45 cal/sq cm and the black specimens were scorched at an input of 55 cal/sq cm; while at Station 6500, identical specimens remained undamaged for a thermal input of 16 cal/sq cm. In the case of the thin specimen, the black T-28 stabilizer at Range 3500 ft suffered severe blistering for a peak skin temperature of $640^{\circ}F$, while those at Station 6500 were undamaged for temperatures up to $414^{\circ}F$. A

295

summary of the peak temperatures attained by the bonded metal panels and the degree of blistering experienced by them tends to place more accurately the threshold temperature for this type of paint failure at approximately 450°F to 470°F. No recommendations regarding a remedy for the situation can be made at this time.

296

DISTRIBUTION

Copy

104 Commander, U.S. Naval Ordnance Test Station, Inyokern, China Lake, Calif.
105 Officer-in-Charge, U.S. Naval Civil Engineering Res. and Evaluation Lab., U.S. Naval Construction Battalion Center, Port Hueneme, Calif. ATTN: Code 753
106 Commanding Officer, U.S. Naval Medical Research Inst., National Naval Medical Center, Bethesda 14, Md.
107 Director, U.S. Naval Research Laboratory, Washington 25, D.C. ATTN: Code 2029
108 Director, The Material Laboratory, New York Naval Shipyard, Brooklyn, N.Y.
109 Commanding Officer and Director, U.S. Navy Electronics Laboratory, San Diego 52, Calif. ATTN: Code 4223
110-113 Commanding Officer, U.S. Naval Radiological Defense Laboratory, San Francisco 24, Calif. ATTN: Technical Information Division
114-115 Commanding Officer and Director, David W. Taylor Model Basin, Washington 7, D.C. ATTN: Library
116 Commander, U.S. Naval Air Development Center, Johnsville, Pa.
117-118 Director, Office of Naval Research Branch Office, 1000 Geary St., San Francisco, Calif.
119 Officer-in-Charge, U.S. Naval Clothing Factory, U.S. Naval Supply Activities, New York, 3rd Avenue and 29th Street, Brooklyn, N.Y. ATTN: R&D Division
120 Commanding Officer and Director, U.S. Naval Engineering Experiment Station, Annapolis, Md. ATTN: Code 155
121-127 Technical Information Service, Oak Ridge, Tenn. (Surplus)

AIR FORCE ACTIVITIES

128 Asst. for Atomic Energy, Headquarters, USAF, Washington 25, D.C. ATTN: DCS/O
129 Director of Operations, Headquarters, USAF, Washington 25, D.C. ATTN: Operations Analysis
130 Director of Plans, Headquarters, USAF, Washington 25, D.C. ATTN: War Plans Div.
131 Director of Research and Development, Headquarters, USAF, Washington 25, D.C. ATTN: Combat Components Div.
132-133 Director of Intelligence, Headquarters, USAF, Washington 25, D.C. ATTN: AFOIN-1B2
134 The Surgeon General, Headquarters, USAF, Washington 25, D.C. ATTN: Bio. Def. Br., Pre. Med. Div.
135 Asst. Chief of Staff, Intelligence, Headquarters, U.S. Air Forces Europe, APO 633, c/o PM, New York, N.Y. ATTN: Air Intelligence Branch
136 Commander, 497th Reconnaissance Technical Squadron (Augmented), APO 633, c/o PM, New York, N.Y.
137 Commander, Far East Air Forces, APO 925, c/o PM, San Francisco, Calif.
138 Commander, Strategic Air Command, Offutt Air Force Base, Omaha, Nebraska. ATTN: Special Weapons Branch, Inspection Div., Inspector General
139 Commander, Tactical Air Command, Langley AFB, Va. ATTN: Documents Security Branch
140 Commander, Air Defense Command, Ent AFB, Colo.
141-142 Commander, Air Materiel Command, Wright-Patterson AFB, Dayton, O. ATTN: MCAIDS
143 Commander, Air Training Command, Scott AFB, Belleville, Ill. ATTN: DCS/O GTP
144 Commander, Air Research and Development Command, PO Box 1395, Baltimore, Md. ATTN: RDDN
145 Commander, Air Proving Ground Command, Eglin AFB, Fla. ATTN: AG/TRB
146-147 Commander, Air University, Maxwell AFB, Ala.

Copy

148-155 Commander, Flying Training Air Force, Waco, Tex. ATTN: Director of Observer Training
156 Commander, Crew Training Air Force, Randolph Field, Tex. ATTN: 2GTS, DCS/O
157 Commander, Headquarters, Technical Training Air Force, Gulfport, Miss. ATTN: TA&D
158-159 Commandant, Air Force School of Aviation Medicine, Randolph AFB, Tex.
160-165 Commander, Wright Air Development Center, Wright-Patterson AFB, Dayton, O. ATTN: WCOESP
166 Commander, Air Force Cambridge Research Center, 230 Albany Street, Cambridge 39, Mass. ATTN: CRW, Atomic Warfare Directorate
167 Commander, Air Force Cambridge Research Center, 230 Albany Street, Cambridge 39, Mass. ATTN: CRQST-2
168-170 Commander, Air Force Special Weapons Center, Kirtland AFB, N. Mex. ATTN: Library
171 Commandant, USAF Institute of Technology, Wright-Patterson AFB, Dayton, O. ATTN: Resident College
172 Commander, Lowry AFB, Denver, Colo. ATTN: Department of Armament Training
173 Commander, 1009th Special Weapons Squadron, Headquarters, USAF, Washington 25, D.C.
174-175 The RAND Corporation, 1700 Main Street, Santa Monica, Calif. ATTN: Nuclear Energy Division
176-182 Technical Information Service, Oak Ridge, Tenn. (Surplus)

OTHER DEPARTMENT OF DEFENSE ACTIVITIES

183 Asst. Secretary of Defense, Research and Development, D/D, Washington 25, D.C.
184 U.S. National Military Representative, Headquarters, SHAPE, APO 55, c/o PM, New York, N.Y. ATTN: Col. J. P. Healy
185 Director, weapons Systems Evaluation Group, OSD, Rm 2E1006, Pentagon, Washington 25, D.C.
186 Armed Services Explosives Safety Board, D/D, Building T-7, Gravelly Point, Washington 25, D.C.
187 Commandant, Armed Forces Staff College, Norfolk 11, Va. ATTN: Secretary
188-193 Commanding General, Field Command, Armed Forces Special Weapons Project, PO Box 5100, Albuquerque, N. Mex.
194-195 Commanding General, Field Command, Armed Forces Special Weapons Project, PO Box 5100, Albuquerque, N. Mex. ATTN: Technical Training Group
196-204 Chief, Armed Forces Special Weapons Project, PO Box 2610, Washington 13, D.C.
205-211 Technical Information Service, Oak Ridge, Tenn. (Surplus)

ATOMIC ENERGY COMMISSION ACTIVITIES

212-214 U.S. Atomic Energy Commission, Classified Technical Library, 1901 Constitution Ave., Washington 25, D.C. ATTN: Mrs. J. M. O'Leary (For DMA)
215-217 Los Alamos Scientific Laboratory, Report Library, PO Box 1663, Los Alamos, N. Mex. ATTN: Helen Redman
218-220 Sandia Corporation, Classified Document Division, Sandia Base, Albuquerque, N. Mex. ATTN: Martin Lucero
221-222 University of California Radiation Laboratory, PO Box 808, Livermore, Calif. ATTN: Margaret Folden
223 Weapon Data Section, Technical Information Service, Oak Ridge, Tenn.
224-280 Technical Information Service, Oak Ridge, Tenn. (Surplus)

AEC Oak Ridge, Tenn. AF1001